# INVESTIGATING PRENATAL STRESS IN A STEM CELL MODEL OF HUMAN NEURONAL DEVELOPMENT

Lilia Papst
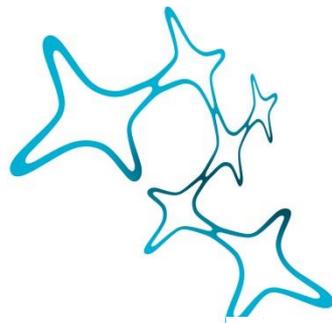
Graduate School of Systemic Neurosciences

LMU Munich

Dissertation at the
Graduate School of Systemic Neurosciences
Ludwig-Maximilians-Universität München

May, 2019

Supervisor
Prof. Dr. Dr. med. Elisabeth Binder
Translational Research in Psychiatry
Max Planck Institute of Psychiatry

First Reviewer: Prof. Dr. Dr. med. Elisabeth Binder
Second Reviewer: Prof. Dr. Moritz Rossner
Third Reviewer: Prof. Dr. Edna Grünblatt
Date of Submission: May 27th 2019
Date of Defense: September 23rd 2019

Contents

ABSTRACT

Prenatal stress is a known risk factor for alterations in brain structure, cognition and behavior associated with neurodevelopmental psychiatric disorders. However, underlying molecular mechanisms are not fully understood and have never been investigated in live human embryonic neuronal cells.

This study aimed at examining the potential molecular effects of prenatal stress on the developing brain by modelling embryonic neurogenesis in human stem cells and inducing glucocorticoid receptor-dependent epigenetic changes.

Embryonic stem cells and induced pluripotent stem cells were differentiated into ventricular zone-like neuronal progenitors and migrating neurons. Glucocorticoid receptor expression and translocation to the nucleus upon stimulation with dexamethasone were traced across neuronal development and epigenomic changes assessed by alterations in methylation profile and differential gene expression.

The results support an intrinsic role of the glucocorticoid receptor during early neurogenesis and suggest that exposure to external glucocorticoids has little effect on neurulating cells up until the start of radial migration towards outer cortical layers. In migrating neurons however, glucocorticoid receptor activation led to hypermethylation of genes with well-established implications in psychiatric disorders, forebrain development, migration, axon development, and Wnt signaling. These effects were mirrored on the transcriptome level in that the number of genes significantly regulated by dexamethasone exposure increased in parallel with glucocorticoid receptor expression and translocation to the nucleus over neural differentiation.

An understanding of the molecular mechanisms linking prenatal stress to psychiatric disorders may both help promote awareness of its impact and the development of targeted interventions.

LIST OF ABBREVIATIONS

bp = base pairs

CpG island = Cytosine-phosphate-Guanine-rich island

DEG = Differentially expressed gene

DEX = Dexamethasone

DMP = Differentially methylated position

DMR = Differentially methylated region

EB = Embryonic Body

GWAS = Genome-wide association studies

hESC = human embryonic stem cell

dN = differentiated Neuron

DNAm = DNA methylation

FDR = False discovery rate (q-value)

GR = Glucocorticoid Receptor

GW = Gestational week

hiPSC = human induced pluripotent stem cell

hSC = human stem cell (hiPSC or ESC)

NP = Neuronal Progenitor

NPC = Neuronal Progenitor Cell

OR = Odds Ratio

TSS = Transcription Start Site

VIF = Variance Inflation Factor

1.　　INTRODUCTION

1.1　　THEORETICAL BACKGROUND

1.1.1　　EPIDEMIOLOGY OF PSYCHIATRIC DISORDERS

Psychiatric disorders pose a global health challenge with a lifetime prevalence of 29.2% and a 12-month prevalence of 17.6% worldwide for any diagnosis (Steel et al., 2014). Overall, they account for over one fifth of years lived with disability and 6.2% of years of life lost due to premature mortality (WHO, 2015). In addition to the personal costs, mental disorders inflict a considerable economic burden on society made up of direct financial costs such as medication, physician services, and hospitalisation as well as indirect costs caused by losses in productivity and income, which together amounted to an estimated €798 billion in the EU in 2010 (Gustavsson et al., 2011) or 6.2% of the European GDP that same year.

1.1.2　　PRENATAL STRESS IN PSYCHIATRIC DISORDERS

1.1.2.1　　DEVELOPMENTAL ORIGINS OF HEALTH AND DISEASE

The "Developmental Origins of Health and Disease" (DOHaD) Hypothesis proposes that the predisposition to non-communicable diseases can be traced back to embryonic development, a sensitive period when plasticity is especially high and susceptible to environmental factors (Barker, 1990). While environmental influences accumulate and become more diverse with time, biological plasticity decreases, meaning that later experiences are less likely to result in (neuro-)biological embedding. Prenatal stress may therefore prime the young organism's

epigenetic signature with lasting effects on stress reactivity and the immune system until long after birth, thus increasing vulnerability to psychiatric disorders.

1.1.2.2   DEFINITION OF PRENATAL STRESS

Prenatal stress is a blanket term in psychiatric research used to describe embryonic and foetal exposure to excessive glucocorticoids in the womb. Its experimental operationalisation ranges from the direct assessment of maternal cortisol to more indirect measures such as maternal anxiety, depression, or experience of trauma, and may also include administration of synthetic glucocorticoids such as dexamethasone or betamethasone.

The unborn child is usually spared from high glucocorticoid levels by a protective barrier of placental 11β-hydroxysteroid dehydrogenase type 2 (11β-HSD2). It rapidly metabolises cortisol to its inactive form (Benediktsson et al., 1997) and thus helps maintain the relatively low physiological concentration of foetal serum cortisol at an average of 8.4 ng/ml mid-gestation, and 45.1 ng/ml towards delivery, respectively (Peffer et al., 2015). This mechanism is compromised when maternal stress levels are high and the placental barrier either becomes saturated with cortisol or levels of placental 11β-HSD2 are depleted as a result of maternal stress (Mairesse et al., 2007), depression (Seth et al., 2015), or non-clinical factors such as liquorice consumption (Tanahashi et al., 2002). Increased numbers of active cortisol are then allowed to enter foetal circulation. Synthetic glucocorticoids such as dexamethasone on the other hand are a poor substrate to 11β-HSD2 and can readily pass the placental barrier to exert their effects (**Fig. 1**). Interestingly, betamethasone was found to increase placental 11β-HSD2 expression in mice (Ni et al., 2018).
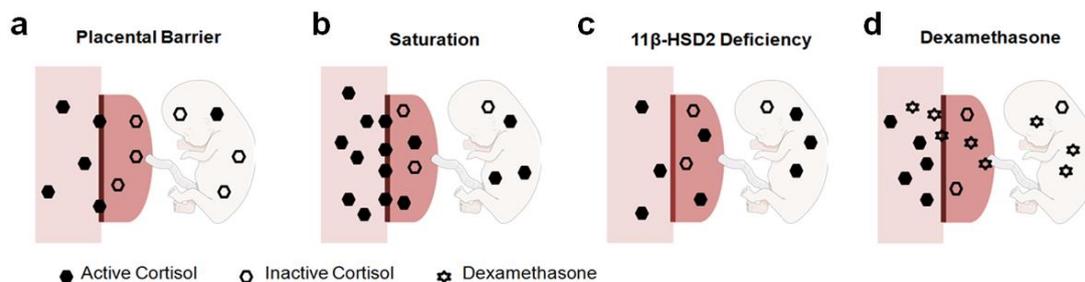
Figure 1. Functioning and Compromised Placental Barrier. a) Placental 11β-HSD2 converts active cortisol to its inactive form. Conversion may be compromised under b) high levels of cortisol or c) low levels of 11β-HSD2. d) Dexamethasone does not bind 11β-HSD2 and can pass the placental barrier under normal physiological conditions. Adapted from Seckl & Holmes (2007).

1.1.2.3   PREVALENCE OF PRENATAL STRESS

Depression affects between 7.4% and 12.8% of mothers during pregnancy (Bennett et al., 2004), while 5.3% (Sausenthaler et al., 2009) to 35% (Pantha et al., 2014) of pregnant women experience daily stressors, traumatic events, physical, sexual, or emotional abuse. Dexamethasone administration in expectant mothers is considered controversial but may be applied within the first seven weeks of pregnancy in pre-emptive treatment of congenital adrenal hyperplasia (Nimkarn & New, 2007) and in preparation for IVF treatment (Basirat et al., 2016), sometimes continuing until the first weeks following implantation. Due to its category A classification in some countries (Australian Government, Department of Health, 2018), it may even be prescribed against nausea during pregnancy. The most common application however is to promote lung maturation in infants at risk for preterm delivery, in which case it is usually not prescribed prior to embryonic weeks 32-34 at a dosage of 6 mg.

Both naturally and artificially elevated glucocorticoid levels during gestation have been linked to a number of alterations in cognition and behaviour, brain structure, stress and immune systems, and molecular processes presumed to contribute to psychiatric conditions.

1.1.2.4   IMPACT ON COGNITION AND BEHAVIOUR

Prenatal stress has reliably been shown to increase the probability of negative affect, internalising and externalising behaviour, disturbed motor development, attention deficits, and cognitive deficits in infants (review of 91 prospective longitudinal studies from 2010 to 2017; van den Bergh et al., 2017). These effects were observed while controlling for confounding factors such as maternal mental health prior to and following pregnancy, socioeconomic status, offspring sex, gestational age, genotype, age at symptom screening, and APGAR (Appearance, Pulse, Grimace, Activity, Respiration) values (Li et al., 2010; Chong et al., 2016; Ronald et al., 2011; Robinson et al., 2011; Velders et al., 2012; Nulman et al., 2012; O'Donnell et al., 2014; Rouse & Goodman, 2014). Similarly, foetal exposure to dexamethasone led to psychopathology, disturbed attention (Khalife et al., 2013), higher emotionality, internalising behaviours and lowered sociability (Trautmann et al., 1995). Some studies also reported no differences in terms of psychopathology, behavioural problems, adaptive functioning (Hirvikoski et al., 2008), or motor and cognitive development (Meyer-Bahlburg et al., 2004) between exposed and non-exposed individuals. Equally, prenatal exposure to betamethasone had no adverse effects on cognitive development in children (MacArthur et al., 1982), or on cognitive functioning, working memory, attention, psychiatric morbidity, or health related quality of life in adults (Dalziel et al., 2005). Associations between different

prenatal stressors and psychiatric diagnoses are listed in **Table 1**. Interventional studies in both animals and humans suggest that the negative outcomes of prenatal stress can be attenuated by tactile stimulation and positive parental attention postnatally (Sharp et al., 2012; Sharp et al., 2015; Pickles et al., 2017; Liu et al., 1997; Francis et al., 1999). This does not seem to be the case however when such behaviour is not explicitly encouraged (Schechter et al., 2017; Sharp et al., 2015).

Table 1. Associations between prenatal stressors and psychiatric diagnoses.

Type of prenatal stress	Sample size (N)	Timing of prenatal stress	Offspring age	Results	Publication
Maternal depression	2.847	GW 32	18 years	Increased risk of depression (OR= 1.28; p = .003)	Pearson et al. (2013)
	103	GW 36	18-25 years	Increased risk of depression (OR=3.4; p = 0.004)	Plant et al. (2015)
	4.303	GW 18	18 years	Increased risk of anxiety disorders (OR=1.75; p = 0.01)	Capron et al. (2015)
	6.050	GW 18, 32	11-12 years	Increased risk of Borderline Personality Disorder (OR=1.31-1.59; CI:1.14-2.32)	Winsper et al. (2015)
Maternal bereavement	1.015.912	1st, 2nd, 3rd trimester	3 years – late adolescence	Increased risk of ADHD in boys (HR=1.47-2.10; CI:1-2.16)	Li et al. (2010)
	1.045.336	1st, 2nd, 3rd trimester	birth – early adulthood	No association with risk of psychosis (OR=0.46-1.66; CI: 0.96-1.62)	Abel et al. (2014)
	738.144 (childhood), 2.155.221 (adulthood)	1st, 2nd, 3rd trimester	birth – early adulthood	Increased risk of autism (HR=1.58; CI: 1.15–2.17) & ADHD (HR=1.31; CI: 1.04–1.66) but not bipolar disorder (HR=1.2; CI: 0.95–1.51) & schizophrenia (1.32; CI: 0.88–1.97)	Class et al. (2014)
Maternal cortisol levels	65	GW 15, 19, 25, 31, 37	7.5 years	GW 15 → higher risk of affective problems in females (p=0.04)	Buss et al. (2012)
Maternal stressful life events	2.868	GW 18, 34	2 years	Increased risk of ADHD (β=0.1, p=0.01-0.03), increased risk of autism in boys only (β=0.1, p=0.04)	Ronald et al. (2011)

	89	1st, 2nd, 3rd trimester	6.5 years	Increased autism spectrum disorder symptoms (β=-0.842 (inverse), p=0.001)	Walder et al. (2014)
	54	1st, 2nd, 3rd trimester	13 years	3rd trimester → increased eating disorder symptoms (β=0.37, $p\leq$0.001)	St-Hilaire et al. (2015)
	1.765	1st, 2nd, 3rd trimester	4 years	2nd & 3rd trimester → Increased ADHD symptoms (OR = 2.41; CI: 1.03-5.66)	Zhu et al. (2015)
	95 (SCZ) 206 (CTRL)	GW 16	Adulthood	Increased risk of schizophrenia in males (OR=1.24; p=0.388)	Fineberg et al. (2016)
	10.569	GW 18	10 – 18 years	Increased depressive symptoms (β = 0.07, $p\leq$0.01)	Kingsbury et al. (2016)
	743	GW 20	6 years	Increased autistic traits (β = 0.16, $p\leq$0.001)	Rijlaarsdam et al. (2017)
Maternal anxiety	4.704	GW 32	15 years	Increased symptoms of anxiety and depression (β = 0.2, $p\leq$0.01)	O'Donnell et al. (2014)
Dexamethasone	56	GW 1-21	0.5 – 5.5 years	Increased shyness, emotionality, avoidance, internalizing & total problem scores decreased sociability (t=1.77-3.33, $p\leq$0.05-$p\leq$0.002)	Trautman et al. (1995)
	61	3rd trimester	2.5 years	No differences in psychopathology (U=447, p=0.907)	Hirvikoski et al. (2008)
	222	3rd trimester	8, 16 years	Increased general psychiatric disturbance at 8 years follow-up (β=8.34, CI: .23-16.45)	Khalife et al. (2013)
Betamethasone	250	3rd trimester	7 years	No differences in cognitive development	MacArthur et al. (1982)
	192	3rd trimester	31 years	No differences in psychiatric morbidity (OR=0, p=0.78)	Dalziel et al. (2005)

Annotations. GW = Gestational week, OR = Odds Ratio, HR = Hazard Ratio, CI = Confidence Interval, ADHD = Attention-deficit hyperactivity disorder.

At the same time, prenatal stress itself has occasionally been associated with

enhanced motor development and cognitive performance (Di Pietro et al., 2006;

Davis et al., 2017) as well as lower levels of depressive symptoms (Zohsel et al., 2017). These findings support the stress inoculation hypothesis stating that stress exposure early in life can actually improve subsequent stress resistance. Which factors decide over the benefit or harmfulness of prenatal stress is currently unknown, although both the duration and intensity of the stressor (Popoli et al., 2012) and individual differences in stress sensitivity (Arloth et al., 2015) are likely contributors.

Taken together, empirical findings support the notion of prenatal stress as a risk factor for psychopathology. However, effects may be attenuated with adequate postnatal care or indeed be advantageous due to factors yet to be determined.

1.1.2.5   ORGANISATIONAL EFFECTS ON BRAIN STRUCTURE

Prospective longitudinal data indicate that pregnancy anxiety at gestational week (GW) 19 but not later is associated with gray matter reductions in prefrontal and premotor cortex, temporal lobe, postcentral gyrus, cerebellum, occipital gyrus and fusiform gyrus in six- to nine-year-old offspring (Buss et al., 2010). Similar effects were reported for maternal depression, which was associated with offspring cortical thinning throughout pregnancy, but especially following exposure at GW 25 with thinning in 19% of the whole cortex and in 24% of the prefrontal cortex and frontal lobes (Sandman et al., 2015). Lending support to the functional significance of these findings, cortical thinning in prefrontal areas of the right hemisphere moreover mediated an association between maternal depression and child externalising behaviour. Prenatal administration of dexamethasone at GW 23 to 31 resulted in a 35% reduction in cerebral cortical grey matter volume in premature infants at birth compared to premature infants not treated with dexamethasone, but

no differences in subcortical gray matter volume (Murphy et al., 2001). Only one study found that elevated cortisol levels at GW 19 and 31 resulted in greater cortical thickness in predominantly frontal regions, mediating enhanced child cognitive performance (Davis et al., 2017). Higher cortisol levels at GW 15 were furthermore associated with larger right amygdala volume and affective problems in girls but not boys, whereas hippocampal volume remained unaffected (Buss et al., 2012). The large-scale prospective longitudinal "Growing Up in Singapore Towards Healthy Outcomes" (GUSTO) study examined the effects of maternal depression at GW 26 on child grey matter measures two weeks postnatally. An interaction between maternal depression and infant genomic profile risk score for Major Depressive Disorder (MDD) predicted increased right amygdala volume, in the Asian cohort also increased right hippocampal volume and shape, and increased orbitofrontal and ventromedial prefrontal cortex thickness (Qiu et al., 2017). At four and a half years of age however, effects were limited to larger right amygdala volume in girls, but not boys (Wen et al., 2017) emphasizing the role of postnatal plasticity.

As for white matter, maternal stressful life events during pregnancy positively correlated with fractional anisotropy values in the right uncinate fasciculus of affected individuals (Sarkar et al., 2014), a white matter tract connecting the amygdala to inferior prefrontal regions bilaterally. Fractional anisotropy is a measure of the degree to which water diffuses directionally throughout the axon, indicating strength of myelination. In other studies, however, prenatal exposure to dexamethasone or maternal stress had no effects on white matter volume (Murphy et al., 2001), or fractional anisotropy (Wen et al., 2017).

In sum, frontal cortical regions, the right amygdala, and possibly their axonal tract connections are the brain areas most likely to be affected by prenatal stress exposure (**Fig. 2**), which falls in line with cognitive-behavioural changes.
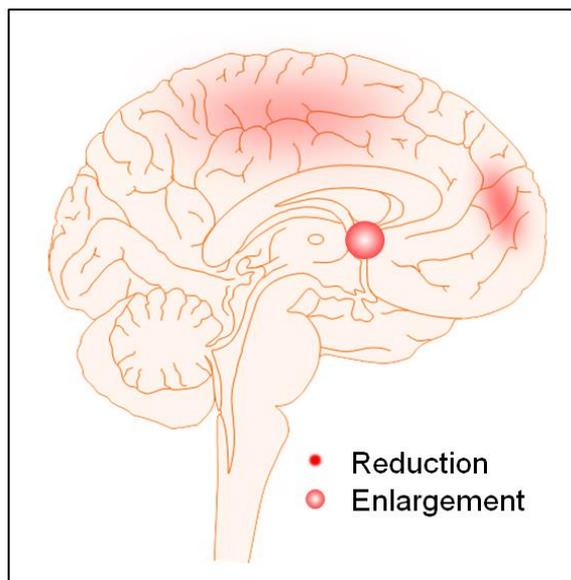
Figure 2. Brain Regions Differentially Affected by Prenatal Stress. Prenatal stress has been found to cause reductions in (frontal) cortical grey matter volume and increases in amygdala volume.

1.1.2.6   HYPOTHALAMIC-PITUITARY-ADRENAL AXIS PROGRAMMING

The psychological experience of an environmental challenge and its physiological effects on the body are mediated by signaling cascades in the central nervous system (Hypothalamic-Pituitary-Adrenal (HPA) axis) and sympathetic nervous system (Catecholaminergic system and Renin-Angiotensin-Aldosterone system) which receive modulating inputs from the amygdala, hippocampus, and prefrontal cortex. The initial reaction to stress is generated in the amygdala (Robinson, 1963; Hill et al., 2009). Efferent signals from the amygdala to the paraventricular nucleus (PVN) of the hypothalamus regulate the production of

corticotrophin releasing factor (CRF), which is then transported to the anterior pituitary gland through a vascular connection, stimulating the production of adrenocorticotropic hormone (ACTH). Released ACTH enters the blood stream and travels to the adrenal gland on top of the kidneys where it initiates an increase in the release of cortisol, norepinephrine, epinephrine, testosterone, and renin into the blood. Cortisol then provides a negative feedback loop to the stress response in binding to glucocorticoid receptors in the hippocampus, hypothalamus, and the pituitary gland, alongside other brain regions and body tissues (**Fig. 3**).
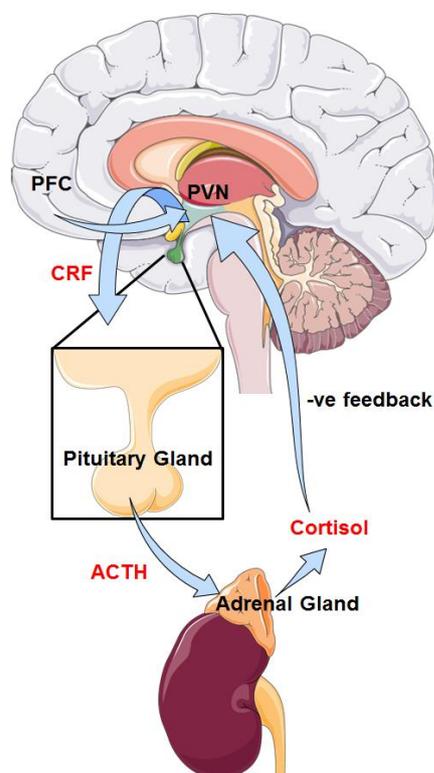
Figure 3. Hypothalamic Pituitary Adrenal axis. PFC = Prefrontal Cortex, PVN = Paraventricular Nucleus of the Hypothalamus, CRF = Corticotrophin Releasing Factor, ACTH = Adrenocorticotropic Hormone.

HPA axis function can be altered by stress-induced epigenetic molecular changes such as DNA methylation (DNAm), histone acetylation, and microRNAs, especially in cells of the amygdala, frontal cortex, and hippocampus as major regulatory regions. The modified epigenome then influences gene expression and

ultimately higher-level features such as stress sensitivity, emotion regulation, and the immune system. In this manner, prenatal stress can lead to long-term programming of the HPA axis.

Impact on stress sensitivity. Prenatal stress was found to both reduce baseline cortisol levels and simultaneously increase the cortisol response to stressors across the lifespan (Yehuda et al., 2005; Entringer et al., 2009; Alexander et al., 2012). Further, maternal trait anxiety was associated with a flattened diurnal cortisol profile with lower values in the morning and higher values in the evening in teenage offspring exposed in the first trimester but not later. This profile was associated with depressive symptoms in girls (van den Bergh et al., 2008). Finally, chronically heightened inflammation levels following prenatal adversity were found in adults up to 39-47 years of age (Slopen et al., 2015; Plant et al., 2016), suggesting that HPA axis programming effects carry over well into adulthood.

Overall, prenatal stress has been connected to dysregulation of the HPA axis, specifically in terms of lowered circulating cortisol levels and larger spikes in response to stressors, as well as chronically heightened inflammation levels.

Epigenetic modifications preceding imbalances in HPA axis homeostasis. Being a key element of the HPA axis, the glucocorticoid receptor gene (*NR3C1*) itself is the most commonly studied in targeted methylation studies. Maternal depression (Oberlander et al., 2008; Conradt et al., 2013; Conradt et al., 2016; Braithwaite et al., 2015), stress (Mulligan et al., 2012; Perroud et al., 2014), and anxiety (Hompes et al., 2013) were consistently associated with heightened methylation levels in the *NR3C1* exon 1F promoter region in offspring cord blood and neonatal blood draws.

Only one study examining stressful experiences in pregnancy found no significant differences in methylation status (Ostlund et al., 2016). Hypermethylation in *NR3C1* was associated with an increased cortisol stress response at three months of age (Oberlander et al., 2008), and lower birth weight (Mulligan et al., 2012). Increased methylation was also reported in *FKBP5* CpGs as a result of maternal stress (Monk et al., 2016). The *FKBP5* gene encodes for a co-chaperone of the GR that reduces the affinity of the glucocorticoid receptor complex for cortisol (Denny et al., 2000). Hypomethylation following prenatal stress on the other hand is reported for *SLC6A4* (Devlin et al., 2010) and *BDNF* (Braithwaite et al., 2015) gene promoters. Both genes are relevant to hippocampal neurogenesis and stress regulation (Alboni et al., 2017). However, a hypothesis-free meta-analysis using data from the Generation R study (n=912) and the Avon Longitudinal Study of Parents and Children (n=828) revealed no epigenome-wide associations of prenatal maternal stress exposure and neonatal cord blood DNA methylation (Rijlaarsdam et al., 2016).

1.1.2.7   ALTERED GENE TRANSCRIPTION AND SIGNALING PATHWAYS

Transcriptional responses to stress and downstream effects in human foetal brain tissue are thus far best characterized in human hippocampal progenitor cell line HPC03A/07 (ReNeuron Ltd., Surrey, UK). High concentrations of 100 µM cortisol were found to upregulate posteriorising patterning factor Homeobox C12 (*HOXC12*) and downregulate BMP And Activin Membrane Bound Inhibitor (*BAMBI*). Pathway enrichment analyses revealed that both TGFβ-SMAD2/3- and Hedgehog signaling were inhibited by cortisol. Interestingly, dual SMAD inhibition using SB431542 and Noggin, followed by optional Hedgehog inhibition with cyclopamine, is a common *in vitro* stem cell differentiation protocol favouring dorsal telencephalic

cell fate (Chambers et al., 2009; van den Ameele et al., 2014). In HPC03A/07 cells, cortisol-induced decreases in proliferation and neuronal differentiation were mimicked by GR agonist dexamethasone and blocked by GR antagonist RU486. In addition, astrogliogenesis was increased by low cortisol concentrations but not affected by high, GR-activating, cortisol concentrations (Anacker et al., 2013).

More experimental evidence on the transcriptome altering effects of prenatal stress comes from mouse studies. Hypothalamic neural progenitor stem cells dissected from mouse embryos on E14.5 and treated with 100 nM of dexamethasone showed differential expression of genes involved in the stress response such as Family With Sequence Similarity 107 Member A (*FAM107A*), TSC22 Domain Family Member 3 (*TSC22D3*), and FK506 binding protein 5 (*FKBP5*) and genes important in embryonic patterning such as Wingless-Type MMTV Integration Site Family, Member 3 (*WNT3*) and Zinc Finger And BTB Domain Containing 16 (*ZBTB16*; Frahm et al., 2016). Wnt signaling was also enhanced in frontal cortex on D21 postnatally following foetal exposure to maternal stress during E12-16 (Mychasiuk et al., 2011). Dexamethasone administration to pregnant mice during mid-to-late gestation confirmed reduced proliferation in neuronal progenitors reported in HPC03A/07 cells. Conversely, it also led to enhanced untimely neurogenesis and reduced complexity of neuronal processes in the prefrontal cortex and hippocampus, with all factors together resulting in lowered cortical thickness (Tsiarli et al., 2017). An increase in neurogenesis following the application of cortisol was further observed in zebrafish larvae (Best et al., 2017) suggesting evolutionary conservation. Prenatal betamethasone exposure on the other hand led to oxidative damage to fetal hippocampus in sheep (Miller et al., 2007) and decreased MAP2 expression in adult

male rats (Bruschettini et al., 2006), but equally reduced proliferation (Scheepens et al., 2003).

In sum, prenatal stress has been shown to affect signaling pathways important in proliferation, neurogenesis, and embryonic axis formation. While it is unclear how altered transcription of patterning genes would influence cells dissected from distinguishable regions such as the hippocampus or hypothalamus, it may conceivably disrupt the course of migrating neuronal cells traversing critical sites of signaling gradients. All factors together, reduced proliferation, increased differentiation, and altered expression of patterning genes may therefore contribute to changes in frontal and limbic brain architecture as observed by magnetic resonance imaging studies.

1.1.3 PRENATAL BRAIN DEVELOPMENT *IN VIVO* AND *IN VITRO*

1.1.3.1 *IN VIVO* NEUROGENESIS

Embryonic stem cells are derived from the inner cell mass (ICM) at the blastocyst stage of embryonic development (E3.5 – E4.5) and express pluripotent marker genes Octamer-binding transcription factor 4 (*OCT4*) which gives the first binary cell fate decision to form the ICM, and Nanog, which instructs cells to give rise to the pluripotent epiblast, the founder tissue of the embryo proper (Arnold et al., 2009). Further marker genes are Sex determining region Y-box 2 (*SOX2*), which is involved in the regulation of embryonic development and in the determination of ectodermal cell fate and Podocalyxin (*TRA1-60*), which is involved in the formation of the preapical plasma membrane subdomain to set up initial epithelial polarisation. Early embryonic asymmetry is induced on E5.5 when the proximal-

distal axis of the pre-gastrulation embryo is established by nodal signaling at the proximal epiblast. Nodal upregulates the production of bone morphogenetic protein 4 (BMP4), which in turn signals to enhance WNT3 expression at the posterior epiblast. Cells at the distal tip of the pre-gastrula embryo initiate the expression of nodal and Wnt signaling inhibitors Cerberus-like-1 (CER1) and left-right determination factor 1 (LEFTY1), which help establish the anterior-posterior axis (**Fig. 4**). Induced pluripotent stem cells are considered equal to embryonic stem cells in terms of marker expression and differentiation potential, although residual lineage-specific methylation marks may persist and prime induced pluripotent stem cells for differentiation towards their lineage of origin (Kim et al., 2010).
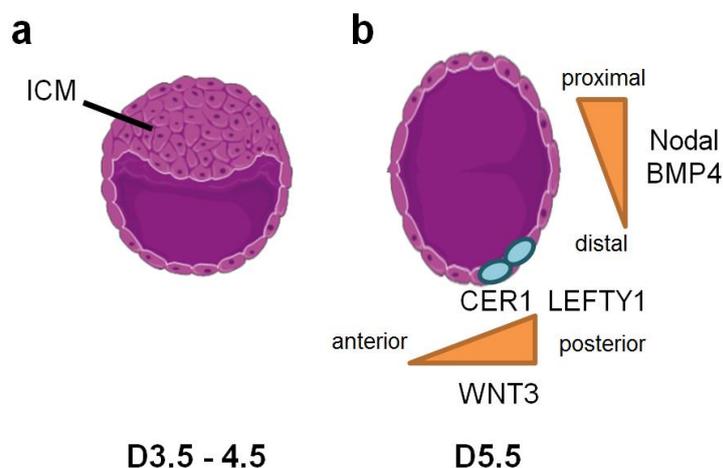
Figure 4. Establishment of early embryonic asymmetry in the epiblast. a) Embryonic stem cells are derived from the inner cell mass of the blastocyst on E3.5 - E4.5 of embryonic development. b) Early embryonic asymmetry is established on E5.5 with Nodal and then BMP4 signaling defining the proximal-distal axis and WNT3 initiating anterior-posterior patterning supported by CER1 and LEFTY1.

The onset of gastrulation is marked by the formation of the primitive streak and the primitive node on embryonic day 13 (**Fig. 5a**).
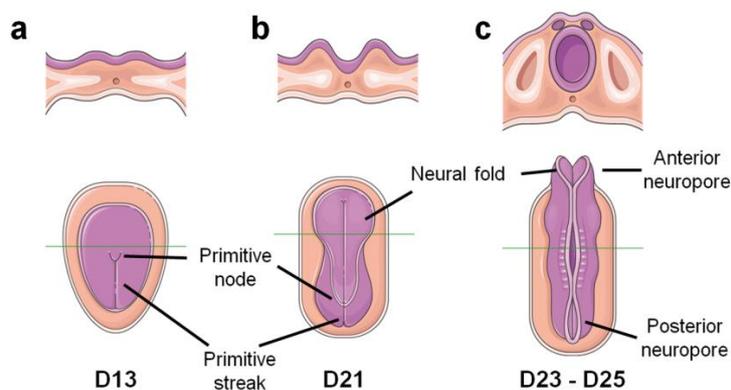
Figure 5. Development of the neural plate and neural tube. a) The primitive node and streak form on top of the epiblast on E13. Cells migrating towards the node and streak signal neural progenitor identity and positioning to the underlying epiblast layer, thus giving rise to the neural plate. b) The neural plate contains the neural progenitor cells. Around E21 it starts to fold inwards producing the neural fold. c) The developing neural tube begins to fuse in the middle and proceeds in both directions towards the anterior and posterior neuropores, which close last. A single layer of neural progenitor cells forming the ventricular zone now lines the inside of the neural tube.

Cells from the epiblast layer begin to migrate towards the primitive node and streak. As the cells pass the node, they receive molecular signals that induce gene expression instructing the first migrating cells to establish the most rostral regions of the newly forming endodermal and mesodermal layers, and later migrating cells to form progressively more caudal regions. Cells that migrate along the axial midline send molecular signals that differentiate cells of the overlying epiblast layer into neuroectodermal cells, giving rise to the neural plate. In addition, the primitive node

sends a second signal to all migrating cells instructing them to produce proteins specifying a regional identity for the neural progenitor cells of the neural plate with each successive wave (Stiles & Jernigan, 2010).

The neural tube forms between E20-27 of gestation. Neural tube development begins with the appearance of two ridges along the sides of the neural plate on E21 (**Fig. 5b**). Within several days, the ridges rise, fold inward and fuse to form a hollow tube enclosing the neural progenitor cells on the inside. Fusion begins in the centre of the developing neural tube and then proceeds in both the rostral and caudal direction. The anterior neuropore at the most rostral end of the neural tube and the posterior neuropore at the caudal end are the last segments to close. When the neural tube is complete, the neural progenitors form a single layer of cells that lines its centre (**Fig. 5c**). This layer is called the ventricular zone. Neural progenitor cells in its most rostral region will give rise to the brain forming around the three primary vesicles (prosencephalon, mesencephalon, rhombencephalon), while more caudally positioned cells will form the spinal column.

Neuron production begins around E42 with the onset of asymmetric cell division. Most neurons are produced in the ventricular zone and migrate radially from the centre of the brain out to the developing neocortex, first by somal translocation and once the cortex becomes larger guided by radial glia cells (Götz & Huttner, 2005).

1.1.3.2   *IN VITRO* NEUROGENESIS

Neural progenitor cells and neurons derived *in vitro* from human embryonic stem cells (hESC) and human induced pluripotent stem cells (hiPSC) show gene

transcription profiles that most closely correspond to those of embryonic and foetal brain up until weeks 16-19 post conception (Johnson et al., 2009; Brennand et al., 2014; Miller et al., 2014; Stein et al., 2014). More specifically, rosette neural stem cells on D14 of *in vitro* differentiation have been equalled to primary neural tissue at the neural plate stage representing the earliest neural stem cell stage *in vivo*. Cells at this stage respond well to spatial patterning cues, whereas the continuous loss of rosette structure demarcated by shrinking Zona-occludens-1 (*ZO1*)-positive lumen size with subsequent passages was accompanied by decreased differentiation potential (Elkabetz et al., 2008). An intact rosette structure was found to be essential for orderly neural development due to preventing premature neurogenesis and astrogliogenesis (Hříbková et al., 2018).

In addition, *in vitro* neuronal differentiation has been shown to recapitulate major *in vivo* neurogenic events such as sequential anterior-posterior patterning, with early neural progenitors (NPs) expressing anterior markers such as Forkhead box protein G1 (*FOXG1*), Paired box 6 (*PAX6*) and Orthodenticle Homeobox 2 (*OTX2*) and later NPs expressing more posterior markers such as POU Class 3 Homeobox 2 (*POU3F2*), and Fatty Acid Binding Protein 7 (*FABP7*), alongside the less specific marker Nestin (*NES*). Similarly, *in vitro* neuronal differentiation mimics the sequential generation of cortical layers, with early progenitors giving rise to deeper layer neurons and later progenitors giving rise to neurons of more superficial layers, as well as the switch from neurogenic to gliogenic cell fate (Edri et al., 2015; Ziller et al., 2015).

These transitions are accompanied by epigenetic events such as histone modifications and DNA methylation (DNAm) which sequentially reduce the variety

of cell types a stem cell can generate with each consecutive stage of development. Embryonic stem cells are derived from blastocysts following a global demethylation event and show little DNA methylation at Cytosine-phosphate-Guanine (CpG)-rich islands. Such hypomethylation at CpG islands associated with major developmental genes provides for a poised state in embryonic stem cells, which allows them to differentiate into any germ layer and cell type depending on signaling cues. Only few CpG island promoters are hypermethylated at this stage. Of those that are, many control germline-specific genes, just like CpG-poor promoters, that are mostly methylated at this stage as well (Mohn et al., 2008; Hirabayashi & Gotoh, 2010, Tsankov et al., 2015). Transition from a pluripotent state to the ectoderm lineage is characterised by predominant loss of DNAm, whereas terminal neuronal differentiation is characterised by predominant gain (Gifford et al., 2013).

1.1.3.3   THE GLUCOCORTICOID RECEPTOR IN EMBRYOGENESIS

The glucocorticoid receptor gene *NR3C1* plays an important role in early neurogenesis, acting as stage-specific transcription factor to co-modulate neural progenitor identity and differentiation potential (Ziller et al., 2015). Indeed, the glucocorticoid receptor was found to regulate gene transcripts functionally implicated in neurogenesis and eye development, as well as skeletal and cardiac muscle formation (Nesan & Vijayan, 2013). Knockdown of *NR3C1* translation resulted in apoptosis and subsequent craniofacial and caudal deformities with severe malformations of neural, vascular, and visceral organs in zebrafish embryos (Pikulkaew et al., 2011). Similarly, knockdown of the glucocorticoid receptor caused massive reductions in bone morphogenetic protein, which is a key regulator of axis formation in the developing neural tube (Nesan et al., 2012). Further, crosstalk with

morphogens is reported between nuclear hormone receptors and the Wnt signaling pathway in differentiating stem cells (Beildeck et al., 2010). Most importantly however, an ascending rostro-caudal GR reporter gradient reminiscent of morphogen signaling gradients was detected in zebrafish embryos (Benato et al., 2014), supporting an independent role of the GR in embryogenesis. Thus, despite the relative sparsity of circulating cortisol during embryonic and foetal development, the glucocorticoid receptor may exert an important role in the formation of the nervous system.

1.2   TECHNICAL BACKGROUND

1.2.1   HIPSC AND HESC AS MODEL SYSTEM

Induced pluripotent stem cells and embryonic stem cells complement prospective longitudinal studies in humans in allowing for the assessment of gene x environment interactions in a laboratory experimental setting free of retrospective confounders. They provide access to live human neuronal cells of different types and developmental time points and enable the manipulation of putative molecular mechanisms underlying phenotypic changes, setting them apart from *post mortem* studies. While the method precludes direct inferences from experimental manipulation to behaviour as in animal studies, it allows for 'quasi-prospective' predictions of donor phenotype and helps to overcome issues of species-specific differences, such as in the amount and type of intermediate zones during cortex formation (Fietz et al., 2012) or human-gained enhancers (de la Torre-Ubieta et al., 2018). Overall comparability of *in vitro* hiPSC-derived neuronal cells to *in vivo* development is discussed in section 1.1.3.2.

However, the stem cell and differentiation field is not devoid of its own limitations and challenges. First, iPSCs have been found to retain an "epigenetic memory" resulting in an intrinsic bias to differentiate towards cell types related to the original donor cell (Kim et al., 2010). Therefore, some iPSC lines may be biased against neuronal differentiation as the lineage of interest. Second, even lines with good inducibility of neural cell fate generate other cell types during the process of directed differentiation and require measures of purification such as neural rosette selection, magnetic beads, or Fluorescence-Activated Cell Sorting (FACS). Third, the transcriptional profile of neuronally differentiating cells is subject to an intrinsic cell fate specification program determining anterior-posterior patterning and the neurogenic-to-gliogenic switch in neural progenitor cells as a function of time in culture (Edri et al., 2015; Ziller et al., 2015). To date, there is no method known to influence this property of stem cells undergoing directed neuronal differentiation. The isolation of progenitor cells with an anterior profile proved inefficient as time in culture remained the determining factor of cell fate (Elkabetz et al., 2008).

These challenges need to be addressed by the choice of differentiation protocol and the experimental design.

1.2.2   ILLUMINA METHYLATIONEPIC BEADCHIP DESIGN

The Illumina MethylationEPIC Bead Chip provides a comprehensive genome-wide coverage of over 850 000 potential methylation sites, including CpG islands, CpG sites outside of CpG islands and non-CpG methylated sites identified in human stem cells, FANTOM5 enhancers, ENCODE open chromatin and transcription factor binding sites and miRNA promoter regions. Every MethylationEPIC BeadChip has

eight slots, respectively, meaning eight samples can be analysed per chip in parallel. Individual slots within a chip equal the array or sentrix position (**Fig. 6**).

Figure 6. Illumina MethylationEPIC BeadChip setup. Left: One chip with 8 array slots. Right: Hybridization chamber in which samples are hybridized to EPIC BeadChips. Modified from http://emea.support.illumina.com/infinium-hd-methylation-guide-15019519-01.pdf.

Following bisulfite conversion, each sample is hybridized to a single array slot on the chip, which contains red and green colour channels (**Figure 7**). The EPIC BeadChip array design includes both Infinium I and Infinium II type beads. With the Infinium I design every CpG is assessed by a methylated and an unmethylated bead type, whereas the Infinium II design involves only one bead type. Both give an average measurement of methylation. Methylated probes are coded by the green signal, while unmethylated probes are coded by the red signal.
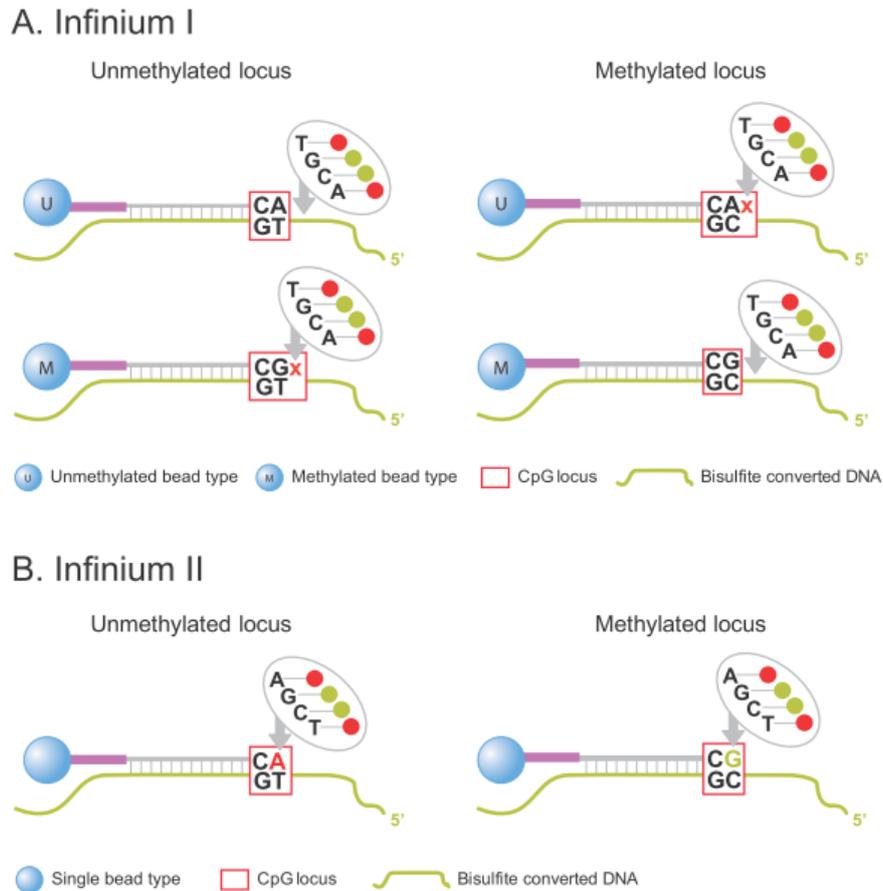
Figure 7. Illumina MethylationEPIC BeadChip design. The Infinium MethylationEPIC BeadChip kit employs both Infinium I and Infinium II assays. Infinium I assay design employs two bead types per CpG locus, one each for the methylated and unmethylated states. The Infinium II design uses one bead type, with the methylated state determined at the single base extension step after hybridization. Figure from Illumina's Infinium MethylationEPIC BeadChip data sheet (http://emea.support.illumina.com/infinium-methylation-epic-ds-1070-2015-008.pdf).

Methylation levels are then reported as beta values

$$\beta = \frac{M}{M + U + a}$$

with M and U denoting the methylated and unmethylated signal intensity, respectively, and α denoting a constant regulating the β-value when both M and U are small. By default, α is set to 100. The resulting β-value for a probe can range between 0 and 1, or 0% and 100%, with 0% meaning that all copies of the CpG site were unmethylated in a sample, and 100% meaning that every copy was methylated.

Advantages of the methylation array approach include its cost-efficiency, reliability and requirement of comparatively low input quantities. Disadvantages on the other hand are a limited coverage of the genome and the focus on promoters as opposed to other features of DNA, such as enhancers, for example. Such disadvantages are better overcome by Whole-Genome Bisulfite-Sequencing (WGBS), which allows for a truly genome-wide assessment of the DNA methylation landscape. While generally cost-prohibitive for large-scale studies, a systematic analysis of requirements on the experimental design found that a 10x sequencing depth and at least two replicates per group would be enough to detect differentially methylated regions between different tissues (Ziller et al., 2015).

1.2.3   TRANSCRIPTOME ANALYSIS BY 3' RNA-SEQ

The development of novel high-throughput DNA sequencing methods has also resulted in a new method for both mapping and quantifying transcriptomes. In contrast to microarray-based methods, these new approaches determine the cDNA

sequence without a priori knowledge of the sequence order. The overarching principle is that total or fractionated RNA is converted to a library of cDNA fragments with adaptors attached to one or both ends. Every fragment is then sequenced in a high-throughput manner to obtain short sequences from one end (single-end sequencing) or both ends (paired-end sequencing). Apart from the possibility to capture previously unknown sequences, advantages of mRNA-Seq include a low or non-existent background signal and a large dynamic range of expression levels, among others (Wang et al., 2009). The most common RNA-Seq application is probably the sequencing of polyadenylated RNA, where total cellular RNA is enriched for poly(A)-tail RNA by magnetic beads. When sample quality does not allow for poly(A) selection, it is also possible to perform a depletion for ribosomal RNA, which is the most common type of RNA but not of interest in most studies. One limitation of the paired-end RNA-seq method is that long transcripts are represented by more reads than shorter transcripts, resulting in a biased estimation of expression levels. The 3′ RNA-seq method, which yields only one sequence per transcript, bypasses this limitation and does not need to be adjusted for sequence length (Tandonnet & Teixera-Torres, 2017). However, it can have higher variability than methods capturing a transcript by multiple fragments. That is, biases from fragmentation, adapter ligation and PCR can make tag-based data more prone to batch effects (Hrdlickova et al., 2017).

Regarding statistical analysis for identifying differentially expressed genes from RNA-Seq data, there is no consensus about the most appropriate pipeline or protocol to date (Costa-Silva et al., 2017) and no single approach is expected to perform optimally for all datasets. A comparison of differential gene expression

tools on 48 biological replicates per condition identified five tools to give results consistent with other tools and pass examination for false positive rates (Schurch et al., 2016): DESeq (Anders & Huber, 2010), DESeq2 (Love et al., 2014), EBSeq (Leng et al., 2013), edgeR (exact) (Robinson et al., 2010), and limma (Law et al., 2014). These tools showed good performance for fold change thresholds above 0.5 in at least six biological replicates. However, limma assumes a log-normal distribution, while RNA-Seq data follow the negative binomial distribution, which underlies the remaining approaches. Both DESeq and DESeq2 rely on shrinkage variance for the estimation of differentially expressed genes, which impacts on suitability for replicates with differing baselines. The remaining tools edgeR and EBSeq on the other hand employ the empirical bayes method, which has long been well established in the analysis of microarray data (Smyth, 2004). Lastly, normalization is performed by Trimmed Mean of M-values (TMM) in edgeR and by median normalization (Anders & Huber, 2010) in EBSeq. The median normalization method finds the ratio of each read count to the geometric mean of all read counts for a gene across all samples and uses the median of these ratios for one sample to scale it. The TMM approach on the other hand chooses one sample as reference to calculate fold changes and absolute expression levels relative to that sample, trim genes by these two values to remove differentially expressed genes and find the trimmed mean of the fold changes for each sample (Evans et al., 2017). Hence, the median normalization approach was assumed to perform better for data sets with high variance between replicates due to relying on a mean rather than one sample as reference. However, both normalization methods have been criticized for being based on the *a priori* assumption that all or most genes are not differentially expressed (Roca et al., 2017). Against the backdrop of these considerations, the

EBSeq package was expected to perform best for the data set at hand. Indeed, it has been successfully employed in developmental studies and especially studies with biological replicates differentiated from stem cells or induced pluripotent stem cells, which share the challenge of relative variability from one differentiation batch to the other (Schwartz et al., 2015; Mo et al., 2015; Tran et al., 2015; Zanotelli et al., 2016; Tomov et al., 2016; Yoon et al., 2017; Jones et al., 2018; Uenishi et al., 2018).

1.3 CONFOUNDERS IN HIGH-THROUGHPUT EXPERIMENTS

Statistical models assume that measured values are affected by noise produced by batch effects such as technical variation, sex, age and other factors which may introduce systematic biases. Random noise is generally captured by the error term in a given statistical model and simply decreases the power to detect significant differences. Batch effects confounded with a variable of interest however are more problematic since they may produce statistically significant results in the absence of real biological effects or obscure real biological effects by producing diametrically opposed systematic bias. Confounders can be addressed at multiple levels by experimental design and by statistical solutions. At the level of study design, systematic biases can be controlled by randomization and parallelization with respect to variables of interest. However, even in well-designed studies, it may be useful to adjust for batches (Leek et al., 2010). Statistical solutions can involve batch correction (Johnson & Rabinovic, 2007; Leek & Storey, 2007) or inclusion of the confounding factor as covariate in the model. Controlling confounding variables by either one or a combination of these approaches is then expected to give a better approximation of the true values and consequentially of true differences between study groups.

1.4 AIM AND SCOPE OF STUDY

The current study aimed to assess the effects of excessive glucocorticoids on the earliest cell types of the developing nervous system. It meant to provide an unbiased assessment of the potential effects of prenatal stress on the epigenome in the germinal zone of the developing telencephalon using embryonic stem cells and neuronal derivatives as model system. The goal was to differentiate embryonic stem cells and induced pluripotent stem cells into highly distinctive populations of neuronal progenitors and neurons in order to 1) characterise glucocorticoid receptor expression and translocation to the nucleus upon stimulation across neuronal development and 2) to assess epigenomic changes by identifying altered DNA methylation and differential gene expression following the application of a stress stimulus. Notably, adult neurogenesis and newly produced neurons may exhibit fundamentally different properties from those observed in embryonic development and therefore fall beyond the scope of this study.

2.   PILOT STUDIES

Preliminary studies were conducted to 1) establish an assay to capture the extent to which stress receptors are expressed and functional in human embryonic and induced pluripotent stem cells as well as their neuronal derivatives, 2) establish a protocol for directed neuronal differentiation yielding reliable neural rosette formation and purification of emerging neural cell populations, and 3) identify the appropriate time in culture for differentiating neuronal cells to approximate a telencephalic profile and account for their inherent cell fate program, which cannot be influenced by external factors to date.

2.1   ESTABLISHMENT OF GR EXPRESSION AND TRANSLOCATION ASSAY

2.1.1 BACKGROUND

Although the stress system and the glucocorticoid receptor as its key player are the subjects of a great research field, little data was available on GR expression and functionality in human embryonic cells at the start of this study. Indeed, data from newly born mice even suggested that developing neurons may not express GR at all during certain stages of neurogenesis (García et al., 2004). In contrast, an early study using human iPSC-derived neural progenitor cells did detect low GR expression in both hiPSC and neural cell derivatives, and dexamethasone-induced effects on proliferation starting at a concentration of 500 nM (Ninomiya et al., 2014). However, neural progenitor cells and neurons were not well-characterised in this study, which is important given their dynamic fate specification in culture. In addition, GR stainings in embryonic mouse brain indicated a shift in subcellular

receptor localisation with outward migration of neural progenitors originating from the ventricular zone (Tsiarli et al., 2013). Due to the overall paucity of data in human embryonic cells, the first pilot aimed to establish an assay to capture the expression, subcellular localisation, and translocation dynamics of GR in hiPSC and neuronally differentiating cells as a model system for human embryonic neurogenesis.

2.1.2 METHODS

Comparison of Glucocorticoid Receptor Antibodies. Glucocorticoid receptor antibodies sc-8992 (H300) (Santa Cruz) binding to amino acids 121-420 within an internal region of GR α of human origin and sc-1002 (P-20) (Santa Cruz) binding to the C-Terminus of GR α were tested for performance in low-GR expressing human neuroblastoma cell line BE-M17 (ATCC CRL-2267) and high-GR expressing human foetal cortex progenitor cell line ReN-CX (ReNeuron Ltd., Surrey, UK). Prior to staining, BE-M17 neuroblastoma were transfected using 1μg of FLAG-tagged GR DNA plasmid on a 24-well plate and the TurboFect Transfection reagent (Thermo Fisher Scientific, Waltham, Massachusetts, USA) according to manufacturer instructions and fixed for analysis 24h after transfection. Immunofluorescence experiments were conducted as described in section 3.7.

Establishment of GR Translocation Assay. The GR translocation assay was established in BE-M17 neuroblastoma cells which showed predominantly cytoplasmic GR localisation under unstimulated culture conditions. BE-M17 cells were cultured in DMEM-F12 with 10% foetal bovine serum, which was switched to stripped serum one day prior to the stimulation experiment. Cells were then stimulated with 1μM dexamethasone for 1h, 2h, and 4h, using EtOH as vehicle control condition and fixed for immunocytochemistry.

2.1.3 RESULTS

Comparison of Glucocorticoid Receptor Antibodies. **Figure 8** shows BE-M17 cells overexpressing GR in successfully transfected cells. Both the sc-1002 P-20 and sc-8992 H300 antibodies against GR correctly identified GR expression as evidenced by control staining for FLAG-tagged GR plasmid.
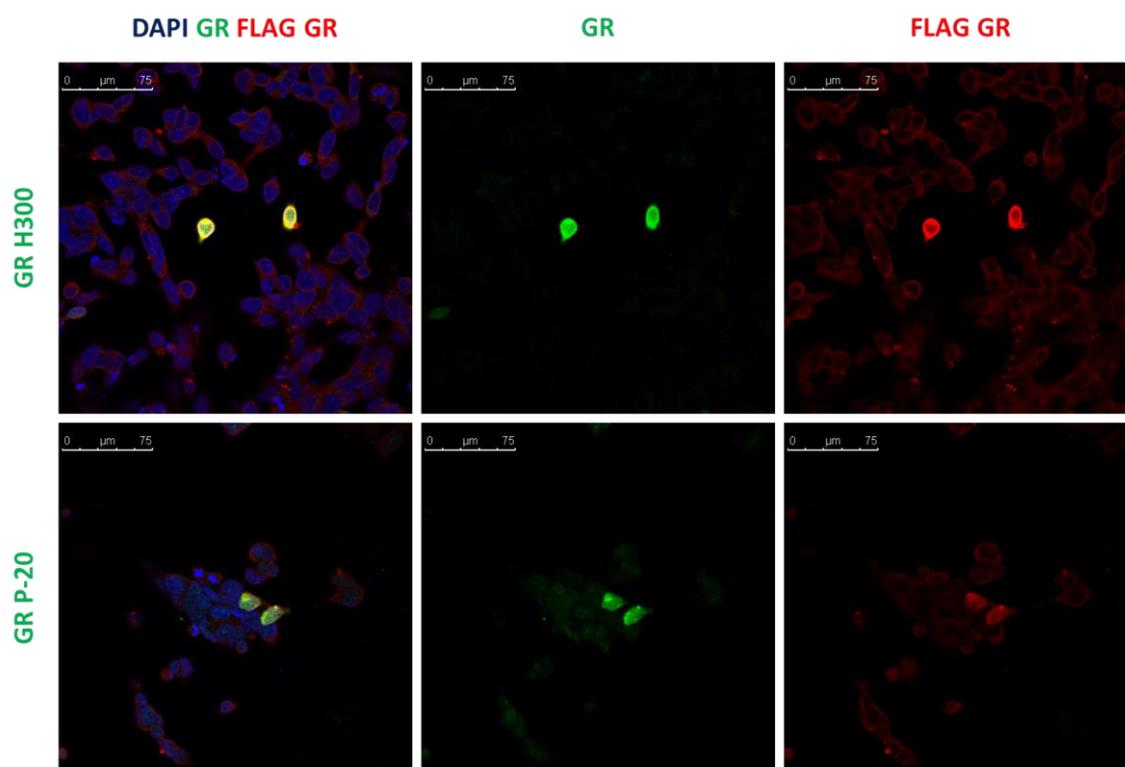
Figure 8. Comparison of P-20 and H300 antibodies against GR in BE-M17 Neuroblastoma cell line transfected with GR DNA plasmid.

Further, both antibodies were tested in untransfected BE-M17 human neuroblastoma (**Fig. 9**) and ReN-CX human foetal cortex cells (**Fig. 10**). Here, the sc-8992 H300 outperformed the sc-1002 P-20 antibody in that it correctly identified the cytoplasmic expression of GR in BE-M17 (compare FLAG GR in **Fig. 8**). In ReN-CX human foetal cortex cells, the H300 showed both nuclear and cytoplasmic GR

staining, whereas P-20 provided a pattern of nuclear GR clusters. Overall, the H300 was considered more reliable in terms of correctly identifying subcellular GR localisation.
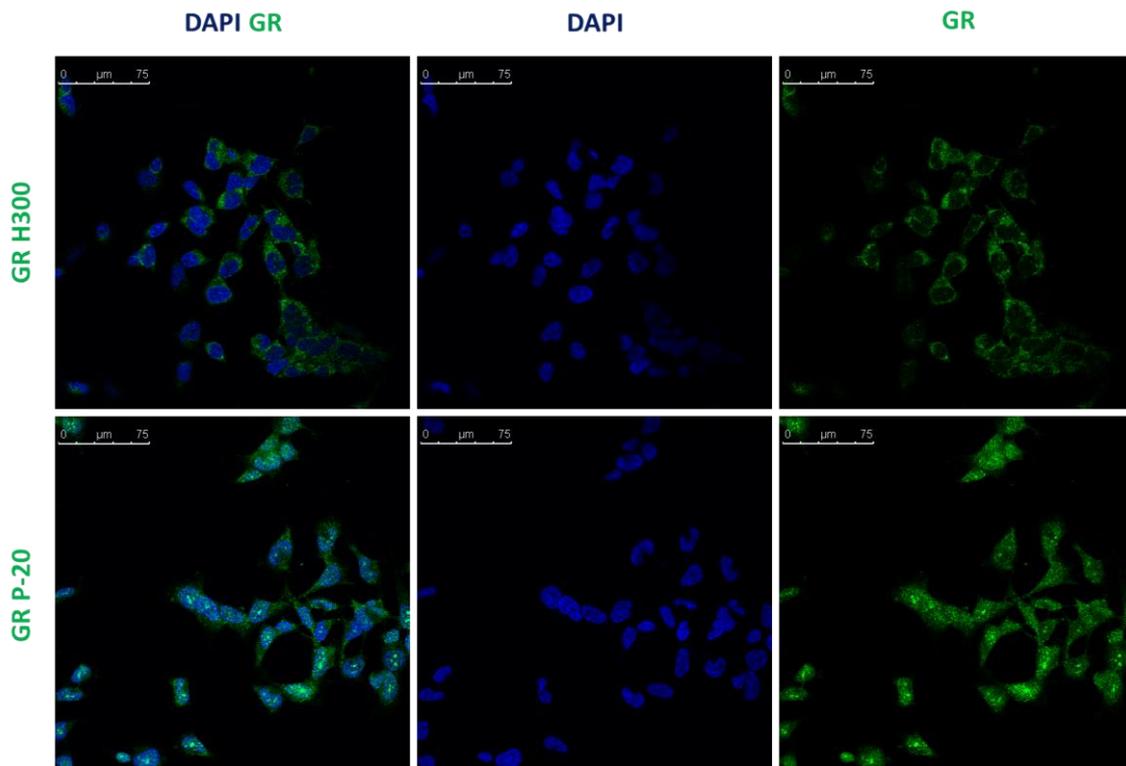
Figure 9. Comparison of P-20 and H300 antibodies against GR in unstimulated BE-M17 Neuroblastoma cells.
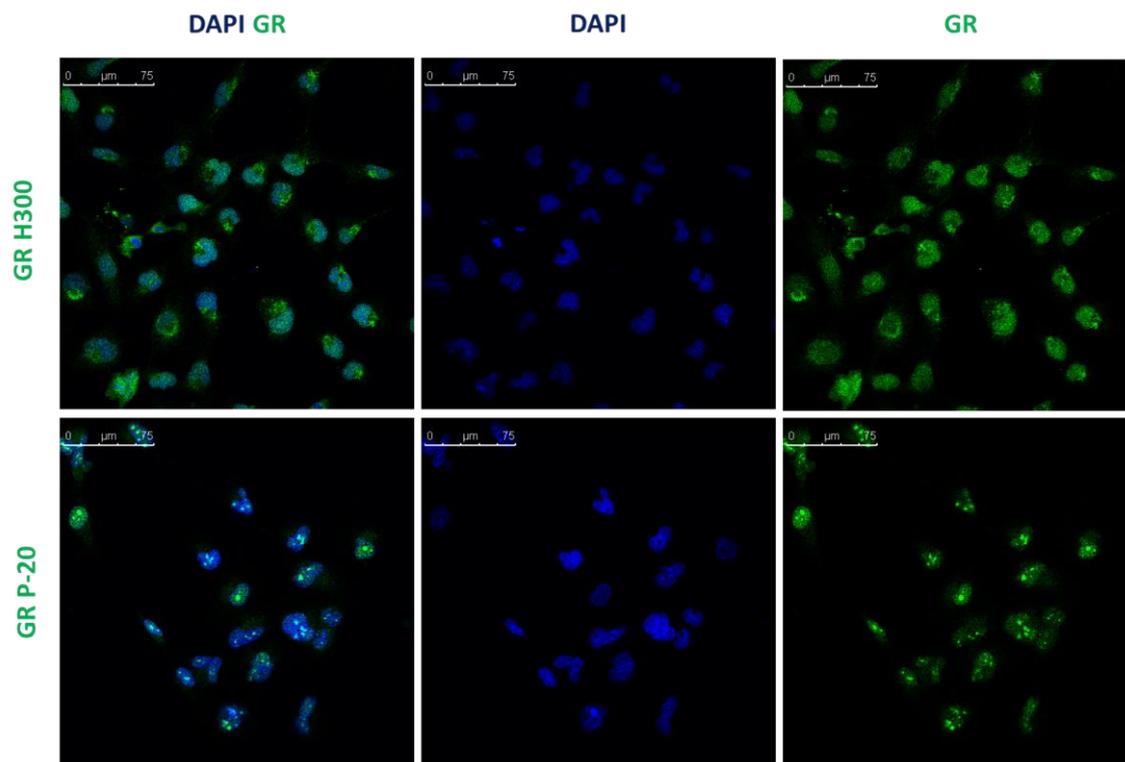
Figure 10. Comparison of P-20 and H300 antibodies against GR in unstimulated ReN-CX foetal cortex cells.

Establishment of GR Translocation Assay. Subsequent experiments were conducted using the sc-8992 H300 GR antibody. **Figure 11** shows a representative result for stimulation of BE-M17 cells with 1μM dexamethasone for 4h. In this figure, the unstimulated condition seems to show more clumping, which however was not representative of all experiments. Cell distributions may vary and are not representative. In the unstimulated vehicle condition, both nuclear and cytoplasmic fractions of the cells were positive for GR, the signal being stronger in the cytoplasm. In the DEX stimulation condition on the other hand, GR signal was predominantly nuclear. Thus, sensitivity of the antibody was considered high enough to distinguish between unliganded GR in the cytoplasm and compound-bound GR in the nucleus.
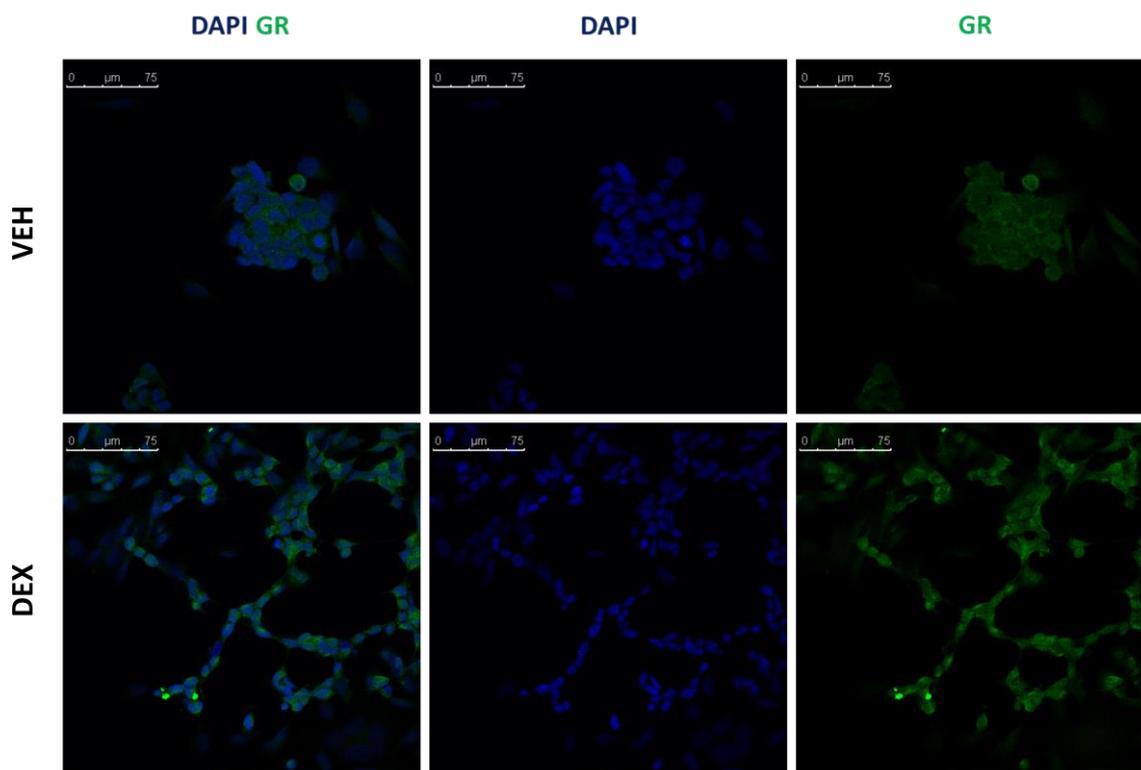
Figure 11. GR translocation experiment in BE-M17 neuroblastoma cells. VEH = Vehicle (EtOH), DEX = Dexamethasone.

2.1.4 DISCUSSION

The evaluation of GR antibodies in human foetal cell lines enabled the identification of an antibody with good sensitivity for both cytoplasmic and nuclear GR expression. It was also confirmed that the process of GR translocation to the nucleus following ligand binding could be traced by immunocytochemistry. These studies were especially important to disambiguate the patterns of GR expression found in hiPS cells and their neuronal derivatives.

2.2   ESTABLISHMENT OF DIFFERENTIATION PROTOCOL

2.2.1 BACKGROUND

The choice of a differentiation protocol can influence the reliability of neural induction, quality of generated cell populations, and thereby overall reproducibility and external validity of obtained results. In addition, an experimental design would have to account for the limited window of opportunity to study a cell type of interest (Elkabetz et al., 2008). In preparation for this study, two differentiation protocols and variations of individual aspects were chosen to test for efficiency and reliability of neural induction as evidenced by the formation of neural rosettes. The tested approaches included two embryoid body-based protocols, which were modifications of the original publication by Chambers et al. (2009). The first protocol relies on neural induction by SMAD inhibition and will be referred to as SMADi protocol (Topol et al., 2015) and the second employs a micropatterning system to improve neuronally enriched embryoid body formation and will be referred to as Aggrewell protocol (STEMdiff Neural System Version 2.1.0; STEMCell Technologies, Vancouver, Canada).

2.2.2 METHODS

Performance of differentiation protocols was evaluated in a total of n=4 blood-derived and n=1 fibroblast-derived hiPSC lines. The original protocols are described in detail in Topol et al. (2015), and the technical manual of the STEMdiff Neural System Version 2.1.0 (STEMCell Technologies). In short, the SMADi protocol relies on dual SMAD inhibition using small molecules LDN193189 and SB431542

and the formation of embryoid bodies from single cell iPS cells in suspension. A schematic of the differentiation process is presented in **Figure 12**.
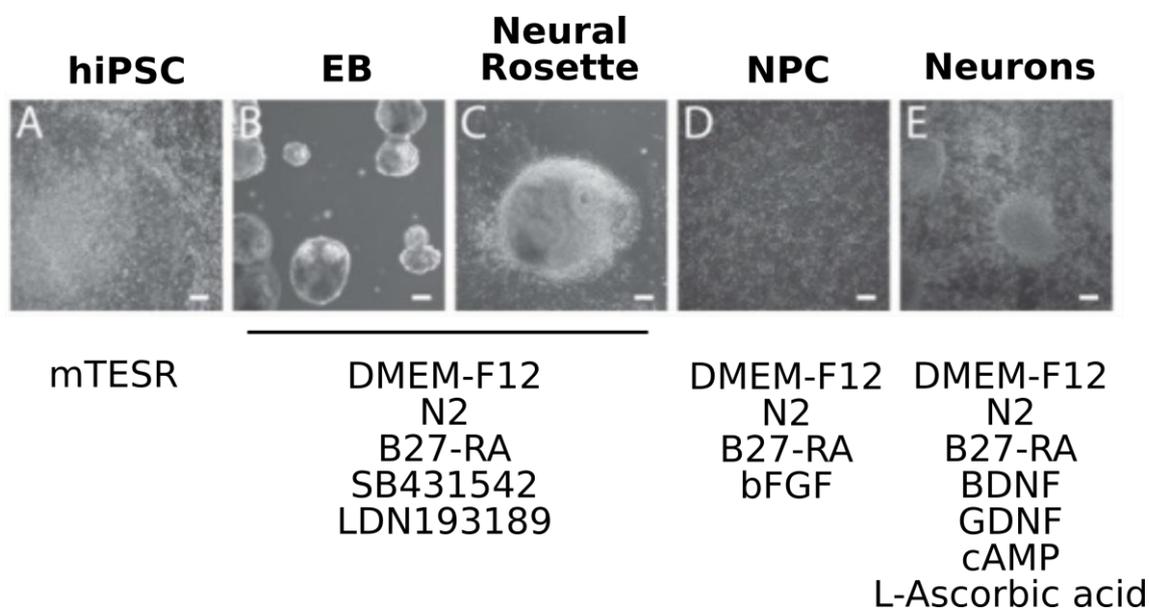
Figure 12. Schematic representation of the SMADi differentiation protocol. Brightfield images of hiPSC neural differentiation, from hiPSCs (A), to embryoid bodies (B), neural rosettes (C), NPCs (D) and neurons (E), with differentiation media components indicated below. Figure adapted from Topol et al., 2015, scale bar 100μm.

The Aggrewell protocol employs Aggrewell 800 plates to standardise embryoid body formation using a predetermined number of hiPSC starting material on a surface area of 800 μm. Earlier works on micropatterning embryoid bodies had established 800 μm as the appropriate starting size to achieve an optimal ratio of PAX6+ (ectoderm) to GATA6+ (endoderm) cells (Bauwens et al., 2009). The Aggrewell protocol further used an optimised medium composition tested for successful neural rosette induction in a large panel of different hiPS cell lines, called

Neural Induction Medium. The original Aggrewell protocol for neural differentiation by embryoid body formation is depicted in **Figure 13**.
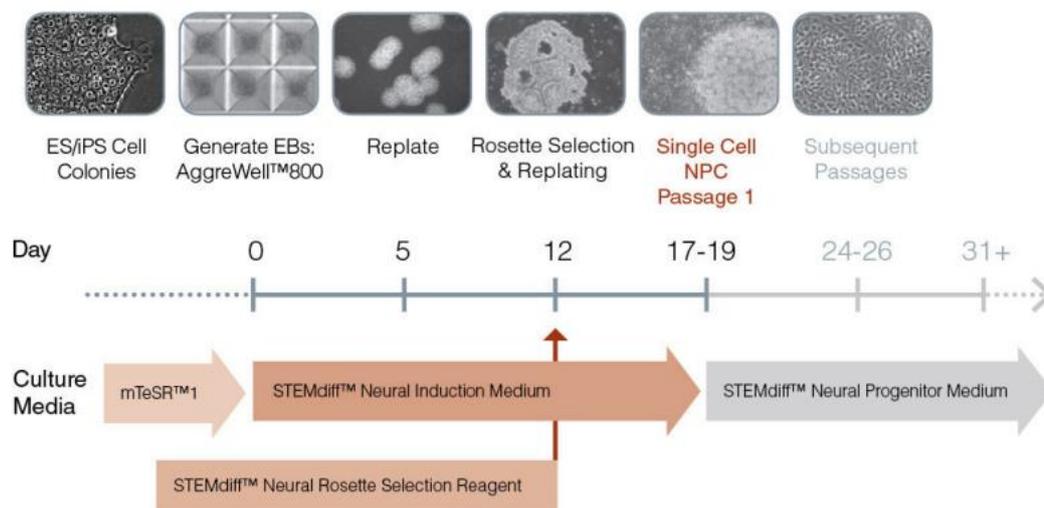
Figure 13. Schematic representation of the Aggrewell differentiation protocol. Brightfield images of hiPSC neural differentiation, from hiPSCs, to embryoid bodies, plated embryoid bodies, rosette selection & replating, and NPCs, respectively NPCs with subsequent passages. Figure from Technical Manual of the STEMdiff Neural System Version 2.1.0.

In addition, following variations of the protocols were tested, respectively adjusted: 1) growth of hiPSC in E8 versus mTESR medium prior to neural induction, 2) influence of medium formulation and embryoid body formation method on the efficiency of neural rosette induction, 3) neural rosette selection by Neural Rosette Selection Reagent versus manual microdissection, and 4) choice of medium for terminal neuronal differentiation. Efficiency of neural induction was then assessed by visual inspection of neural rosette morphology.

Initially, terminal neuronal differentiation of neuronal progenitor cells was induced using a DMEM-F12-based medium supplemented with pro-neural factors

as described in Topol et al. (2015). However, it was found that this type of basal media impaired synaptic communication between differentiating neurons (Bardy et al., 2015), thus diminishing the quality of the neuronal culture as well as the external validity of obtained results. Terminal neuronal differentiation was subsequently performed in BrainPhys medium (STEMCell Technologies), developed by Bardy et al. (2015).

Ultimately, the protocol used for directed neuronal differentiation in this study underwent multiple modifications and is described in detail in section 3.3.

2.2.3 RESULTS

While both the SMADi and Aggrewell approach eventuated in neural induction, the SMADi protocol resulted in immediate outgrowth of neurites from the plated embryoid body with individual neural rosettes being difficult to discriminate (**Fig. 14**).

Figure 14. Differently sized plated embryoid bodies generated by SMADi neural induction protocol. Plated embryoid bodies derived from MPI3 hiPSC vary largely in size and exhibit neurite outgrowth and premature differentiation to neurons.

Specifically, differently sized embryoid bodies caused heterogeneity with respect to the differentiation stage of generated neural progenitor cells, as reported previously (Ma et al., 2008). This outgrowth pattern complicated the subsequent selection of neural rosettes and resulted in heterogeneous neural progenitor populations. However, the disadvantage may have been caused by the random formation of embryoid bodies in suspension culture, rather than the SMAD inhibition approach per se.

In order to discriminate between the effects of media formulation and the method of embryoid body formation on differentiation outcomes, the SMADi protocol was modified for more homogeneous embryoid body formation using the Aggrewell 800. Differentiation experiments were performed varying the medium used to induce neural cell fate (SMAD inhibition by small molecules versus Neural Induction Medium) and the mode of embryoid body formation (in Aggrewells for one day followed by six days in suspension culture versus formation and culture in Aggrewells for five days followed by plating of embryoid bodies on day five). On day twelve of differentiation, plated embryoid bodies were then subjected to neural rosette selection reagent and replated. Representative results are shown in **Figure 15**. Although formation of embryoid bodies in Aggrewell plates resulted in overall improved homogeneity, plated aggregates cultured in SMADi medium nevertheless showed lower efficiency in generating neural progenitor cells compared to those cultured in Neural Induction Medium.
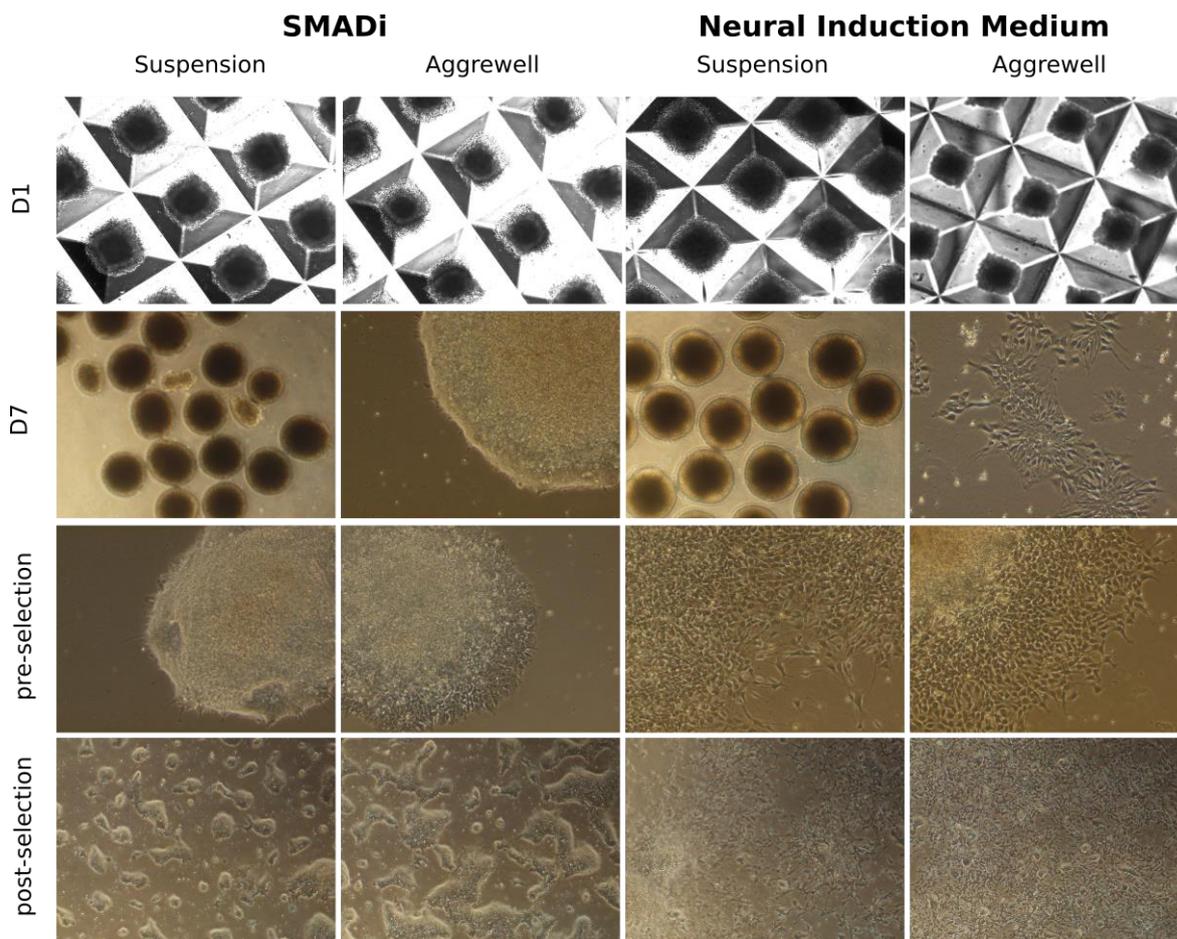
Figure 15. Comparison of protocols and embryoid body formation. Neural induction by SMAD inhibition compared to Neural Induction Medium in MPI4 hiPSC.

However, the efficiency of neural rosette induction was also highly dependent on hiPSC line, with the HMGU1 line derived from fibroblasts (ectodermal lineage) outperforming MPI lines derived from blood (endodermal lineage) (**Figure 16**).
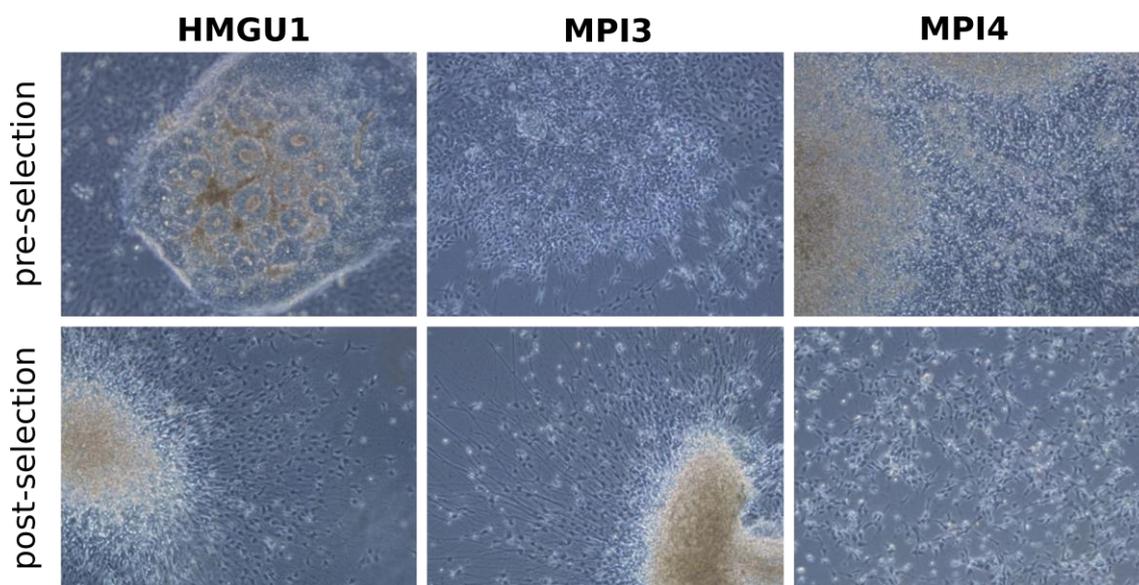
Figure 16. Comparison of neural rosette formation in hiPSC lines. The upper panel shows neural rosettes generated using the Aggrewell protocol on D12. The lower panel depicts replated rosettes selected with Neural Rosette Selection Reagent (STEMCell).

In hiPS cell lines with favourable properties for differentiation to the neural lineage, the Aggrewell protocol resulted in plated embryoid bodies forming distinctive neural rosette colonies surrounded by non-target cell types on the outer margins. While initial plating showed little premature outgrowth of neurites and terminal neuronal differentiation, rosette selection by Neural Rosette Selection Reagent (STEMCell, Vancouver, Canada) amounted to neurite outgrowth patterns similar to those observed with the SMADi protocol. In addition, selectivity of the reagent proved inefficient as non-target cells were often removed alongside neural rosettes. The protocol was therefore adapted, and neural rosettes subsequently selected by manual microdissection under the microscope using a syringe needle. Representative outcomes using selection reagent versus microdissection are shown in **Figure 17**.
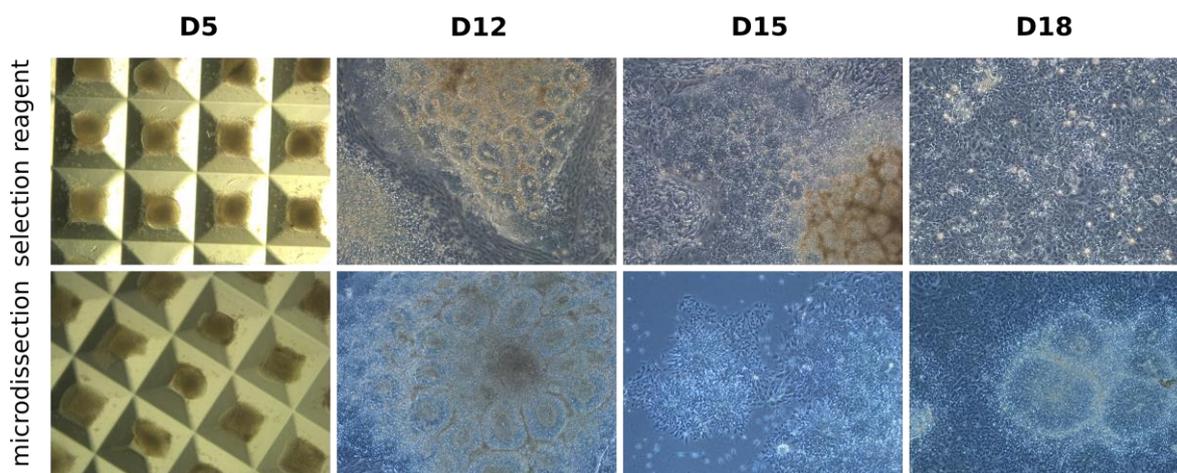
Figure 17. Neural rosette selection by Neural Rosette Selection Reagent compared to manual microdissection. Differentiation of fibroblast-derived HMGU1 hiPS cell line.

Neural progenitor cultures on D15 and D18 following rosette selection on D12 were more homogeneous with less contamination by non-target cell types when obtained by microdissection. Upon repeated replating, some neural rosettes however continued to generate non-target cell types on their outer margins. These were removed by light scraping with a plastic tip. When contaminating cell types prevailed after rosette colonies were dissociated to single cells, additional purification was obtained by positive magnetic bead selection using beads labelled with pan-neuronal progenitor marker PSA-NCAM (Miltenyi).

A comparison between neural induction starting from E8 medium or mTESR medium revealed more pronounced neural rosette formation from hiPS cells previously cultured in mTESR (**Figure 18**).
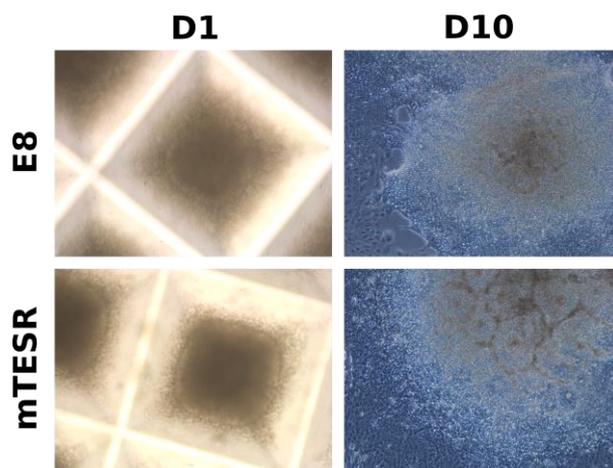
Figure 18. Comparison of neural rosette formation starting from E8 or mTESR hiPSC medium. Differentiation of blood-derived MPI2 line.

2.2.4 DISCUSSION

Neuronal differentiation was first successfully initiated using a SMAD inhibition protocol (Brennand et al., 2011; Topol et al., 2015). Neural rosette formation and purification of neural progenitor populations were then subsequently optimised by standardising embryoid body formation, testing different media for neural induction, adjusting the process of neural rosette selection and purification, and adapting the medium used for terminal neuronal differentiation. The adjustments eventually resulted in highly pure neural progenitor and neuronal cultures displaying homogeneous morphologies. A disadvantage of the approach remained the high amount of required hands-on time.

2.3   ESTABLISHMENT OF DEXAMETHASONE EXPERIMENTS

2.3.1 BACKGROUND

A pilot microarray study was conducted to test for overall DEX-reactivity of hiPSC and neuronal derivatives on the transcriptome level. Because neuronal progenitor populations were not initially anticipated to undergo an intrinsic fate-specification program as has since been described (Edri et al., 2015; Ziller et al., 2015), neural progenitors were classified by passage but not day at the time point of data collection.

2.3.2 METHODS

Stimulation experiments were performed on HMGU1 human induced pluripotent stem cells (hiPSC) and neuronal derivates, which originate from the same clone and thus represent technical replicates on the levels of differentiation. In this pilot, hiPSC (n=2 technical replicates), neuronal progenitors (NP) (n=2 technical replicates), and differentiated neurons (dN) (n=1 technical replicate) were stimulated with 1µM of dexamethasone diluted in ethanol for 3h, 6h, and 12h. In the vehicle condition cells were treated with 0,001% ethanol. Neuronal progenitors ranged in passage number between passages 7 and 12. RNA was extracted using the miRNeasy kit (Qiagen) and hybridized to HumanHT-12 v4 Expression BeadChips. RNA quality was assessed by NanoDrop and TapeStation with RIN values ranging between 8 and 10. Microarrays were scanned using the Illumina Bead Array Reader and summarized raw probe intensities exported using Illumina's GenomeStudio Gene Expression module. Statistical analyses were conducted in R Studio using the

limma package (Ritchie et al., 2015). Limma contrasts were first computed between individual stages of differentiation in order to assess the identity of differentiated cell types, and then between the stimulated and unstimulated condition for 3h, 6h, and 12h in hiPSC and NP. Due to the low sample number for differentiated neurons in the pilot study, timepoints were collapsed for contrasts between stimulated and unstimulated cells. The cutoff was set at $\log_2 FC \geq 1$ and $p \leq 0.01$ in hiPSC and NP, and $q \leq 0.01$ in dN.

2.3.3 RESULTS

Characterisation of stimulated cell types by mRNA expression profile revealed that gene transcripts with the strongest upregulation in neuronal progenitor cells were pan-neuronal progenitor marker Hes Family BHLH Transcription Factor 5 (*HES5*), Neurocalcin Delta (*NCALD*), and anterior-posterior patterning factor Homeobox B7 (*HOXB7*) (**Table 2**).

Table 2. Top 25 gene transcript fold changes between hiPSC and NP.

ILMN probe	Gene	$\log_2$ FC	M	T	*p*-value	*q*-value
ILMN_1744398	ZSCAN10	-7.75	8.39	-33.87	3.86e-08	0.00035
ILMN_1705403	CYP2S1	-7.66	7.88	-17.09	2.34e-06	0.00080
ILMN_1713995	SCNN1A	-7.16	8.26	-32.05	5.38e-08	0.00035
ILMN_1794742	HES5	7.07	10.03	22.37	4.68e-07	0.00055
ILMN_2124802	MT1H	-7.02	8.34	-27.71	1.30e-07	0.00035
ILMN_1788538	NCALD	6.99	9.89	28.73	1.04e-07	0.00035
ILMN_1702125	HOXB7	6.99	8.43	27.83	1.26e-07	0.00035
ILMN_2052373	RAB17	-6.94	7.72	-28.87	1.01e-07	0.00035
ILMN_1762696	FAM181A	6.85	8.16	23.67	3.34e-07	0.00054
ILMN_1745299	FABP7	6.81	10.82	28.53	1.09e-07	0.00035
ILMN_2132982	IGFBP5	6.44	8.88	15.95	3.52e-06	0.00096
ILMN_1759652	C1ORF61	6.42	9.93	29.26	9.33e-08	0.00035
ILMN_1744604	CYBA	-6.38	8.71	-12.12	1.78e-05	0.00181
ILMN_1696339	ZIC2	-6.38	9.68	-10.60	3.89e-05	0.00261
ILMN_1811238	ALPK2	6.35	8.59	8.37	0.0002	0.00541
ILMN_1679060	LOC642559	-6.31	9.28	-11.21	2.81e-05	0.00229
ILMN_2384122	GPR56	6.26	9.36	16.17	3.26e-06	0.00095
ILMN_2343097	NCALD	6.18	9.51	26.30	1.77e-07	0.00039
ILMN_2237428	SCD5	6.13	8.12	15.68	3.91e-06	0.00102
ILMN_1699750	ABHD9	-6.12	8.32	-26.50	1.69e-07	0.00039
ILMN_1664265	EPHA1	-6.10	8.81	-20.76	7.33e-07	0.00058
ILMN_1804531	CLDN6	-6.08	7.85	-21.33	6.23e-07	0.00058
ILMN_1726204	SCRG1	5.99	8.28	13.72	8.59e-06	0.00144
ILMN_1770940	CDH1	-5.96	8.43	-10.03	5.34e-05	0.00312
ILMN_1674908	HOXB5	5.93	9.13	16.92	2.48e-06	0.00082

Annotations. ILMN probe = Illumina probe identifier, Gene = gene name, $\log_2$ FC = $\log_2$ fold change, M = mean value, t = t statistic, *p*-value = unadjusted significance value, *q*-value = False discovery rate-corrected *p*-value.

Contrasts between hiPSC and differentiated neurons on the other hand resulted in strongest upregulation of Neurotrophic Receptor Tyrosine Kinase 2 (*NTRK2*), Stathmin 2 (*STMN2*), and astrocyte marker Glial Fibrillary Acidic Protein (*GFAP*) (**Table 3**).

Table 3. Top 25 gene transcript fold changes between hiPSC and dN.

ILMN probe	Gene	log$_2$ FC	M	T	*p*-value	*q*-value
ILMN_1748903	LIN28	-9.55	10.15	-28.96	4.44e-11	9.69e-07
ILMN_1744398	ZSCAN10	-7.73	9.69	-23.76	3.21e-10	2.10e-06
ILMN_1714067	NTRK2	7.66	7.166	23.706	3.29e-10	2.10e-06
ILMN_1801246	IFITM1	-7.53	10.57	-23.18	4.12e-10	2.10e-06
ILMN_1795679	STMN2	7.33	9.23	22.82	4.81e-10	2.10e-06
ILMN_1697176	GFAP	7.29	7.35	21.68	7.99e-10	2.21e-06
ILMN_2124802	MT1H	-7.23	9.44	-21.60	8.29e-10	2.21e-06
ILMN_1696339	ZIC2	-7.23	10.46	-20.77	1.22e-09	2.23e-06
ILMN_2126038	STMN2	7.12	8.89	20.78	1.22e-09	2.23e-06
ILMN_2310814	MAPT	7.12	7.48	20.35	1.50e-09	2.26e-06
ILMN_1715401	MT1G	-7.05	10.71	-21.39	9.13e-10	2.21e-06
ILMN_1759652	C1ORF61	6.96	9.04	21.59	8.33e-10	2.21e-06
ILMN_1713995	SCNN1A	-6.87	9.55	-21.17	1.02e-09	2.22e-06
ILMN_1705403	CYP2S1	-6.80	9.45	-20.52	1.38e-09	2.26e-06
ILMN_2316236	HOPX	6.74	5.59	17.64	6.16e-09	3.95e-06
ILMN_1679060	LOC642559	-6.72	10.19	-11.63	3.48e-07	3.25e-05
ILMN_2384122	GPR56	6.62	8.43	17.26	7.64e-09	4.28e-06
ILMN_1702125	HOXB7	6.61	7.14	19.34	2.48e-09	2.58e-06
ILMN_1744604	CYBA	-6.61	9.70	-19.79	1.97e-09	2.54e-06
ILMN_1788538	NCALD	6.59	8.59	20.12	1.68e-09	2.29e-06
ILMN_1745299	FABP7	6.59	9.61	20.28	1.55e-09	2.26e-06
ILMN_1674908	HOXB5	6.57	8.36	16.51	1.18e-08	4.65e-06
ILMN_1726204	SCRG1	6.54	7.47	13.61	7.74e-08	1.25e-05
ILMN_1719449	DCLK2	6.42	7.06	19.07	2.85e-09	2.70e-06
ILMN_1701603	ALPL	-6.40	10.99	-19.14	2.75e-09	2.70e-06

Annotations. ILMN probe = Illumina probe identifier, Gene = gene name, log$_2$ FC = log$_2$ fold change, M = mean value, t = t statistic, *p*-value = unadjusted significance value, *q*-value = False discovery rate-corrected *p*-value.

Results for regulated genes following DEX stimulation in hiPSC are shown in **Table 4**. Upregulated transcripts included *WNT3*, Annexin A1 (*ANXA1*), HOP Homeobox (*HOPX*), and NK6 Homeobox 2 (*NKX6-2*), whereas Inhibin Subunit Beta E (*INHBE*), Cyclin Dependent Kinase Inhibitor 1A (*CDKN1A*), Growth factor Beta 2 (*TGFB2*), and Neuronal Membrane Glycoprotein M6-A (*GPM6A*), were among those transcripts that were downregulated.

Table 4. Regulated gene transcripts in hiPSC with log$_2$ FC ≥ 1 and *p* ≤ 0.01.

ILMN probe	Gene	log$_2$ FC	M	t	*p*-value
3h DEX					
UPREGULATED					
ILMN_1794501	HAS3	1.73	7.72	6.36	0.0001
ILMN_1708934	ADM	1.41	10.25	6.13	0.0002
ILMN_1773117	BCOR	1.33	9.36	5.72	0.0003
ILMN_1803593	WNT3	1.28	6.87	5.94	0.0002
ILMN_1770035	NCOA5	1.28	8.84	5.71	0.0003
ILMN_1668760	HAS3	1.22	6.59	4.10	0.003
ILMN_2184184	ANXA1	1.19	4.67	4.68	0.001
ILMN_1819384	HS.543887	1.19	8.33	3.53	0.006
ILMN_1801077	PLIN2	1.15	8.61	5.47	0.0004
ILMN_1803825	CXCL12	1.15	9.24	4.86	0.0009
ILMN_2412384	CCNE2	1.15	6.54	4.50	0.001
ILMN_2370208	CMTM3	1.14	7.40	4.69	0.001
ILMN_2316236	HOPX	1.13	4.17	3.82	0.004
ILMN_1713561	C20ORF103	1.13	5.62	3.88	0.004
ILMN_1741021	CH25H	1.06	7.60	5.04	0.0007
ILMN_1667577	LCMT2	1.05	8.55	3.43	0.007
ILMN_2395375	GABBR1	1.03	8.53	3.48	0.007
ILMN_1795285	PHF15	1.01	9.58	4.45	0.002
DOWNREGULATED					
ILMN_1811767	INHBE	-1.94	9.68	-8.45	1.29E-05
ILMN_1784602	CDKN1A	-1.74	10.16	-8.26	1.56E-05
ILMN_2074860	RN7SK	-1.71	10.07	-5.95	0.0002
ILMN_2399363	CLEC4A	-1.69	7.14	-6.61	9.15E-05
ILMN_1697448	TXNIP	-1.47	8.96	-6.19	0.0002
ILMN_2300664	CACNA1I	-1.40	7.75	-5.86	0.0002
ILMN_1739241	CHAC1	-1.26	5.94	-3.32	0.009
ILMN_1668592	STON1	-1.24	6.21	-5.24	0.0005
ILMN_1799600	STARD8	-1.23	6.82	-4.80	0.0009
ILMN_1766171	SNF8	-1.20	8.81	-3.62	0.005
ILMN_3213167	LOC100132739	-1.18	5.52	-4.81	0.0009
ILMN_1724806	RAPSN	-1.14	6.14	-4.09	0.003
ILMN_3288755	LOC646808	-1.11	8.40	-3.40	0.008
ILMN_1737561	LOC88523	-1.06	9.13	-5.61	0.0003
ILMN_1744621	CCDC35	-1.06	6.84	-3.82	0.004
ILMN_3240220	RNU1F1	-1.04	7.56	-3.54	0.006
ILMN_1742382	RIMS3	-1.02	10.13	-4.63	0.001
6h DEX					
UPREGULATED					
ILMN_1809972	CADPS	1.56	3.80	4.57	0.001
ILMN_1784756	ACOT7	1.10	4.48	4.22	0.002
ILMN_2118663	ERV3	1.07	5.10	4.72	0.001
DOWNREGULATED					
ILMN_1814221	NPTX1	-2.01	7.87	-4.04	0.003
ILMN_2341254	STARD13	-1.63	4.37	-3.50	0.007
ILMN_1811767	INHBE	-1.51	9.68	-6.60	9.28E-05
ILMN_1784602	CDKN1A	-1.33	10.16	-6.31	0.0001
ILMN_1812526	TGFB2	-1.32	4.38	-5.20	0.0005
ILMN_1739241	CHAC1	-1.30	5.94	-3.41	0.008
ILMN_2397646	GPM6A	-1.20	4.22	-3.66	0.005
ILMN_1697448	TXNIP	-1.07	8.96	-4.50	0.001
ILMN_1770085	BTG2	-1.05	7.13	-4.77	0.001

		12h DEX			
ILMN probe	**ID**	**log$_2$ FC**	**M**	**T**	***p*-value**
		UPREGULATED			
ILMN_1714569	PCTK1	1.35	5.08	4.30	0.002
ILMN_1809972	CADPS	1.32	3.80	3.88	0.004
ILMN_2118663	ERV3	1.31	5.10	5.78	0.0003
ILMN_2316236	HOPX	1.27	4.17	4.29	0.002
ILMN_1710408	LGR4	1.22	6.75	3.64	0.005
ILMN_2383934	ITGB1	1.15	8.95	3.38	0.008
ILMN_1786989	NKX6-2	1.11	4.49	5.84	0.0002
ILMN_3204434	LOC100132934	1.02	6.07	3.75	0.004
ILMN_1768260	GAS6	1.02	4.40	3.32	0.009
		DOWNREGULATED			
ILMN_1736817	LOC642118	-1.11	5.95	-3.46	0.007
ILMN_3213167	LOC100132739	-1.09	5.52	-4.46	0.002

Annotations. ILMN probe = Illumina probe identifier, Gene = gene name, log$_2$ FC = log$_2$ fold change, M = mean value, t = t statistic, *p*-value = unadjusted significance value.

Dexamethasone regulated transcripts in neural progenitor cells are shown in **Table 5**. Following stimulation, Chromosome 13 Open Reading Frame 15 (*C13ORF15*), Receptor Activity Modifying Protein 1 (*RAMP1*), and *TSC22D3* were among the upregulated transcripts, while Matrix Metallopeptidase 9 (*MMP9*) was found to be decreased.

Table 5. Regulated gene transcripts in NP with log$_2$ FC ≥ 1 and *p* ≤ 0.01.

		3h DEX			
ILMN probe	**ID**	**log$_2$ FC**	**M**	**T**	***p*-value**
		UPREGULATED			
ILMN_1658494	C13ORF15	2.13	10.83	3.50	0.009
ILMN_1752526	RNF144B	1.26	5.34	4.64	0.002
ILMN_2064725	METTL7B	1.08	5.99	4.11	0.004
		6h DEX			
ILMN probe	**ID**	**log$_2$ FC**	**M**	**T**	***p*-value**
		UPREGULATED			
ILMN_1752526	RNF144B	1.02	5.34	3.78	0.006
		12h DEX			
ILMN probe	**ID**	**log$_2$ FC**	**M**	**T**	***p*-value**
		UPREGULATED			
ILMN_1764754	RAMP1	2.37	8.57	4.22	0.003
ILMN_1658494	C13ORF15	2.19	10.83	3.59	0.008
ILMN_2373062	RHBDF2	1.24	6.78	3.79	0.006
ILMN_1748124	TSC22D3	1.23	8.68	4.26	0.003
ILMN_1752526	RNF144B	1.02	5.34	3.78	0.006
ILMN_2064725	METTL7B	1.01	5.99	3.86	0.005
		DOWNREGULATED			
ILMN_1796316	MMP9	-3.13	3.95	-5.78	0.001

Annotations. ILMN probe = Illumina probe identifier, Gene = gene name, log$_2$ FC = log$_2$ fold change, M = mean value, t = t statistic, *p*-value = unadjusted significance value.

[57]

Finally, transcripts regulated in differentiated neurons are shown in **Table 6**. Among those upregulated by Dexamethasone exposure were *C13ORF15*, *FAM107A*, *FKBP5*, *TSC22D3*, Drebrin 1 (*DBN1*), and Microtubule-associated protein 1B (*MAP1B*), whereas downregulation occurred in A Disintegrin-Like And Metalloprotease With Thrombospondin Type 1 Motif 3 (*ADAMTS3*), among others.

Table 6. Regulated gene transcripts in dN with log$_2$ FC ≥ 1 and *q* ≤ 0.01.

ILMN probe	ID	log$_2$ FC	M	T	*p*-value	*q*-value
UPREGULATED						
ILMN_1658494	C13ORF15	2.07	10.66	8.36	6.19E-17	1.35E-12
ILMN_1675947	MT3	1.69	9.96	6.86	7.13E-12	7.78E-08
ILMN_1743445	FAM107A	1.62	11.94	6.57	5.03E-11	3.66E-07
ILMN_1690566	RASSF4	1.56	9.40	6.33	2.43E-10	1.32E-06
ILMN_2290808	RPL21	1.40	10.37	5.67	1.45E-08	6.34E-05
ILMN_1670926	CHST15	1.37	9.74	5.54	3.09E-08	0.000103
ILMN_1895227	HS.204481	1.36	8.75	5.53	3.3E-08	0.000103
ILMN_1778444	FKBP5	1.32	8.65	5.35	9.07E-08	0.000248
ILMN_2276952	TSC22D3	1.30	5.95	5.26	1.42E-07	0.000344
ILMN_1805543	ADAMTS9	1.29	8.65	5.21	1.86E-07	0.000406
ILMN_1708890	RASSF4	1.24	7.23	5.02	5.17E-07	0.000915
ILMN_1686664	MT2A	1.24	11.22	5.01	5.45E-07	0.000915
ILMN_3247533	LOC100133840	1.21	7.32	4.89	1.01E-06	0.001467
ILMN_2303912	SCD5	1.17	8.09	4.74	2.14E-06	0.002742
ILMN_3215954	LOC653079	1.16	10.49	4.70	2.58E-06	0.002959
ILMN_3225795	LOC730032	1.13	5.46	4.58	4.68E-06	0.004504
ILMN_1757270	DBN1	1.13	7.11	4.58	4.7E-06	0.004504
ILMN_1680154	MAP1B	1.13	10.95	4.58	4.75E-06	0.004504
ILMN_2246134	PDE4DIP	1.11	5.74	4.50	6.73E-06	0.006118
ILMN_1761281	LOC441019	1.10	7.49	4.46	8.35E-06	0.006822
ILMN_1677814	ABCC3	1.10	7.38	4.45	8.44E-06	0.006822
ILMN_1774387	ZHX3	1.08	9.24	4.38	1.17E-05	0.008787
ILMN_1663080	LFNG	1.08	10.31	4.37	1.26E-05	0.00887
ILMN_1775170	MT1X	1.07	10.92	4.34	1.43E-05	0.009611
DOWNREGULATED						
ILMN_1703803	ADAMTS3	-1.28	5.54	-5.19	2.16E-07	0.000429
ILMN_2131177	GUCY1A3	-1.21	5.65	-4.91	9.04E-07	0.001409
ILMN_3240989	LOC729278	-1.20	5.59	-4.87	1.13E-06	0.001547
ILMN_1796099	LOC644380	-1.16	4.87	-4.71	2.48E-06	0.002959
ILMN_1842578	HS.539384	-1.15	6.10	-4.65	3.31E-06	0.003617
ILMN_1778985	PRMT10	-1.10	5.46	-4.47	7.86E-06	0.006822
ILMN_1812898	ZNF132	-1.09	4.95	-4.41	1.03E-05	0.008062
ILMN_2382245	KIRREL2	-1.08	5.49	-4.38	1.21E-05	0.008787
ILMN_1787434	OR10H1	-1.07	5.57	-4.34	1.45E-05	0.009611

Annotations. ILMN probe = Illumina probe identifier, Gene = gene name, log$_2$ FC = log$_2$ fold change, M = mean value, t = t statistic, *p*-value = unadjusted significance value, *q*-value = False discovery rate-corrected *p*-value.

2.3.4 DISCUSSION

A pilot transcriptome study was conducted to characterise differentiated cell types and assess reactivity to GR ligand binding in hiPSC and their neuronal derivatives.

First, while highest upregulation of pan-neural progenitor marker *HES5* positively identified the generated cell population as neuronal progenitor cells, concurrent upregulation of anterior-posterior patterning factor *HOXB7* pointed to an unexpected spatial profile. Indeed, HOX genes are known as specifiers of the hindbrain and some are even involved in somitogenesis (Veraksa et al., 2000). The desired cell population on the other hand should have shown an anterior profile to accommodate the fact that prenatal stress was found to primarily affect frontal brain structures and associated functions (see section 1.1.2.5). The anterior–posterior and dorsal–ventral axes of the forebrain and midbrain are specified by the OTX (orthodenticle homolog) and EMX (empty spiracles homolog) gene families. The first patterning genes to be expressed in the fore- and midbrain are OTX genes, starting with *OTX2* followed by *OTX1*. Expression of EMX genes follows subsequently, with *EMX2* being expressed first, succeeded by *EMX1*. While *OTX2* and *OTX1* are expressed in fore- and midbrain, *EMX2* and *EMX1* expression is restricted to the forebrain (Tan et al., 2013).

In line with the transcriptional profile found in neural progenitors, one of the most strongly upregulated genes in differentiated neuronal cultures alongside Microtubule-Associated Protein Tau (*MAPT*) was *GFAP*. Both observations led to the conclusion that the time that stimulated neuronal cells had been in culture resulted in an advanced state of their internal fate-specification program (Edri et al., 2015).

Therefore, stimulation experiments would need to be performed within a short time span after neural induction in order to capture effects of glucocorticoid stimulation on cells with predominantly anterior and neurogenic properties. A temporal transcriptome analysis of *in vitro* derived neuronal cells from human embryonic stem cells found highest expression of *FOXG1* between D20 and D30 following neural induction (van de Leemput et al., 2014).

Dexamethasone stimulation experiments in hiPSC revealed an upregulation of early embryonic asymmetry patterning factor *WNT3*. Interestingly, also *NODAL* was found to be upregulated following dexamethasone exposure for 3h ($\log_2$ FC = 1.09, *p* = 0.049). High expression levels of *NODAL* and *WNT3* are characteristic of the proximal and posterior axes of the developing epiblast, respectively. Similarly, upregulated gene transcript *NKX6-2* was found to play a role in ventral midbrain development (La Manno et al., 2016). Glucocorticoid-induced gene activation in hiPSC may therefore introduce an early bias regarding embryonic axis formation. In addition, downregulated transcripts included *GPM6A*, which was found to be involved in the differentiation and migration of neurons derived from human embryonic stem cells (Michibata et al., 2009) and *TGFB2*, which was equally shown to promote neuronal cell fate (Roussa et al., 2006). The transcript for *HOPX* on the other hand was increased following dexamethasone administration and is reported to prime neural stem cells in the subventricular zone towards an astrocyte cell fate (Zweifel et al., 2018). Several regulated transcripts were also involved in inflammation, such as the upregulated *ANXA1* gene transcript (Zhao et al., 2016) and downregulated inflammatory response gene *CDKN1A* (Ring et al., 2003), which moreover has a well-established role in the stress system (Gorospe et al., 1999).

Only few transcripts were regulated in neural progenitor cells following dexamethasone stimulation. However, this finding may have been caused by the relative heterogeneity of neural progenitor populations used in the pilot study, found to occur with an increasing number of passages and time in culture (Edri et al., 2015). Nevertheless, results showed an increase in *TSC22D3*, previously reported to be upregulated following dexamethasone stimulation of mouse hypothalamic neural progenitor cells (Frahm et al., 2016). Also, expression of *RAMP1* was heightened, which encodes for a receptor associated with migraine (Edvinsson, 2018). Meanwhile, decreased expression was detected for *MMP9*, which is known to be implicated in the stress response. For example, inhibition of *MMP9* was shown to prevent stress-induced behavioural alterations in mice (van der Kooij et al., 2014).

As discussed, the neuronal culture subjected to dexamethasone should more appropriately be described as a mixed culture of neurons and astrocytes. Upregulated gene transcripts included several genes with well-established roles in the stress response. One of them was *FAM107A*, previously reported to increase following stress, bind to actin, promote bundling and stabilization of actin filaments, and impact on actin-dependent neurite outgrowth, synaptic function, and cognition (Schmidt et al., 2011). Furthermore, heightened expression was shown for *FKBP5*, a co-chaperone of the glucocorticoid receptor implicated in the negative feedback loop of the stress response (Denny et al., 2000; Russell et al., 2010), and *TSC22D3*, which was also regulated in neural progenitor cells. With *ZBTB16*, an additional stress-responsive gene was increased following dexamethasone exposure at a significance level slightly above the chosen cutoff ($\log_2$ FC = 1.07, *q* = 0.0101). Some

of the upregulated genes were moreover associated with actin dynamics and neurite outgrowth of developing neuronal cells. For instance, *DBN1* is reported to stabilize actin filaments (Mikati et al., 2013) and thereby protect dendritic spine density from stress-induced alterations (Kreis et al., 2019). Similarly, *MAP1B* was found to be implicated in the density of presynaptic and postsynaptic terminals (Bodaleo et al., 2016). Downregulated transcripts following dexamethasone exposure included *ADAMTS3*. It was identified as the major enzyme responsible for cleaving and inactivating Reelin in the cerebral cortex and hippocampus (Ogino et al., 2017).

2.4 CONCLUSIONS

The preliminary studies described here resulted in an immunocytochemistry assay with established sensitivity to capture subcellular GR localisation and translocation, a differentiation protocol yielding high quality neural rosettes and defined neural progenitor populations, and crucial information for further planning of experiments as the characterisation of stimulated cells revealed a posterior gliogenic profile but also confirmed reactivity to known stress-reactive genes on the transcriptome level.

3. METHODS

3.1 STUDY DESIGN
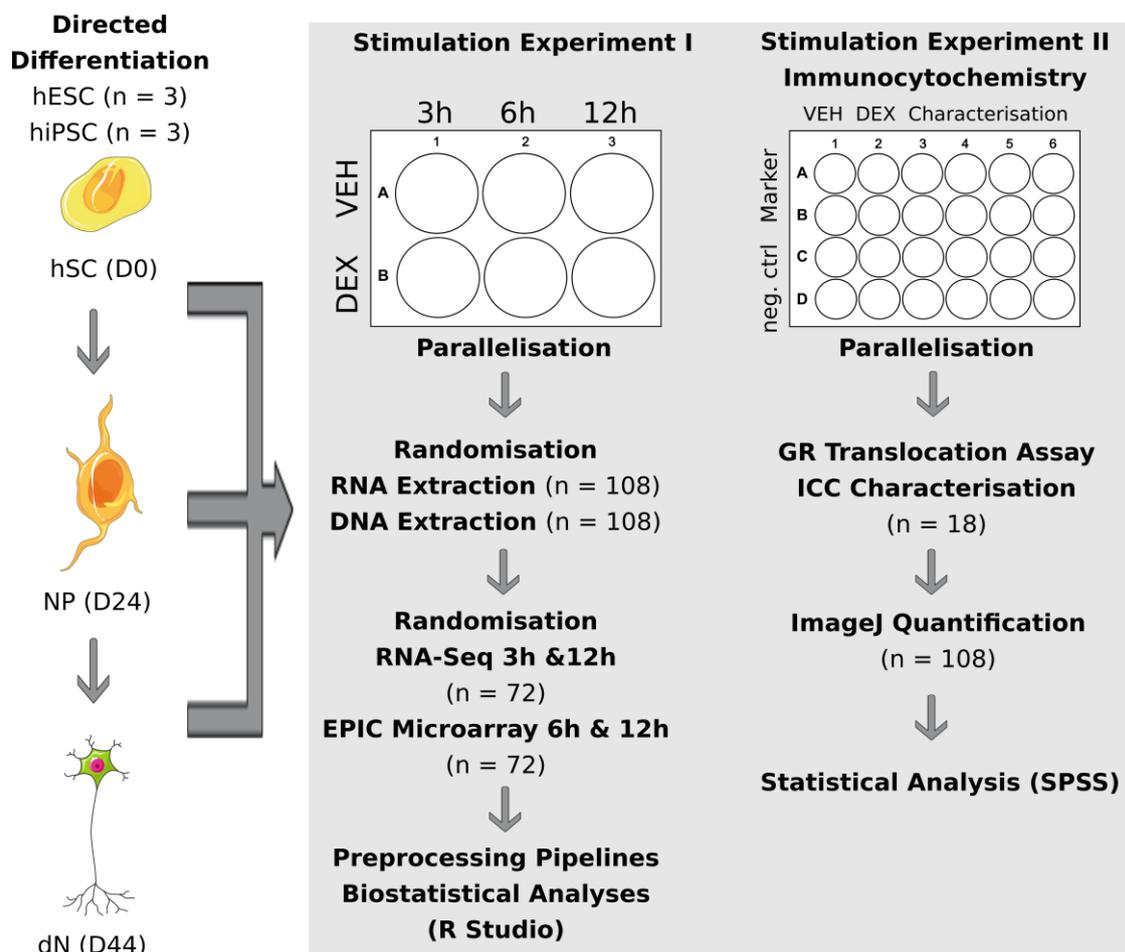
Figure 19. Schematic representation of the experimental design. hESC = human embryonic stem cells, hiPSC = human induced pluripotent stem cells, hSC = human stem cells, NP = neural progenitors, dN = differentiated neurons, VEH = Vehicle (EtOH), DEX = Dexamethasone.

A schematic of the experimental design is shown in **Figure 19**. Biological replicates were obtained from two cell lines (hESC and hIPSC) subjected to repeated induction of directed differentiation to neuronal progenitors and neurons in order

to produce independent technical replicates from the two biological replicates for all developmental stages. A panel of experiments was conducted for each replicate, involving a time course stimulation experiment with 1µM dexamethasone for high-throughput experiments and a second stimulation experiment for quantification of GR translocation following 3h of stimulation and respective downstream analyses. Dexamethasone was dissolved in ethanol and further diluted in water before application to the respective culture media. The control condition was treated with 0,001% ethanol as vehicle. With respect to downstream analyses, only the 6h and 12h stimulation conditions were used for analyses of DNA methylation due to the assumption that no methylation changes can be expected after 3h, while only 3h and 12h conditions were used for RNA-Seq analyses due to cost-restrictions and showing most regulated transcripts in the pilot study across stages of differentiation. For every independent replicate, the study design was parallelised with respect to treatment and duration as primary outcomes of interest. In addition, samples were randomised both for extraction of RNA and DNA, as well as for RNA-Seq library preparation and positioning on EPIC microarray chips.

3.2 CELL LINES

Experiments were performed on embryonic stem cell line H1 (WA01) and HMGU1, an induced pluripotent stem cell line derived from fibroblast line CRL-2522 (ATCC) at the German Research Center for Environmental Health, Institute of Stem Cell Research. The reprogramming process is described in detail elsewhere (O'Neill et al., 2018). Both cell lines are derived from male donors. Another three blood-derived and two fibroblast-derived hiPSC lines were tested for differentiation potential but failed to produce neural rosettes with sufficient reliability or to

differentiate into the target lineage and cell types. An overview of the cell lines is given in **Table 7**. Additional independent technical replicates were obtained by repeated induction of directed differentiation. Three of these replicates were chosen from each line for further downstream analysis based on visual inspection of marker gene expression and homogeneity, yielding a total of n = 6 replicates per experimental condition and N=108 samples in total.

Table 7. Cell lines.

Cell line	Sex	Ethnicity	Primary tissue (if applicable)	Reprogramming method	Passage	Reliable induction
H1	male	caucasian	none (ICM of blastocyst)	none	24-29	Y
HMGU1	male	caucasian	Fibroblasts	episomal reprogramming	30-35	Y
#20	male	caucasian	Fibroblasts	episomal reprogramming	11-16	N
#60	male	caucasian	Fibroblasts	episomal reprogramming	15-20	N
MPI1	female	caucasian	PBMCs	episomal reprogramming	12-24	N
FOK1-4	male	caucasian	PBMCs	episomal reprogramming	17-23	N
FOK1-5	male	caucasian	PBMCs	episomal reprogramming	20-24	N

Annotations. PBMCs = peripheral blood mononuclear cells; ICM= inner cell mass; Y=yes; N=no.

3.3   CELL CULTURE AND HESC/ HIPSC DIFFERENTIATION

H1 human embryonic stem cells (hESC) and HMGU1 human induced pluripotent stem cells (hiPSC) were grown on Matrigel diluted 1:40 (Corning), maintained in mTESR (STEMCell Technologies) and split 1:6 with 1 mg/mL Collagenase IV (Gibco) approximately once or twice a week. Neuronal differentiation was induced using the Aggrewell protocol (**Fig. 20**). hESC / hiPSC colonies were dissociated with Accutase (Sigma-Aldrich) into single cells, resuspended in Neural Induction Medium (STEMCell) supplemented with 10 µM

ROCK Inhibitor (STEMCell), and plated at a density of 3 million cells per well into Aggrewell 800 plates to generate embryonic bodies (EBs) consisting of approximately 10 000 cells. Three-fourths of the medium was exchanged every day for 5 days until aggregates were replated on Matrigel. Induction of neural rosettes (NR-NP) in the chosen lines was highly efficient approximating 100%, and visible from as early as day 6. Rosettes were washed with DMEM/F-12 (Gibco) and Neural Induction Medium was refreshed daily. On day 12, rosettes were manually selected by microdissection using a syringe needle and replated onto Poly-L-Ornithine / Laminin coated plates. On day 17-19, replated rosettes were then dissociated with Accutase and seeded at a density of 1 million cells per well of a 12-well plate in order to ensure close cell-to-cell contact.
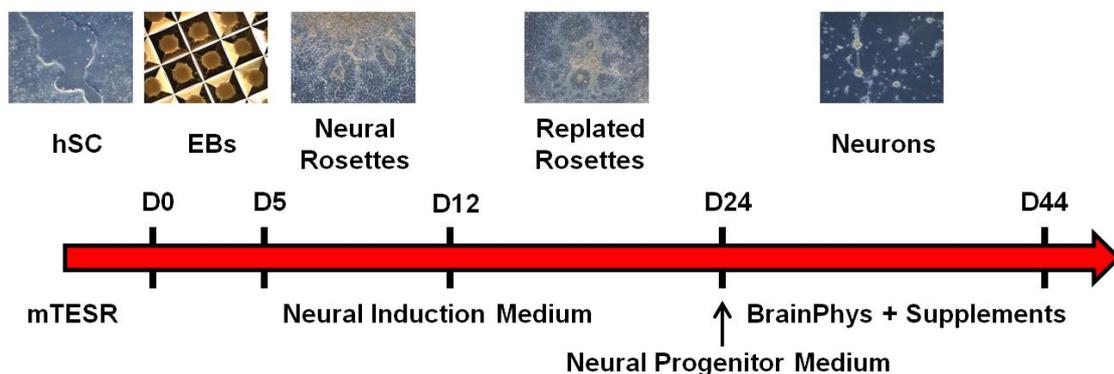
Figure 20. Schematic representation of the neural differentiation process. Neural induction was performed using the Aggrewell protocol. Induced pluripotent stem cells / embryonic stem cells (hSC) are considered D0 of differentiation. Terminal neural differentiation was induced on D24.

When necessary, the neural progenitor (NP) population was additionally purified by magnetic bead selection for PSA-NCAM positive cells using anti-PSA-NCAM MicroBeads (Miltenyi) and the MiniMACS separator (Miltenyi).

Differentiation to neurons (dN) was induced on day 24. Neuronal progenitors were plated at a density of 200 000 cells per 6-well plate in Neural Progenitor Medium (STEMCell). On day 1 of neuronal differentiation, half of the medium was replaced with BrainPhys Medium (STEMCell), supplemented with 1 x N2 (Gibco), 1 x B27 without Vitamin A (Gibco), 20 ng/ml BDNF (PeproTech), 20 ng/ml GDNF (PeproTech), 200 nM L-Ascorbic acid (Sigma-Aldrich), and 1 mM dibutyryl-cyclic AMP (Sigma-Aldrich). Half a medium change was subsequently performed every 2-3 days. From day 10 of neuronal differentiation (i.e. D34 after neural induction), 1 µg/ml Laminin was added to the medium in order to prevent detachment of emerging neuronal hubs alongside 1 µg/ml cytosine arabinoside (Jena BioScience) to eliminate differentiating cells from the culture.

3.4 DEXAMETHASONE STIMULATION EXPERIMENTS

Culture media were switched to a glucocorticoid-free equivalent the day prior to the experiment. hESC / hiPSC were stimulated in E8 which does not contain glucocorticoids, neuronal progenitors in DMEM/F-12 supplemented with 1 x N2 and 20 ng/ml bFGF, and neurons in DMEM/F-12 supplemented with 1 x N2. Media were not depleted of progesterone due to its low affinity to bind GR (Attardi et al., 2008) and a final concentration in N2-containing media of 2 nM. Cells were plated at a density of 1 million per well and stimulated with 1 µM dexamethasone dissolved in ethanol and diluted in DPBS for 3h, 6h, and 12h on a shaker at 40 rpm following a reverse time-course stimulation protocol. The control condition was treated with 0,001% ethanol as vehicle. The plates were placed on a shaker in order to promote equal distribution of the ligand in the culture media during the stimulation experiment. Cells were collected with Accutase, counted, centrifuged at 300 x g for

3 minutes, washed with DPBS and split to separate tubes for RNA and DNA extraction, centrifuged again, and frozen at -80°C.

3.5   RNA EXTRACTION AND LIBRARY PREPARATION

RNA was extracted in randomised order on the Chemagic 360 automated system using magnetic beads (Perkin Elmer). RNA quantity and quality were assessed using the Nanodrop 2000 spectrophotometer (NanoDrop Technologies) and Agilent TapeStation (Agilent Technologies). RNA libraries were prepared for samples stimulated for 3h and 12h using 100 ng input mRNA and the QuantSeq 3′ mRNA-Seq Library Prep Kit FWD for Illumina following manufacturer instructions.

3.6   DNA EXTRACTION AND EPIC METHYLATION ARRAY

Genomic DNA was extracted in randomised order on the Chemagic 360 automated system using magnetic beads (Perkin Elmer). DNA of samples stimulated for 6h and 12h (14-400 ng) was bisulfite converted using the EZ-96 DNA Methylation Kit (Zymo Research). DNA methylation levels were assessed with the Illumina Infinium MethylationEPIC BeadChip Kit. Hybridization and processing were performed according to manufacturer instructions.

3.7   IMMUNOFLUORESCENCE ASSAYS

Cells were fixed in 4 % PFA for 10 minutes and blocked in 1% FBS, 5% donkey serum, and 0.5 % Triton-X 100 for 1h. Primary antibodies were diluted in blocking solution and added overnight at 4°C. Secondary antibodies were incubated for 1h at room temperature. Immunofluorescence was performed using the following primary antibodies: OCT4 (1:500, Millipore ABD116), Nanog (1:250, Millipore MABD24), Tra1-60 (1:250, Millipore MAB4360), SOX2 (1:500, Cell Signaling 2748),

FOXG1 (1:50, abcam ab18259), PAX6 (1:250, Biozol BLD-901301), OTX2 (1:100, R&D AF1979), Nestin (1:500, Santa Cruz sc-23927), ZO1 (1:100, BD Bioscience 610966), MAP2 (1:500, abcam AB5392), vGLUT1 (1:1000, Synaptic Systems 135303), vGAT2 (1:500, Synaptic Systems 131011), SYN1 (1:1000, Synaptic Systems 106001), PSD95 (1:500, Invitrogen 51-6900), GFAP (1:1000, Dako Z0334), and GR H-300 (1:500, sc8992 X). Secondary antibodies were raised in donkey: Alexa 488 anti-rabbit (1:1000, Dianova), Alexa 488 anti-mouse (1:1000, Dianova), Alexa 488 anti-chicken (1:1000, Dianova), Alexa 594 anti-rabbit (1:500, Life Technologies), Alexa 594 anti-mouse (1:500, Dianova), Alexa 594 anti-goat (1:500, Dianova), DyLight 647 anti-rabbit (1:1000, Dianova), and Alexa 647 anti-mouse (1:1000, Life Technologies). Images were obtained on a Leica Confocal microscope TCS SP8.

3.8 QUANTIFICATION OF GLUCOCORTICOID RECEPTOR TRANSLOCATION

Dexamethasone stimulation experiments were performed as described in section 3.4 on glass cover slips in 24-well plates but limited to the 3h condition and fixed for immunocytochemistry. Image analysis was run in ImageJ software. A total of n = 6 experiments were conducted for each developmental stage. Three individual frames of randomly selected regions of interest were taken per condition at a 40x magnification, resulting in n = 18 frames per developmental stage and treatment condition covering 129 cells/frame on average. Glucocorticoid receptor signal intensity was defined in terms of mean integrated density (area x mean gray value) in order to account for different area sizes occupied by nuclear and cytoplasmic fractions. Nuclear and cytoplasmic GR intensities were extracted from thresholded

pictures and values normalised to the absolute GR signal per frame. Translocation of GR to the nucleus was then calculated as a function of the difference between the mean integrated density signal in the nucleus and cytoplasm (GR $_{\Delta ID}$ =M$_{IDN}$-M$_{IDC}$). Thus, positive values indicate more protein in the nucleus while negative values indicate more protein in the cytoplasm. Statistical analysis was carried out in PASW Statistics version 18 (2009).

3.9 WESTERN BLOT

Protein extraction from cell pellets (n=3 for hSC, NP, and dN, respectively) was conducted in RIPA buffer (50 mM Tris pH 8.0, 150 mM NaCl, 1% NP-40, 0.5% sodium deoxycholate, and 0.1% SDS) supplemented with cOmplete protease inhibitor cocktail (Roche) and phosphatase inhibitor (Sigma-Aldrich). Following incubation on ice for 30 min, the solution was sonicated, centrifuged at 14 000 rpm (20 817 x g) for 15 min and the supernatant collected for western blot. The homogenized lysate was centrifuged at 16 000 x g for 15 min and protein sample concentration quantified by Bradford protein assay (Bio-Rad, Hercules, California, USA). The protein solution (15-20 µg) was resuspended in Roti-Load (Roth) loading buffer and boiled for 5 min at 95°C. Samples were run in a 10% acrylamide gel and then transferred to nitrocellulose membranes (Merck-Millipore). Membranes were blocked in 5% low-fat milk Tris buffer containing 0.1% Tween20 for 1h at room temperature and incubated with primary antibodies overnight followed by 1h incubation with corresponding HRP-conjugated secondary anti-goat (1:5000, Santa Cruz, sc-2028) or anti-rabbit (1:2000, Cell Signaling, 7074S) antibodies at room temperature. β-ACTIN served as loading control for protein lysates. Protein bands were developed by enhanced chemiluminescence (Immobilon Western HRP

Substrate, Merck) and intensity measures taken in Image Lab 5.2 (Bio-Rad). The following primary antibodies were used: GR (1:2000, Cell Signaling, 12041), HSP70 (1:2000, Cell Signaling, 4872), HSP90 (1:1000, Thermo Scientific, PA3-013), FKBP51 (1:500, Santa Cruz, 11518 (F14)), and β-ACTIN (1:4000, Cell Signaling, 4967).

3.10 QPCR

Dexamethasone treatment effect on gene expression in differentiating cells was additionally evaluated using PrimeTime qPCR primer assays (IDT) for stress-reactive genes *TSC22D3* and *ZBTB16*. RNA (100 ng) was reverse-transcribed using Maxima H Minus Reverse Transcriptase (ThermoFisher Scientific) following manufacturer recommendations and the cDNA diluted in H_2O to a working concentration of 1 ng/μl. The qPCR was run with four independent replicates of the 12h stimulation condition (n=4 treated, n=4 untreated) per stage of differentiation using 2 ng of cDNA, the respective primer, TaqMan Master Mix (ThermoFisher Scientific), and the LightCycler 480 (Roche). Threshold cycle values were determined in quadruplicates and averages normalised to *YWHAZ*, which had shown good stability in previous experiments conducted in the lab. Fold changes were calculated using the $2^{-\Delta CP}$ method. A paired Student's t-test (2-tailed) was run between the ΔCP values of stimulated and unstimulated samples in every stage of differentiation (n=4). For visualisation, mean $\log_2$-transformed values were normalised to the untreated control.

3.11 Biostatistical Analyses of Differential Methylation

All biostatistical analyses were carried out in R Version 3.5.1 and R Studio. Samples chosen for DNAm downstream analysis had been stimulated for 6h and 12h, reducing the total number of samples from N=108 to N=72. The 3h stimulation condition was expected to show negligible changes in DNAm and was therefore omitted. Preprocessing was conducted using the minfi package. Raw data (**Fig. 21a**) were normalised by Subset-quantile Within Array Normalisation (SWAN) (Maksimovic et al., 2012) (**Fig. 21b**). Density plots were visually inspected for artefacts and n = 2 samples excluded due to their flattened distribution profiles, resulting in N = 70 samples considered in downstream analyses.

Prior to statistical analyses, probes that failed to reach a detection *p*-value of 0.01 in more than 25% of samples were eliminated (n = 1 715). No samples had to be removed due to low call rates. Probes known to be cross-hybridising (n = 44 088) or polymorphic with a minor allele frequency (MAF) ≥ 5% in European samples (n = 9 508) were removed, as well as probes located on the X and Y chromosomes (n = 18 000), leaving a total of n = 792 780 probes that were considered in analyses of differential methylation.
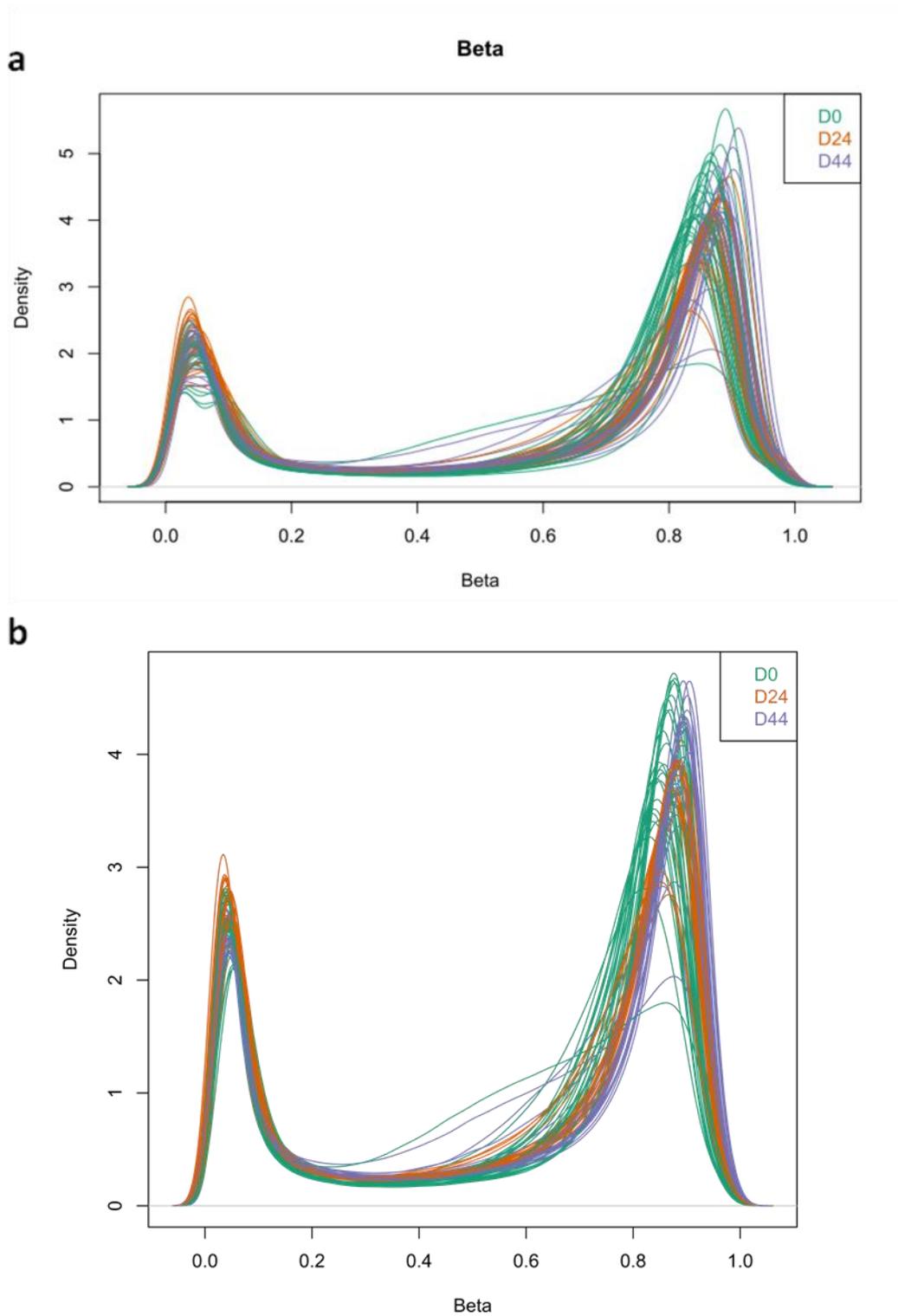
Figure 21. Density plots. a) Uncorrected beta values (N=72). **b)** Beta values after SWAN normalisation (N=72).

3.11.1 ASSESSMENT OF POTENTIAL CONFOUNDERS

Potential confounders were assessed using multidimensional scaling, correlation analyses with principal components, and variance partition.

Multidimensional scaling plots showed samples separating along the factors differentiation stage and cell line on the first and second dimension, respectively (**Fig. 22**). Within individual stages of differentiation, differences between cells were accordingly best described by the factor cell line. Meanwhile, the differentiation batch or biological replicate specifically discriminated differentiated HMGU1-derived neurons and, to a lesser degree, neuronal progenitors (**Fig. 23**).

A correlation heatmap between the first 20 principal components (PCs) and potential explanatory variables is shown for raw (**Fig. 24a**) and SWAN normalised data (**Fig. 24b**). The PCA for normalised data identified highest loadings of differentiation stage and cell line on PC1 and PC2. In addition, amount of DNA (μg) for bisulfite conversion and number of live cells loaded on PC3 and PC4, while column loaded on PC5.

Overall, variance in the data set was well explained by the combination of study variables and known technical batches both before (**Fig. 25**) and after SWAN normalisation (**Fig. 26**). Variance partition suggested EPIC methylation chip and array sentrix position as the most influential batches on both a global level and within individual stages of differentiation. Also, biological replicate captured a high percentage of variance, presumed to include both dependent and independent variance (Blainey et al., 2014).
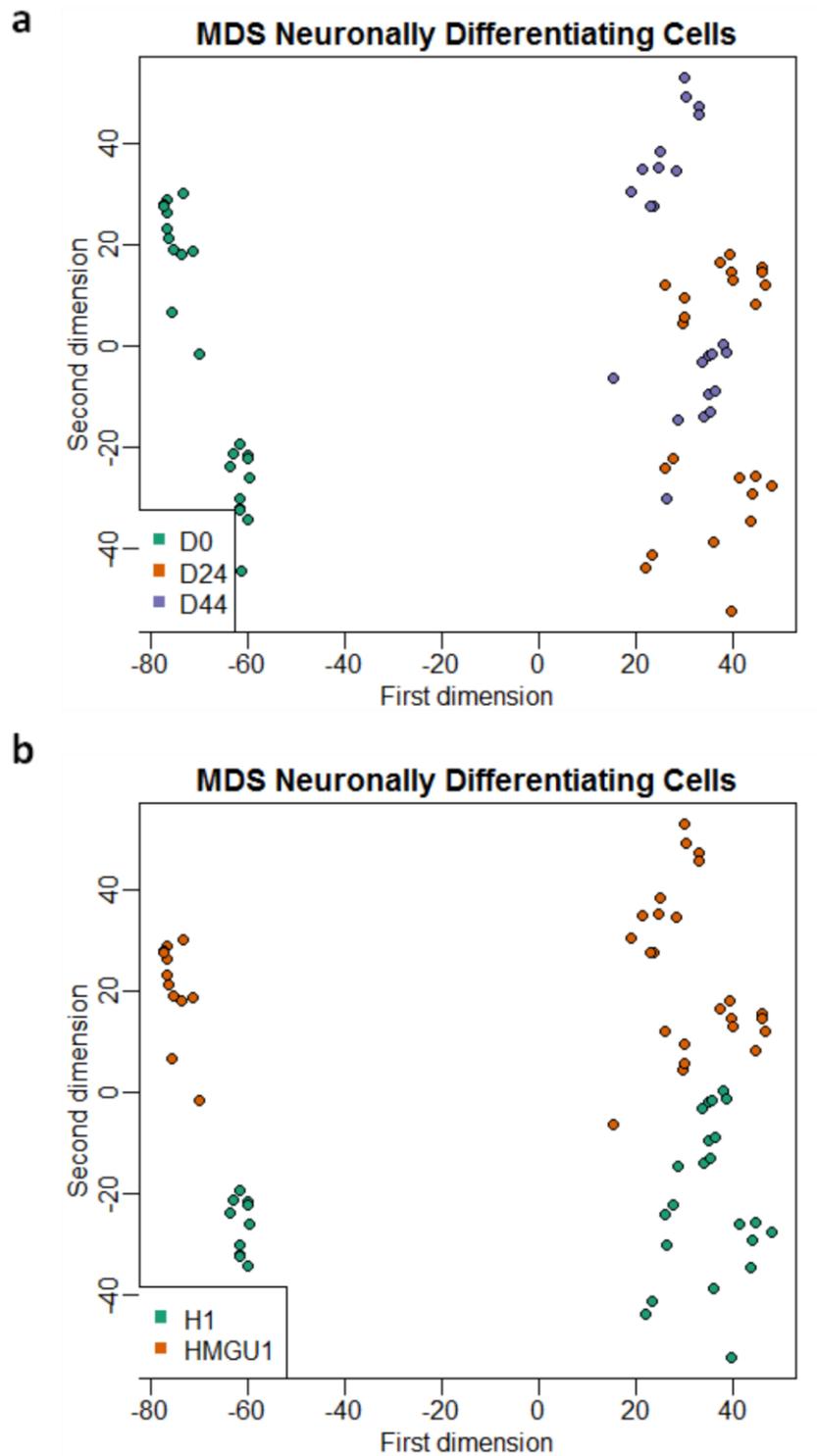
Figure 22. Multidimensional scaling plots (MDS) a) MDS for SWAN normalised data (n=866 091 probes) separating by **a)** differentiation stage and **b)** cell line.

SWAN normalised betas
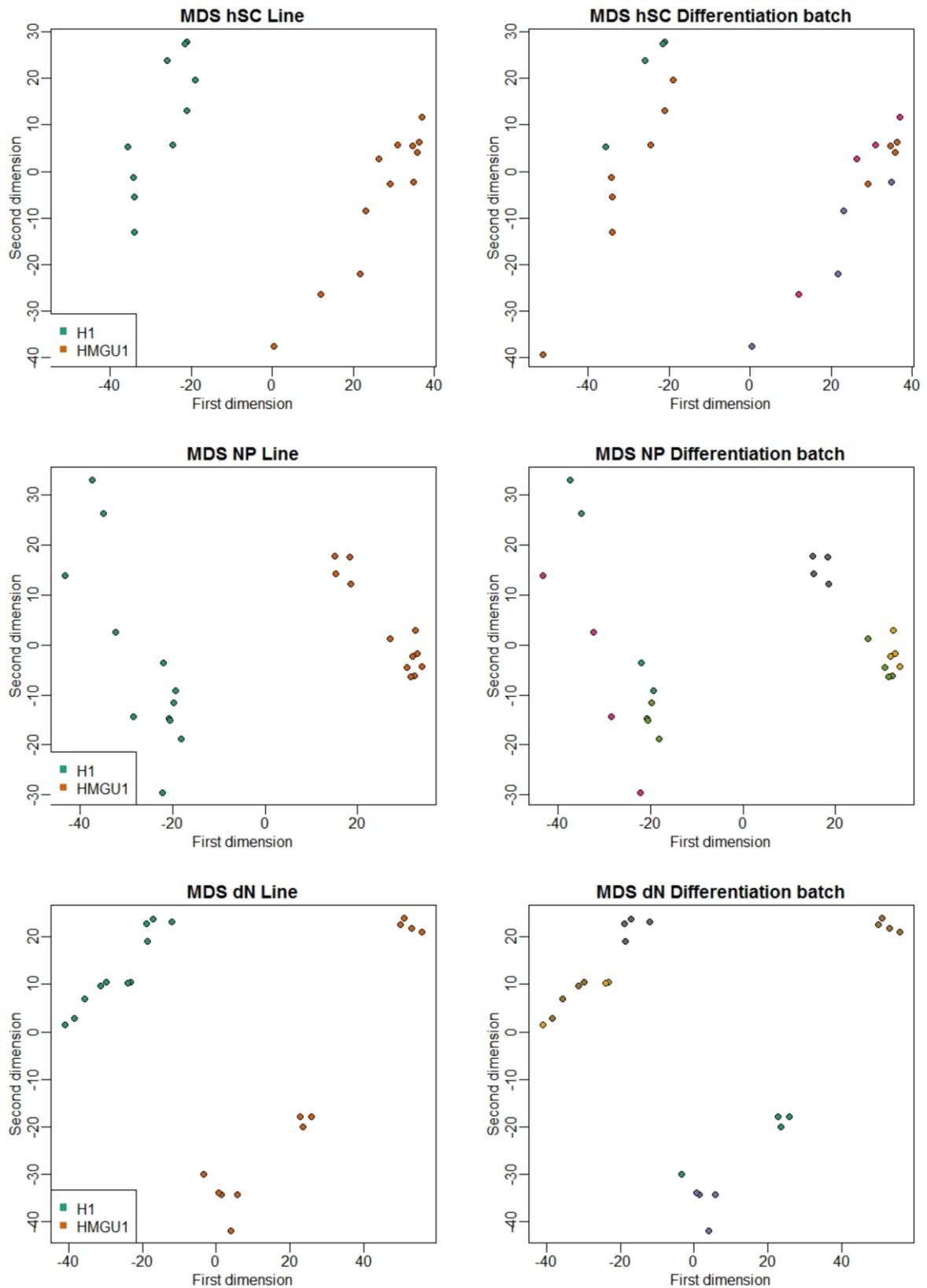
Figure 23. Multidimensional scaling plots (MDS) for individual stages of differentiation. Beta values after SWAN normalisation (N=72, n=866 091 probes).
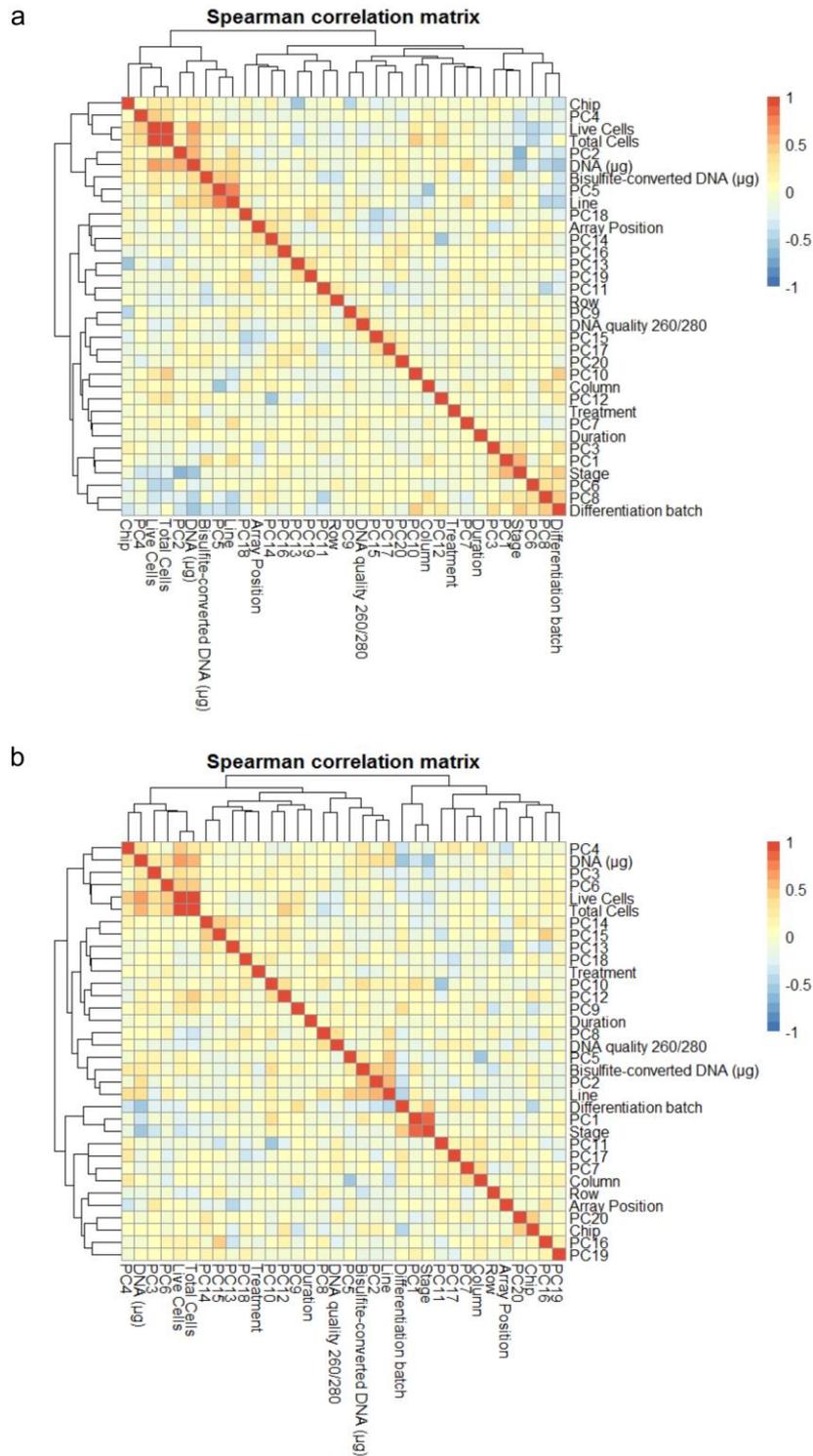
Figure 24. Correlation matrices between PCA 1-20 and potential predictor variables in raw and normalised data. a) Raw methylation beta values (N=72 samples; n=866 091 probes). **b)** SWAN normalised methylation beta values (N= 70 samples; n=866 091 probes).
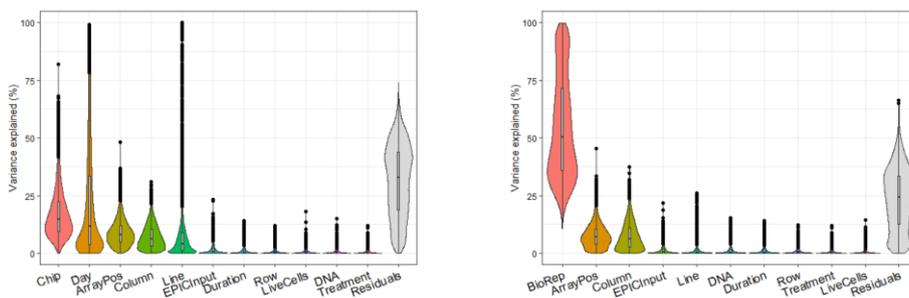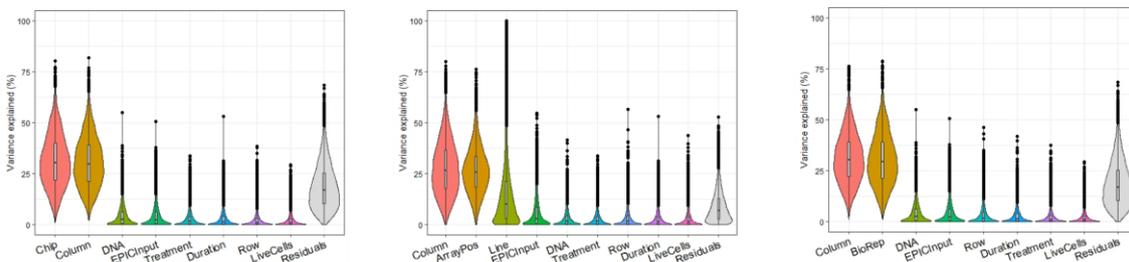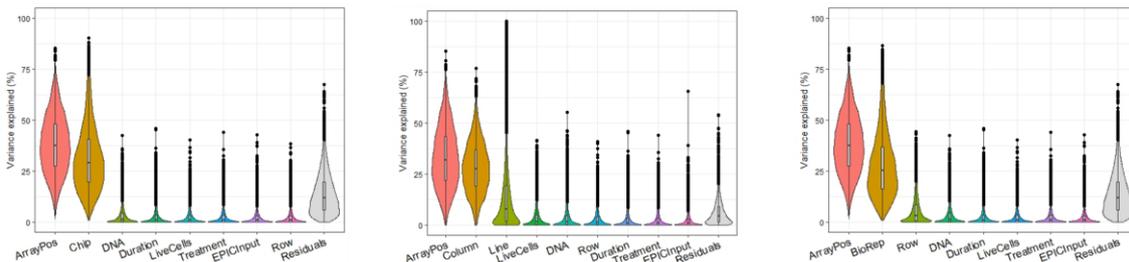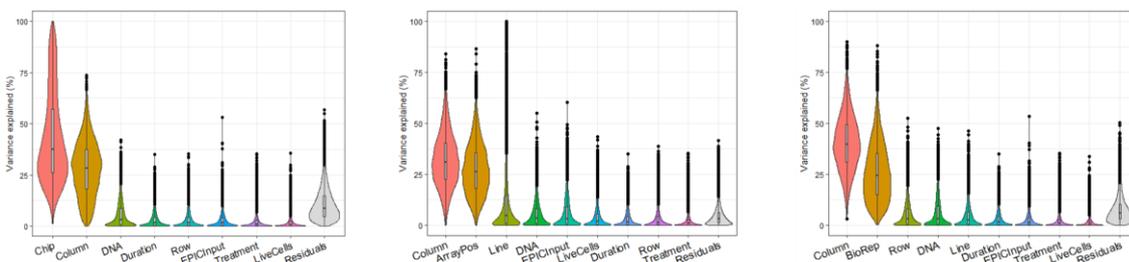
Figure 25. Variance partition in raw methylation beta values (N=72 samples; n=10 000 probes). Chip = EPIC methylation chip, ArrayPos = sentrix position, LiveCells = number of living cells, DNA = DNA input amount for bisulfite conversion, EPICInput = amount of bisulfite-converted DNA.
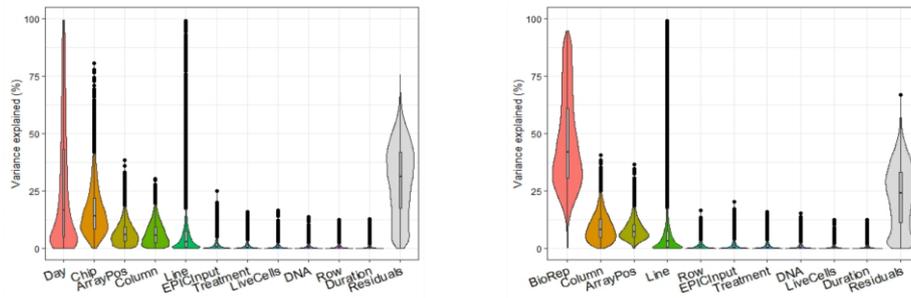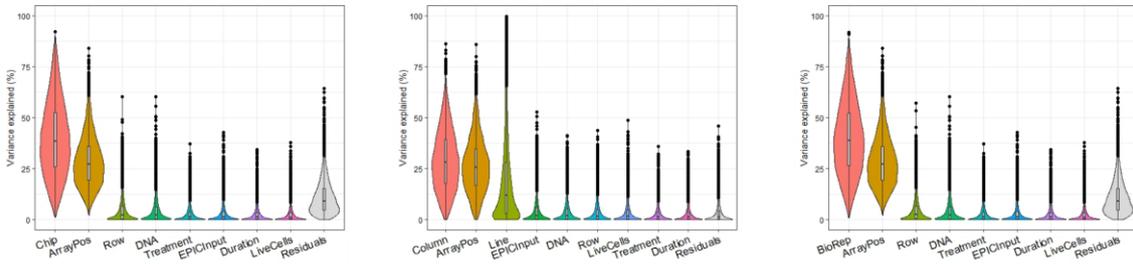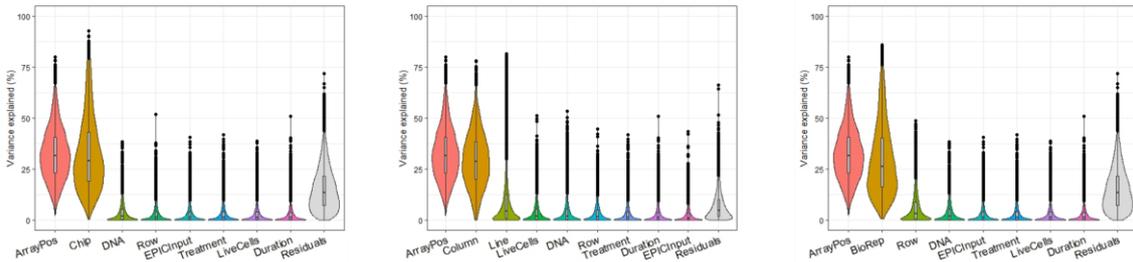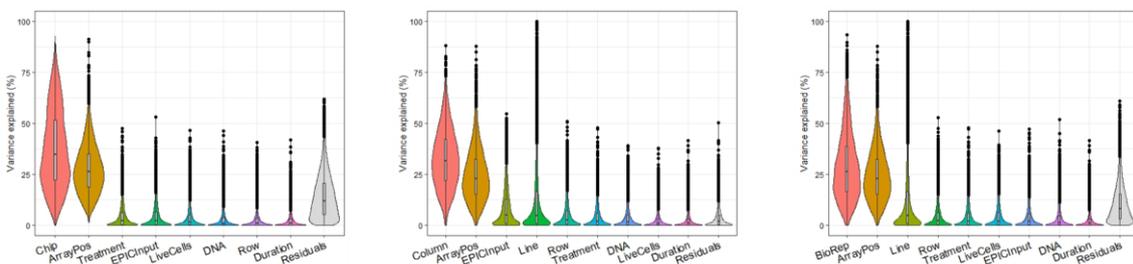
Figure 26. Variance partition in SWAN normalised methylation beta values (N=70 samples; n=10 000 probes). Chip = EPIC methylation chip, ArrayPos = sentrix position, LiveCells = number of living cells, DNA = DNA input amount for bisulfite conversion, EPICInput = amount of bisulfite-converted DNA.

In sum, the assessment of potential confounding variables by MDS and correlation structure with principal components as well as explained variance suggested that cell line, EPIC methylation chip, array sentrix position, and either number of live cells or DNA (µg) may need to be accounted for in the statistical model. Corrections are possible by batch correction as part of data pre-processing, e.g. with ComBat in the sva package (Leek et al., 2012), or by inclusion of the confounding factor as covariate in the regression model (Leek et al., 2010).

3.11.2 REGRESSION MODELLING

During data preprocessing, EPIC methylation chip and array position were chosen for ComBat batch correction due to explaining a high percentage of variance overall, and because samples were randomized with respect to their distribution. Therefore, both factors were expected to introduce random noise that would otherwise have contributed to the error term and decreased statistical power to detect significant effects.

Cell line and DNA (µg) were chosen as covariates, since both loaded on the second, respectively third and fourth principal components.

Because shared variance may cause batch correction for technical variables to indirectly alter test variables and their relations to each other, the ComBat function allows to define the regression model when removing unwanted variance. Therefore, normalised data were batch corrected for array position and EPIC methylation chip while preventing alterations to test variables stage of differentiation, treatment and duration as well as cell line and DNA (µg) as covariates in order to not distort subsequent regression analyses. The resulting

model yielded satisfactory scores on collinearity ($r = 0.57$) and variance inflation (all multilinear model VIF ≤ 2.12).

Consequences of the preprocessing pipeline on the data structure were assessed by observation of changes with respect to multidimensional scaling, correlation with principal components, and variance partition. Multidimensional scaling plots following the preprocessing procedure indicated that individual stages of differentiation clustered closer together (**Fig. 27a**), but also that cell line remained an influential factor, since it was meant to be addressed as covariate in the regression model (**Fig. 27b**). Within individual stages of differentiation, variance between independent replicates was reduced following batch correction (**Fig. 28**).

The correlation structure of potential predictor variables with principal components presented with overall reduced correlation coefficients between principal components and technical batches after correction (**Fig. 29**). High correlation coefficients were retained between principal components and variables specified in the regression model. In addition, corrected data showed test variables duration loading on PC9 and treatment loading on PC17.

Variance partition plots for EPIC methylation chip and array position show a reduction of variance explained by these factors in the complete data set from up to 75% and 30% before batch correction down to around 30% and 10% after correction, respectively (**Fig. 30**). Within individual stages of neuronal development, reductions were less pronounced. Meanwhile, variance explained by predictor variables stage of differentiation, treatment, and duration was heightened in the corrected data set.
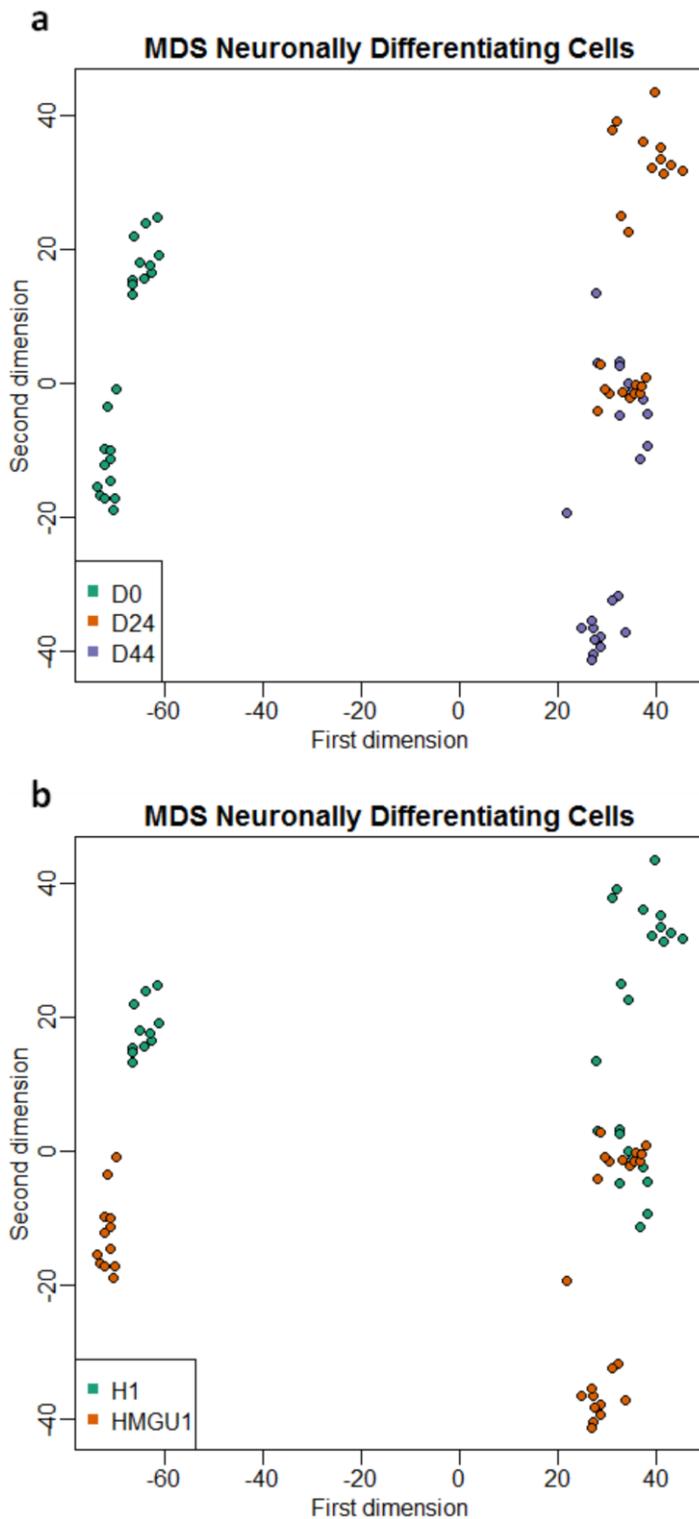
Figure 27. Multidimensional scaling plots (MDS) following batch correction.
SWAN normalised batch-corrected data separating by **a)** differentiation stage and
b) cell line (N=70 samples; n=792 780 probes).

combat corrected betas
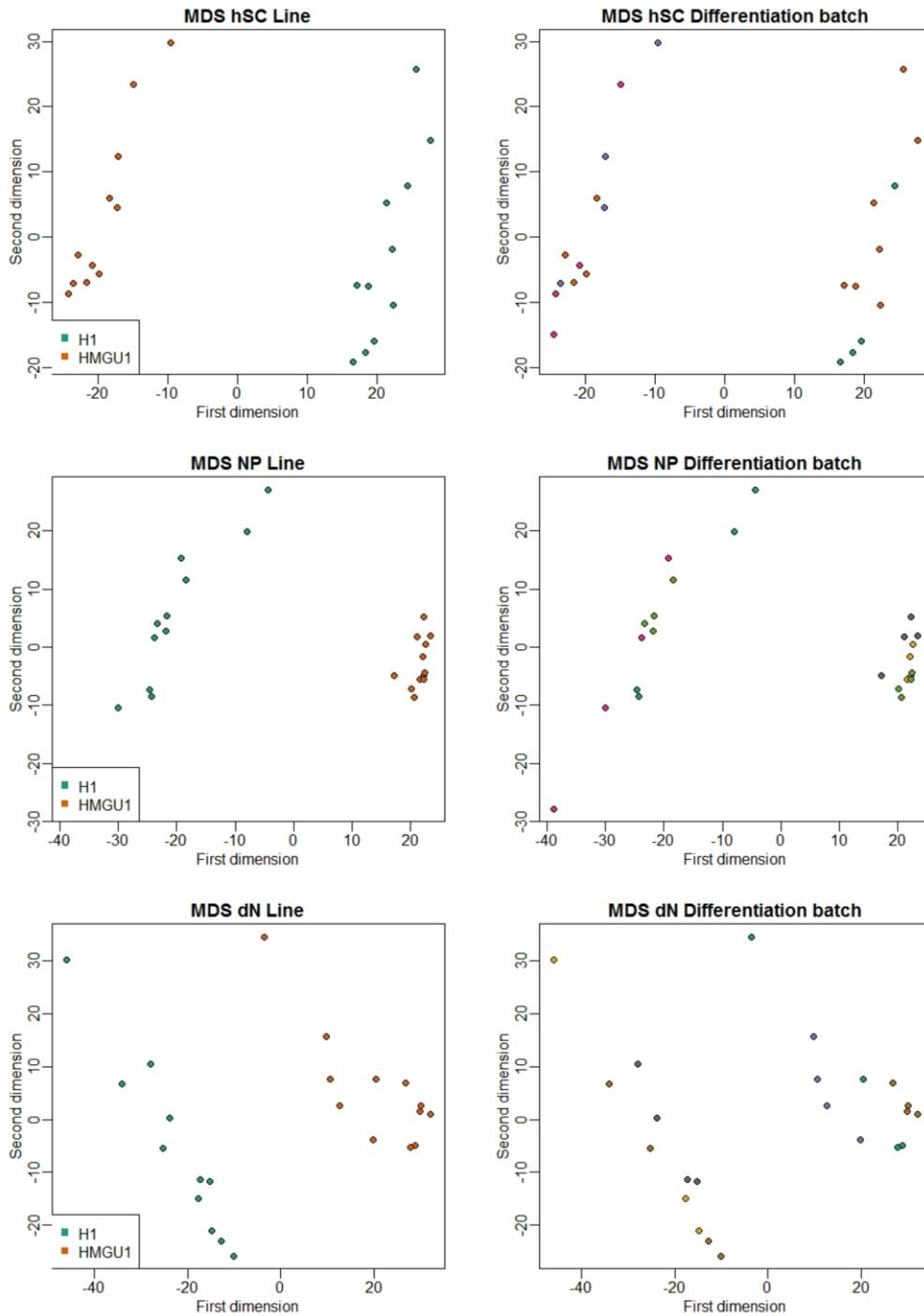
Figure 28. Multidimensional scaling plots (MDS) for individual stages of differentiation. SWAN normalised batch-corrected data (N=70, n=792 780 probes).
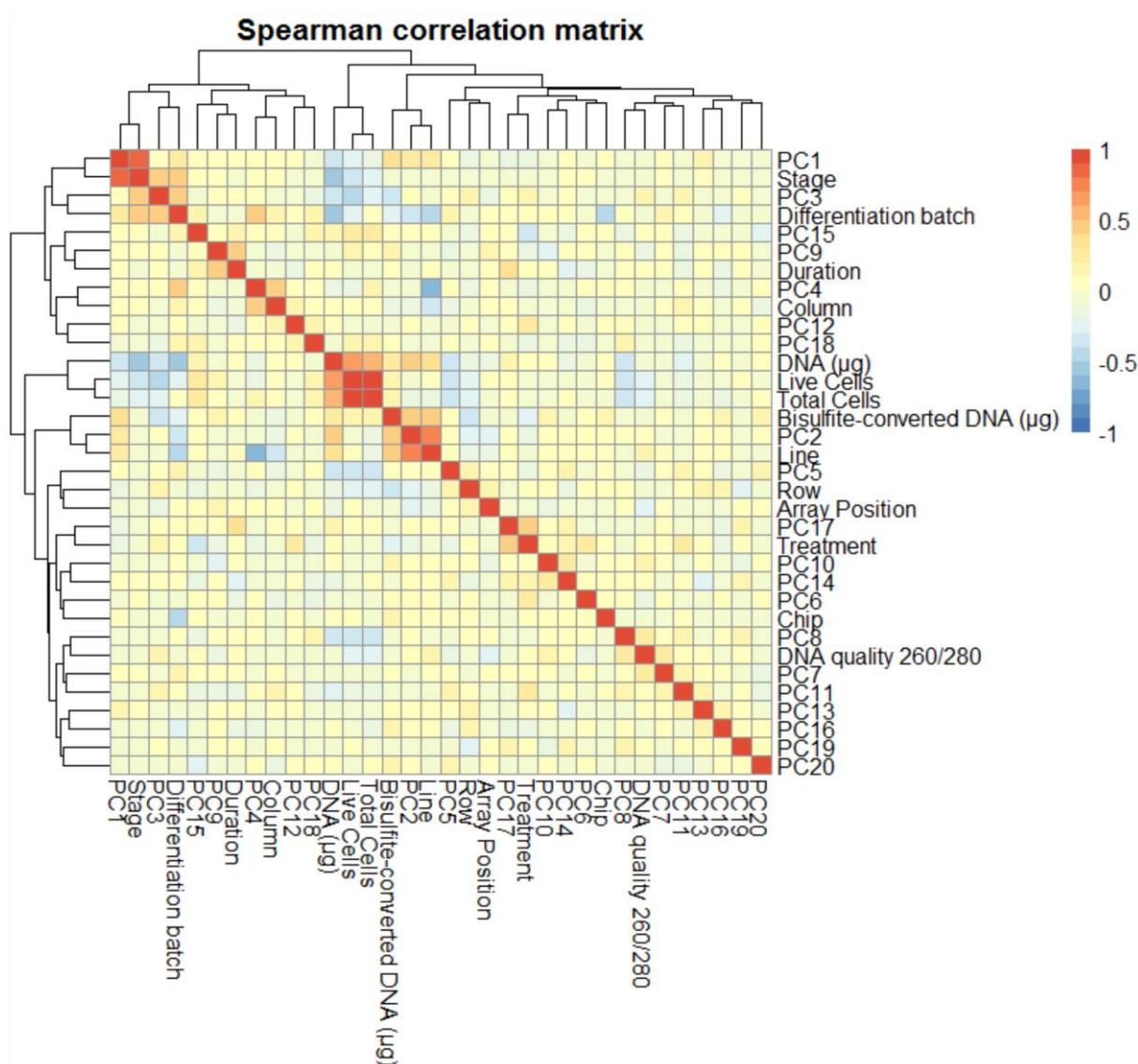
Figure 29. Correlation matrix between PCA 1-20 and potential predictor variables following batch correction. SWAN normalised batch-corrected data (N=70 samples; n=792 780 probes).
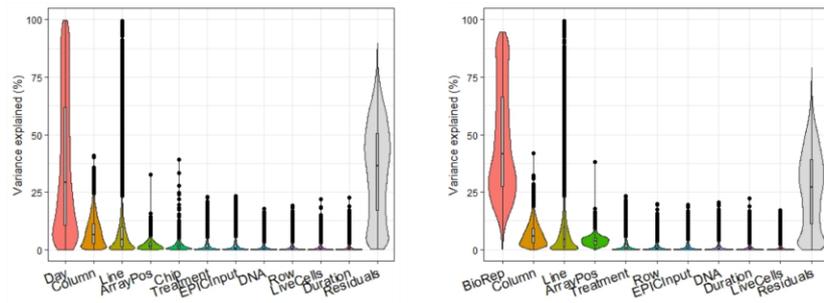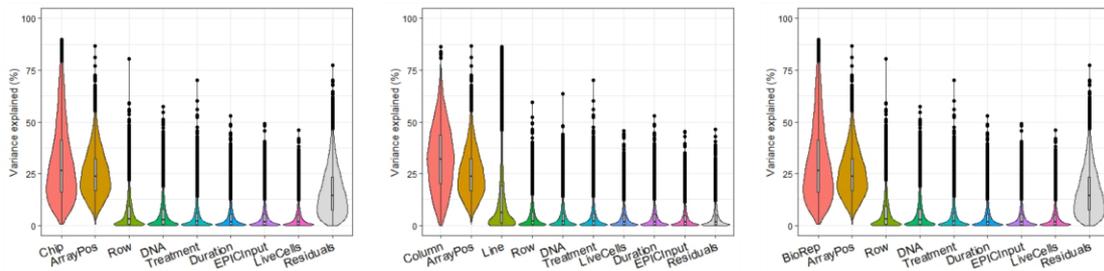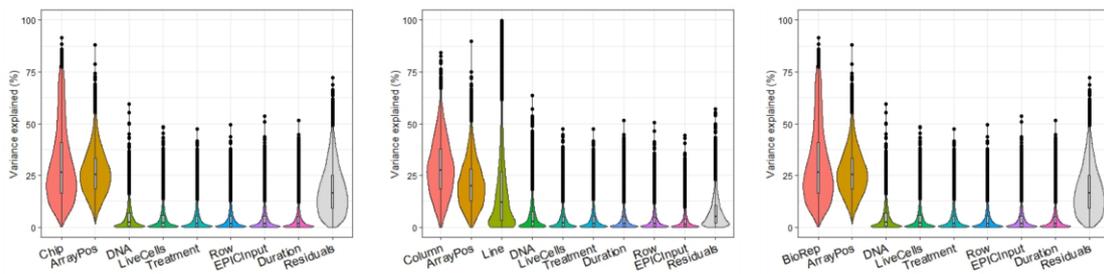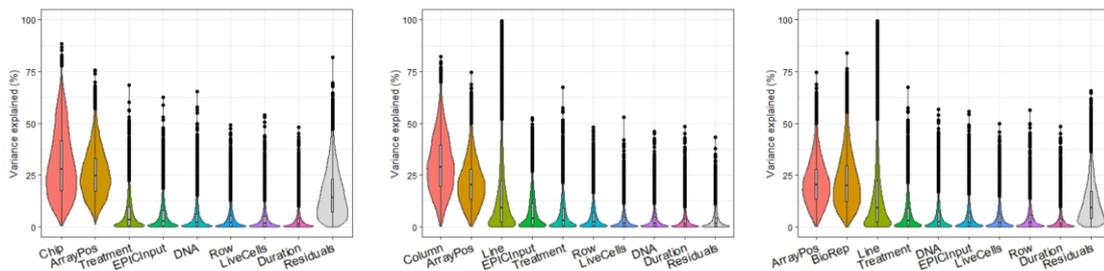
Figure 30. Variance partition following combat correction (N=70 samples; n=10 000 probes). Chip = EPIC methylation chip, ArrayPos = sentrix position, LiveCells = number of living cells, DNA = DNA input amount for bisulfite conversion, EPICInput = amount of bisulfite-converted DNA.

In order to confirm that the preprocessing procedure indeed served the intended purpose of unmasking effects by reducing error variance rather than introducing bias itself, supplementary analyses were performed and are described in detail in section 7.1 Supplementary Analyses.

Differential methylation analyses were conducted using the limma package and differentially methylated probes identified by contrasts. Probes were annotated with the IlluminaHumanMethylationEPICanno.ilm10b2.hg19 package and uniquely assigned to the closest gene 500 base pairs (bp) upstream or downstream of the probe (UCSC knownGene, hg19) with ChIPseeker (Yu et al., 2015). First, differential methylation was computed between the hSC and NP stage as well as between NPs and dNs in unstimulated samples to account for global events of consecutive methylation and demethylation. Probes were considered differentially methylated at beta changes over 10% and q-values ≤ 0.01. Analyses of dexamethasone response were carried out for each of the three developmental stages separately. Because there were no differentially methylated probes between cells stimulated for 6h or 12h in any of the stages of differentiation (FDR = 5%), time points were collapsed into a single treatment variable for analyses of treatment effect. Primary analyses were carried out at the level of individual probes and considered significant at the conventional FDR-cutoff of $q ≤ 0.1$ and a change in methylation beta values of at least 5%. A second cutoff was set at $q ≤ 0.05$ in order to reduce results for presentation in the print part of this thesis.

Where ranges were required in downstream analyses, differentially methylated regions consisting of at least two probes within no more than 1000 nucleotides distance between each other were computed with the DMRcate package

making use of the design and contrast matrices from limma analyses. FDR-cutoffs were set at $q \leq 0.01$ and mean beta changes $\geq 10\%$ for contrasts between stages of differentiation and $q \leq 0.1$ and mean beta changes $\geq 3\%$ for contrasts between treated and untreated samples, respectively. Where both contrasts are displayed in the same graph, the higher cutoff was applied. Secondary analyses on differentially methylated regions were conducted for dexamethasone treatment effect and visualized using the Gviz package with gene region track annotations (refGene, hg19) retrieved from the UCSC website (http://genome.ucsc.edu/cgi-bin/hgTables?command=start).

Functional Enrichment Analyses. Gene set enrichment analyses for differentially methylated regions were carried out using the rGREAT toolbox (McLean et al., 2010) and the GeneCodis3 online tool (Carmona-Saez et al., 2007; Nogales-Cadenas et al., 2009; Tabas-Madrid et al., 2012). For contrasts between stages of neuronal differentiation, DMRs with q-values ≤ 0.01 and beta changes over 10% were considered in the analyses, for comparisons between DEX-stimulated and unstimulated cells q-values ≤ 0.1 without restrictions on beta cutoffs. Enrichment for DMRs between stages of differentiation were conducted separately for DNAm gains and losses. Following recommendations for different sample sizes of tested gene sets, the hypergeometric test was used to assess functional enrichment of DEX-dependent DMRs, and the binomial test for DMRs between stages of differentiation which covered a larger proportion of the genome (Rivals et al., 2006).

Enrichment Analyses for Chromatin States and Glucocorticoid Response Elements. Differentially methylated regions between differentiation stages ($q \leq 0.01$) were analysed regarding enrichment or depletion for chromHMM states using

Fisher's exact test. A cutoff on changes in beta values was omitted due to the special role of bivalent and poised chromatin states in neuronal differentiation (Hirabayashi & Gotoh, 2010), where even small changes may have major impact. An in-house compiled set of chromHMM states for hiPSC, hESC, brain, and neurospheres was used as reference for enrichment analyses. Fisher's exact test was also applied to examine overrepresentation of blood Glucocorticoid Response Elements in DMRs between differentiation stages and following dexamethasone stimulation ($q \leq 0.1$, beta change $\geq 3\%$).

3.12 BIOSTATISTICAL ANALYSES OF DIFFERENTIAL GENE TRANSCRIPTION

RNA-Seq analyses were conducted for the 3h and 12h stimulation conditions due to having shown most DEX-regulated genes across stages of differentiation in the pilot study. Sequencing was performed on a HiSeq4000 system generating 8 million 100 bp reads per sample on average. Quality control of sequencing data was performed by FASTQC version 0.11.4 (Andrews et al., 2010) and reads subsequently trimmed with cutadapt version 1.11 (Martin, 2011). Read maps were aligned to RefSeq (GRCh38) and transcript expression quantified with Salmon 0.11.3 (Patro et al., 2017). Non-default salmon parameters --noLengthCorrection and –perTranscriptPrior were set due to the 3'prime tag library preparation approach. The R package tximport (Soneson et al., 2015) was used to summarise transcript quantification to gene level resulting in n = 28 764 genes in total. In contrast to conventional array analysis pipelines, analyses of differential gene expression in RNA-Seq data rely on unnormalized raw counts as input, performing normalization in conjunction with the analysis and estimating measurement precision within the

algorithm (Love et al., 2014). Visualization of RNA-Seq data however requires normalised read counts. Thus, normalisation was performed by variance stabilizing transformation implicated in the DESeq2 package (Love et al., 2014).

RNA-Seq data structure was evaluated using MDS plots and analyses of variance partition. One biological replicate of differentiated neurons showed unusual clustering on the mRNA level and was omitted from transcriptome analyses (**Supplementary Fig. 7**). The remaining dataset consisted of N = 68 samples.

The complete data set separated into clusters demarcating the stage of differentiation (**Fig. 31**). Variance in hSC was minimal and remained low despite progressively increasing with ongoing neuronal differentiation.
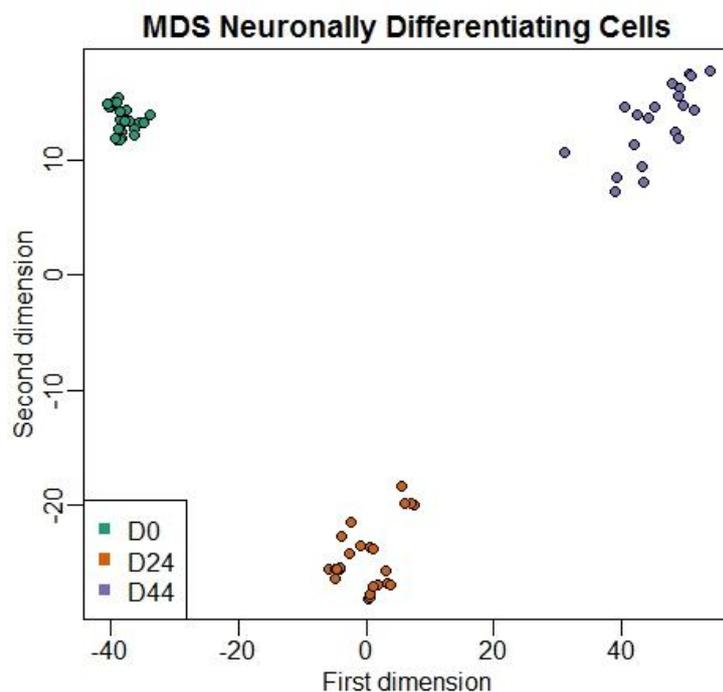
Figure 31. Multidimensional scaling plot of mRNA-Seq data (stage of differentiation). Read counts normalised by variance stabilizing transformation, N=68 samples, n=28 764 genes.
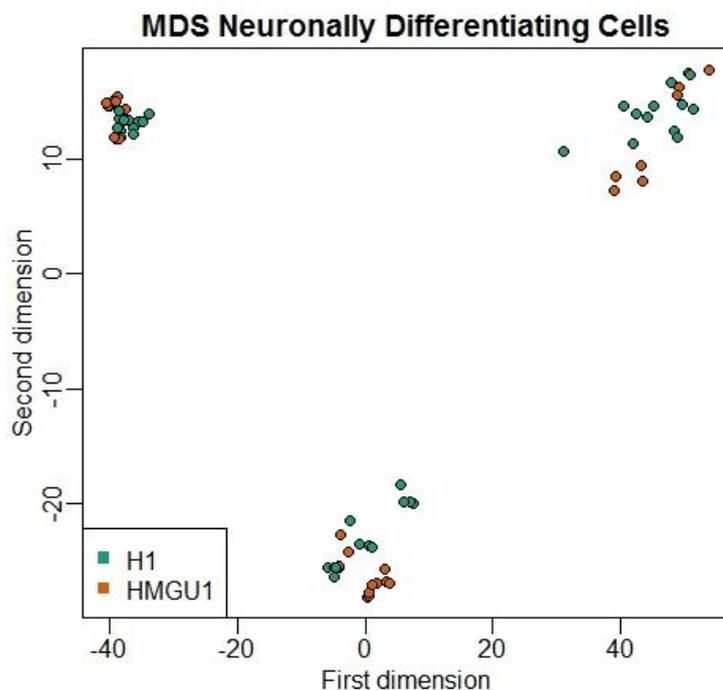
Figure 32. Multidimensional scaling plot of mRNA-Seq data (cell line). Read counts normalised by variance stabilizing transformation**,** N=68 samples, n=28 764 genes.

Contrasting methylation data, cell line was not a defining factor of the first two dimensions in the RNA-Seq data set (**Fig. 32**).

At the level of individual stages of differentiation however, samples separated by cell line in undifferentiated hiPS and ES cells (**Fig. 33**). With ongoing differentiation to neuronal progenitors and neurons, the influence of cell line decreased, whereas overall variance increased leaving no clear separation along the first and second dimension. Thus, in neuronal progenitors and neurons, study samples were best discriminated by the individual differentiation batch or biological replicate.

Because variance in RNA-Seq data is estimated directly from raw counts in any particular analysis of differential gene expression, variance partition plots are given for data subsets that contrasts were run on, respectively (**Fig. 34**).

In the unstimulated subset used to compare stages of differentiation, the highest percentage of variance was explained by day (i.e. stage of differentiation), whereas error variance was mostly caused by individual differences between differentiation batches (i.e. independent replicates) followed by row, column, and cell line.

Biological replicate, row and column also had the highest percentages of explained error variance in dexamethasone treatment subsets, followed by cell line and number of live cells. Potential biases were controlled for by randomisation for row and column, and by parallelisation for treatment and duration within a biological replicate and cell line. The number of live cells was not significantly different between stimulated and unstimulated samples in any of the test sets as determined by two-tailed t-test (t = -0.61, p=0.55 (hSC 3h), t = -0.62, p=0.55 (hSC 12h), t = 0.29, p=0.78 (NP 3h), t = 0.44, p=0.66 (NP 12h), t = -0.05, p=0.96 (dN 3h), and t = -0.12, p=0.90 (dN 12h)).

Variance partition showed the highest variance explained by treatment effect in differentiated neurons compared to earlier stages of differentiation.
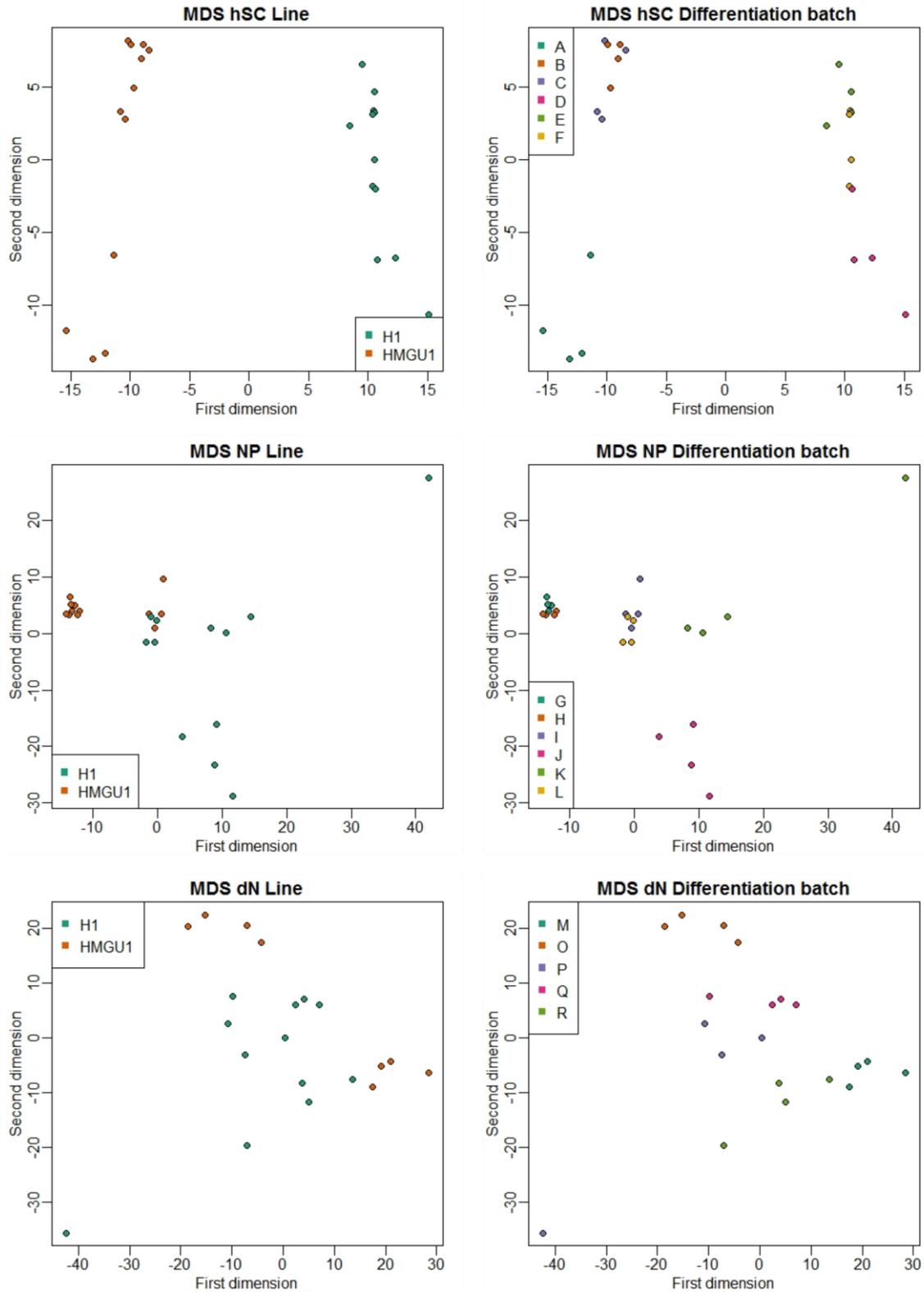
Figure 33. Multidimensional scaling plots (MDS) for individual stages of differentiation. Read counts normalised by variance stabilizing transformation, N=68 samples, n=28 764 genes.
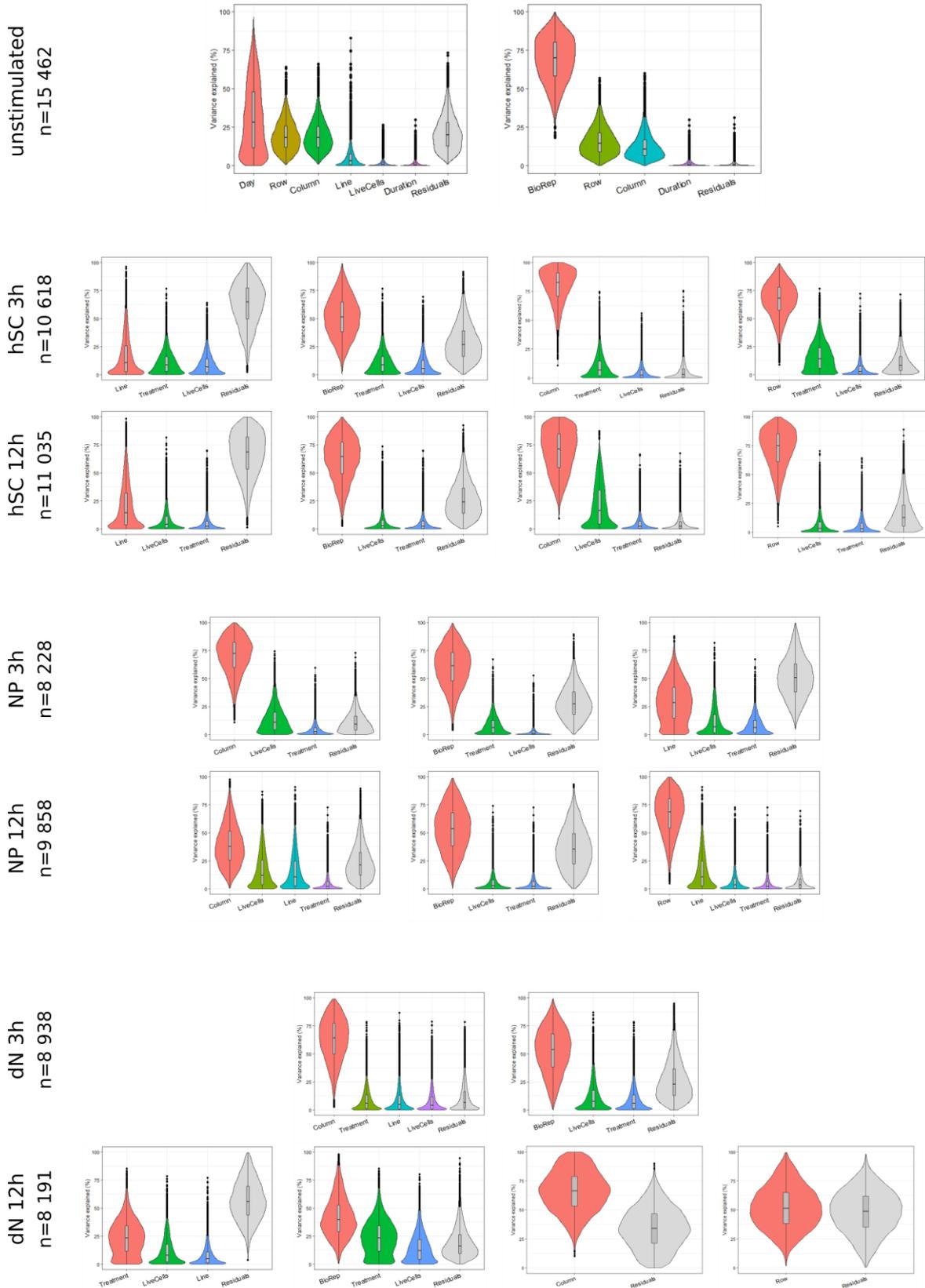
Figure 34. Variance partition plots of RNA-Seq raw count data. Variance partition for genes with counts ≥ 10 in all samples within a subset.

Analyses of differential gene expression were conducted using EBSeq (Leng et al., 2013). Normalisation was performed using the median normalisation procedure (Anders & Huber, 2010) implemented in the package. Results are reported as posterior probabilities for genes to be differentially expressed (PPDE) or equally expressed (PPEE).

Differential gene expression between stages of differentiation was computed with settings for multiple comparisons on unstimulated samples only. Genes quantified in at least one stage of differentiation (i.e., in at least n = 10 samples) at a minimum count of 10 were included in the analysis, comprising n = 15 462 genes. Genes were considered significantly differentially expressed at $\log_2$ fold changes ≥ 1.5 in either the NP compared to hSC or dN compared to hSC conditions and a posterior probability to be differentially expressed of PPDE ≥ 0.99.

Analyses of DEX-induced differential gene expression were carried out within individual stages of differentiation for simple contrasts between stimulated and unstimulated samples for 3h and 12h, respectively. Filtering for genes with counts ≥ 10 in all samples prior to analyses resulted in n = 10 618 (hSC 3h), n = 11 035 (hSC 12h), n = 8 228 (NP 3h), n = 9 858 (NP 12h), n = 8 938 (dN 3h), and n = 8 191 (dN 12h) genes for analyses of treatment effect. The cutoff was set at $q ≤ 0.1$ without restrictions on fold changes.

Functional Enrichment Analyses. Analyses of functional enrichment were performed using enrichr (Chen et al., 2013; Kuleshov et al., 2016), the ConsensusPathwayDB (Kamburov et al., 2010), and The Database for Annotation, Visualization and Integrated Discovery (DAVID) (Sherman & Lempicki, 2009) for differentially expressed genes (DEGs) following dexamethasone stimulation for 3h

and 12h combined in the respective stages of differentiation. Enrichment analyses included all genes with log$_2$ fold changes ≥ 0.5 in the respective contrasts. Cutoffs for significantly enriched terms are indicated in the results section.

4. RESULTS

4.1 *IN VITRO* DIFFERENTIATING CELLS RECAPITULATE EMBRYONIC NEUROGENESIS

Within a matter of days, neuronally differentiating hSCs underwent major changes in morphology, DNAm and transcriptome profiles, as well as protein marker expression. First, hSC and differentiating neuronal cells were characterized by morphology and expression of proteins marking the target cell type (**Fig. 35**).
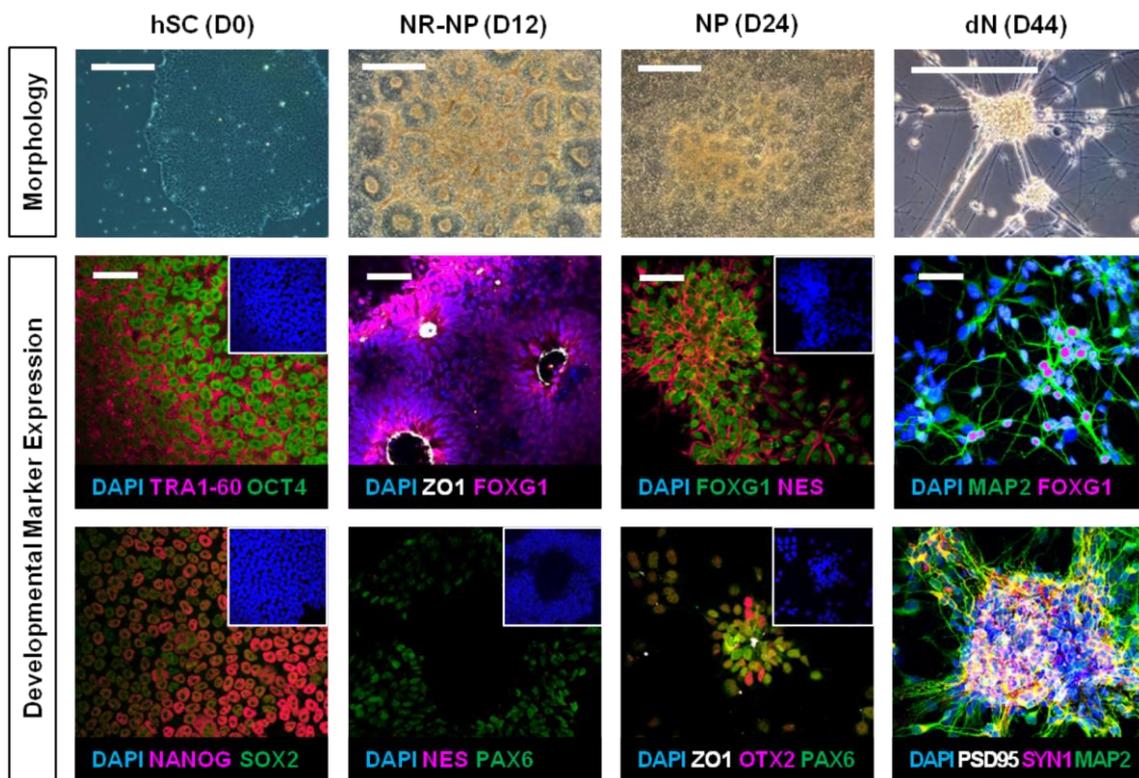
Figure 35. Characterisation of differentiated cell types (morphology & marker protein expression). Morphological transitions under the light microscope (upper panel, scale bars: 1 mm) with marker expression indicating differentiating neural cells of the telencephalon (lower panel, scale bars: 50 μm) in HMGU1 hiPSC. hSC = human stem cells, NR-NP = neural rosette neuronal progenitors, NP = neuronal progenitors, dN = differentiated neurons.

Morphologically, undifferentiated hSC on D0 grew in flat colonies with a smooth surface structure and without contamination by spontaneous differentiation on the margins. Following the plating of embryoid bodies, plated aggregates started to form neural tube-like neural rosettes with large lumen sizes of about 25 µm on average by D12. Lumen sizes decreased with dissociation to single cells, but neural rosette structure remained intact in neural progenitors on D24 of neuronal differentiation. Induction of terminal neuronal differentiation and elimination of differentiating cells resulted in neuronal cultures with minimal contamination by non-target cell types on D44. Neuronal cultures were further characterized by partial formation of interconnected neuronal clusters and neuroblasts migrating between clusters.

In addition, hSC and neuronal derivatives showed characteristic protein marker expression. That is, hSC were positive for OCT4 (instruction to form the ICM), Nanog (formation of the pluripotent epiblast), SOX2 (determination of ectodermal cell fate) and TRA1-60 (formation of initial epithelial polarisation), as major markers of pluripotency. Secondly, neural rosettes on D12 of differentiation were characterized by luminal expression of ZO1 defining the apical side of rosette structure (Elkabetz et al., 2008), lined by expression of FOXG1 indicating anterior forebrain cell fate (Fasano et al., 2009). Meanwhile, expression of PAX6 as marker of both frontal and mid-brain structures (Stoykova et al., 1997) was low and Nestin not yet detectable. On D24 of neuronal differentiation, neural progenitors were positive for both FOXG1 and PAX6 as well as OTX2, which acts in concert with PAX6 to regulate forebrain/midbrain patterning (Kurokawa et al., 2004; Kimura et al., 2005). Expression of ZO1 had progressively decreased and on D24 was restricted to the center of neural rosettes, while Nestin expression had increased above detection

threshold marking intermediate filaments (Lendahl et al., 1990). Neuronal cultures maintained FOXG1 expression at a reduced level. They were characterized by Microtubule Associated Protein 2 (MAP2), which is expressed in dendrites and axons (Chen et al., 1992), as well as Synapsin 1 (SYN1) localized to the pre-synapse (Bennett et al., 1991) and postsynaptic density protein 95 (PSD95) localized to the post-synapse (Irie et al., 1997). In addition, neurons were found to express vesicular Glutamate Transporter 1 (VGLUT1), indicating glutamatergic signaling, but no vesicular GABA Transporter 2 (VGAT2) (**Fig. 36**).
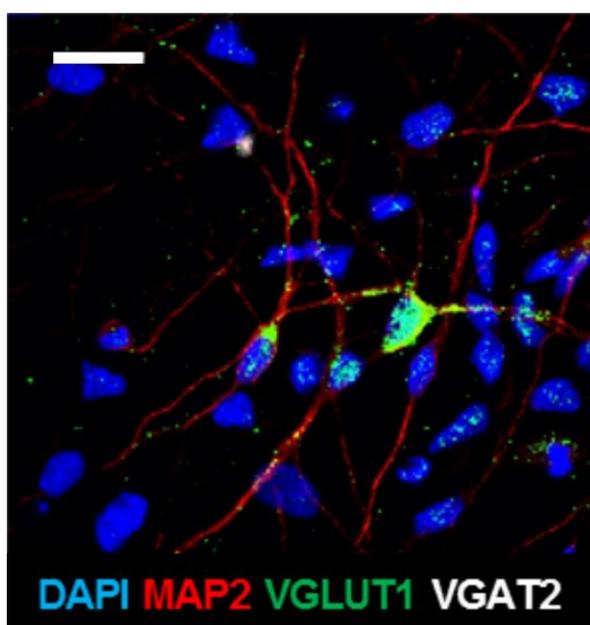
Figure 36. Characterisation of differentiated cell types (neurotransmitter). Differentiated MAP2+ neurons express vesicular transporter proteins for glutamate (VGLUT1), but not for GABA (VGAT2) (scale bar: 10 μm).

Initial characterization of differentiated cell types by protein markers was then corroborated by bioinformatic analyses of gene transcription (**Tables 8 & 9**).

Differential expression was found in a total of n = 9 461 genes between stages of neuronal differentiation.

Table 8. Top 25 gene transcripts with highest fold changes between hSC and NP.

Gene	log$_2$FC			PPEE	PPDE
	hSC Over NP	hSC Over dN	NP Over dN		
ZIC1	**-5.74**	-4.76	0.98	1.03e-157	1
EMX2	**-5.37**	-4.32	1.05	3.44e-41	1
DMRTA2	**-5.15**	-3.40	1.76	7.17e-26	1
C1orf61	**-5.15**	-2.32	2.83	3.49e-26	1
FABP7	**-4.93**	-1.33	3.60	7.81e-56	1
ZNF503	**-4.80**	-2.79	2.01	5.68e-43	1
WNT7B	**-4.67**	-3.50	1.17	4.17e-66	1
NR2F1	**-4.66**	-6.32	-1.66	5.18e-26	1
FAM181B	**-4.62**	-0.14	4.49	9.98e-61	1
POU3F3	**-4.55**	-4.60	-0.05	2.02e-101	1
MAP6	**-4.53**	-5.63	-1.10	2.19e-185	1
FEZF2	**-4.44**	-2.21	2.23	3.88e-36	1
PAX6	**-4.23**	-2.79	1.44	1.17e-53	1
LHX2	**-4.23**	-4.25	-0.02	4.66e-64	1
FOXG1	**-4.17**	-3.18	0.99	4.55e-30	1
CRH	**-4.11**	-3.72	0.39	3.31e-29	1
KLHDC8A	**-4.07**	-1.84	2.24	4.52e-32	1
ISLR2	**-4.07**	-5.71	-1.63	1.32e-83	1
AMER2	**-4.05**	-4.34	-0.29	2.64e-123	1
RSPO3	**-4.01**	-1.60	2.41	4.24e-28	1
DACH1	**-4.01**	-2.80	1.21	1.03e-16	1
ARX	**-3.99**	-0.97	3.02	9.33e-32	1
HES5	**-3.96**	-0.60	3.36	1.19e-33	1
SOX1	**-3.94**	-0.23	3.70	8.79e-45	1
CCDC80	**-3.92**	-2.16	1.76	2.21e-38	1

Annotations. hSC = human stem cells; NP = neuronal progenitor cells; dN = differentiated neurons; log$_2$ FC = log$_2$ fold change, PPEE = posterior probability of equal expression; PPDE = posterior probability of differential expression.

In this hypothesis-free analysis, strongest upregulation was detected for Zic Family Member 1 (*ZIC1*), *EMX2*, and Doublesex- and Mab-3–Related Transcription Factor A2 (*DMRTA2*) in neural progenitors (**Table 8**). Expression of *ZIC1* begins at the neural plate stage, and consecutively shifts with neural tube formation until reaching the most dorsal regions of the developing brain (Rohr et al., 1999).

Functionally, *ZIC1* is implicated in the maintenance of neural progenitor cells in an undifferentiated state (Inoue et al., 2007), as is *DMRTA2* (Konno et al., 2012; Young et al., 2017). Expression of *EMX2* is regulated by Wnt and BMP signaling (Theil et al., 2002) and is specific to the forebrain (Tan et al., 2013), where it is implicated in regional patterning (Yoshida et al., 1997). Fatty Acid-binding Protein 7 (*FABP7*) is a downstream target of transcription factor *PAX6* (Arai et al., 2005), which was equally among the most strongly upregulated transcripts. With *FOXG1*, another marker used for characterisation by immunocytochemistry was confirmed as one of the genes with highest induction upon neuronal differentiation. Further genes with known roles in forebrain specification were *WNT7B* (Garda et al., 2002), Forebrain Embryonic Zinc Finger-Like Protein 2 (*FEZF2*) (Zhang et al., 2014), LIM Homeobox 2 (*LHX2*) (Porter et al., 1997), Immunoglobulin Superfamily Containing Leucine Rich Repeat 2 (*ISLR2*) (Abudureyimu et al., 2018), Aristaless Related Homeobox (*ARX*) (Kitamura et al., 2002), and SRY-box 1 (SOX1) (Ekonomou et al., 2005), with some of these genes presumed to act in concert. For example, LHX2 was found to affect the number of layer 5 *FEZF2*-expressing neurons (Muralidharan et al., 2017).

Some of the genes with highest increases in transcript levels were furthermore found to be specific to neural rosette neuronal progenitors, such as Dachshund Family Transcription Factor 1 (*DACH1*) and Nuclear Receptor Subfamily 2 Group F Member 1 (*NR2F1*), while some were found in both neural rosettes and neural stem cells, such as *ZIC1*, *FABP7*, *LHX2*, POU Class 3 Homeobox 3 (*POU3F3*), *SOX1*, Chromosome 1 Open Reading Frame 61 (*C1orf61*). and *ARX* (Elkabetz et al., 2008).

In addition, three of the most strongly upregulated transcripts had equally been among the top 25 highest expressed genes in neuronal progenitors with an

overall posterior profile in the pilot study. These genes indicating pan-neuronal progenitor properties were Hes Family BHLH Transcription Factor 5 (*HES5*), *FABP7*, and *C1orf61*.

Table 9. Top 25 gene transcripts with highest fold changes between hSC and dN.

Gene	log$_2$FC			PPEE	PPDE
	hSC Over NP	hSC Over dN	NP Over dN		
MAPT	-2.61	**-6.86**	-4.25	1.81e-169	1
STMN4	-3.73	**-6.77**	-3.04	2.50e-130	1
NSG2	-2.55	**-6.65**	-4.11	2.68e-131	1
SCG2	-1.84	**-6.63**	-4.78	8.75e-46	1
NR2F1	-4.66	**-6.32**	-1.66	5.18e-26	1
CELF3	-3.63	**-6.20**	-2.57	1.76e-267	1
APC2	-3.65	**-6.15**	-2.50	9.83e-81	1
DCX	-3.07	**-6.13**	-3.06	3.91e-113	1
ELAVL3	-4.17	**-6.06**	-1.89	1.24e-237	1
GPM6A	-3.81	**-6.04**	-2.23	4.94e-311	1
LHX9	-2.52	**-5.99**	-3.47	6.55e-70	1
NCAM1	-2.94	**-5.92**	-2.98	1.25e-169	1
SCN3A	-2.60	**-5.90**	-3.30	9.87e-145	1
CDK5R2	-2.24	**-5.83**	-3.59	1.62e-52	1
THSD7A	-2.23	**-5.77**	-3.54	5.98e-50	1
RELN	-2.42	**-5.76**	-3.35	1.94e-45	1
MAP2	-3.66	**-5.71**	-2.05	6.22e-174	1
ISLR2	-4.07	**-5.71**	-1.63	1.32e-83	1
NR2F2	-3.91	**-5.65**	-1.74	1.73e-19	1
MAP6	-4.53	**-5.63**	-1.10	2.19e-185	1
SLIT1	-3.27	**-5.56**	-2.29	4.97e-28	1
SCN3B	-1.80	**-5.44**	-3.64	2.11e-57	1
DNER	-2.75	**-5.43**	-2.68	3.55e-66	1
SLC17A6	-2.08	**-5.42**	-3.35	5.90e-47	1
ELAVL4	-3.82	**-5.41**	-1.58	2.79e-92	1

Annotations. hSC = human stem cells; NP = neuronal progenitor cells; dN = differentiated neurons; log$_2$ FC = log$_2$ fold change, PPEE = posterior probability of equal expression; PPDE = posterior probability of differential expression.

Meanwhile, neurons on D44 of differentiation (**Table 9**) were characterised by gene transcripts associated with the establishment and stabilization of the cytoskeleton, such as Microtubule-Associated Protein Tau (*MAPT*), Microtubule-Associated Protein 2 (*MAP2*), Microtubule-Associated Protein 6 (*MAP6*), Stathmin 4

(*STMN4*), and Doublecortin (*DCX*). While *MAPT* and *MAP2* promote microtubule assembly and stability (Goedert et al., 1991), members of the stathmin family destabilize microtubules, thus enabling reorganization of the cytoskeleton (Charbaut et al., 2001).

Other genes like *GPM6A* are implicated in filopodium formation (Brocco et al., 2010) and cell migration (Michibata et al., 2009). Also, Neural Cell Adhesion Molecule 1 (*NCAM1*) affects migration by reducing cell adhesion (Petridis et al., 2004), whereas Reelin (*RELN*) inhibits neuronal migration (Dulabon et al., 2000) and Slit Guidance Ligand 1 (*SLIT1*) regulates midline crossing of migrating neurons (Plump et al., 2002).

Top upregulated gene transcripts furthermore pointed to glutamatergic signaling as primary neurotransmitter system in differentiated neurons. Concomitant with positive immunocytochemistry results for VGLUT1, one of these gene transcripts was *SLC17A6*, the gene encoding for VGLUT1. Further upregulated transcripts were ELAV Like RNA Binding Protein 3 (*ELAVL3*) and 4 (*ELAVL4*), which control glutamate levels (Ince-Dunn et al., 2012) and Neuronal Vesicle Trafficking Associated 2 (*NSG2*), which encodes for one of the most abundant nervous system proteins during perinatal development and interacts with AMPA receptor subunits (Chander et al., 2019). Additionally, upregulation was found for Sodium Voltage-Gated Channel Alpha Subunit 3 (*SCN3A*) and Sodium Voltage-Gated Channel Beta Subunit 3 (*SCN3B*), which are implicated in the regulation of action potential generation (Holland et al., 2008; Baum et al., 2014).

Lastly, the transcript for corticotropin releasing hormone (*CRH*), an important agent of HPA axis regulation, was also among the most strongly

upregulated genes in both neural progenitors and neurons compared to undifferentiated hSC (**Fig. 37**). This was despite the fact that analyses were run on unstimulated samples only.

The complete list of genes regulated during neuronal differentiation can be found in **Supplementary Table 1**. The top 100 most significantly regulated gene transcripts are additionally depicted in **Figure 37**.
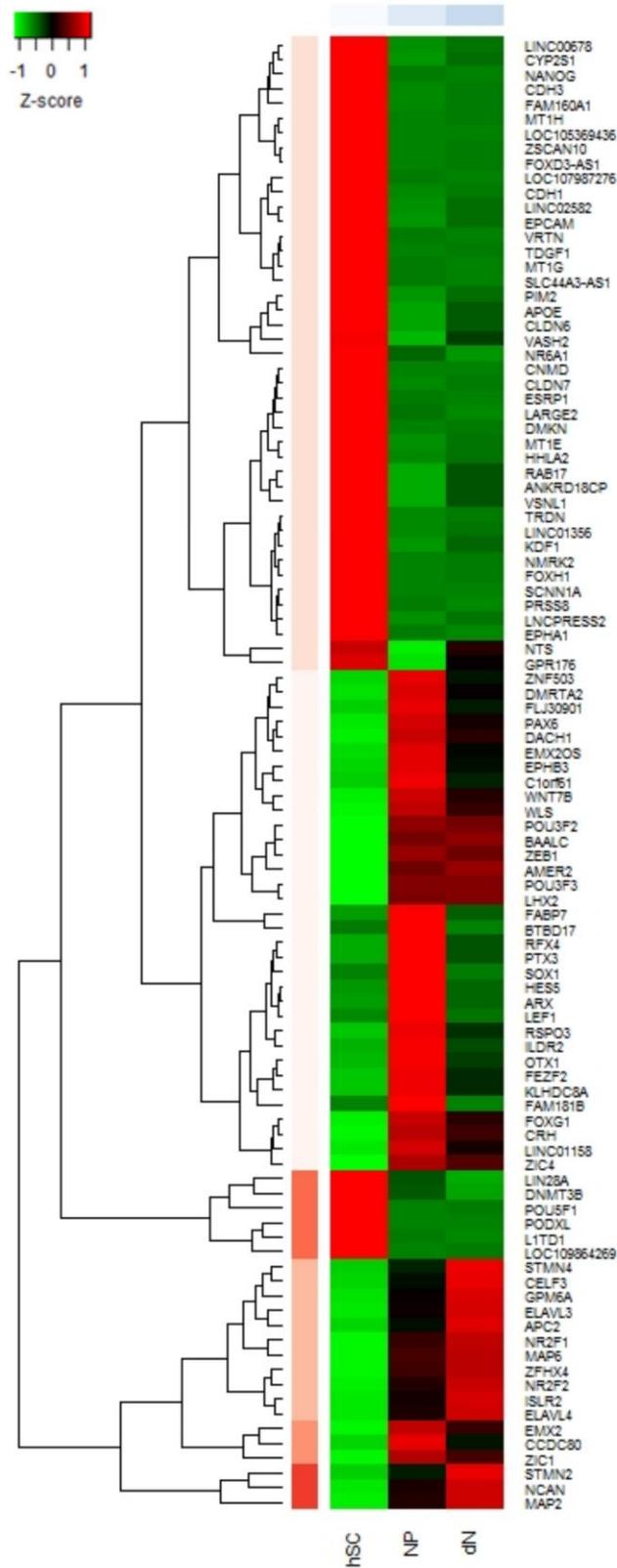
Figure 37. Top 100 most significantly differentially expressed genes between stages of differentiation.

Principal component analysis with publically available brain transcriptome data sets showed a developmental trajectory stretching from stem cells and induced pluripotent stem cells as the earliest possible cell types over stages of germinal zone development to prenatal samples and ultimately postnatal brain samples (**Fig. 38**).
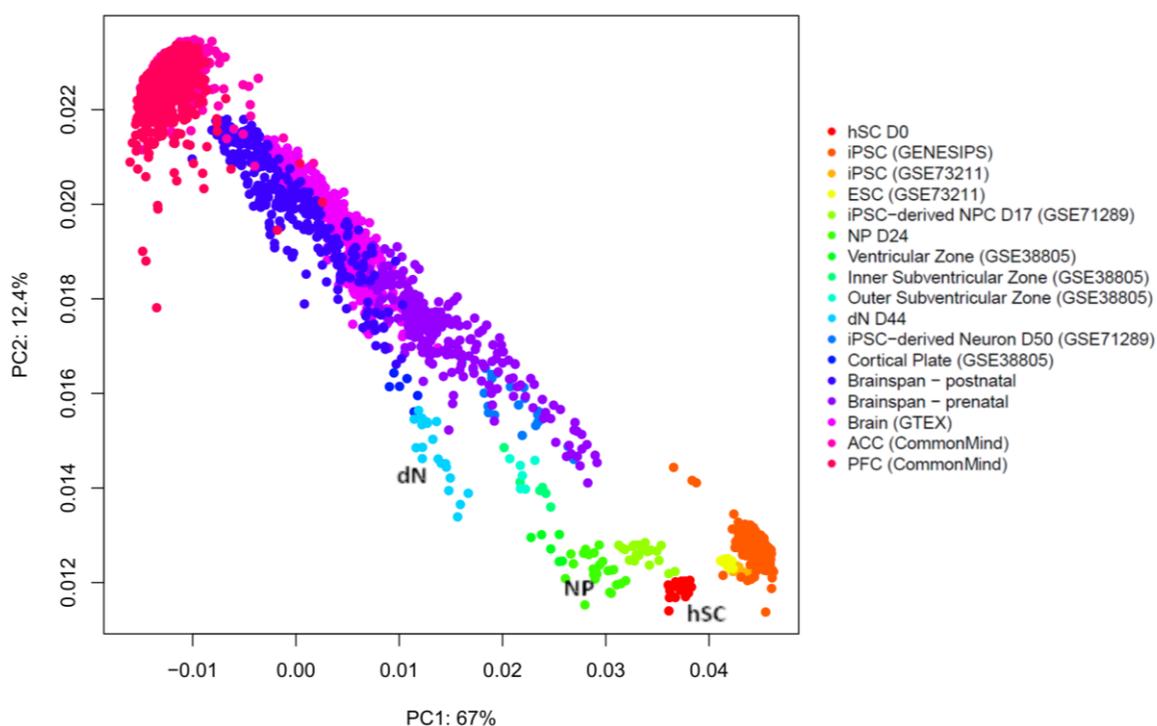
Figure 38. Neuronally differentiating cells recapitulate embryonic neurogenesis from E 3.5 to PCW 8-16. Principal component plot of transcript expression in differentiated neuronal cells and publically available data sets of stem cells, induced pluripotent stem cells, human brain and *in vitro* neuronally differentiated cells.

Although germinal zone data was obtained from foetal brain 13-16 weeks post-conception (Fietz et al., 2012), individual layers formed noticeably distinct clusters within the temporal trajectory. Neuronal progenitors (D24) grouped with the ventricular zone and a published set of D17 iPSC-derived NPC, as should be

expected, while differentiated neurons (D44) mapped between the outer subventricular zone and the cortical plate, lining up in parallel to D50 iPSC-derived neurons and the younger stages of prenatal brainspan samples starting at eight weeks post-conception.

Finally, neuronally differentiated cells underwent characterization by assessment of consecutive changes in DNA methylation profiles.

A cluster dendrogram computed from DNAm data of neurulating cells shows the underlying similarity structure of the dataset (**Fig. 39**).
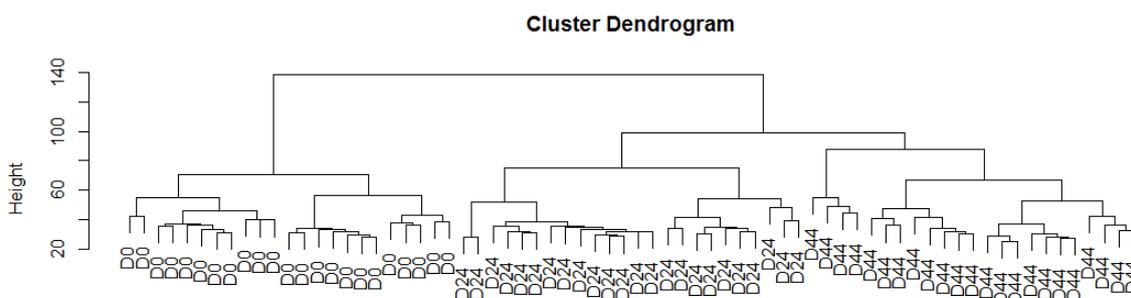
Figure 39. Cluster dendrogram of differentiated cells. Normalized and batch-corrected methylation beta values (N=70, n=792 780 probes).

The two major clusters are formed by hSC and neural cells, the latter being comprised of D24 progenitors and D44 neurons. The structure reflects the relative reduction in DNAm dynamics during terminal differentiation compared to initial commitment to neuroectoderm fate (Mohn et al., 2008). A dendrogram computed on normalized data before batch correction confirmed it had not been altered during preprocessing (**Supplementary Fig. 6**).

Overall, there were n=88 122 differentially methylated positions or n=11 784 differentially methylated regions between undifferentiated hSC and neuronal progenitor cells (**Supplementary Table 2**), and n=34 998 differentially methylated positions, respectively n=3 080 differentially methylated regions between neuronal progenitor cells and neurons (**Supplementary Table 3**), approximating orders of magnitude reported in the Epigenome Roadmap Project (Ziller et al., 2015).

The number of differentially methylated positions that either lost or gained in DNAm between consecutive stages of differentiation ($q \leq 0.01$, beta change $\geq$ 10%) is depicted in venn diagrams (**Fig. 40**). Predominant loss in DNAm during the transition from hSC to NP and predominant gain during terminal neuronal differentiation was consistent with neuroectoderm differentiation (Gifford et al., 2013).
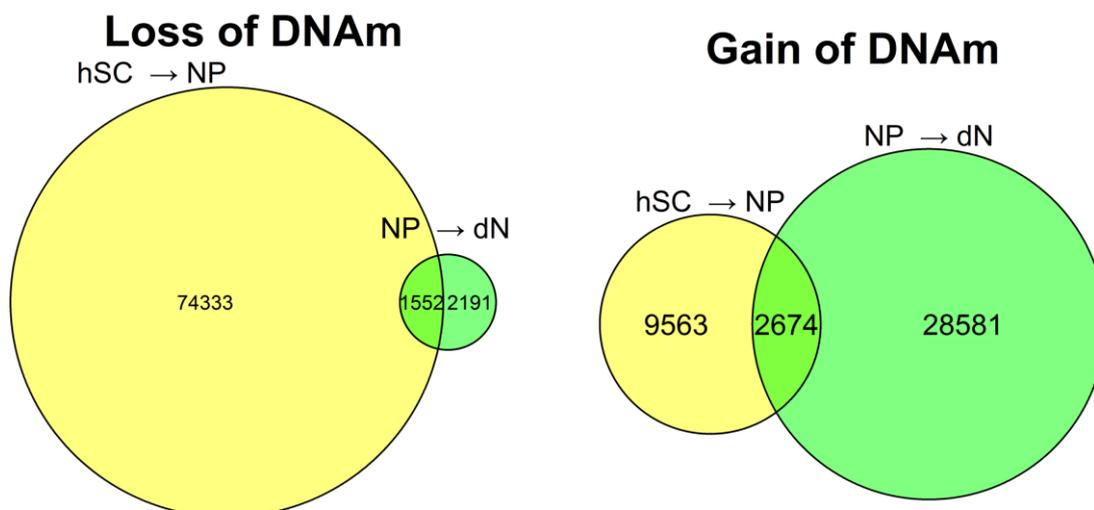
Figure 40. Venn diagrams showing overlaps in gains and losses in DNAm over the course of neuronal differentiation. Based on differentially methylated

positions between hSC and NP, and NP and dN, respectively (beta change ≥ 10%, *q* ≤ 0.01).

It is noteworthy that only a fraction of the sites underwent gradual increases (↗) (n=2 674) or decreases (↘) (n=1 552) in methylation, indicated by small overlaps in the venn diagrams. Indeed, the majority of DMPs switched methylation status only once during differentiation, indicated in the bar plot as ↓ (n=76 524) or ↑ (n=12 421). A U-shaped pattern was the third most common methylation trajectory (n=17 423), while sites that gained DNAm during neural differentiation rarely proceeded to lose it again (n=31) (**Fig. 41**).
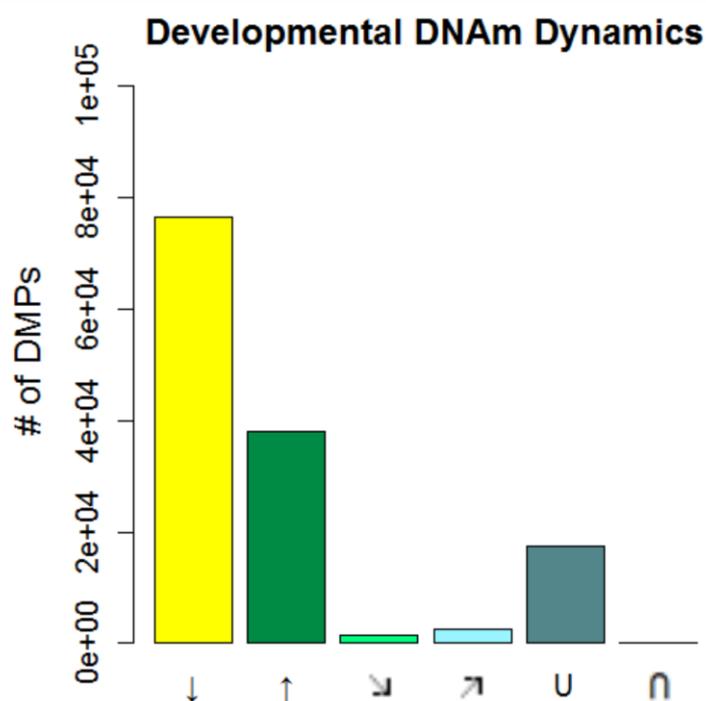
Figure 41. DNAm trajectories over the course of neuronal differentiation. Based on differentially methylated positions between hSC, NP, and dN (beta change ≥ 10%, *q* ≤ 0.01).

The top 25 most significantly differentially methylated positions between consecutive stages of neuronal differentiation are shown in **Tables 10 & 11**.

Table 10. Top 25 most significantly regulated DMPs between hSC and NP.

ILMN probe	UCSC hg19 gene (-500, +500 bp)	Chr	position	$\log_2$ beta FC	*p*-value	*q*-value
cg09511421	NDST4	chr4	116034871	-0.81	3.05E-88	2.42E-82
cg06214213	ATG4C	chr1	63476757	-0.84	4.85E-84	1.92E-78
cg23344761	DAB1	chr1	58525591	-0.79	1.76E-82	4.66E-77
cg03233918	NKX6-1	chr4	84991657	-0.80	3.24E-81	6.42E-76
cg19039481	ALKAL2	chr2	394115	-0.80	5.52E-81	8.74E-76
cg21216522	MCF2L	chr13	113656041	-0.72	7.80E-81	1.03E-75
cg09740450	SCARB1	chr12	125223650	-0.82	1.11E-80	1.26E-75
cg17290371	LINC00861	chr8	126781197	-0.81	2.33E-80	2.31E-75
cg14081465	SNORA70C	chr9	119722239	-0.86	5.47E-80	4.81E-75
cg07279442	SLC12A8	chr3	124848635	-0.71	3.33E-79	2.40E-74
cg26217483	MCF2L	chr13	113656010	-0.76	3.26E-79	2.40E-74
cg02593989	HK2	chr2	75064185	0.82	8.08E-79	5.34E-74
cg08917985	COMMD9	chr11	36300646	-0.82	1.00E-78	6.12E-74
cg05256043	DCT	chr13	95131951	-0.80	4.37E-78	2.48E-73
cg12166819	NCALD	chr8	102962229	-0.77	6.62E-78	3.50E-73
cg05947357	GRIK4	chr11	120703894	-0.68	1.08E-77	5.01E-73
cg14568259	MIR181A2HG	chr9	127421654	-0.74	1.07E-77	5.01E-73
cg07759833	LINC00284	chr13	44619208	-0.78	2.30E-77	1.01E-72
cg03623878	MCF2L	chr13	113655560	-0.70	2.62E-77	1.09E-72
cg23805719	SH2B2	chr7	101773510	-0.82	3.59E-77	1.42E-72
cg09799980	CCND2	chr12	4398618	-0.82	3.82E-77	1.44E-72
cg14042988	THBS1	chr15	39719453	-0.76	6.22E-77	2.15E-72
cg16721359	MTDH	chr8	98610787	-0.73	5.97E-77	2.15E-72
cg03264106	ZNF532	chr18	56510609	-0.71	1.59E-76	5.25E-72
cg19376097	FAT1	chr4	187765617	-0.81	1.91E-76	6.04E-72

Annotations. ILMN probe = Illumina methylation probe; UCSC hg19 gene (-500, +500 bp) = UCSC hg19 closest annotated gene name 500 bp upstream or downstream of the probe; chr = chromosome; $\log_2$ beta FC = $\log_2$ beta fold change, *q*-value = FDR-corrected *p*-value.

During transition from the undifferentiated state to neural progenitors, probes that exhibited the most significant changes exclusively underwent a loss in DNAm (**Table 10**). Probes closest to N-Deacetylase And N-Sulfotransferase 4 (*NDST4*), implicated in neural lineage commitment (Oikari et al., 2016), Autophagy Related 4C Cysteine Peptidase (*ATG4C*), associated with folic acid and GR-mediated

pathways important in brain formation (Sun et al., 2016) and DAB Adaptor Protein 1 (*DAB1*), regulating migration in close interaction with Reelin (Franco et al., 2011) were found to be most significantly demethylated.

Further strongly demethylated probes were annotated to NK6 Homeobox 1 (*NKX6-1*), which is implicated in ventral neural tube progenitor fate specification (Briscoe et al., 2000), ALK And LTK Ligand 2 (*ALKAL2*), which has a role in neural crest development (Fadeev et al., 2018, Vieceli & Bronner, 2018), and MCF2 Transforming Sequence-Like Protein (*MCF2L*), known to become demethylated during embryonic mouse brain development (Hirabayashi et al., 2013). Other genes close to hypomethylated probes had similar functions. For instance, COMM Domain-Containing Protein 9 (*COMMD9*) modulating Notch signaling (Li et al., 2015) or Protocadherin Fat 1 (*FAT1*) regulating neural progenitor proliferation and neural tube closure (Badouel et al., 2015).

During terminal differentiation from neuronal progenitors to neurons, probes most significantly regulated were exclusively hypermethylated (**Table 11**). Three of these probes were annotated to Stimulated By Retinoic Acid 6 (*STRA6*), a gene encoding for a retinoic acid receptor protein (Bouillet et al., 1997) and two for Intercellular adhesion molecule 3 (*ICAM3*), which is involved in the removal of apoptotic cells (Torr et al., 2012). Overall, many hypermethylated probes were located in the vicinity of genes regulating cell cycle progression and proliferation, such as Lemur Tyrosine Kinase 3 (*LMTK3*) (Giamas et al., 2011), Endothelin Converting Enzyme 1 (*ECE1*) (Awano et al., 2006), and ER Lipid Raft Associated 2 (*ERLIN2*) (Zhang et al., 2015).

Table 11. Top 25 most significantly regulated DMPs between NP and dN.

ILMN probe	UCSC hg19 gene (-500, +500 bp)	Chr	position	$\log_2$ beta FC	*p*-value	*q*-value
cg14275207	STRA6	chr15	74495401	0.47	1.88E-61	1.49E-55
cg19949931	MIR1225	chr16	2141745	0.45	6.95E-57	2.76E-51
cg18717554	STRA6	chr15	74495119	0.46	1.84E-56	4.85E-51
cg18418538	LMTK3	chr19	48997000	0.36	2.72E-56	5.38E-51
cg07359545	SEPT5-GP1BB	chr22	19711327	0.35	3.82E-55	5.06E-50
cg26774156	STRA6	chr15	74495384	0.64	3.83E-55	5.06E-50
cg00365672	MRPS18A	chr6	43670600	0.54	4.89E-55	5.48E-50
cg09948374	RABGAP1L	chr1	174844517	0.38	5.53E-55	5.48E-50
cg00590639	ICAM3	chr19	10464771	0.50	7.36E-55	6.49E-50
cg19925475	ICAM3	chr19	10464767	0.43	9.62E-55	7.63E-50
cg23764158	ECE1	chr1	21606057	0.51	1.33E-54	9.55E-50
cg09709600	KCNK7	chr11	65359521	0.43	1.58E-54	1.05E-49
cg04227087	ERLIN2	chr8	37585009	0.37	2.68E-54	1.64E-49
cg10859605	RBPMS-AS1	chr8	30255368	0.56	3.29E-54	1.86E-49
cg08953826	OPA3	chr19	46119023	0.37	3.92E-54	2.07E-49
cg06857690	USP12	chr13	27608835	0.40	4.41E-54	2.19E-49
cg09712464	CLUH	chr17	2627328	0.38	4.87E-54	2.27E-49
cg21631439	SLC44A2	chr19	10736448	0.37	6.56E-54	2.89E-49
cg09414325	CABLES1	chr18	20714084	0.41	7.67E-54	3.20E-49
cg14678774	DNASE2	chr19	12978360	0.52	9.76E-54	3.87E-49
cg27436259	PRSS8	chr16	31147017	0.43	1.24E-53	4.69E-49
cg04395593	C9orf106	chr9	132044732	0.51	1.55E-53	5.57E-49
cg24690588	FYB2	chr1	57285399	0.33	3.21E-53	1.11E-48
cg05566966	KREMEN1	chr22	29493092	0.49	4.30E-53	1.40E-48
cg23621097	HIC1	chr17	1962236	0.39	4.41E-53	1.40E-48

Annotations. ILMN probe = Illumina methylation probe; UCSC hg19 gene (-500, +500 bp) = UCSC hg19 closest annotated gene name 500 bp upstream or downstream of the probe; chr = chromosome; $\log_2$ beta FC = $\log_2$ beta fold change, *q*-value = FDR-corrected *p*-value.

Analyses of functional enrichment had been performed separately for losses and gains in DNAm between individual stages of differentiation. Exhaustive results lists of the respective annotation data bases can be found in **Supplementary Tables 8 & 9**. Due to the large number of enriched gene sets and dissimilar distribution of enriched pathways throughout DNAm losses and gains in differentiation, a selected subset of the results is shown in the different figures.

Functionally, DMRs ($q \leq 0.01$, beta change $\geq 10\%$) that lost DNAm during transition from hSC to NP were most significantly overrepresented in genes implicated in the Notch signaling pathway (**Fig. 42**). Notch activation in stem and progenitor cells has been found to link major neural lineage transitions, confer CNS rostrocaudal patterning ability, and consequentially enable the process of cortical lamination (Edri et al., 2015). Highly significant enrichment in the Notch pathway was also found for DMRs that gained DNAm during terminal differentiation to dN. A similar pattern of consecutive demethylation and gain in methylation was observed for the majority of enriched pathways. Overall, these included several morphogen signaling pathways, such as the Wnt, Hedgehog, and FGF signaling pathways. However, enrichment was also found for angiogenesis, i.e. the development of blood vessels, which were morphologically not discernible in cell culture. Nevertheless, also Vascular endothelial growth factor (VEGF) and Platelet-derived growth factor (PDGF) signaling pathways were enriched for, both of which are associated with blood vessel formation (Chen et al., 2007) and cell migration (Duchek et al., 2001). Multiple enriched pathways were associated with functions important in cell-to-cell interactions or proliferation, such as the integrin signaling pathway (Giancotti & Ruoslahti, 1999), cytoskeletal regulation by Rho GTPase (Hall, 1998), and the PI3 kinase pathway (Kim et al., 2007). Further, differentially methylated regions were overrepresented in genes associated with the apoptosis signaling pathway, important in embryonic morphogenesis (Qu et al., 2007), as well as several pathways of particular interest to neuropsychiatric developmental disorders such as the oxytocin receptor mediated signaling pathway (Tyzio et al., 2014), inflammation mediated by chemokine and cytokine signaling pathway (Goeden et

al., 2016), 5HT2 type receptor mediated signaling pathway (Seckl, 1997), or the Alzheimer presenilin pathway (Ye et al., 1999).
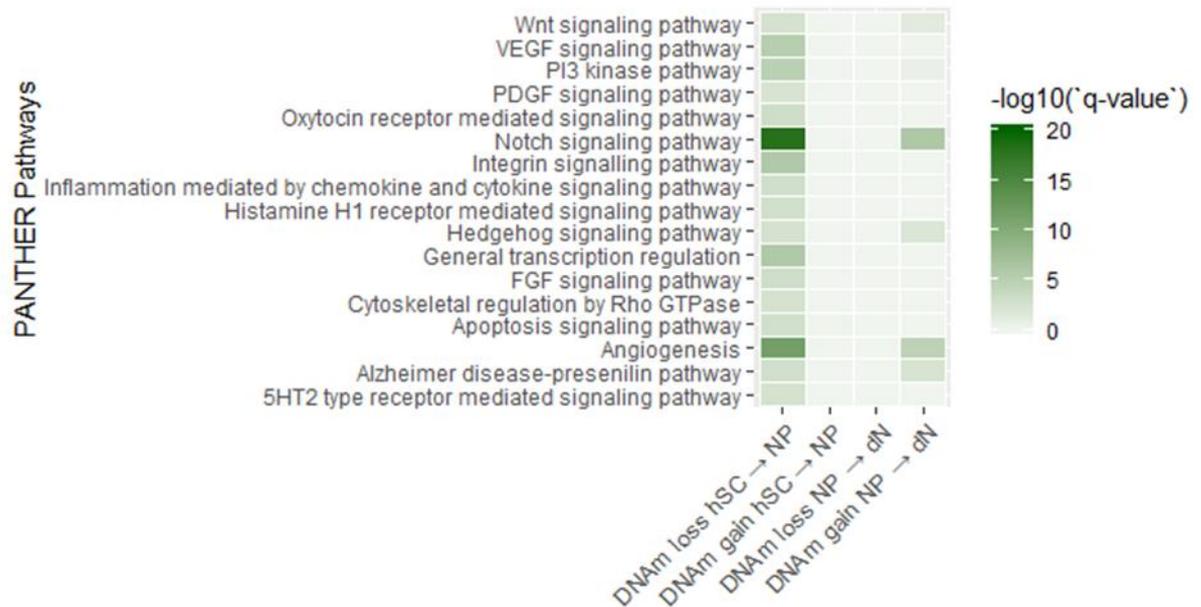
Figure 42. Characterisation of differentiated cells (DNAm). Functional enrichment analysis for PANTHER Pathways. Significantly enriched terms ($q \leq$ 0.05) for DMRs (beta change $\geq$ 10%, $q \leq$ 0.01).

Enrichment analyses conducted for GO Biological Process terms are depicted in **Figure 43**. Again, DMRs becoming hypomethylated during the initial neuroectoderm cell fate transition from hSC to NP, and DMRs becoming hypermethylated upon terminal differentiation to neurons were enriched for in most categories.

These included many terms related to embryogenesis in general (stem cell development, lung development, floor plate morphogenesis, face morphogenesis, nose morphogenesis, eye development, embryonic placenta development, palate development, embryonic morphogenesis, development of primary sexual characteristics, negative regulation of auditory receptor cell differentiation, and cochlea development), or to the formation of embryonic axes in particular (regulation of BMP signaling pathway, rostrocaudal neural tube patterning, dorsal / ventral neural tube patterning, left / right axis specification, anterior / posterior axis specification, and forebrain dorsal / ventral pattern formation). Many terms further referred to specific brain regions, such as telencephalon development, positive regulation of anterior head development, nucleus accumbens development, hippocampus development, forebrain ventricular zone progenitor cell division, forebrain radial glial cell differentiation, forebrain neuron fate commitment, or forebrain neuron differentiation. Others were associated with the processes of neurogenesis or neuronal migration and synapse formation, like the terms neurogenesis, Wnt receptor signaling pathway, synapse maturation, regulation of cell migration, positive regulation of cell adhesion, neuron fate commitment, neuron projection morphogenesis, layer formation in cerebral cortex, lateral motor column neuron migration, gliogenesis, ERBB signaling pathway, dopaminergic neuron differentiation, commissural neuron axon guidance, cerebral cortex radially

oriented cell migration, axonogenesis, axon guidance, or actin filament polymerization. Lastly, while overrepresentation of DMRs in the notch signaling pathway was high, response to stress was more significantly enriched by a margin for DNAm loss during transition from hSC to NP, and to a lesser degree for DNAm gain during terminal differentiation. In addition, multiple enriched terms pointed to an involvement of the stress system during neurogenesis, such as response to steroid hormone stimulus, response to corticosterone stimulus, regulation of stress-activated MAPK cascade, and regulation of response to stress. Others were associated with the immune system, namely immune system development and negative regulation of NF-kappaB transcription factor activity.

Enriched Biological Process categories for all differentially methylated regions without distinction by direction of methylation changes are shown in **Table 12**. In addition, enrichment analysis results conducted using GeneCodis are depicted in **Figure 44**.
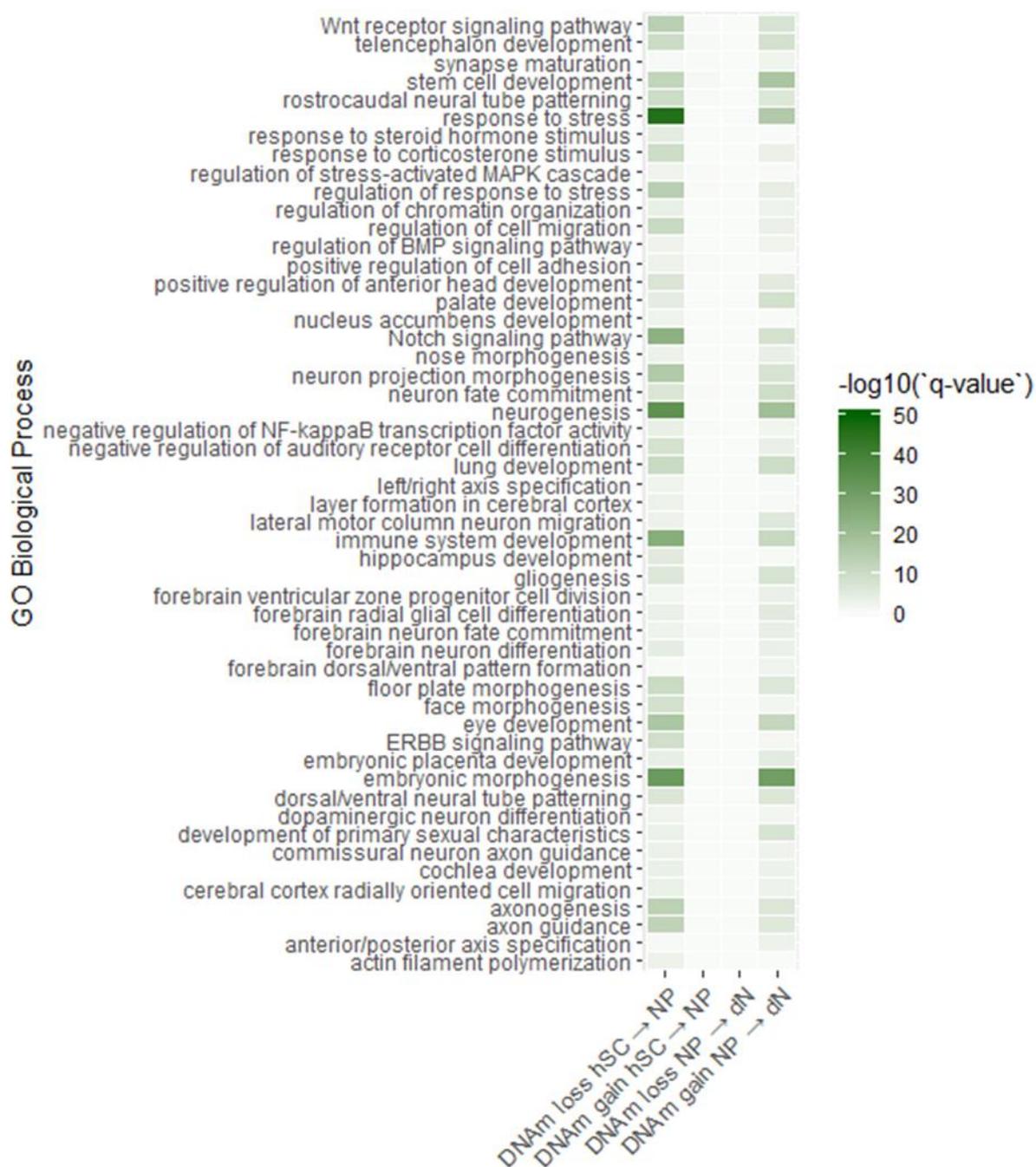
Figure 43. Characterisation of differentiated cells (DNAm). Functional enrichment analysis for Gene Ontology Biological Process terms. Significantly enriched terms (*q* ≤ 0.05) for DMRs (beta change ≥ 10%, *q* ≤ 0.01).

Table 12. Characterisation of differentiated cells (DNAm). Functional enrichment analysis for Gene Ontology Biological Process terms.

GO Biological Process	Fold Enrichment	q-value	Stage
regulation of cellular ketone metabolic process by regulation of transcription from RNA polymerase II promoter	7.8	4.90E-14	hSC → NP
regulation of cellular ketone metabolic process by negative regulation of transcription from RNA polymerase II promoter	9.75	6.17E-14	hSC → NP
floor plate formation	6.48	2.31E-11	hSC → NP
notochord regression	6.32	3.80E-11	hSC → NP
floor plate morphogenesis	6.04	9.68E-11	hSC → NP
peroxisome transport along microtubule	11.18	4.96E-10	hSC → NP
protein import into peroxisome matrix, substrate release	11.18	4.96E-10	hSC → NP
protein import into peroxisome matrix, translocation	10.46	1.18E-09	hSC → NP
rhombomere 2 development	6.01	2.89E-08	hSC → NP
regulation of phosphatidylcholine catabolic process	6.48	6.58E-08	hSC → NP
positive regulation of anterior head development	6.39	7.96E-08	hSC → NP
negative regulation of protein homotetramerization	7.42	9.12E-08	hSC → NP
lipopolysaccharide transport	6.73	1.08E-07	hSC → NP
cerebellar Purkinje cell layer maturation	6.14	9.10E-07	hSC → NP
cerebellar cortex maturation	6.01	1.18E-06	hSC → NP
negative regulation of hepatocyte growth factor biosynthetic process	6.37	1.56E-06	hSC → NP
cerebellar molecular layer formation	7.21	3.28E-06	hSC → NP
Notch signaling pathway involved in arterial endothelial cell fate commitment	7.21	3.28E-06	hSC → NP
histone citrullination	7.04	1.19E-05	hSC → NP
prechordal plate formation	7.98	1.22E-05	hSC → NP
midbrain-hindbrain boundary initiation	7.98	1.22E-05	hSC → NP
regulation of cell motility involved in somitogenic axis elongation	7.92	1.30E-05	hSC → NP
positive regulation of non-canonical Wnt signaling pathway via JNK cascade	7.92	1.30E-05	hSC → NP
negative regulation of convergent extension involved in axis elongation	7.92	1.30E-05	hSC → NP
notochord cell development	1.28	2.46E-05	hSC → NP
tRNA wobble position uridine thiolation	6.23	8.57E-05	hSC → NP
regulation of growth plate cartilage chondrocyte proliferation	8.18	0.0001	hSC → NP
cell-abiotic substrate adhesion	1.24	0.0001	hSC → NP
calcium ion regulated lysosome exocytosis	7.81	0.0001	hSC → NP
establishment of protein localization to juxtaparanode region of axon	7.65	0.0002	hSC → NP
positive regulation of phosphorylation of RNA polymerase II C-terminal domain serine 2 residues	11.51	0.0002	hSC → NP
response to nickel cation	14.84	0.0003	hSC → NP
axial mesoderm formation	6.77	0.0003	hSC → NP
negative regulation of Notch signaling pathway involved in somitogenesis	6.72	0.0004	hSC → NP
glucose import in response to insulin stimulus	9.46	0.0005	hSC → NP
leukocyte adhesive activation	8.69	0.0008	hSC → NP
amino acid homeostasis	8.22	0.001	hSC → NP
positive regulation of exit from mitosis	6.59	0.001	hSC → NP
mitotic DNA replication initiation	8.07	0.001	hSC → NP
malonate catabolic process	7.89	0.001	hSC → NP

[117]

GO Biological Process	Fold Enrichment	*q*-value	Stage
Cajal body organization	6.14	0.002	hSC → NP
smooth muscle hyperplasia	9.04	0.002	hSC → NP
positive regulation of chylomicron remnant clearance	12.62	0.003	hSC → NP
sphingoid catabolic process	10.89	0.004	hSC → NP
nitrate catabolic process	7.44	0.005	hSC → NP
nitric oxide catabolic process	7.44	0.005	hSC → NP
cellular organofluorine metabolic process	7.44	0.005	hSC → NP
smooth muscle cell-matrix adhesion	7.27	0.005	hSC → NP
allantoin catabolic process	10.12	0.005	hSC → NP
Mastication	6.99	0.006	hSC → NP
learned vocalization behavior	6.99	0.006	hSC → NP
negative regulation of saliva secretion	6.99	0.006	hSC → NP
hard palate morphogenesis	6.99	0.006	hSC → NP
biosynthetic process of antibacterial peptides active against Gram-negative bacteria	38.88	0.008	hSC → NP
neutrophil mediated killing of fungus	38.88	0.008	hSC → NP
regulation of the force of skeletal muscle contraction	14.16	0.008	hSC → NP
regulation of slow-twitch skeletal muscle fiber contraction	14.17	0.008	hSC → NP
cerebellar Purkinje cell-granule cell precursor cell signaling involved in regulation of granule cell precursor cell proliferation	7.27	1.34E-11	NP → dN
positive regulation of cerebellar granule cell precursor proliferation	6.55	3.90E-11	NP → dN
regulation of cerebellar granule cell precursor proliferation	6.22	1.09E-10	NP → dN
regulation of somitogenesis	7.26	9.62E-09	NP → dN
comma-shaped body morphogenesis	9.16	4.97E-08	NP → dN
enzyme-directed rRNA 2'-O-methylation	16.19	6.03E-08	NP → dN
rRNA 2'-O-methylation	15.26	1.02E-07	NP → dN
compartment pattern specification	8.86	2.59E-07	NP → dN
uterine epithelium development	21.72	2.61E-07	NP → dN
nephric duct elongation	2.172.017	2.61E-07	NP → dN
horizontal cell localization	21.72	2.61E-07	NP → dN
smoothened signaling pathway involved in ventral spinal cord interneuron specification	6.52	3.42E-07	NP → dN
smoothened signaling pathway involved in spinal cord motor neuron cell fate specification	6.52	3.42E-07	NP → dN
smoothened signaling pathway involved in ventral spinal cord patterning	6.31	5.12E-07	NP → dN
midbrain-hindbrain boundary morphogenesis	7.38	6.17E-07	NP → dN
paramesonephric duct development	11.73	1.01E-06	NP → dN
negative regulation of inner ear receptor cell differentiation	8.25	1.83E-06	NP → dN
metanephric comma-shaped body morphogenesis	12.99	1.99E-06	NP → dN
positive regulation of anterior head development	12.94	2.05E-06	NP → dN
peroxisome transport along microtubule	19.96	3.22E-06	NP → dN
protein import into peroxisome matrix, substrate release	19.96	3.22E-06	NP → dN
positive regulation of ovulation	6.29	3.48E-06	NP → dN
S-shaped body morphogenesis	6.23	3.86E-06	NP → dN
negative regulation of follicle-stimulating hormone secretion	6.22	3.94E-06	NP → dN
protein import into peroxisome matrix, translocation	18.68	4.76E-06	NP → dN
floor plate morphogenesis	9.24	6.95E-06	NP → dN

[118]

GO Biological Process	Fold Enrichment	*q*-value	Stage
rhombomere 2 development	10.88	7.16E-06	NP → dN
ectoderm formation	8.88	9.65E-06	NP → dN
positive regulation of nephron tubule epithelial cell differentiation	12.39	1.22E-05	NP → dN
neuroblast division in subventricular zone	15.96	1.22E-05	NP → dN
inhibition of neuroepithelial cell differentiation	7.31	1.56E-05	NP → dN
floor plate formation	8.92	3.08E-05	NP → dN
skeletal muscle satellite cell differentiation	7.66	3.10E-05	NP → dN
negative regulation of protein homotetramerization	13.24	3.61E-05	NP → dN
notochord regression	8.70	3.66E-05	NP → dN
mitotic spindle organization in nucleus	13.07	3.89E-05	NP → dN
mesendoderm development	6.42	4.68E-05	NP → dN
positive regulation of hyaluranon cable assembly	8.39	4.74E-05	NP → dN
N-terminal peptidyl-alanine trimethylation	12.38	5.26E-05	NP → dN
N-terminal peptidyl-glycine methylation	12.38	5.26E-05	NP → dN
N-terminal peptidyl-proline dimethylation	12.38	5.26E-05	NP → dN
N-terminal peptidyl-serine demethylation	12.38	5.26E-05	NP → dN
N-terminal peptidyl-serine trimethylation	12.38	5.26E-05	NP → dN
negative regulation of auditory receptor cell differentiation	6.99	6.14E-05	NP → dN
skeletal muscle satellite cell commitment	14.79	9.38E-05	NP → dN
regulation of keratinocyte apoptotic process	6.03	0.0002	NP → dN
metanephric S-shaped body morphogenesis	6.38	0.0003	NP → dN
re-entry into mitotic cell cycle	8.89	0.0003	NP → dN
negative regulation of Notch signaling pathway involved in somitogenesis	16.07	0.0003	NP → dN
detection of chemical stimulus involved in sensory perception of sweet taste	15.93	0.0004	NP → dN
proepicardium development	6.24	0.0004	NP → dN
negative regulation of hepatocyte growth factor biosynthetic process	10.44	0.0005	NP → dN
growth hormone secretion	6.65	0.0006	NP → dN
cellular response to raffinose	6.43	0.0008	NP → dN
lateral inhibition	6.42	0.0008	NP → dN
positive regulation of intracellular mRNA localization	6.36	0.0008	NP → dN
coronary vein morphogenesis	9.29	0.0009	NP → dN
peptidyl-glycine modification	7.39	0.0009	NP → dN
glomerular mesangial cell development	9.05	0.001	NP → dN
nephrogenic mesenchyme morphogenesis	7.06	0.001	NP → dN
cerebellar molecular layer formation	11.49	0.001	NP → dN
Notch signaling pathway involved in arterial endothelial cell fate commitment	11.49	0.001	NP → dN
negative regulation of pro-B cell differentiation	6.87	0.001	NP → dN
medium-chain fatty acid transport	34.94	0.001	NP → dN
N-terminal protein amino acid methylation	6.69	0.002	NP → dN
regulation of lateral mesodermal cell fate specification	8.21	0.002	NP → dN
antigen processing and presentation, exogenous lipid antigen via MHC class Ib	6.28	0.002	NP → dN
nuclear inner membrane organization	15.19	0.002	NP → dN
commitment of multipotent stem cells to neuronal lineage in forebrain	9.16	0.003	NP → dN
Cajal body organization	13.42	0.003	NP → dN
axial mesoderm formation	12.96	0.004	NP → dN
adenosine catabolic process	8.87	0.004	NP → dN
inosine biosynthetic process	8.87	0.004	NP → dN

GO Biological Process	Fold Enrichment	q-value	Stage
response to hydrostatic pressure	6.70	0.005	NP → dN
regulation of cell motility involved in somitogenic axis elongation	12.12	0.005	NP → dN
positive regulation of non-canonical Wnt signaling pathway via JNK cascade	12.12	0.005	NP → dN
negative regulation of convergent extension involved in axis elongation	12.12	0.005	NP → dN
inosine metabolic process	8.22	0.005	NP → dN
cell migration involved in endocardial cushion formation	7.38	0.008	NP → dN
lactose biosynthetic process	7.35	0.008	NP → dN
cerebellar Purkinje cell layer structural organization	7.06	0.01	NP → dN

Annotations. Significantly enriched terms ($q \leq 0.01$, Fold Enrichment ≥ 6) for DMRs (beta change $\geq$ 10%, $q \leq 0.01$).
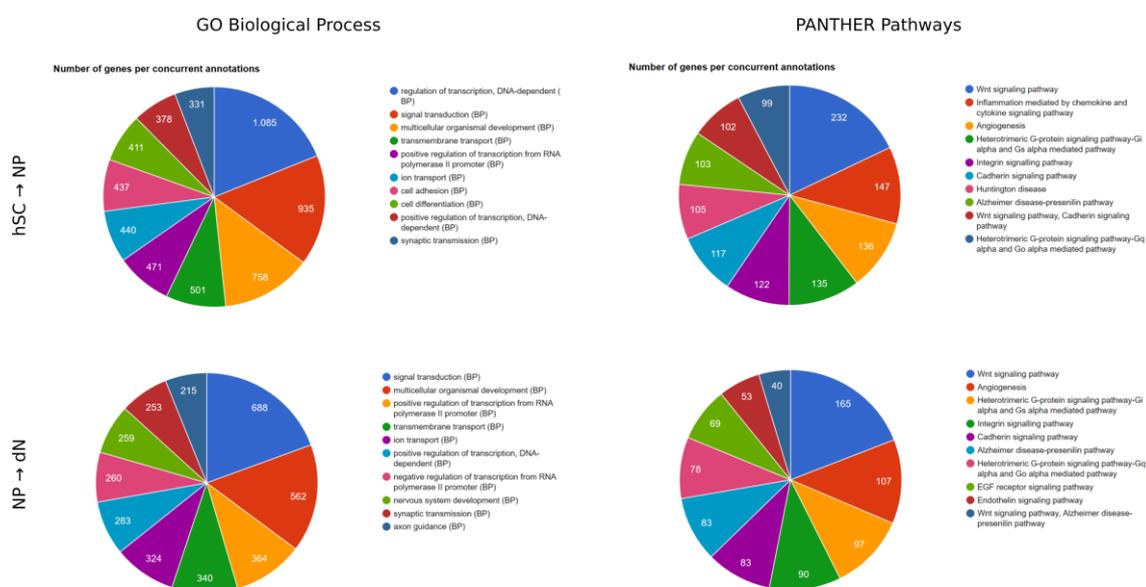
Figure 44. Functional enrichment (GeneCodis). Enrichment for differentially methylated positions over the course of development (beta change $\geq 10\%$, $q \leq 0.01$).

Overrepresentation of differentially methylated regions ($q \leq 0.01$) during neuronal differentiation for chromatin conformation states is depicted in **Figure 45**. Differentially methylated regions were enriched for flanking bivalent transcription start sites (TSS)/Enhancers (hSC → NP: OR=7.21; permuted *p*-value $\leq 10^{-50}$; NP →

dN: OR=6.83, permuted p-value $\leq 10^{-50}$), bivalent/ poised TSS (hSC $\rightarrow$ NP: OR=6.23; permuted p-value $\leq 10^{-50}$; NP $\rightarrow$ dN: OR=4.74, permuted p-value $\leq 10^{-50}$), flanking active TSS (hSC $\rightarrow$ NP: OR=6.28; permuted p-value $\leq 10^{-50}$; NP $\rightarrow$ dN: OR=4.20, permuted p-value $\leq 10^{-50}$), active TSS (hSC $\rightarrow$ NP: OR=5.60; permuted p-value $\leq 10^{-50}$; NP $\rightarrow$ dN: OR=3.72, permuted p-value $\leq 10^{-50}$), (bivalent) enhancers (hSC $\rightarrow$ NP: OR=5.54; permuted p-value $\leq 10^{-50}$; NP $\rightarrow$ dN: OR=6.29, permuted p-value $\leq 10^{-50}$), transcription at 5' and 3' sites (hSC $\rightarrow$ NP: OR=4.66; permuted p-value $\leq 10^{-50}$; NP $\rightarrow$ dN: OR=2.34, permuted p-value $\leq 10^{-50}$), and (weak) repressed polycomb (hSC $\rightarrow$ NP: OR=1.78; permuted p-value $\leq 10^{-50}$; NP $\rightarrow$ dN: OR=2.04, permuted p-value $\leq 10^{-50}$), as well as genic enhancers (hSC $\rightarrow$ NP: OR=1.50; permuted p-value $\leq 10^{-50}$; NP $\rightarrow$ dN: OR=1.50, permuted p-value $\leq 10^{-50}$), and weak transcription (hSC $\rightarrow$ NP: OR=1.23; permuted p-value $\leq 10^{-15}$; NP $\rightarrow$ dN: OR=1.23, permuted p-value $\leq 10^{-15}$). Depletion on the other hand was found for quiescent/low states (hSC $\rightarrow$ NP: OR=0.67; permuted p-value $\leq 10^{-50}$; NP $\rightarrow$ dN: OR=0.59, permuted p-value $\leq 10^{-50}$), heterochromatin (hSC $\rightarrow$ NP: OR=0.64; permuted p-value $\leq 10^{-50}$; NP $\rightarrow$ dN: OR=0.39, permuted p-value $\leq 10^{-50}$), and strong transcription (hSC $\rightarrow$ NP: OR=0.56; permuted p-value $\leq 10^{-50}$; NP $\rightarrow$ dN: OR=0.51, permuted p-value $\leq 10^{-50}$). Therefore, strongest overrepresentation was detected for bivalent states. Bivalent chromatin marks keep genes poised for activation and thus help to maintain stem and progenitor cells in a state of pluri- and multipotency, respectively. Dynamic processes of methylation and demethylation at these sites help to resolve the poised state towards commitment to a more specific cell fate (Hirabayashi et al., 2010).
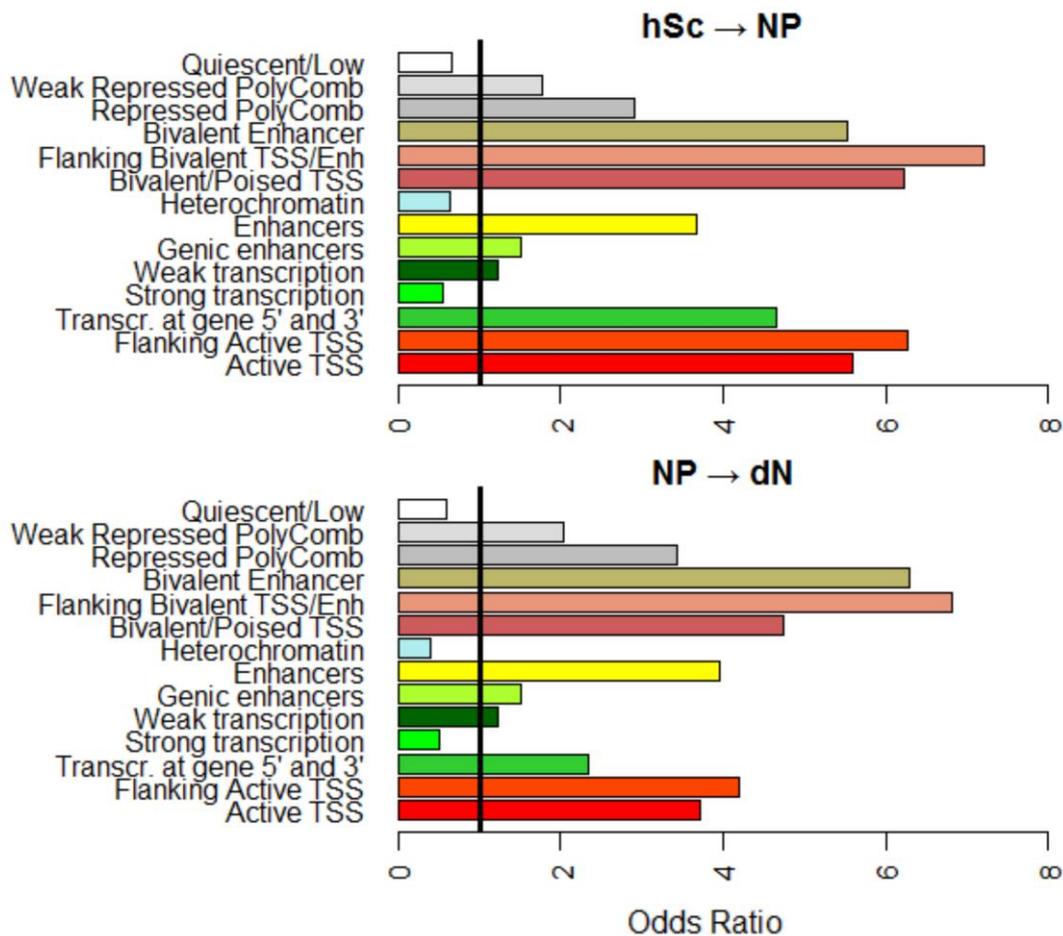
Figure 45. Enrichment for chromHMM chromatin states. Odds ratios for differentially methylated regions over the course of development ($q \leq 0.01$).

4.2 ENDOGENOUS AND DEXAMETHASONE-INDUCED GLUCOCORTICOID RECEPTOR ACTION IN NEUROGENESIS

While the glucocorticoid receptor protein was expressed as early as the stem cell stage, it decreased in expression below background levels on D12 of differentiation when lumen diameter of neural rosettes were at their maximum. Expression then increased with further differentiation to neural progenitors on D24 and migrating neurons on D44 (**Fig. 46**).
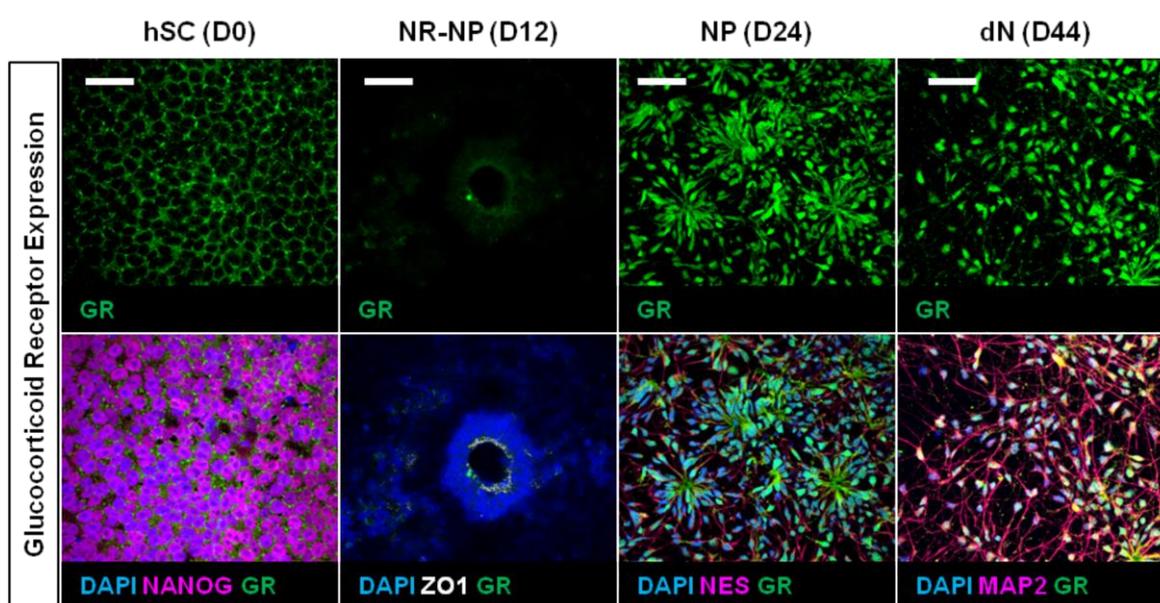
Figure 46. Neurogenesis is accompanied by dynamic expression of GR and its chaperones (ICC). Unliganded GR expression in differentiating neural cells (upper panel) with developmental markers (lower panel). GR is transiently repressed in D12 neural rosettes. hSC = human stem cells, NR-NP = neural rosette neuronal progenitors, NP = neuronal progenitors, dN = differentiated neurons. Scale bars: 50 μm.

Western Blots (**Fig. 47**) confirmed this expression pattern and revealed a concurrent decrease in heat shock protein 90 (HSP90). HSP90 is a chaperone protein of the GR and crucial regulator of its function. It stabilises cytoplasmic GR in a complex with co-chaperones FKBP51 and heat shock protein 70 (HSP70), and binds FKBP52, which initiates GR translocation to the nucleus. In the nucleus, the complex disassembles, the GR dimerises and then binds to DNA, where it can act as both an activator or repressor of gene transcription (Wochnik et al., 2005; Pratt et al., 2006). Increases in both HSP70 and FKBP51 protein levels were further characteristics of the neuronal differentiation process.
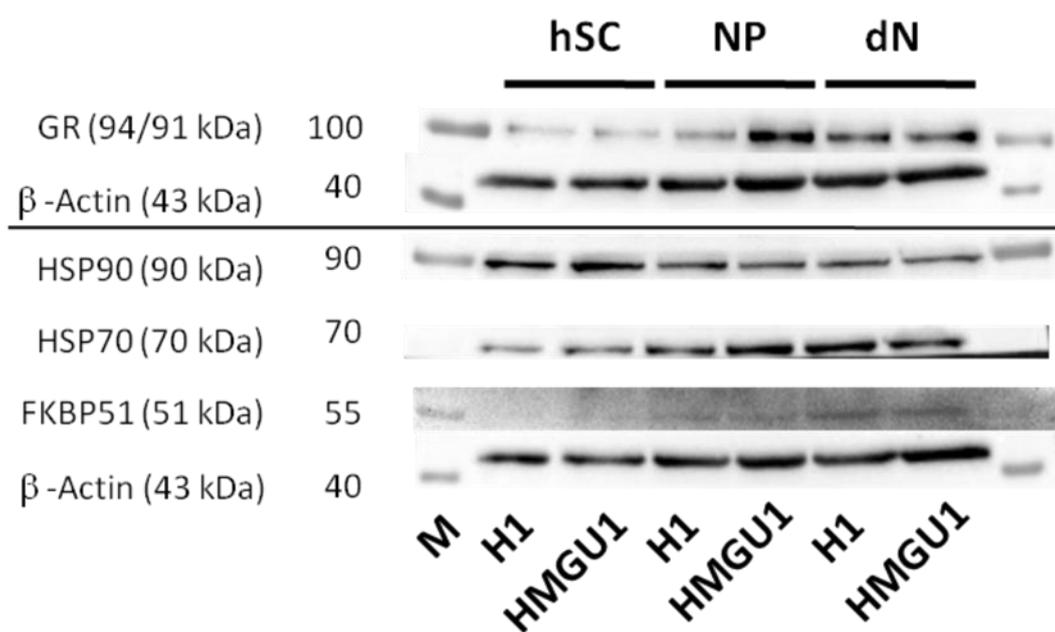
Figure 47. Neurogenesis is accompanied by dynamic expression of GR and its chaperones (Immunoblot). Western Blot of GR and its chaperones in differentiating neural cells.

However, neurogenesis was not only accompanied by a general increase in glucocorticoid receptor levels, but also by a shift in its constituent localisation (**Fig. 48**). A two-factorial ANOVA with development and treatment as independent variables and $GR_{\Delta ID}$ as dependent variable resulted in a significant influence of development (F = 65.43, df = 2, $p \leq 0.0001$), showing a shift of GR to the nucleus in neurulating cells. Neither dexamethasone treatment (F = 2.51, df = 1, $p = 0.12$), nor the interaction between development and treatment (F = 0.02, df = 2, $p = 0.98$) reached statistical significance, although dexamethasone treatment increased the tendency towards nuclear localisation. Levene's test confirmed equality of error variances across groups (F = 1.88, df1 = 5, df2 = 102, $p = 0.10$).
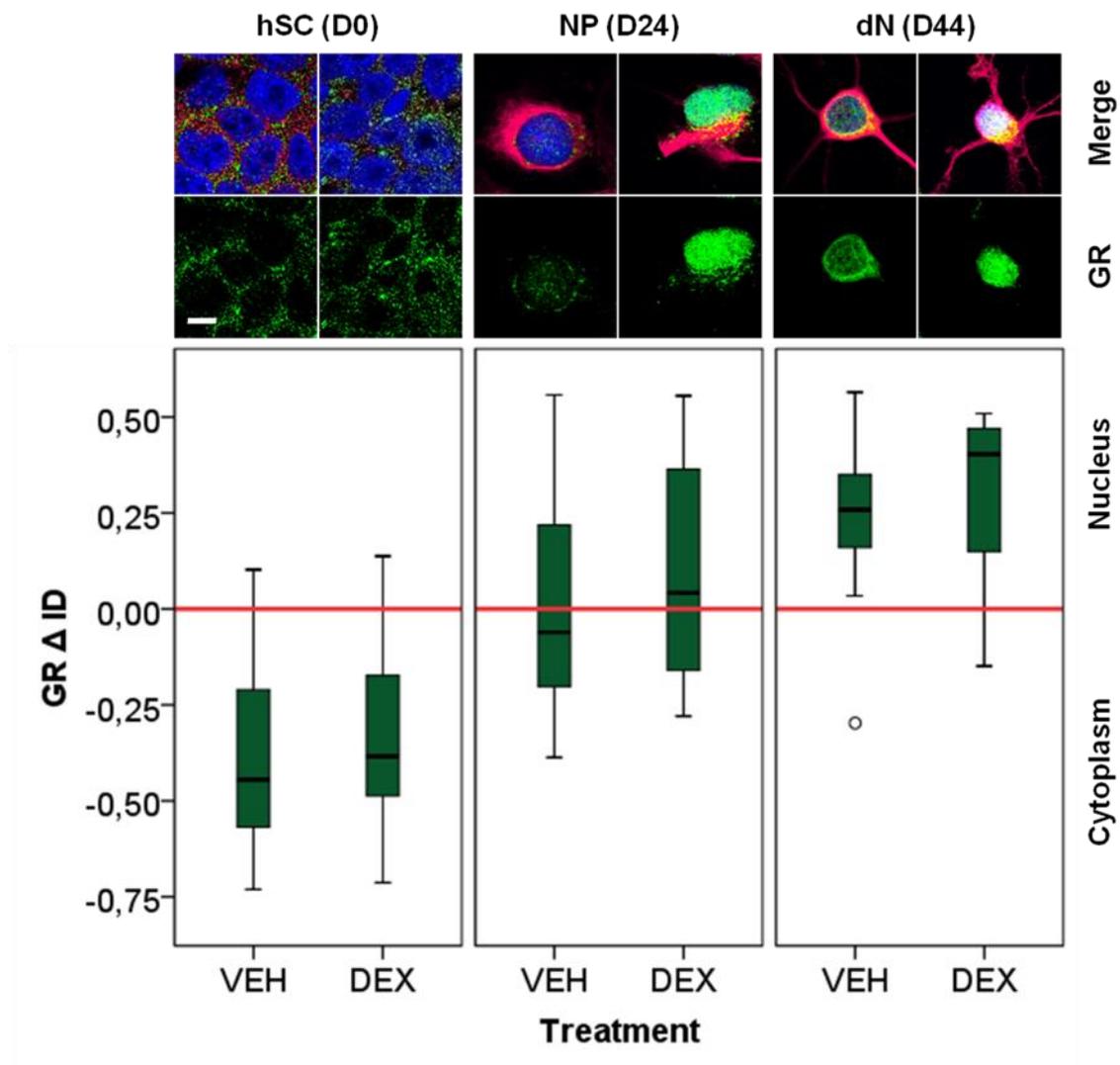
Figure 48. Glucocorticoid receptor undergoes cytoplasmic to nuclear shift during neurogenesis. Upper panel: Confocal microscopy of differentiating neural cells showing GR localisation under VEH and DEX [1 µM] treatment conditions after 3 h (GR = green, Nanog, NES, and MAP2, respectively = red). Scale bar: 7.5 µm (valid for all images). Lower panel: Boxplots of $GR_{\Delta ID}$. $GR_{\Delta ID}$ signifies the difference between the mean integrated density signal in the nucleus and cytoplasm.

In addition, glucocorticoid response elements (GREs) were significantly overrepresented in differentially methylated regions between any two stages of neuronal differentiation (hSC → NP: OR=3.23; permuted *p*-value ≤ 0.001; NP → dN: OR=5.06, permuted *p*-value ≤ 0.001), but subsequently less likely to be located in differentially methylated regions induced by DEX stimulation in migrating neurons (OR=0.05; permuted *p*-value ≤ 0.001) (**Fig. 49**).

Glucocorticoid Response Elements
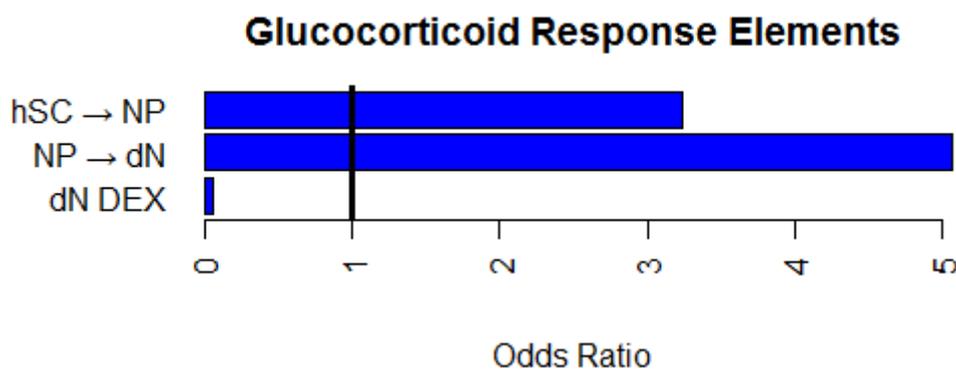
Figure 49. DMR enrichment for Glucocorticoid Response Elements. Contrasts between developmental transitions and DEX-stimulated versus unstimulated D44 neurons (both at *q* ≤ 0.1 and beta change ≥ 3%). Glucocorticoid Response Elements were derived from blood data.

4.3 EFFECTS OF DEXAMETHASONE EXPOSURE ON THE METHYLOME

Dexamethasone treatment did not or minimally affect the methylation landscape in hSC (n = 0 DMPs) and NP (n = 1 DMPs), but led to differential methylation in n = 2 034 ($q \leq 0.1$), respectively n = 218 probes ($q \leq 0.05$) at methylation beta changes $\geq$ 5% on D44 of terminal neuronal differentiation (**Supplementary Tables 5-7**). Results for the cutoff at $q \leq 0.05$ are displayed in **Table 13**.

The majority of all DMPs ($q \leq 0.1$) presented with a gain in DNA methylation. Only n = 17 probes showed a decrease compared to the untreated condition (**Fig. 51**). These included probes annotated for Sprouty RTK Signaling Antagonist 1 (*SPRY1*), an antagonist of FGF signaling (Faedo et al., 2010), Mitogen-Activated Protein Kinase 14 (*MAPK14*) involved in regulation of stress resilience (Bruchas et al., 2011), and Neogenin 1 (*NEO1*), which encodes for a receptor for repulsive guidance molecule families (Rajagopalan et al., 2004).

Table 13. Differentially methylated positions following DEX stimulation in dN (beta change ≥ 5%, *q*-value ≤ 0.05).

ILMN probe	UCSC hg19 gene (-500, +500 bp)	chr	position	log₂ beta FC	*p*-value	*q*-value
cg15745461	LINC01501	chr9	93314587	0.18	0.0000060	0.04
cg25043205	CDH2	chr18	25593477	0.17	0.0000004	0.02
cg19740984	ACOD1	chr13	77522450	0.16	0.0000008	0.02
cg08623623	NRG1	chr8	31883074	0.16	0.0000197	0.04
cg14831325	FBXO38	chr5	147784060	0.15	0.0000019	0.03
cg15031550	VRK2	chr2	57661686	0.15	0.0000252	0.05
cg20043269	CRYBG1	chr6	106867538	0.15	0.0000005	0.02
cg09628356	SEPT2	chr2	242263567	0.15	0.0000051	0.04
cg22312738	CCDC196	chr14	66577514	0.14	0.0000296	0.05
cg22764861	MCPH1	chr8	6277513	0.14	0.0000294	0.05
cg16835955	BBS9	chr7	33196366	0.14	0.0000140	0.04
cg08263875	SLC6A15	chr12	85013118	0.14	0.0000156	0.04
cg23576250	OR4E2	chr14	22519747	0.14	0.0000338	0.05
cg03799736	KIAA0825	chr5	93858506	0.14	0.0000294	0.05
cg19207921	EDNRA	chr4	148451778	0.14	0.0000271	0.05
cg06230971	MIR4437	chr2	182028979	0.14	0.0000199	0.04
cg19564579	ACO1	chr9	32339841	0.14	0.0000347	0.05
cg24395241	CCDC146	chr7	76755312	0.14	0.0000116	0.04
cg15790015	IMPA1	chr8	82543894	0.13	0.0000013	0.03
cg24660376	KRTAP4-1	chr17	39342819	0.13	0.0000222	0.04
cg07369422	FOPNL	chr16	15973723	0.13	0.0000145	0.04
cg23544656	OR1L4	chr9	125486146	0.13	0.0000105	0.04
cg15470192	TAX1BP1	chr7	27803707	0.13	0.0000072	0.04
cg08274723	OR1L6	chr9	125511547	0.13	0.0000152	0.04
cg00337569	CPOX	chr3	98282714	0.13	0.0000106	0.04
cg11831646	SPATA8	chr15	97535477	0.13	0.0000029	0.03
cg07382566	RASSF3	chr12	65021077	0.13	0.0000019	0.03
cg02770728	ADGRG6	chr6	142582173	0.13	0.0000017	0.03
cg23269715	GMDS	chr6	2209967	0.13	0.0000182	0.04
cg10643146	MTPAP	chr10	30595593	0.13	0.0000201	0.04
cg05289636	MPRIP	chr17	16950125	0.12	0.0000120	0.04
cg12969108	DLG2	chr11	84835381	0.12	0.0000176	0.04
cg01691063	MAP2	chr2	210555274	0.12	0.0000110	0.04
cg07566425	RASGEF1B	chr4	82378725	0.12	0.0000146	0.04
cg08385371	SPAM1	chr7	123587371	0.12	0.0000047	0.04
cg06504624	DNAJB6	chr7	157157215	0.12	0.0000222	0.04
cg24544278	CLEC2D	chr12	9822238	0.12	0.0000231	0.05
cg04256394	ITK	chr5	156606860	0.12	0.0000050	0.04
cg14297504	RAI14	chr5	34687533	0.12	0.0000116	0.04
cg26271775	DDIT4L	chr4	101017130	0.12	0.0000095	0.04
cg27041299	KIDINS220	chr2	9008822	0.12	0.0000065	0.04
cg17706188	HIVEP2	chr6	143158337	0.12	0.0000069	0.04
cg14418297	TLE4	chr9	83000016	0.12	0.0000170	0.04
cg07109965	GMPR	chr6	16401143	0.12	0.0000038	0.04
cg25144815	ZNF385D	chr3	22414843	0.12	0.0000288	0.05
cg11782594	MIR548AC	chr3	23441799	0.12	0.0000296	0.05
cg07611507	TFG	chr3	100451548	0.12	0.0000022	0.03
cg23671448	HYKK	chr15	78786397	0.12	0.0000264	0.05

ILMN probe	UCSC hg19 gene (-500, +500 bp)	chr	position	log₂ beta FC	*p*-value	*q*-value
cg00618271	C21orf62	chr21	34186397	0.12	0.0000325	0.05
cg16843058	ALB	chr4	74274175	0.12	0.0000290	0.05
cg26974427	RAB11FIP1	chr8	37727552	0.12	0.0000028	0.03
cg09150550	GS1-279B7,1	chr1	185308635	0.12	0.0000249	0.05
cg07371838	GOLT1B	chr12	21657406	0.11	0.0000021	0.03
cg10276433	ADGRF1	chr6	47011312	0.11	0.0000050	0.04
cg04608399	DYRK2	chr12	68123453	0.11	0.0000025	0.03
cg00127664	RNF125	chr18	29597931	0.11	0.0000325	0.05
cg22694445	OR52H1	chr11	5570731	0.11	0.0000157	0.04
cg00292925	FBN1	chr15	48709005	0.11	0.0000023	0.03
cg00841352	ADGRL4	chr1	79938150	0.11	0.0000221	0.04
cg14555759	FYB1	chr5	39167171	0.11	0.0000373	0.05
cg06629612	HDAC4	chr2	240429462	0.11	0.0000354	0.05
cg15012161	MARCKS	chr6	113955683	0.11	0.0000332	0.05
cg03074604	DIO2-AS1	chr14	80440750	0.11	0.0000205	0.04
cg18427465	FBXO34	chr14	55737629	0.11	0.0000004	0.02
cg10941858	ARID2	chr12	46230405	0.11	0.0000040	0.04
cg14552441	RAD51AP1	chr12	4650518	0.11	0.0000317	0.05
cg06426483	PTEN	chr10	89692507	0.11	0.0000222	0.04
cg07101116	ALDH1A1	chr9	75486850	0.11	0.0000350	0.05
cg23938649	GSAP	chr7	77053943	0.11	0.0000017	0.03
cg16324899	ZEB2	chr2	145298195	0.11	0.0000254	0.05
cg27594634	PPP1R1C	chr2	182838329	0.11	0.0000302	0.05
cg04797820	TMEM132D	chr12	129460559	0.11	0.0000267	0.05
cg16600438	ISX	chr22	35339700	0.11	0.0000134	0.04
cg04486747	LUZP6	chr7	135927795	0.11	0.0000308	0.05
cg00305108	XPC	chr3	14203919	0.11	0.0000020	0.03
cg21245844	SORBS2	chr4	186734417	0.11	0.0000207	0.04
cg24886843	OOEP	chr6	74126975	0.11	0.0000084	0.04
cg24500972	KLHL32	chr6	97369501	0.11	0.0000148	0.04
cg10520863	COL5A2	chr2	190098505	0.11	0.0000035	0.04
cg10565356	DAD1	chr14	22739553	0.10	0.0000137	0.04
cg16644365	BLOC1S6	chr15	45883592	0.10	0.0000219	0.04
cg18333514	LOC100506178	chr7	22636364	0.10	0.0000190	0.04
cg10438034	GBP6	chr1	89831072	0.10	0.0000302	0.05
cg06375876	CNOT6L	chr4	78638815	0.10	0.0000083	0.04
cg22711104	CA2	chr8	86378258	0.10	0.0000106	0.04
cg19608497	GS1-279B7,1	chr1	185402565	0.10	0.0000165	0.04
cg20499528	DARS	chr2	136744435	0.10	0.0000260	0.05
cg08522272	LRBA	chr4	151169929	0.10	0.0000178	0.04
cg09187189	ARHGAP26-AS1	chr5	142209689	0.10	0.0000226	0.05
cg00650939	OR5B12	chr11	58208970	0.10	0.0000346	0.05
cg06394103	DPP10	chr2	116480197	0.10	0.0000185	0.04
cg23501843	LINC00535	chr8	94711282	0.10	0.0000005	0.02
cg10774352	LINC00472	chr6	72206414	0.10	0.0000153	0.04
cg13996593	DNER	chr2	230574596	0.10	0.0000250	0.05
cg25522664	NHLH2	chr1	116384013	0.10	0.0000073	0.04
cg06875305	TANGO6	chr16	68869013	0.10	0.0000142	0.04
cg10459339	TECTA	chr11	120971461	0.10	0.0000101	0.04
cg10195698	GCNT2	chr6	10613040	0.10	0.0000163	0.04
cg04621944	AJAP1	chr1	5080448	0.10	0.0000044	0.04

ILMN probe	UCSC hg19 gene (-500, +500 bp)	chr	position	log₂ beta FC	*p*-value	*q*-value
cg05444548	CFAP70	chr10	75119064	0.10	0.0000052	0.04
cg20318580	TNFAIP8L3	chr15	51398457	0.10	0.0000368	0.05
cg17585395	MCUR1	chr6	13831046	0.10	0.0000222	0.04
cg15140258	LOC285593	chr5	173000823	0.10	0.0000178	0.04
cg11030620	MIR135A2	chr12	97957283	0.10	0.0000337	0.05
cg18355137	NDUFAF2	chr5	60348758	0.10	0.0000109	0.04
cg16635171	FRZB	chr2	183691600	0.10	0.0000014	0.03
cg21729334	TNS3	chr7	46736542	0.10	0.0000238	0.05
cg07041310	LNX1	chr4	54537807	0.10	0.0000281	0.05
cg13329407	LINC01692	chr21	25801374	0.10	0.0000027	0.03
cg16986571	RASA3	chr13	114872102	0.10	0.0000207	0.04
cg21525946	TENM2	chr5	167022853	0.10	0.0000178	0.04
cg20526254	SIPA1L1	chr14	72167842	0.10	0.0000093	0.04
cg20587464	COL1A2	chr7	93976482	0.10	0.0000107	0.04
cg23397168	MESD	chr15	81285343	0.10	0.0000224	0.05
cg01568402	LINC00994	chr3	64074407	0.10	0.0000369	0.05
cg27372170	H19	chr11	2021103	0.10	0.0000007	0.02
cg14801403	LINC01364	chr1	88406191	0.10	0.0000002	0.02
cg02187199	EPHX2	chr8	27379409	0.09	0.0000275	0.05
cg17155818	CCNA1	chr13	37028767	0.09	0.0000347	0.05
cg16958715	CNTN5	chr11	98889455	0.09	0.0000084	0.04
cg18569864	JARID2	chr6	15509337	0.09	0.0000038	0.04
cg08806468	ZEB1	chr10	31593433	0.09	0.0000190	0.04
cg17992876	NEU3	chr11	74698322	0.09	0.0000242	0.05
cg00092349	ACVR1	chr2	158633806	0.09	0.0000168	0.04
cg09066498	SERPINB2	chr18	61553558	0.09	0.0000132	0.04
cg16330062	NA	chr11	31091140	0.09	0.0000112	0.04
cg07649828	NEB	chr2	152591715	0.09	0.0000269	0.05
cg17902703	EGFR	chr7	55195278	0.09	0.0000072	0.04
cg18039268	RNF24	chr20	3961082	0.09	0.0000159	0.04
cg17227839	PTPRC	chr1	198602868	0.09	0.0000258	0.05
cg24647339	IL18R1	chr2	102978605	0.09	0.0000225	0.05
cg09458539	GNRH1	chr8	25282830	0.09	0.0000126	0.04
cg16887607	INHBA-AS1	chr7	41733800	0.09	0.0000085	0.04
cg09654664	PMFBP1	chr16	72280588	0.09	0.0000006	0.02
cg11876048	MSI2	chr17	55337654	0.09	0.0000038	0.04
cg17437856	MIR4308	chr14	55286038	0.09	0.0000122	0.04
cg15533302	WDR72	chr15	53582753	0.09	0.0000367	0.05
cg05998259	MYLK4	chr6	2753514	0.09	0.0000070	0.04
cg00478362	POU2F1	chr1	167300563	0.09	0.0000123	0.04
cg10279072	TANC1	chr2	159975353	0.09	0.0000204	0.04
cg24431879	DCTD	chr4	183787513	0.09	0.0000117	0.04
cg09644422	ADGRL4	chr1	80579223	0.09	0.0000350	0.05
cg13974091	NA	chr15	76218542	0.09	0.0000134	0.04
cg01589054	VGLL4	chr3	11744933	0.09	0.0000047	0.04
cg19977232	FIP1L1	chr4	54325479	0.09	0.0000188	0.04
cg18097834	HIST1H4F	chr6	26239120	0.09	0.0000360	0.05
cg15381326	COG5	chr7	107205253	0.09	0.0000098	0.04
cg21868154	WDFY1	chr2	224790161	0.09	0.0000115	0.04
cg13383689	BCL2L11	chr2	111873229	0.09	0.0000018	0.03
cg16024274	CRISP1	chr6	49877534	0.09	0.0000012	0.03

ILMN probe	UCSC hg19 gene (-500, +500 bp)	chr	position	log$_2$ beta FC	*p*-value	*q*-value
cg08296433	LRMDA	chr10	77382225	0.09	0.0000040	0.04
cg22758653	CAV2	chr7	116066796	0.09	0.0000118	0.04
cg05437226	FAM201A	chr9	38682612	0.09	0.0000053	0.04
cg18236545	ATP2B1-AS1	chr12	90501477	0.09	0.0000204	0.04
cg07795517	PTK2	chr8	141949337	0.09	0.0000004	0.02
cg13120174	ZBED9	chr6	28541462	0.09	0.0000023	0.03
cg00865690	LINC01822	chr2	21976205	0.09	0.0000324	0.05
cg07275634	NCKAP1L	chr12	54879977	0.09	0.0000296	0.05
cg09629734	TGFB2-AS1	chr1	218842928	0.09	0.0000029	0.03
cg17939889	HDAC4	chr2	240174650	0.08	0.0000014	0.03
cg09257208	USP25	chr21	17032658	0.08	0.0000005	0.02
cg14899042	SP140	chr2	231095583	0.08	0.0000305	0.05
cg05372182	XKR9	chr8	71751724	0.08	0.0000005	0.02
cg00155788	SLIT3	chr5	168344748	0.08	0.0000267	0.05
cg17904686	SGK1	chr6	134477852	0.08	0.0000298	0.05
cg24740647	PCBD1	chr10	72681285	0.08	0.0000234	0.05
cg24444631	ZFP57	chr6	29636366	0.08	0.0000356	0.05
cg24542758	MAF	chr16	79751767	0.08	0.0000244	0.05
cg20384075	GPR149	chr3	154258166	0.08	0.0000355	0.05
cg22650030	SPAG6	chr10	22667272	0.08	0.0000040	0.04
cg16341261	SLC30A5	chr5	68390788	0.08	0.0000151	0.04
cg21523751	LAMC1	chr1	182988639	0.08	0.0000117	0.04
cg11757134	C1QTNF7	chr4	15341611	0.08	0.0000202	0.04
cg08672675	TPH2	chr12	72331271	0.08	0.0000005	0.02
cg06681995	BEST1	chr11	61704389	0.08	0.0000180	0.04
cg10496071	DTD1	chr20	18591952	0.08	0.0000228	0.05
cg13968580	GLDN	chr15	51669312	0.08	0.0000359	0.05
cg02761866	ASB8	chr12	48542726	0.08	0.0000104	0.04
cg15283498	FOXO3	chr6	108981550	0.08	0.0000351	0.05
cg06060759	EFCAB2	chr1	245207109	0.08	0.0000130	0.04
cg16488116	PLS1	chr3	142316059	0.08	0.0000323	0.05
cg00743081	MAP3K3	chr17	61724970	0.08	0.0000209	0.04
cg05592335	PLOD2	chr3	145803659	0.08	0.0000309	0.05
cg07945473	PAG1	chr8	81934123	0.08	0.0000257	0.05
cg09642879	WNK1	chr12	958166	0.08	0.0000001	0.02
cg07502249	ACVR1	chr2	158670534	0.08	0.0000344	0.05
cg08757143	LOC100131257	chr7	7143230	0.08	0.0000039	0.04
cg17582698	DGKI	chr7	137529886	0.08	0.0000033	0.04
cg06188663	TNFSF8	chr9	117669965	0.08	0.0000101	0.04
cg10907840	BTBD7	chr14	93736028	0.08	0.0000024	0.03
cg06409217	SEMA6D	chr15	47564943	0.08	0.0000078	0.04
cg13998260	XPNPEP1	chr10	111689701	0.08	0.0000343	0.05
cg17157234	PALMD	chr1	99974022	0.08	0.0000110	0.04
cg13027933	MYL1	chr2	211168547	0.08	0.0000098	0.04
cg19004285	NR2C1	chr12	95468616	0.08	0.0000171	0.04
cg05560321	MIR569	chr3	170984982	0.08	0.0000273	0.05
cg23110890	SIRPB1	chr20	1614192	0.08	0.0000323	0.05
cg04843137	NUDT7	chr16	77760029	0.08	0.0000290	0.05
cg12652240	SVEP1	chr9	113188514	0.08	0.0000166	0.04
cg01696336	SLC25A26	chr3	66311011	0.08	0.0000160	0.04
cg03564473	ELMO1	chr7	37191218	0.08	0.0000037	0.04

ILMN probe	UCSC hg19 gene (-500, +500 bp)	Chr	position	log₂ beta FC	*p*-value	*q*-value
cg26566271	OR2F1	chr7	143651877	0.08	0.0000186	0.04
cg17654821	TAMM41	chr3	11860723	0.08	0.0000188	0.04
cg04937851	COPS8	chr2	237993660	0.08	0.0000181	0.04
cg23981142	MAML3	chr4	141020664	0.07	0.0000098	0.04
cg00378492	SCN5A	chr3	38688954	0.07	0.0000009	0.03
cg17417739	UST	chr6	149072089	0.07	0.0000367	0.05
cg18937354	ARHGAP25	chr2	68943968	0.07	0.0000144	0.04
cg04090117	DNER	chr2	230319995	0.07	0.0000274	0.05
cg03276552	IL1RAP	chr3	190229556	0.07	0.0000279	0.05
cg05124953	ARRDC3-AS1	chr5	90524312	0.07	0.0000181	0.04
cg21220297	FRMD4B	chr3	69359138	0.07	0.0000159	0.04
cg03392759	YES1	chr18	801523	0.07	0.0000262	0.05
cg15962375	RPS6KC1	chr1	213563639	0.07	0.0000094	0.04
cg01587411	RRAS2	chr11	14376514	0.07	0.0000122	0.04
cg15851696	PDE1A	chr2	183183274	0.07	0.0000182	0.04
cg25053332	LINC01432	chr20	22034354	0.07	0.0000188	0.04
cg13918297	MIR3156-1	chr10	45678192	0.07	0.0000113	0.04

Annotations. ILMN probe = Illumina methylation probe; UCSC hg19 gene (-500, +500 bp) = UCSC hg19 closest annotated gene name 500 bp upstream or downstream of the probe; chr = chromosome; log₂ beta FC = log₂ beta fold change, *q*-value = FDR-corrected *p*-value; NA = Not available, i.e. the probe was not within 500 bp upstream or downstream of a known gene.

The highest increases in DNAm gain were found in probes annotated to Long Intergenic Non-Protein Coding RNA 1501 (*LINC01501*) associated with age of onset in major depressive disorder (Gedik, 2017), followed by Neural Cadherin (*CDH2*) important in the formation of cortex layers (Gil-Sanz et al., 2014), Aconitate Decarboxylase 1 (*ACOD1*), which has an anti-inflammatory role (Mills et al., 2018) and Neuregulin 1 (*NRG1*), which is known to be implicated in neural development, synaptic plasticity, and schizophrenia (Mei & Xiong, 2008). In fact, multiple probes annotated to *NRG1* were differentially regulated in different separate regions of the gene (**Supplementary Table 7**). One such differentially methylated region encompassing four probes is shown in **Figure 50**.
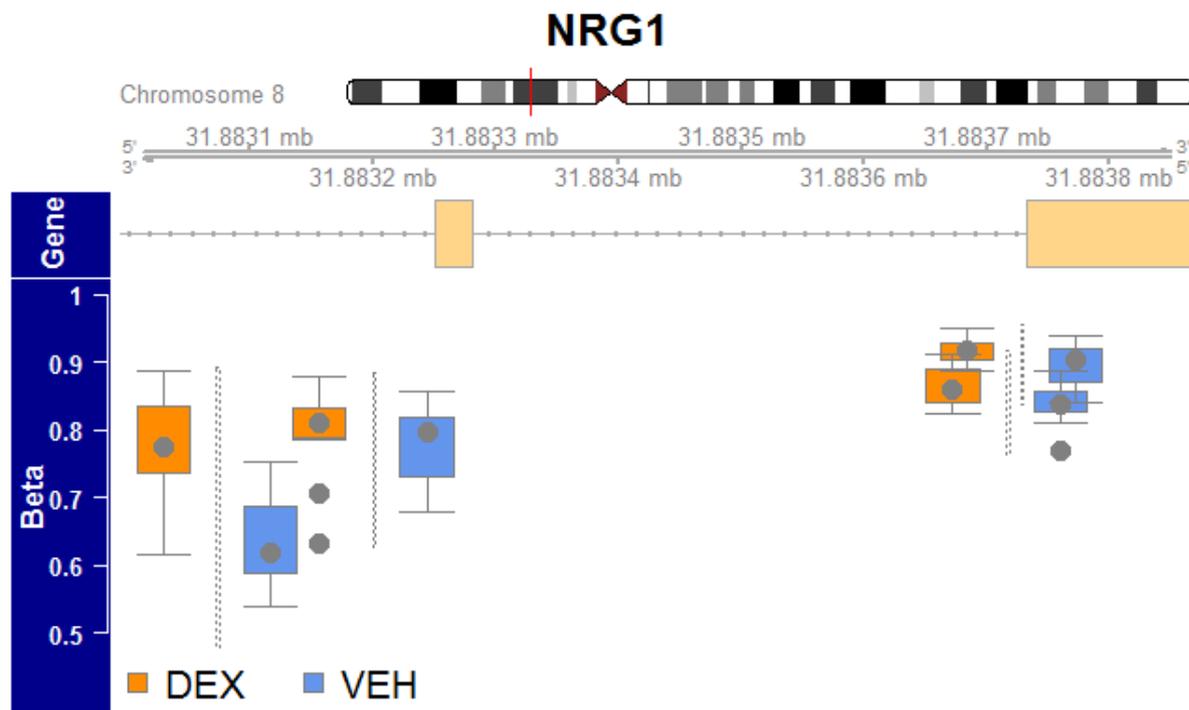
Figure 50. Differentially methylated region in NRG1. Mean beta change ≥ 3%, q ≤ 0.1.

Further gains in DNAm over 10% compared to the unstimulated condition were found in probes annotated to F-Box Protein 38 (*FBXO38*), a coactivator of the Krüppel-like factor 7 (*KLF7*), which regulates genes required for neuronal axon outgrowth and repair (Sumner et al., 2013), VRK Serine/Threonine Kinase 2 (*VRK2*), common variants in which were associated with schizophrenia (Steinberg et al., 2011) and which has recently been proposed as candidate gene for psychiatric and neurological disorders (Li & Yue, 2018), or Crystallin Beta-Gamma Domain Containing 1 (*CRYBG1*), which does not have an established function in brain to date, but was found to be in close proximity to a new locus associated with systemic inflammation in adulthood (Shin et al., 2019). One of these highly hypermethylated probes was moreover annotated to Solute Carrier Family 6 Member 15 (*SLC6A15*),

which was found to be involved in glutamatergic transmission (Santarelli et al., 2016) and confer risk to major depression (Kohli et al., 2011).

Both the results for cutoffs set at $q \leq 0.05$ and $q \leq 0.1$ included probes annotated to genes with well-known implications in neuronal development and psychiatric disorders.

Among probes significant at $q \leq 0.05$, these included *MAP2*, Epidermal Growth Factor Receptor (*EGFR*), implicated in the maturation of neural progenitor cells (Burrows et al., 1997), Musashi 2 (*MSI2*), which is expressed in the ventricular zone and subventricular zone of the developing cortex (Sakakibara et al., 2001), Slit Guidance Ligand 3 (*SLIT3*), which is best known for its role in axon guidance (Long et al., 2004), but was also associated with MDD (Glessner et al., 2010), Serine / threonine-protein kinase 1 (*SGK1*), a gene shown to potentiate GR nuclear translocation, reduce neurogenesis, and inhibit neurogenic Hedgehog signaling (Anacker et al., 2013), and Tryptophan Hydroxylase 2 (*TPH2*), also associated with MDD (Zill et al., 2004).

Results for DMPs at a significance cutoff of $q \leq 0.1$ are shown in **Figure 51**. Among these, notable genes annotated to regulated probes included *GPM6A*, variants in which were associated with schizophrenia (Li et al., 2017), Autism Susceptibility Candidate 2 (*AUTS2*), whose downregulation had previously been found to cause developmental abnormalities in mice by impairing neurite outgrowth and neuronal migration (Hori et al., 2014), Transcription Factor 4 (*TCF4*), variation in which has repeatedly been associated with schizophrenia on a genome-wide level (Ripke et al., 2011; Wray et al., 2018), or Receptor Tyrosine-Protein Kinase 4 (*ERBB4*), which is a receptor for NRG1 and implicated in NMDA receptor hypofunction in schizophrenia (Hahn et al., 2006).

In addition, several DMPs were annotated to genes encoding for crucial actors in the HPA axis (*NR3C1* and Nuclear Receptor Subfamily 3 Group C Member 2 (*NR3C2*)), or to genes important during brain development and axis formation (SMAD Family Member 2 (*SMAD2*), Transforming Growth Factor Beta Receptor 1 (*TGFBR1*), Bone Morphogenetic Proteins 1A (*BMPR1A*), and 2 (*BMPR2*), and Roundabout Guidance Receptor 1 (*ROBO1*)).
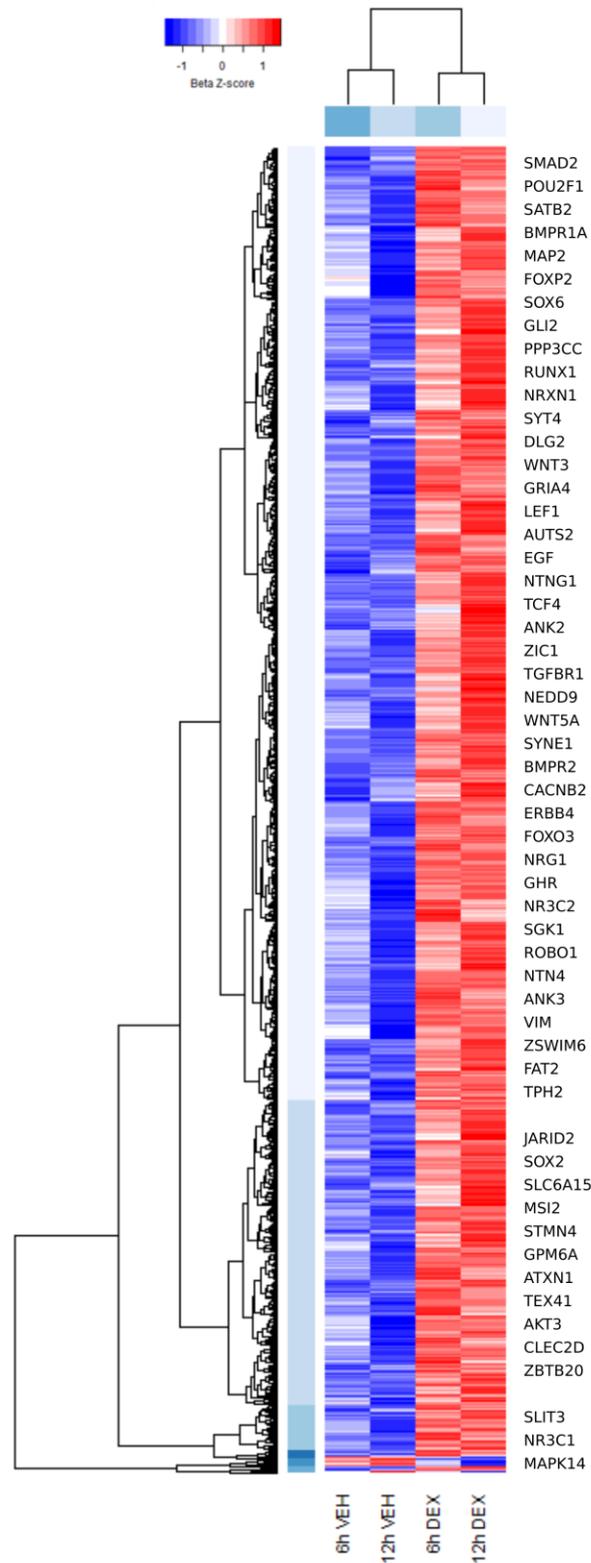
Figure 51. Heatmap of differentially methylated positions in D44 neurons following DEX exposure. DMPs ($q \leq 0.1$, beta change $\geq 5\%$) were annotated to the closest gene 500 bp upstream or downstream (n=2 034).

In addition to findings on *NRG1*, secondary analyses run on differentially methylated regions with a medium beta change cutoff of 3% identified alterations in another candidate gene for schizophrenia susceptibility (Millar et al., 2000): Disrupted in Schizophrenia 1 (*DISC1*) (**Fig. 52**).
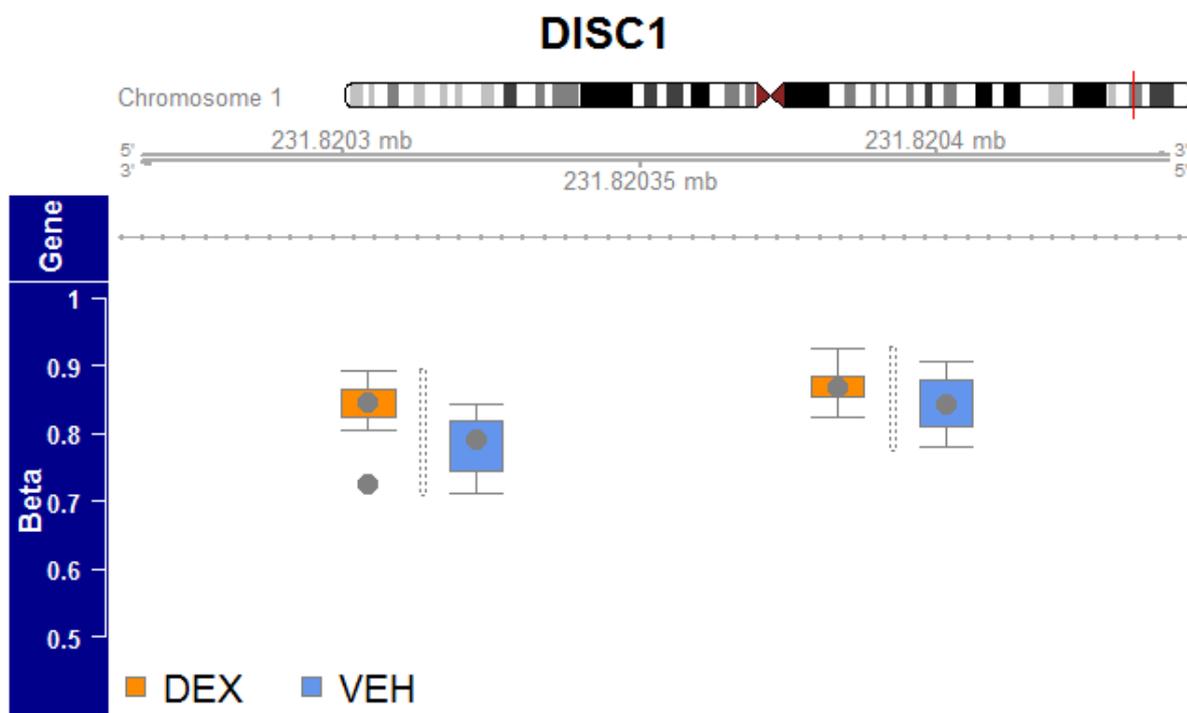
Figure 52. Differentially methylated region in DISC1. Mean beta change ≥ 3%, $q ≤ 0.1$.

Exhaustive results lists for functional enrichment analyses of differentially methylated regions in D44 differentiated neurons can be found in **Supplementary Table 10**. A subset of the results is shown in the different figures.

Functional enrichment analysis for GO Biological Process terms ($q ≤ 0.05$) (**Fig. 53**) revealed that differentially methylated regions following dexamethasone exposure were significantly enriched for neurogenesis and related terms such as neuron development, axon development, neuron projection morphogenesis, axon

guidance, cell migration, apoptotic process, positive regulation of stem cell proliferation, positive regulation of cell migration, or regulation of gliogenesis. Several terms were furthermore associated with embryogenesis in a broader sense, such as embryo development, regulation of growth, palate development, telencephalon development, forebrain development, neural tube development, inner ear development, and lung morphogenesis. Some others referred to either the stress or immune systems, like regulation of stress-activated protein kinase signaling cascade, regulation of MAPK cascade and immune system development. Finally, significant enrichment was also detected for the Wnt receptor signaling pathway.
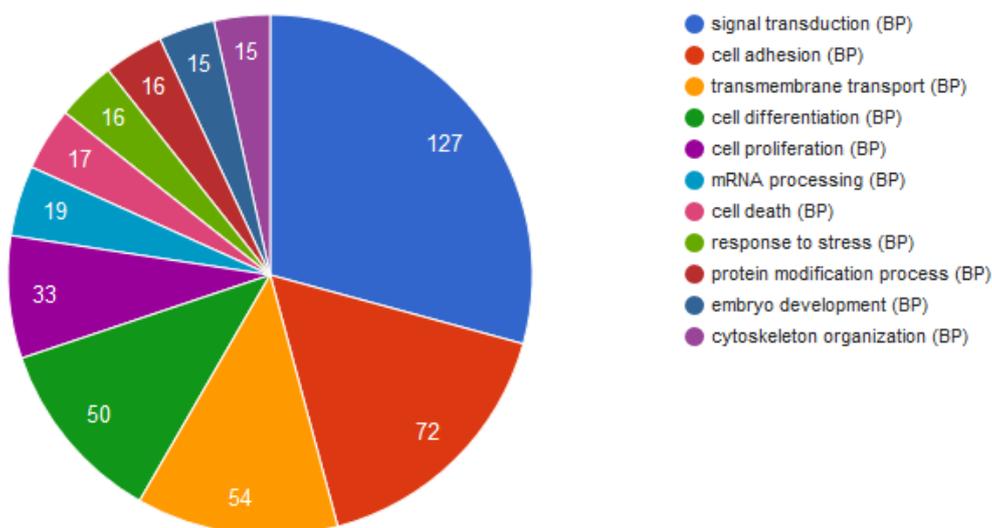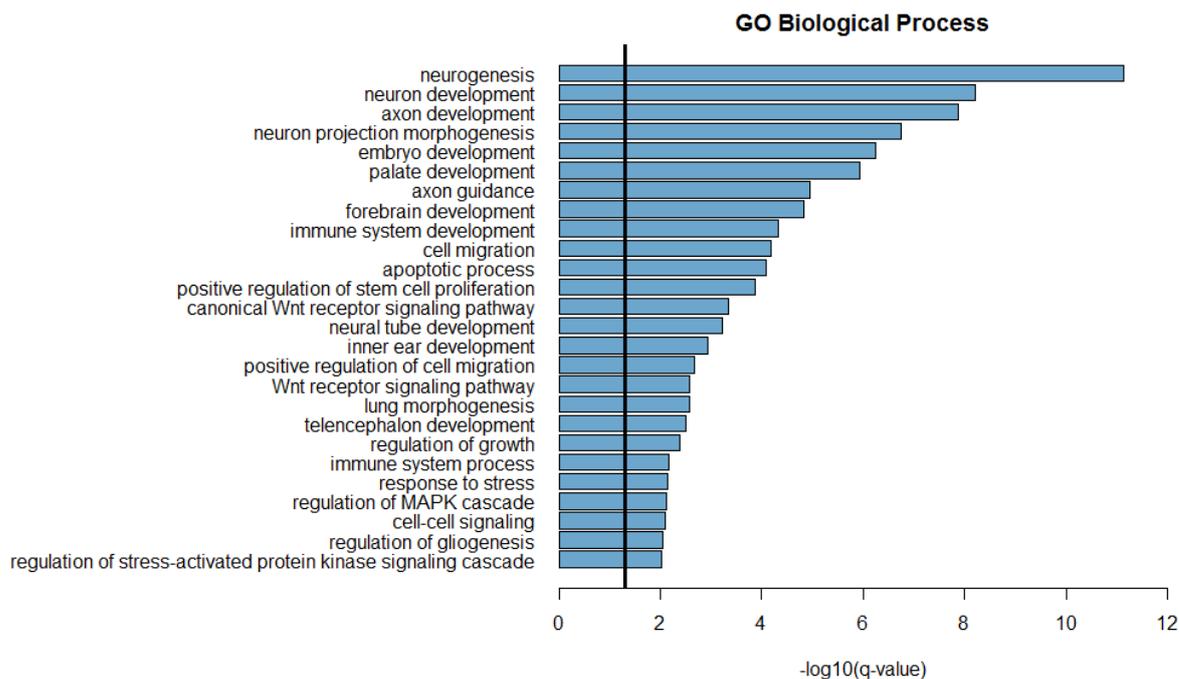
Figure 53. Functional enrichment analysis for DMRs in D44 neurons following DEX exposure (Gene Ontology Biological Process). Significantly enriched terms ($q \leq 0.05$) for DMRs ($q \leq 0.1$).

Indeed, Wnt signaling was the most significantly enriched pathway in the PANTHER pathway database (**Fig. 54**), followed by angiogenesis and the cadherin

signaling pathway. Overrepresentation of DEX-induced DMRs was furthermore found in pathways previously enriched for DMRs showing hypomethylation during transition from hSC to NP, and hypermethylation during terminal neuronal differentiation from NP to dN. These were the Alzheimer disease-presenilin pathway, PDGF signaling pathway, and Integrin signaling pathway.
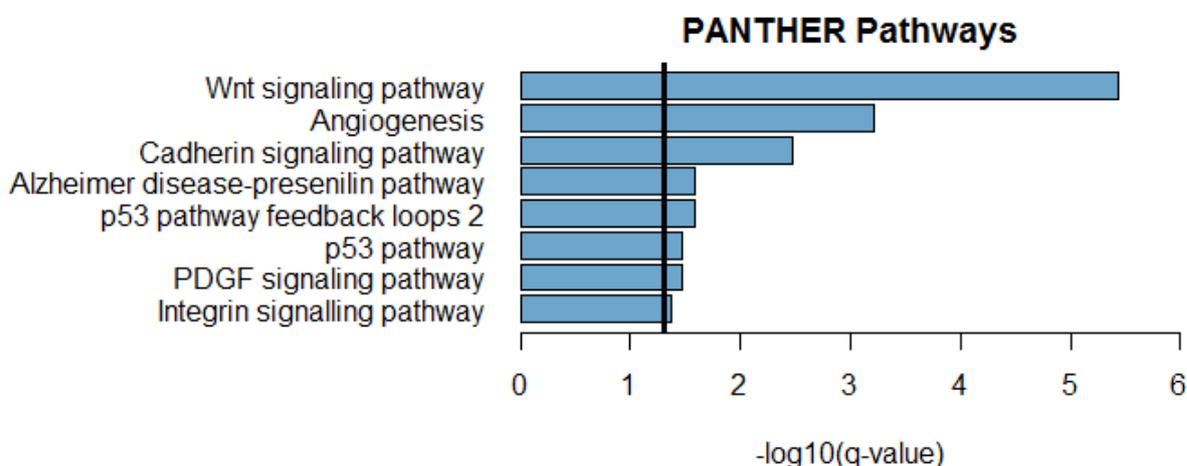
Figure 54. Functional enrichment analysis for DMRs in D44 neurons following DEX exposure (PANTHER Pathways). Significantly enriched terms ($q \leq 0.05$) for DMRs ($q \leq 0.1$).

Lastly, among diseases annotated in the mSigDB Disease Ontology database (**Fig. 55**), DEX-induced DMRs were significantly overrepresented in genes associated with nervous system and immune system disease. Non-psychiatric conditions included diabetes mellitus and asthma, while significant enrichment for specific psychiatric disorders was found for schizophrenia alongside psychotic disease, substance-related disease, anxiety and panic disorders ($q \leq 0.05$). Autism,

bipolar disease, borderline personality disorder, obsessive-compulsive disease, and developmental disease of mental health were additionally significantly enriched for at a cutoff of $q \leq 0.1$.
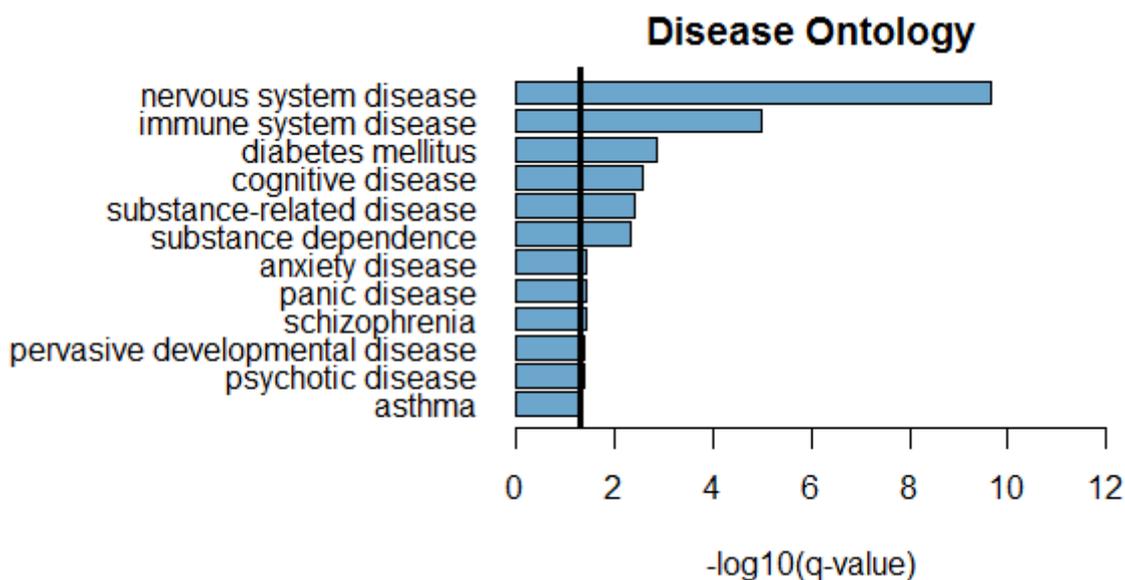
Figure 55. Functional enrichment analysis for DMRs in D44 neurons following DEX exposure (mSigDB Disease Ontology). Significantly enriched terms ($q \leq 0.05$) for DMRs ($q \leq 0.1$).

Overall, dexamethasone exposure resulted in a predominant increase in DNA methylation in D44 neurons as the latest examined stage of differentiation. Functional enrichment analyses of differentially methylated regions implicate that alterations may play a role in neuronal development and specifically the Wnt signaling pathway, as well as neurodevelopmental disorders of mental health.

4.4 EFFECTS OF DEXAMETHASONE EXPOSURE ON THE TRANSCRIPTOME

Concurrent with analyses of methylation, differential gene expression in RNA-seq data showed increased reactivity to dexamethasone with ongoing differentiation (**Supplementary Table 4**). Specifically, n=2 transcripts were upregulated in hSC, n=9 in neural progenitors, and n= 33 in neurons ($q \leq 0.1$).

The two genes regulated by dexamethasone at the stem cell stage (**Fig. 56**) were *CXorf408* and Claudin Domain Containing 1 (*CLDND1*), neither of which is functionally well-defined. However, *CLDND1* encodes for a tight junction protein and might play a role in regulating inflammation (Wang et al., 2017).
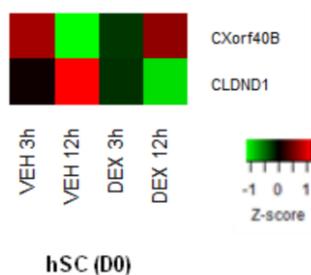
Figure 56. Heatmap of DEX-induced differentially expressed genes in hSC. Based on individual contrasts between stimulated and unstimulated cells for 3h and 12h, respectively ($q \leq 0.1$).

DEX-regulated transcripts in NPs (**Fig. 57**) included PR Domain Zinc Finger Protein 15 (*PRDM15*), which serves as a molecular node in a transcriptional network regulating cell fate decision. It stimulates expression of transcriptional activators and repressors of the Wnt and MAPK/ERK pathways, respectively, and promotes

SPRY1 transcription activation by direct binding in its promoter region (Mzoughi et al., 2017). Furthermore, downregulation in NPs was found for COMM domain containing 5 (*COMMD5*). Depletion in this gene has been associated with decreased cell proliferation and impairments in directional cell migration along the cytoskeleton (Campion et al., 2018). Dynamic DEX-induced regulation over time was also detected for IQ Motif Containing GTPase Activating Protein 3 (*IQGAP3*), which is reported to associate directly with actin filaments and accumulate asymmetrically at the distal region of axons in hippocampal neurons. The depletion of IQGAP3 was found to impair neurite or axon outgrowth in neuronal cells due to disorganization of the cytoskeleton (Wang et al., 2007). It is also assumed to be exclusively expressed in proliferating cells and was found to positively regulate cell proliferation (Nojima et al., 2008). Fatty Acid Binding Protein 5 (*FABP5*) was upregulated following 12h of dexamethasone stimulation. In mice it is expressed in the subgranular zone of the dentate gyrus, where its knockout led to enhanced neuronal differentiation (Matsumata et al., 2012).
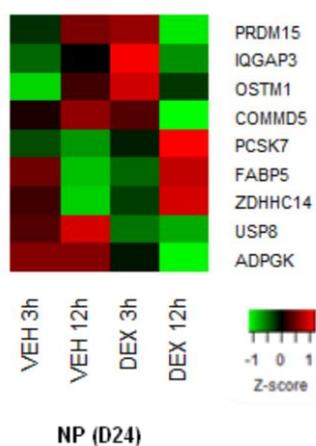
Figure 57. Heatmap of DEX-induced differentially expressed genes in NP. Based on individual contrasts between stimulated and unstimulated cells for 3h and 12h, respectively ($q \leq 0.1$).
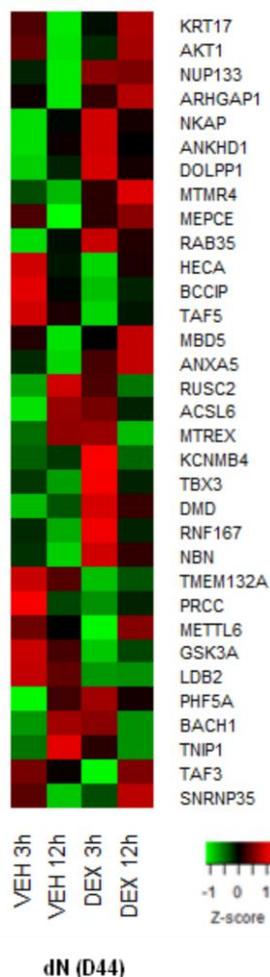
Figure 58. Heatmap of DEX-induced differentially expressed genes in dN. Based on individual contrasts between stimulated and unstimulated cells for 3h and 12h, respectively ($q \leq 0.1$).

In neurons (**Fig. 58**), DEX-induced downregulation was observed for Glycogen Synthase Kinase 3 A (*GSK3A*), while the transcript for AKT Serine/Threonine kinase 1 (*AKT1*) was upregulated. Both genes are part of the same signaling pathway, which in turn has been associated with schizophrenia (Emamian et al., 2004; Emamian, 2012). Nibrin (*NBN*) and Methyl-CpG-Binding Domain 5 (*MBD5*) transcripts were also upregulated following dexamethasone stimulation.

The prior is associated with Nijmegen breakage syndrome, which is characterised by microcephaly, growth retardation, and immunodeficiency (Varon et al., 1998), while the latter has been implicated as a single causal locus of intellectual disability, epilepsy, and autism spectrum disorder (Talkowski et al., 2011). Further upregulation was found for Annexin A5 (*ANXA5*), associated with obstetric complications and miscarriage (Bogdanova et al., 2007; Tiscia et al., 2009; Hayashi et al., 2013).

Dexamethasone effects on the transcriptome level were furthermore evaluated by qPCR for genes known to be regulated by dexamethasone both from the literature (Frahm et al., 2016) and from the HumanHT-12 v4 Expression BeadChip microarray pilot study.
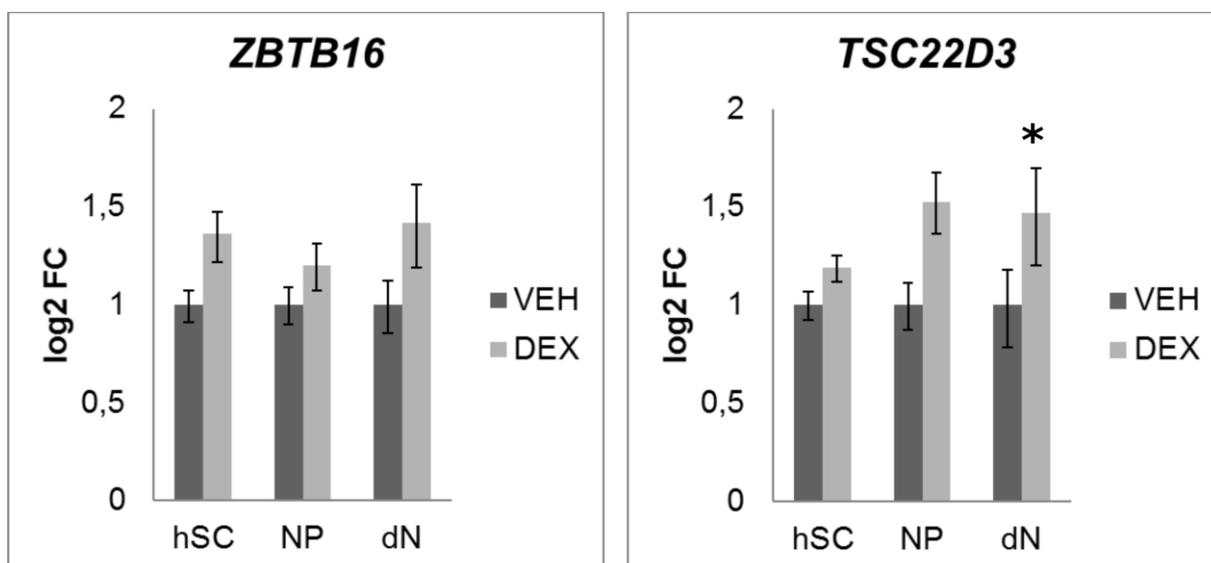
Figure 59. qPCR for stress-reactive genes. Log$_2$ fold change increases in *ZBTB16* and *TSC22D3* transcript levels (Student's t-Test (two-tailed), *p = 0.05).

In line with the general pattern observed for DEX-induced transcriptional activity in neurulating cells, stress-reactive genes *ZBTB16* and *TSC22D3* were not significantly regulated in hSC (**Fig. 59**). Indeed, upregulation of *ZBTB16* did not reach significance in any of the differentiation stages, but *TSC22D3* was significantly heightened in neurons following dexamethasone exposure, and marginally significantly increased in neuronal progenitors (**Table 14**).

Table 14. qPCR for *TSC22D3* and *ZBTB16*.

	TSC22D3		*ZBTB16*	
	log$_2$FC	*p*-value	log$_2$FC	*p*-value
hSC	0.77	0.45	1.41	0.24
NP	1.53	0.07	1.25	0.15
dN	1.47	0.03	1.47	0.11

Annotations. hSC = human stem cells, NP = neuronal progenitor cells, dN = differentiated neurons, log$_2$ FC = log$_2$ fold change, *p*-value = result statistics for paired Student's t-Test (2-tailed).

Results for functional enrichment analyses of DEX-induced transcripts (log$_2$ FC ≥ 0.5) using enrichr for PANTHER pathways ($p ≤ 0.1$) within the respective stages of differentiation are shown in **Table 15**. Overrepresentation of transcripts regulated in hSC was found in synaptic vesicle trafficking, while DEX-regulated transcripts in neuronal progenitors were enriched in the p53, PDGF signaling, JAK/STAT signaling, Histamine H2 receptor mediated signaling, and nicotine pharmacodynamics pathways. Differentially expressed genes in stimulated neurons were associated with integrin signaling, arginine, purine, and cholesterol biosynthesis, as well as synaptic vesicle trafficking, dopamine receptor mediated, metabotropic glutamate receptor, and beta 3 adrenergic receptor signaling pathways, and angiogenesis.

Table 15. Functional enrichment analysis (PANTHER pathways) of DEX-responsive genes (log$_2$FC ≥ 0.5).

Term	*p*-value	*q*-value	Z-score	Combined Score	DEX-regulated Genes (log$_2$FC ≥ 0.5)	Stage
Synaptic vesicle trafficking	0.014	0.49	-1.42	6.07	RIMS1; RAB3A; STXBP1	hSC
General transcription regulation	0.001	0.09	-1.35	9.13	GTF2A1; TAF12; TAF9; GTF2H3; TAF4; GTF2F2	NP
Transcription regulation by bZIP transcription factor	0.002	0.09	-1.42	8.72	GTF2A1; TAF12; PRKAR2B; TAF9; GTF2H3; TAF4; GTF2F2	NP
Nicotine pharmacodynamics pathway	0.007	0.19	-1.30	6.51	CHRNB2; CLIC6; CHRNA4; PRKACA; KCNK3	NP
PDGF signaling pathway	0.01	0.21	-1.36	6.27	VAV3; STAT5B; MAP2K1; RPS6KB1; RASA4; RPS6KC1; SRF; ITPR1; ARAF; PIK3C3; JAK3	NP
p53 pathway	0.01	0.21	-1.12	4.95	KAT6B; SERPINE1; PTEN; PMAIP1; SFN; PIK3C3; PML; DDB2	NP
Hypoxia response via HIF activation	0.02	0.26	-0.6	2.33	EGLN1; PTEN; PIK3C3; MTOR	NP
JAK/STAT signaling pathway	0.02	0.26	0.87	-3.34	PIAS3; STAT5B; JAK3	NP
Histamine H2 receptor mediated signaling pathway	0.06	0.53	0.84	-2.43	PRKAR2B; PRKACA	NP
CCKR signaling map ST	0.06	0.53	-1.04	2.94	TPST1; MAP2K1; RPS6KB1; SRF; SERPINE1; ITPR1; ARAF; PTEN; PRKACA; MEF2D; FOXO1; HDAC7	NP
p53 pathway by glucose deprivation	0.06	0.53	0.59	-1.64	PRKAA2; RPS6KB1; PRKAB1	NP
Integrin signaling pathway	0.004	0.37	-1.78	9.97	ITGB5; SRC; LAMA1; COL11A1; ILK; LAMC1; RAP1A; FLNA; ITGB8; ITGAV; MAP2K1; ITGA3; CAV1; ITGA2; FN1; PTPN12; RHOC; ARHGAP26; PTK2; COL1A1; COL3A1; COL1A2; COL5A1; PIK3CA; COL4A2; COL5A2; VCL	dN
Arginine biosynthesis	0.02	0.67	-0.37	1.53	CPS1; ASL; ASS1	dN
Synaptic vesicle trafficking	0.024	0.67	-0.99	3.72	SYT5; UNC13B; SYT3; STX2; STX1A; SYT7	dN
De novo purine biosynthesis	0.04	0.67	-0.82	2.61	RRM2; GMPS; AK2; AK5; ADSS; GART	dN
Dopamine receptor mediated signaling pathway	0.07	0.67	-1.41	3.68	CLIC6; GNAZ; EPB41L2; SNAP23; FLNA; ADCY2; PRKACA; COMT; SNAP29	dN
Metabotropic glutamate receptor group II pathway	0.08	0.67	-1.03	2.67	GRM2; BDNF; SNAP23; PRKACA; SNAP29; STX1A	dN
Angiogenesis	0.08	0.67	-1.09	2.76	NOTCH2; MAP2K1; FZD2; MAP3K1; SRC; WNT5A; ARHGAP1; HSPB1; FOS; RHOC; PRKCZ; PTK2; EFNB1; PIK3CA; FRZB; DVL2; AKT1; DVL3; PRKD2; EPHB3	dN
Formyltetrahydroformate biosynthesis	0.08	0.67	4.26	-10.61	MTHFD2; TYMS	dN
Beta3 adrenergic receptor signaling pathway	0.09	0.67	0.79	-1.89	SNAP23; ADCY2; SNAP29	dN
Cholesterol biosynthesis	0.09	0.67	2.03	-4.85	SQLE; MVK; FDFT1	dN
p53 pathway	0.10	0.67	-0.51	1.19	CCNB1; RRM2; PIK3CA; APAF1; HDAC1; PERP; IGFBP3; SERPINE1; AKT1; GTSE1; DDB2	dN

Annotations. Combined Score = log of the *p*-value from the Fisher exact test multiplied by the z-score of the deviation from the expected rank. hSC = human Stem Cells, NP = Neuronal Progenitors, dN = differentiated Neurons.

Results for functional enrichment analyses of DEX-induced transcripts (log2 FC ≥ 0.5) using the Consensus Pathway DB for Pathways ($p ≤ 0.01$) within the respective stages of differentiation are shown in **Figure 60**.
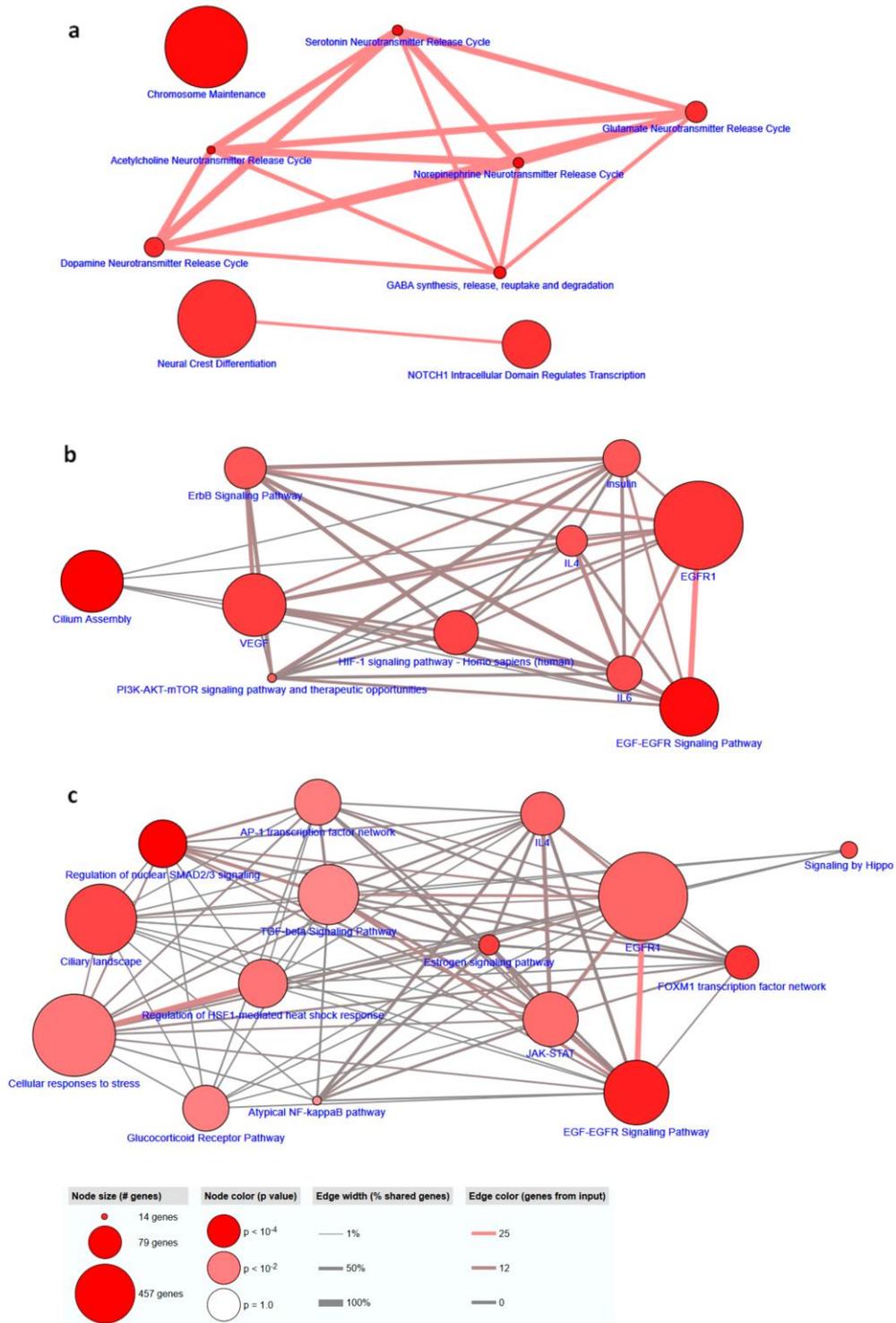
Figure 60. Functional enrichment analysis (ConsensusPathwayDB) of DEX-responsive genes (log₂FC ≥ 0.5). a) Stimulation of hSC, b) Stimulation of NP, c) Stimulation of dN, *p* = 0.01).

Results for functional enrichment analyses of DEX-induced transcripts (log2 FC ≥ 0.5) for KEGG pathways using DAVID ($p \leq 0.1$) within the respective stages of differentiation are shown in **Table 16**.

Table 16. Functional enrichment analysis (KEGG pathways) of DEX-responsive genes (log$_2$FC ≥ 0.5).

Term	Fold Enrichment	*p*-value	BH	DEX-regulated Genes (log$_2$FC ≥ 0.5)	Stage
Peroxisome	4.40	0.01	0.87	HMGCLL1, GSTK1, PEX16, ABCD4, SCP2, ACOX3	hSC
Synaptic vesicle cycle	4.83	0.02	0.82	RAB3A, AP2A1, ATP6V1E2, STXBP1, RIMS1	hSC
Bladder cancer	5.94	0.03	0.83	CDKN2A, HBEGF, THBS1, MYC	hSC
Purine metabolism	2.42	0.07	0.96	NME2, PDE2A, NME1-NME2, NT5M, ADCY5, NPR2, POLA2	hSC
Basal transcription factors	4.16	0.003	0.49	MNAT1, TAF4, TAF12, GTF2A1, GTF2I, GTF2F2, GTF2H3, TAF9	NP
Lysosome	2.51	0.005	0.49	GNPTG, NPC1, AP1S1, GLA, GM2A, SMPD1, ARSA, GALC, ATP6V1H, CD164, ATP6V0A2, CLN5, GLB1	NP
Endocytosis	1.94	0.007	0.44	CAV1, USP8, VTA1, PML, CYTH3, VPS37D, SNX3, ARFGEF2, LDLRAP1, RAB11FIP5, CBLB, SH3GLB2, ARPC3, ACAP3, PSD, DNAJC6, WIPF1, ITCH, ARAP3, EHD4	NP
HIF-1 signaling pathway	2.68	0.007	0.38	PDK1, CUL2, LTBR, MAP2K1, SERPINE1, HK2, ENO3, NFKB1, RPS6KB1, EGLN1, MTOR	NP
Galactose metabolism	4.68	0.008	0.34	PGM2, GALK1, GLA, HK2, PFKM, GLB1	NP
Acute myeloid leukemia	3.34	0.009	0.32	JUP, MAP2K1, STAT5B, ARAF, PML, NFKB1, RPS6KB1, MTOR	NP
Ubiquitin mediated proteolysis	2.05	0.03	0.69	FANCL, CUL2, CBLB, CUL7, PIAS3, TRIM32, PML, DDB2, UBE2F, FBXO4, ITCH, CDC26	NP
Insulin signaling pathway	2.04	0.03	0.66	PRKAR2B, CBLB, MAP2K1, ARAF, PRKAB1, HK2, PDE3B, FOXO1, PRKACA, RPS6KB1, PRKAA2, MTOR	NP
mTOR signaling pathway	2.82	0.04	0.64	CAB39L, ULK2, RPS6KB1, RICTOR, PRKAA2, MTOR, PTEN	NP
RNA degradation	2.43	0.05	0.69	PATL1, SKIV2L, TTC37, EXOSC2, ENO3, PFKM, PABPC1L, CNOT6	NP

Term	Fold Enrichment	*p*-value	BH	DEX-regulated Genes (log$_2$FC ≥ 0.5)	Stage
Sphingolipid metabolism	2.99	0.05	0.68	GLA, SMPD1, ARSA, GALC, B4GALT6, GLB1	NP
Central carbon metabolism in cancer	2.56	0.05	0.69	SLC16A3, PDK1, MAP2K1, HK2, MTOR, PFKM, PTEN	NP
Primary immunodeficiency	3.44	0.06	0.67	ORAI1, RFX5, TAP2, RFXAP, ADA	NP
Amyotrophic lateral sclerosis (ALS)	2.81	0.06	0.68	BID, SLC1A2, TNFRSF1B, GRIA1, CCS, NEFM	NP
ErbB signaling pathway	2.15	0.08	0.74	CBLB, NRG4, MAP2K1, STAT5B, PAK5, ARAF, RPS6KB1, MTOR	NP
Ribosome biogenesis in eukaryotes	2.15	0.08	0.74	TBL3, SNORD3A, UTP15, POP1, POP4, UTP14A, GNL2, POP5	NP
Proteoglycans in cancer	1.64	0.08	0.75	CAV1, MAP2K1, PPP1R12B, ITGB5, RPS6KB1, ITPR1, CBLB, CD44, ITGA5, ARAF, PRKACA, MTOR, FRS2, SLC9A1	NP
Biosynthesis of amino acids	2.28	0.09	0.74	SHMT1, BCAT2, ASS1, MTR, ENO3, PFKM, PC	NP
RNA degradation	2.49	2.47E-4	0.07	NUDT16, PAN3, EXOSC6, PFKL, EXOSC7, EXOSC4, PNPT1, PABPC4, PAPD7, EXOSC2, CNOT2, CNOT1, EXOSC1, CNOT4, DCP2, DCP1B, DCP1A, PABPC1L, ZCCHC7, C1D	dN
Small cell lung cancer	2.37	3.39E-4	0.05	E2F1, CKS1B, COL4A2, XIAP, RXRB, SKP2, NFKBIA, ITGA2, NFKB1, ITGA3, CDK4, AKT1, LAMA1, PTK2, CDKN1B, ITGAV, IKBKG, PIK3CA, LAMC1, APAF1, FN1	dN
Ribosome biogenesis in eukaryotes	2.21	0.001	0.11	NOL6, NXT1, GTPBP4, GAR1, TCOF1, MPHOSPH10, GNL3L, NXF1, FCF1, NOP10, NVL, WDR36, SNORD3A, POP1, WDR3, POP5, GNL2, UTP14A, SPATA5, WDR43	dN
Purine metabolism	1.75	0.002	0.14	ADSS, GMPR2, ADCY2, POLR2K, PNPT1, ADCY6, ZNRD1, PDE4A, PDE4B, PDE1A, GUCY1A2, ENTPD4, IMPDH1, NUDT16, POLR3H, POLR1A, AK2, NPR2, AK5, POLR1B, AK4, DGUOK, GMPS, POLR3E, AK9, APRT, GART, POLD3, ITPA, RRM2, PGM1, PAICS	dN
ECM-receptor interaction	1.99	0.0077	0.34	COL4A2, COL3A1, HSPG2, ITGA2, ITGB5, ITGA3, SDC4, COL5A2, COL5A1, LAMA1, CD44, ITGB8, ITGAV, COL1A2, COL1A1, LAMC1, COL11A1, FN1	dN

[151]

Term	Fold Enrichment	*p*-value	BH	DEX-regulated Genes (log$_2$FC ≥ 0.5)	Stage
p53 signaling pathway	2.15	0.008	0.31	CDK1, CDK4, SESN1, GTSE1, SESN3, CCNB1, CDKN2A, CCND2, RRM2, SERPINE1, DDB2, APAF1, PERP, ADGRB1, IGFBP3	dN
Basal transcription factors	2.35	0.02	0.45	TAF2, GTF2E1, TAF10, TAF1, GTF2E2, TAF5L, TAF3, TAF6, TAF5, GTF2H1, ERCC2	dN
Focal adhesion	1.49	0.02	0.53	CAV1, XIAP, DIAPH1, COL3A1, ITGB5, SRC, VCL, AKT1, PTK2, ITGB8, ITGAV, ILK, PIK3CA, COL11A1, FN1, PARVG, COL4A2, MAP2K1, ROCK1, ITGA2, ITGA3, MYL12A, COL5A2, FLNA, COL5A1, VEGFB, LAMA1, CCND2, COL1A2, RAP1A, COL1A1, LAMC1	dN
Thyroid hormone signaling pathway	1.67	0.03	0.57	BMP4, THRA, MAP2K1, RXRB, PFKFB2, ESR1, FOXO1, SRC, AKT1, NOTCH2, SLC16A2, NCOA1, HDAC1, DIO2, NCOA3, MED16, DIO3, ITGAV, PIK3CA, PRKACA	dN
Glycosaminoglycan biosynthesis - heparan sulfate / heparin	2.80	0.03	0.59	NDST4, NDST2, HS3ST1, B4GALT7, EXTL2, EXT2, HS2ST1	dN
Hippo signaling pathway	1.53	0.04	0.63	PPP2R1B, DVL2, WNT5A, BMP4, DVL3, PRKCZ, BMP2, TP53BP2, TGFBR1, WWC1, PATJ, FZD2, LATS1, LATS2, CCND2, CTGF, ID1, RASSF1, SERPINE1, DLG3, YAP1, WNT9A, BMP7, BMPR1A	dN
Non-homologous end-joining	3.69	0.04	0.59	DCLRE1C, POLM, PRKDC, LIG4, NHEJ1	dN
Lysosome	1.59	0.04	0.61	CTSZ, LIPA, GM2A, LGMN, ABCA2, CTSS, CD164, ASAH1, AP1S3, NAGPA, NPC2, SMPD1, GAA, ARSA, NEU1, CTSC, ENTPD4, MAN2B1, GGA3, CLN5	dN
Hepatitis B	1.52	0.04	0.59	E2F1, MAVS, MAP2K1, TGFBR1, STAT5B, HSPG2, NFKBIA, NFKB1, CDK4, SRC, ATF2, IFNAR1, AKT1, FOS, CDKN1B, MAP3K1, TICAM1, IKBKG, ATF6B, DDB2, CREB3L1, PIK3CA, APAF1	dN

Term	Fold Enrichment	*p*-value	BH	DEX-regulated Genes (log$_2$FC ≥ 0.5)	
Endocytosis	1.36	0.06	0.67	VPS29, PRKCZ, CAV1, USP8, STAM2, CYTH3, SNX3, ARFGEF1, SRC, CXCR4, WWP1, GIT2, RAB11B, DNAJC6, SPG21, IQSEC3, EHD3, MVB12B, RAB8A, VPS45, TGFBR1, RAB4A, HLA-C, HLA-B, TFRC, ARRB1, RAB35, GRK5, RAB10, GRK3, RAB11FIP1, DNM1, EPN1, VPS25	dN
Glycerophospholipid metabolism	1.62	0.07	0.69	GPD2, ACHE, CRLS1, CDIPT, DGKQ, LYPLA1, PISD, CDS1, GPCPD1, LPIN2, CHPT1, LPCAT3, DGKA, CEPT1, LPCAT1, DGKD	dN
Chronic myeloid leukemia	1.74	0.07	0.67	E2F1, AKT1, CDKN2A, CDKN1B, HDAC1, MAP2K1, TGFBR1, IKBKG, STAT5B, NFKBIA, PIK3CA, NFKB1, CDK4	dN
Arginine and proline metabolism	1.92	0.07	0.67	SAT1, ALDH18A1, SRM, CNDP2, P4HA1, SAT2, ALDH4A1, GAMT, ALDH3A2, ALDH9A1	dN
Glutathione metabolism	1.88	0.08	0.69	GSTM1, GPX1, TXNDC12, G6PD, SRM, RRM2, GSTK1, GPX8, GCLM, MGST2	dN
Platelet activation	1.48	0.08	0.68	PRKCZ, ADCY2, ROCK1, COL3A1, ADCY6, STIM1, ITGA2, MYL12A, COL5A2, COL5A1, SRC, AKT1, COL1A2, GUCY1A2, PIK3CA, RAP1A, PRKACA, COL1A1, SNAP23, COL11A1	dN

Annotations. BH = Benjamini-Hochberg-corrected *p*-value. hSC = human Stem Cells, NP = Neuronal Progenitors, dN = differentiated Neurons.

In sum, the number of differentially expressed transcripts following stimulation with dexamethasone increased progressively with ongoing neuronal differentiation. Altered expression was found in genes associated with neuronal migration, cytoskeleton organization, and neurodevelopmental conditions such as intellectual disability, epilepsy, autism or schizophrenia.

[153]

5. DISCUSSION

The current study investigated the potential molecular effects of prenatal stress on the developing brain by modelling embryonic neurogenesis in human stem cells and inducing GR-dependent epigenetic changes. Pilot studies were conducted in order to establish a differentiation protocol yielding homogeneous formation of neural rosettes, establish an assay to identify subcellular localization of the glucocorticoid receptor, and assess the reactivity of differentiating cells to GR binding on the transcriptome level.

In order to understand the developmental context in which dexamethasone-induced epigenetic changes occur, neuronally differentiating cells were first characterised by marker protein expression, spatiotemporal gene expression profile, events of consecutive methylation and demethylation, as well as enrichment for Gene Ontology terms, pathway data and chromatin states. Since cells at this stage of development undergo rapid changes, an in-depth characterisation was deemed essential to understand the biological significance of dexamethasone-induced alterations. These analyses indicated that *in vitro* differentiated cells emulated the earliest cell types of the developing nervous system on embryonic days 3.5 to ~ week 8-16 post conception. Transcriptionally mapping onto fetal *post mortem* tissue of the ventricular zone and between the outer subventricular zone and cortical plate, respectively, they were considered to best represent cells found in the germinal zone of the developing telencephalon.

Intrinsic glucocorticoid receptor activity was then assessed by means of protein expression levels, intracellular localisation, translocation dynamics, as well

as by enrichment for glucocorticoid response elements (GREs) in developmentally and dexamethasone-induced differentially methylated regions. Not only was neuronal development accompanied by a gradual increase in absolute GR levels, but also by a constitutive shift in subcellular receptor localization under unstimulated conditions.

Finally, epigenetic effects were analysed separately for individual stages of differentiation. In line with increased GR expression and translocation, differentiated neurons showed the strongest response to dexamethasone on both the transcript and methylation level compared to earlier stages of differentiation. Potential functional consequences were evaluated using enrichment analyses, which suggested a possible role of GR activation in brain development and neurodevelopmental psychiatric disorders.

Overall, the data presented here suggested that a) the GR may have an endogenous role during the early stages of neurogenesis, b) sensitivity of neurulating cells to external glucocorticoids may arise progressively with differentiation, and c) migrating neurons might undergo a sensitive phase for disruption by external glucocorticoids, which act on genes implicated in Wnt signaling, cell migration, axon guidance, and as a consequence on developmental neuropsychiatric disorders.

The discussion will first focus on technical aspects concerning the use of directed differentiation from stem cells and induced pluripotent stem cells as model system, limitations imposed by microarray-based and 3'sequencing-based

techniques, and the process of statistical decision-making. The second part will then elaborate on potential functional implications of presented results.

5.1 TECHNICAL ASPECTS

5.1.1 INDUCED PLURIPOTENT STEM CELLS AS MODEL SYSTEM.

The possibilities associated with induced pluripotent stem cells and embryonic stem cells as model system have inspired a great amount of research both on the optimization of protocols, and regarding translation to clinical applications. Major challenges on the technical level included the biased differentiation propensity of individual cell lines towards their lineage of origin, the generation of homogeneous populations of differentiated target cells, and the intrinsic cell fate specification program following induction of differentiation.

Here, stimulation experiments were conducted on cell lines with well established competence regarding differentiation towards the ectodermal lineage. However, this would not be possible in experiments that require specific lines, such as patient studies. Clinical studies are more likely to rely on blood as tissue of origin due to its accessibility and would then need to circumvent the problem of differentiation bias in a different manner. In induced pluripotent stem cells derived from mice, epigenetic differentiation bias was shown to attenuate with repeated series of differentiation and reprogramming or by treatment with chromatin-modifying drugs (Kim et al., 2010). Similar approaches could be applied to improve neural differentiation in human induced pluripotent stem cells derived from blood. However, serial differentiation and reprogramming would mean an enormous burden on the experimental timeline. Pre-treatment of pluripotent cells with

Dimethylsulfoxide (DMSO) on the other hand is a simple, low-cost method shown to improve differentiation into multiple lineages (Chetty et al., 2013).

In addition, differentiation protocols are undergoing continuous optimization. For example, there are methods for direct trans-differentiation of neurons from either fibroblasts (Thier et al., 2012; Vadodaria et al., 2016) or blood (Tanabe et al., 2018), bypassing the step of reprogramming to induced pluripotent stem cells. Such approaches are reported to maintain hallmarks of aging in neurons, which are otherwise erased during the process of reprogramming (Mertens et al., 2015; Tang et al., 2017). Thus, they may be useful to study the effects of stress on the adult brain or to conduct screenings for drug discovery. Neurons differentiated from hiPS cells on the other hand are better suited to examine the Developmental Origins of Health and Disease hypothesis.

Concerning the optimization of differentiation techniques, a more recent version of the original protocol employed in this study suggests SMAD inhibition in combination with Neural Induction Medium (STEMdiff Neural System Version 2.4.0; STEMCell Technologies, Vancouver, Canada) for improved differentiation towards the neural lineage. Indeed, a small molecule named XAV939 was shown to enhance differentiation towards FOXG1+ neuronal progenitors (Maroof et al., 2013). Using a small molecule screen, a combination of LDN193189, SB431542, XAV939, SU5402, PD0325901, and DAPT was furthermore identified to result in the highest efficiency regarding differentiation to FOXG1+ neuronal progenitors and cortical neurons positive for FOXG1, Reelin, TBR1, and DCX (Qi et al., 2017).

However, transcriptome analyses conducted on differentiated neuronal cells confirmed that the protocol used in this thesis yielded satisfactory results regarding

differentiation towards the target cell types. While differentiated cells used for stimulation experiments in the pilot study had progressed towards a posterior profile due to repeated passaging, upscaling of the starting material and early stimulation of neuronal progenitors in passages 2 or 3 on D24 resulted in the desired study population of anterior neuronal progenitors. Nevertheless, future studies may profit from newly developed protocols, especially regarding required hands-on-time.

Finally, an open question may be the usefulness of human iPS cells in comparison to other model systems, such as neuroblastoma cell lines or mice. Regarding the prior, the crucial point is certainly the study objective. Stable cell lines facilitate experiments by providing a homogeneous study population of defined cell fate, however at the expense of lacking the external validity of pluripotent stem cells undergoing an intrinsic cell fate specification program. The latter may be an important factor influencing sensitive phases for disruption, such as by external glucocorticoids. Mice on the other hand may indeed go through developmental phases akin to humans, but hiPS cells offer the opportunity to examine these phases against the backdrop of a complex genetic background, with a high number of individual gene variants contributing to disease risk. Interestingly, a study examining the effects of stress exposure on mouse brain reported alterations to neuronal migration as suggested by results of differential methylation and gene expression lined out here, albeit mediated by an entirely different set of regulated gene transcripts (Fukumoto et al., 2009). Therefore, alterations that are seemingly parallel in humans and animals may be conferred by different processes on the molecular level.

[158]

5.1.2 MICROARRAY AND SEQUENCING-BASED TECHNIQUES

Both the pilot transcriptome study with HumanHT-12 v4 Expression BeadChip, and the DNA methylation study using MethylationEPIC BeadChip microarrays relied on array-based techniques with hybridization of samples to predetermined probes. Microarrays have the advantage of good replicability and well-established analysis pipelines. However, they provide a limited range of genes or positions within the gene sequence and are thus restricted with respect to their potential for new discoveries.

Transcriptome analysis in the main study was based on 3' mRNA sequencing. The technique promised to facilitate analysis by eliminating the need to perform transcript length normalization. Indeed, 3' mRNA-Seq was shown to assign equal numbers of reads to transcripts irrespective of their lengths. However, it was also found to have lower power to detect differentially expressed genes compared to whole transcriptome sequencing (Xiong et al., 2017; Ma et al., 2019), meaning it may require higher sequencing depth to achieve the same statistical power. Key differences between the 3' and whole transcriptome sequencing approaches are that 3' mRNA-Seq comes from a restricted region of the exome, which may have reduced sequence entropy. In addition, 3'mRNA-Seq does not allow for the identification of differential splicing events and alignment is performed to an mRNA RefSeq transcriptome instead of the comprehensive reference genome (Xiong et al., 2017).

Indeed, the sequencing experiment was performed generating only 8 million 100 bp reads per sample on average. While power to detect differentially expressed genes was found to improve moderately above 10 million reads by a study using a

single cell line (Liu et al., 2013), another systematic comparison on sequencing depth suggested at least 100 million reads may be necessary to detect differentially expressed genes in human adipose tissue (Liu, Ferguson, et al., 2013). Considering that detection of differential gene expression may have been reduced owing to the 3' end approach to library construction, it is likely that at least 10 million, but possibly even more reads would have been necessary to give a proper estimate of differentially expressed transcripts between stimulated and unstimulated cells. This may also explain why a qPCR for *TSC22D3* detected significantly heightened upregulation of the transcript in neurons following dexamethasone stimulation, which was not captured by RNA-Seq. On the other hand, the method chosen to analyze RNA-Seq data did not allow for a paired analysis, which may also have impacted on power to detect significant differences. In fact, a Student's t-Test for unpaired samples on the same qPCR resulted in a reduced significance estimate of $p=0.09$. Moreover, there was overall little convergence between transcripts differentially regulated by dexamethasone in the pilot and RNA-Seq studies. Importantly, it is unclear whether the dissimilarities were caused by differences in the techniques or by the fact that differentiated cell types ultimately belonged to different populations. After all, stimulated cells in the pilot study had a posterior gliogenic profile, whereas those investigated by RNA-Seq were characterized by high expression of *FOXG1*, respectively *DCX* and *RELN*.

5.1.3 STATISTICAL CONSIDERATIONS

High-throughput experiments pose considerable challenges regarding experimental design and statistical decision-making. In this study, confounders were controlled by means of parallelization and randomization at the level of study

design, as well as by batch correction and inclusion of covariates in methylation data. Because RNA-Seq analyses rely on statistical methods requiring raw data as input, no normalization or batch correction was performed prior to analyses of differential gene expression.

Generally, it is assumed that measured values are influenced by technical error and that correcting for this error gives an improved estimate of true values and therefore their differences. However, high-throughput data are often influenced by a variety of technical batches that may additionally be confounded either with each other or with a variable of interest. Results may therefore vary with every statistical decision made in the data analysis process. Here, supplementary analyses were run in order to assess the influence of batch correction and covariates in this respect (see section 7.1 Supplementary Analyses).

Moreover, differentiated hiPS cells posed the challenge of relatively high batch-to-batch variation between independent replicates. On the one hand, this property supports their external validity as independent replicates given that true inter-individual differences are likely to be even greater in actual human embryos. On the other hand, it complicated analyses and reduced the options with respect to the choice of statistical tools. In methylation data, variation between independent replicates was indirectly corrected for with batch correction for EPIC chip, and additionally addressed in the Supplementary Analyses by explicit inclusion in the model as random factor. In transcriptome data, biological variation prohibited analysis by tools using variance shrinkage such as DESeq and DESeq2 regardless of the popularity of these packages. The empirical bayes method employed by the EBSeq package in turn was well suited to handle the different baselines between

differentiation batches. Unfortunately, inclusion of covariates or blocking of paired samples to improve the statistical model was not possible in the EBSeq package.

5.2 THEORETICAL ASPECTS

Theoretical considerations will focus on the potentially intrinsic role of the glucocorticoid receptor during neurogenesis, as well as the functional implications of epigenetic changes on the methylome and transcriptome level.

5.2.1 INTRINSIC GLUCOCORTICOID RECEPTOR ACTION IN NEUROGENESIS

Firstly, the differentiated cell types exposed to dexamethasone in this study were extensively characterized revealing a strong developmental component against the backdrop of which dexamethasone exerts its effects. The data presented here suggested an endogenous role of stress signaling during neurogenesis by showing rising expression levels of HPA axis agent *CRH* with neural differentiation, a gradual increase in total and nuclear GR levels, and enrichment of developmentally induced methylation switches for glucocorticoid response elements, as well as gene ontology categories "response to stress", "response to corticosterone stimulus", "regulation of stress-activated MAPK cascade", or "response to steroid hormone stimulus". Such stage-specific neurodevelopmental regulation of the glucocorticoid receptor implies the existence of a developmental mechanism guiding intrinsic GR transcription factor activity. Indeed, the *NR3C1* gene has previously been identified as one of the transcription factors dynamically modelling neural progenitor identity and differentiation potential in neural progenitors up until *in vitro* day 35 of differentiation in the Epigenome Roadmap Project (Ziller et al., 2015). Earlier research works have already reported increasing brain glucocorticoid receptor

[162]

levels with development in both rodents (Meaney et al., 1985; Androutsellis-Theotokis et al., 2013) and human iPSC-derived neurons (Lieberman et al., 2017). Also, accumulation of nuclear GR in outer germinal zones and with increasing proximity to birth has been described in the brains of E11.5 mouse embryos (Tsiarli et al., 2013). In the embryos, cells in the apical ventricular zone expressed cytoplasmic GR, while radial glia, intermediate progenitor cells, and neurons of the cortical plate had a nuclear GR profile noticeable throughout the ventral telencephalon, hippocampus and olfactory bulb. In line with these observations, research on non-neuronal cells revealed a relationship between increases in total GR levels and nuclear receptor levels in that high receptor protein density led to enhanced GR dimerisation and translocation in the absence of ligands (Robertson et al., 2013). Moreover, there are reports of glucocorticoids actually misplacing promoter-bound unliganded GR rather than increasing GR binding (Ritter & Mueller, 2014).

In addition, glucocorticoid response elements were overrepresented in differentially methylated regions induced by neuronal differentiation but underrepresented in those induced by dexamethasone in differentiated neurons. This finding seems to suggest that the usual binding sites of GR as observed in adult tissues (in this case blood) may not yet be accessible to exogenous glucocorticoids. Other sites might in turn be open specifically in migrating neurons, leading to the observed changes in DNAm status in genes associated with neurodevelopmental disorders. Indeed, there is evidence that potential GR binding sites in H3K27ac regions change chromatin status during early neuronal development (Ziller, personal communication), thus becoming either more or less accessible to ligands.

Finally, glucocorticoid receptor autoregulation by dexamethasone was found to be absent in rat embryos as opposed to adult animals, suggesting that embryonic cells may have a unique mode of GR regulation (Ghosh et al., 2000).

5.2.2 DEXAMETHASONE-INDUCED DIFFERENTIAL METHYLATION

On the methylome level, glucocorticoid receptor activation by dexamethasone predominantly affected differentiated neurons and led to heightened methylation levels, as opposed to demethylation. This was consistent with the overall pattern that most sites gained DNAm during neuronal differentiation rather than losing it. Because stimulated cells had a prefrontal profile, the altered methylome in this important regulatory region might impact on functions such as cognitive, emotional, and inhibitory control. Additionally, the prefrontal cortex is the last brain region to mature, so that the adverse impact of prenatal stress may not become fully apparent until adolescence or early adulthood (Pfefferbaum et al., 1994) when most psychiatric disorders have their onset (Kessler et al., 2005). Moreover, stimulated neuronal populations exhibited high expression of Reelin, which is depleted in *post mortem* prefrontal brain tissue of schizophrenic patients (Impagnatiello et al., 1998; Guidotti et al., 2000). Given that many differentially methylated positions were either in or adjacent to risk genes for schizophrenia, autism, or MDD, RELN+ neuronal cells might be an interesting target population to study gene by environment interactions in psychiatric disorders.

In sum, alterations in methylation profile suggested potential implications for the stress system, brain development, cleft palate, Wnt signaling, and neurodevelopmental psychiatric disorders.

[164]

Stress system. Results suggest that prenatal stress may impact on HPA axis homeostasis by showing increased DNA methylation in genes encoding for the glucocorticoid and mineralocorticoid receptor. The mineralocorticoid receptor, encoded for by *NR3C2,* is mostly expressed in the hippocampus and has a higher affinity for cortisol than the GR, leading to saturation under baseline levels. The GR on the other hand only substantially becomes occupied under conditions of stress and is much more widely expressed (review by Reul et al., 2000). Heightened methylation in the *NR3C1* gene is already one of the most well-replicated findings on the epigenetic effects of prenatal stress (Oberlander et al., 2008; Conradt et al., 2013; Conradt et al., 2016; Braithwaite et al., 2015; Mulligan et al., 2012; Perroud et al., 2014; Hompes et al., 2013). A glucocorticoid-induced epigenetic mark on these genes may further help to explain heightened inflammation levels in individuals exposed to prenatal stress up until middle to late adulthood (Slopen et al., 2015; Plant et al., 2016).

Brain development. Regulated DMPs included several probes annotated to genes important in dorsal-ventral axis formation, such as *SMAD2*, *TGFBR1*, *BMPR1A*, and *BMPR2*. The latter two encode for receptor proteins binding BMP4, which is one of the major regulators of axis formation in the developing neural tube and all four have roles in SMAD signaling. Binding in BMPR1A for instance was shown to directly stimulate the SMAD2/3 signaling pathway (Wang et al., 2014).

Further regulated DMPs were annotated to *SLIT3* and *ROBO1*, both of which are implicated in left-right axis formation. They have important roles in the guidance of migrating neurons along the axial midline establishing commissural axon connections during brain development (Long et al., 2004). Both genes were shown

[165]

to be negatively regulated by cortisol in ovarian cancer tissue (Dickinson et al., 2011), which might be mediated by promoter hypermethylation (Narayan et al., 2006). Functionally, deficiencies in Slit/Robo signaling were found to impact on language, which relies on highly lateralised networks in the human brain. Decreased *ROBO1* expression for example has been shown to impair development of the auditory pathway (Lamminmäki et al., 2012). Also, gene expression in hiPSC-derived neurons of patients with schizophrenia was enriched for the Slit/Robo pathway (Brennand et al., 2011). Concurrently increased methylation in a probe annotated to Forkhead Box P2 (*FOXP2*) equally points to an impact on the development of language functions. It was found to have an evolutionary role in the acquisition of human speech (Enard et al., 2002) and mutations were associated with severe language and speech impairments (Lai et al., 2001). Congruently, differentially methylated regions were significantly enriched for inner ear development, which was found to be implicated in hearing impairments in children with autism (Bennetto et al., 2017). In addition, a single nucleotide polymorphism in *FOXP2* was found to differentiate between schizophrenia patients with auditory hallucinations and healthy controls (Sanjuán et al., 2006). Auditory hallucinations are a hallmark symptom of schizophrenia, while patients with autism spectrum disorder show language impediments ranging from absence of speech to difficulties with figurative language use.

Cleft palate. Special AT-Rich Sequence-Binding Protein 2 (*SATB2*) is another gene associated with both autism and schizophrenia on a genome-wide level (Talkowski et al., 2012; Pardiñas et al., 2018; Whitton et al., 2018). However, further functional annotations of *SATB2* include not only intellectual disability (Döcker et

al., 2014), but also craniofacial patterning (Dobreva et al., 2006) and cleft palate (FitzPatrick et al., 2003). Indeed, differentially methylated regions in DEX-stimulated neurons were significantly enriched for palate development. Previous studies have shown that both dexamethasone administration and an increase in maternal stressful life events accompanied by little emotional support were associated with increased risk of orofacial malformations such as cleft lip, cleft palate and neural tube defects (Goldman et al., 1978; Carmichael et al., 2007; Suárez et al., 2003). Accordingly, boys with cleft lip and palates had higher ratings of hyperactivity, impulsivity, and inattention accompanied by increased right ventromedial prefrontal cortex volumes relative to the comparison group (Nopoulos et al., 2010). Altogether, these findings suggest that prenatal stress may not only affect frontal brain regions but generalize to frontal phenotypes.

Wnt signaling. A particularly interesting aspect of the current study was the association of DEX-induced epigenetic changes with Wnt signaling and genes known to be implicated in schizophrenia and other neurodevelopmental psychiatric disorders. As reported initially, Wnt signaling was previously found to be affected by prenatal stress (Mychasiuk et al., 2011; Frahm et al., 2016). It may therefore act as a unifying pathway for both the effects of prenatal stress exposure and genetic variability associated with pervasive developmental disorders of mental health. For instance, altered Wnt signaling was found in hiPSC-derived neuronal cells from schizophrenic and bipolar patients, sometimes accompanied by ventralising or dorsalising effects (Chen et al., 2014; Topol et al., 2015; Madison et al., 2015; Srikanth et al., 2015; Srikanth et al., 2018). Deficient Wnt signaling was also shown to cause a delay in neuronal migration, altered interhemispheric connections and

impaired social behaviour in rats (Bocchi et al., 2017). Moreover, schizophrenia is characterised by prefrontal loss of function and limbic gain of function with increased activity of the dopaminergic signaling pathway (Meyer-Lindenberg et al., 2002). This makes Wnt signaling a potential target system due to its key role in patterning cells towards midbrain identity and in the neurogenic conversion of the midbrain floor plate into dopaminergic neurons (Kirkeby et al., 2012; Kriks et al., 2011; Studer, 2017).

Neurodevelopmental psychiatric disorders. A striking number of probes was annotated to genes with well-known associations to neurodevelopmental psychiatric disorders, including *DISC1*, *NRG1*, *GPM6A*, or *TCF4*.

A translocation in chromosome 1 disrupting *DISC1* has first been described to co-segregate with schizophrenia in a large Scottish family (Millar et al., 2000) and has since become one of the best characterised candidate genes for the disorder, including detailed molecular signaling pathways and phenotyping.

Knockdown of *DISC1 in utero* for instance has been shown to disturb postnatal maturation of mesocortical dopaminergic projections to the medial prefrontal cortex in mice and reduce prepulse inhibition (Niwa et al., 2010). Suppression of *DISC1* has furthermore been related to disturbed radial migration, resulting in a reduced number of neurons reaching the cortical plate due to accumulation in the intermediate zone and subventricular zone (Kamiya et al., 2005). These findings suggest that increased methylation in *DISC1* following dexamethasone exposure may impact on the developmental trajectory of Reelin expressing neurons by disrupting mesocortical connections and the proper formation of cortical layers.

[168]

While genetic variance in *GPM6A* has been associated with schizophrenia in genome-wide association studies (GWAS) (Li et al., 2017), the role of *NRG1* polymorphisms in the disorder has actually been challenged by GWAS due to lack of significant associations (Ripke et al., 2014; review by Mostaid et al., 2016). Nevertheless, *post mortem* brain tissue of affected individuals was indeed shown to exhibit altered expression of *NRG1* on the mRNA and protein level (Law et al., 2006; Bertram et al., 2007). Perhaps these discrepancies could be explained by environmental factors becoming epigenetically embedded in the diseased brain. Hypermethylation of several regions in the *NRG1* gene following DEX exposure suggest this may be the case. Functionally, both *NRG1* (López-Bendito et al., 2006) and *CDH2* (Horn et al., 2018) are implicated in neuronal migration, subtle aberrations in which are presumed to precede disease onset (Muraki & Tanigaki, 2015). High expression of genes such as *RELN* or *DCX* in differentiated neuronal cells suggest they may in fact have been vulnerable to aberrations in neuronal migration.

Compared to other risk genes, the function of *TCF4* is relatively less well characterised. On a phenomenological level, it may be implicated in attention (Zhu et al., 2013) while molecular functions seem to include interactions with the basic helix-loop-helix (bHLH) factors Neurogenic Differentiation Factor 1 (*NEUROD1*) and 2 (*NEUROD2*) *in vivo* (Brzózka et al., 2010). It is therefore most likely to act on neurogenesis, possibly in relation to the establishment of frontally mediated attention networks.

5.2.3 DEXAMETHASONE-INDUCED DIFFERENTIAL GENE EXPRESSION

The number of gene transcripts regulated by dexamethasone increased progressively with neuronal maturation and rising levels of GR expression. Regulated transcripts in hSC were therefore sparse. Those that were regulated however suggest a possible effect on inflammation. In neuronal progenitors and neurons, dexamethasone exposure affected expression of genes associated with proliferation and neuronal migration, which is in line with functional implications of differentially methylated positions. Most notably, dexamethasone regulated two members of the same pathway, *GSK3A* and *AKT1*. Apart from being associated to schizophrenia (Emamian, 2012), signaling in this pathway is reportedly involved in neural development (Hur & Zhou, 2010), and itself regulated by the dopaminergic signaling pathway (Beaulieu et al., 2011). Accordingly, regulated transcripts in differentiated neurons were overrepresented in the dopamine-receptor mediated signaling pathway and synaptic vesicle trafficking, as well as metabotropic glutamate receptor signaling. The combination of enrichment for both the dopaminergic and glutamatergic pathways is particularly interesting in light of the dopamine and glutamate hypotheses of schizophrenia (Coyle, 2006; Stone et al., 2007; Benamer et al., 2018), which have recently been extended to other psychiatric disorders (Moghaddam & Javitt, 2012). The dopamine hypothesis may be one of the most enduring in psychiatry, stating that hyperdopaminergic signaling in the limbic system is causally related to positive, i.e. psychotic, symptoms (Mackay, 1980; Weinstein et al., 2017). The glutamate hypothesis on the other hand was based on the observation that N-methyl-D-aspartate receptor (NMDAR) antagonists can induce schizophrenia-like symptoms. It assumes that reduced NMDAR activity on

inhibitory neurons leads to the disinhibition of glutamatergic neurons and increases the synaptic activity of glutamate, especially in the prefrontal cortex (Moghaddam & Javitt, 2012). Since excessive glutamate in the synaptic cleft has indeed been associated with neurotoxicity (Popoli et al., 2012), it may provide yet another explanation for reduced frontal cortex size observed in schizophrenic or depressed patients (Lai et al., 2000; Hirayasu et al., 2001).

5.3 LIMITATIONS

1) The data presented here were generated from two male-derived lines. While further independent replicates have been obtained by repeated directed differentiation, more replication in different sexes is necessary to consolidate results. Specifically, sex-dependent differences are expected due to the higher incidence rate of neurodevelopmental disorders in males compared to females. For instance, autism was found to occur more often in males with a likelihood of 3:1 (Loomes et al., 2017). The incidence risk ratio for men to develop schizophrenia was found to be 1.42 relative to women (Aleman et al., 2003). Prior research suggests that this bias might be mediated at the intra-uterine environment level, involving polygenic risk, early life complications during pregnancy, and offspring sex (Ursini et al., 2018).

2) Further replication is also needed in order to determine the effect of glucocorticoid concentration on observed changes. While even higher doses of 100 μM have been used to study effects of GR activation on neurogenesis (Anacker et al., 2013), 1 μM of dexamethasone is a considerably high concentration. The effects

described here should therefore be considered at the upper end of possible molecular changes.

3) Similarly, it is unknown how much cortisol or dexamethasone actually pass the placenta, so it is unclear what concentration would indeed be appropriate.

4) Dexamethasone was used to model prenatal stress, which is known to have longer GR residence times compared to corticosterone (Paakinaho et al., 2017). While clinical phenotypes associated with prenatal exposure to either maternal stress or dexamethasone were similar, molecular mediators do not necessarily need to be equal.

5) The method of dexamethasone application did not model the naturally occurring pulsatility of cortisol (Young et al., 2004), which is an important factor in HPA axis regulation and homeostasis (Lightman & Conway-Campbell, 2010).

6) Dexamethasone may be dissolved in ethanol or dimethyl sulfoxide, both of which can have detrimental effects on cell physiology and survival. In this study, dexamethasone was initially dissolved in ethanol and further diluted in H_2O resulting in a final concentration of 0.001% after application to growth media. Physiological changes of cells were not detectable under the light microscope at the conclusion of individual experiments. However, interaction effects between low concentrations of ethanol and dexamethasone cannot be excluded.

7) Overall, stem cell-derived neural rosettes have been shown to closely recapitulate early neurulation events, such as transition from neural plate-like cells to neural tube-like cells, apical-basal polarity, anterior-posterior patterning, neurogenic to gliogenic switch, and cortical lamination (Elkabetz & Studer, 2008;

Elkabetz et al., 2008; Curchoe et al., 2012; Banda et al., 2014; Edri et al., 2015). However, *in vitro* differentiated neuronal cells ultimately represent a simplified model of a much more complex system, all the while introducing confounders specific to the culture conditions.

8) Lastly, DNAm and gene expression data were annotated to different versions of the reference genome (hg19 and hg38, respectively) and cannot be interpreted in direct relation to one another.

5.4 CONCLUSIONS

While exposure to alcohol during pregnancy is a well-known risk factor for neurodevelopmental complications, exposure to prenatal stress has never received similar attention despite epidemiological evidence of heightening the risk for schizophrenia (van Os & Selten, 1998) or autism (Rai et al., 2012; Walder et al., 2014). The current study suggests that increased risk of neurodevelopmental psychiatric disorders following prenatal stress might be conferred by epigenetic marks in psychiatrically relevant genes. However, earlier research in mice and humans has shown that these epigenetic marks and their adverse effects may be attenuated postnatally with positive parental attention and physical contact (Sharp et al., 2012; Sharp et al., 2015; Pickles et al., 2017; Liu et al., 1997; Francis et al., 1999). Knowledge about the epigenetic changes following prenatal stress exposure will hopefully help to identify and develop further treatment options.

5.5 OUTLOOK

For the first time, embryonic stem cells and induced pluripotent stem cells allow to disambiguate influences of genes and environment from as early as the equivalent

[173]

of the blastocyst stage only few days post-fertilization. Mental illness may constitute a heavy burden on the lives of expecting parents and be a major cause of stress itself. Taking into account gene by environment interactions from the onset of cell division in the newly formed organism may therefore improve our current understanding of the true effect sizes of genetic and environmental contributors to psychiatric disorders. Perhaps fortunately, current results suggest only the methylation status of post-mitotic neuronal cells may be affected by exposure to prenatal stress. As such, alterations cannot be transmitted to daughter cells upon cell division, restricting the impact of stress exposure. In addition, prenatal stress may need to be followed by subsequent stress exposure to significantly increase risk to psychiatric disorders.

Furthermore, the results laid out in this thesis may hint at treatment options to attenuate the impact of prenatal stress. For instance, hypermethylation in migrating neurons caused by prenatal stress exposure may be addressed by provision of a methyl-balanced diet. A similar approach has proven successful in reducing binge eating behaviour in mice exposed to prenatal stress (Schroeder et al., 2017). Early diet-based interventions have further been developed to treat conditions such as phenylketonuria. The disease is characterised by an excess of phenylalanine building up in the body and associated with skin rashes, seizures, microcephaly, intellectual disability and psychiatric disorders when going untreated. Foods low in protein and free of phenylalanine have shown to ameliorate brain development and disease symptoms to a point below observability (van Wegberg et al., 2017). Moreover, foods rich in folic acid have been found to counteract neural tube defects

(Moreno et al., 2012), which studies in zebrafish suggest the Glucocorticoid Receptor may have a role in (Pikulkaew et al., 2011).

In order to prove the efficiency of such potential interventions, future studies on prenatal stress may include a rescue paradigm in the experimental setup.

6.   REFERENCES

Abel, K. M., Heuvelman, H. P., Jörgensen, L., Magnusson, C., Wicks, S., Susser, E., ... & Dalman, C. (2014). Severe bereavement stress during the prenatal and childhood periods and risk of psychosis in later life: population based cohort study. *Bmj, 348*, f7679.

Abudureyimu, S., Asai, N., Enomoto, A., Weng, L., Kobayashi, H., Wang, X., ... & Takahashi, M. (2018). Essential role of Linx/Islr2 in the development of the forebrain anterior commissure. *Scientific reports*, 8.

Alboni, S., Van Dijk, R. M., Poggini, S., Milior, G., Perrotta, M., Drenth, T., ... & Cirulli, F. (2017). Fluoxetine effects on molecular, cellular and behavioral endophenotypes of depression are driven by the living environment. *Molecular psychiatry*, *22*(4), 552.

Aleman, A., Kahn, R. S., & Selten, J. P. (2003). Sex differences in the risk of schizophrenia: evidence from meta-analysis. *Archives of general psychiatry*, *60*(6), 565-571.

Alexander, N., Klucken, T., Koppe, G., Osinsky, R., Walter, B., Vaitl, D., ... & Hennig, J. (2012). Interaction of the serotonin transporter-linked polymorphic region and environmental adversity: increased amygdala-hypothalamus connectivity as a potential mechanism linking neural and endocrine hyperreactivity. *Biological Psychiatry*, *72*(1), 49-56.

Anacker, C., Cattaneo, A., Luoni, A., Musaelyan, K., Zunszain, P. A., Milanesi, E., ... & Price, J. (2013). Glucocorticoid-related molecular signaling pathways regulating hippocampal neurogenesis. *Neuropsychopharmacology*, *38*(5), 872.

Anacker, C., Cattaneo, A., Musaelyan, K., Zunszain, P. A., Horowitz, M., Molteni, R., ... & Thuret, S. (2013). Role for the kinase SGK1 in stress, depression, and glucocorticoid effects on hippocampal neurogenesis. *Proceedings of the National Academy of Sciences*, *110*(21), 8708-8713.

Anders, S., & Huber, W. (2010). Differential expression analysis for sequence count data. *Genome biology*, *11*(10), R106.

Andrews, S. (2010). FastQC: a quality control tool for high throughput sequence data. http://www.bioinformatics.babraham.ac.uk/projects/fastqc.

Androutsellis-Theotokis, A., Chrousos, G. P., McKay, R. D., DeCherney, A. H., & Kino, T. (2013). Expression profiles of the nuclear receptors and their transcriptional coregulators during differentiation of neural stem cells. *Hormone and Metabolic Research*, *45*(02), 159-168.

Arai, Y., Funatsu, N., Numayama-Tsuruta, K., Nomura, T., Nakamura, S., & Osumi, N. (2005). Role of Fabp7, a downstream gene of Pax6, in the maintenance of neuroepithelial cells during early embryonic development of the rat cortex. *Journal of Neuroscience, 25*(42), 9752-9761.

Arloth, J., Bogdan, R., Weber, P., Frishman, G., Menke, A., Wagner, K. V., ... & Altmann, A. (2015). Genetic differences in the immediate transcriptome response to

stress predict risk-related brain function and psychiatric disorders. *Neuron*, *86*(5), 1189-1202.

Arnold, S. J., & Robertson, E. J. (2009). Making a commitment: cell lineage allocation and axis patterning in the early mouse embryo. *Nature reviews Molecular cell biology*, *10*(2), 91.

Attardi, B. J., Zeleznik, A., Simhan, H., Chiao, J. P., Mattison, D. R., Caritis, S. N., & Network, O. F. P. R. U. (2007). Comparison of progesterone and glucocorticoid receptor binding and stimulation of gene expression by progesterone, 17-alpha hydroxyprogesterone caproate, and related progestins. *American journal of obstetrics and gynecology*, *197*(6), 599-e1.

Australian Government, Department of Health (2018, June 7). Prescribing medicines in pregnancy database. Retrieved from https://www.tga.gov.au/prescribing-medicines-pregnancy-database#.U1Yw8Bc3tqw

Awano, S., Dawson, L. A., Hunter, A. R., Turner, A. J., & Usmani, B. A. (2006). Endothelin system in oral squamous carcinoma cells: Specific siRNA targeting of ECE-1 blocks cell proliferation. *International journal of cancer, 118*(7), 1645-1652.

Badouel, C., Zander, M. A., Liscio, N., Bagherie-Lachidan, M., Sopko, R., Coyaud, E., ... & McNeill, H. (2015). Fat1 interacts with Fat4 to regulate neural tube closure, neural progenitor proliferation and apical constriction during mouse brain development. *Development, 142*(16), 2781-2791.

Banda, E., McKinsey, A., Germain, N., Carter, J., Anderson, N. C., & Grabel, L. (2014). Cell polarity and neurogenesis in embryonic stem cell-derived neural rosettes. *Stem cells and development, 24*(8), 1022-1033.

Bardy, C., Van Den Hurk, M., Eames, T., Marchand, C., Hernandez, R. V., Kellogg, M., ... & Bang, A. G. (2015). Neuronal medium that supports basic synaptic functions and activity of human neurons in vitro. *Proceedings of the National Academy of Sciences, 112*(20), E2725-E2734.

Barker, D. J. (1990). The fetal and infant origins of adult disease. *BMJ: British Medical Journal*, *301*(6761), 1111.

Basirat, Z., Rad, H. A., Esmailzadeh, S., Jorsaraei, S. G. A., Hajian-Tilaki, K., Pasha, H., & Ghofrani, F. (2016). Comparison of pregnancy rate between fresh embryo transfers and frozen-thawed embryo transfers following ICSI treatment. *International Journal of Reproductive BioMedicine*, *14*(1), 39.

Baum, L., Haerian, B. S., Ng, H. K., Wong, V. C., Ng, P. W., Lui, C. H., ... & Tan, H. J. (2014). Case–control association study of polymorphisms in the voltage-gated sodium channel genes SCN1A, SCN2A, SCN3A, SCN1B, and SCN2B and epilepsy. *Human genetics, 133*(5), 651-659.

Bauwens, C. L., Peerani, R., Niebruegge, S., Woodhouse, K. A., Kumacheva, E., Husain, M., & Zandstra, P. W. (2008). Control of human embryonic stem cell colony and aggregate size heterogeneity influences differentiation trajectories. *Stem cells, 26*(9), 2300-2310.

[179]

Beaulieu, J. M., Del'Guidice, T., Sotnikova, T., Lemasson, M., & Gainetdinov, R. (2011). Beyond cAMP: the regulation of Akt and GSK3 by dopamine receptors. *Frontiers in molecular neuroscience*, 4, 38.

Beildeck, M. E., Gelmann, E. P., & Stephen, W. B. (2010). Cross-regulation of signaling pathways: an example of nuclear hormone receptors and the canonical Wnt pathway. *Experimental cell research, 316*(11), 1763-1772.

Benamer, N., Marti, F., Lujan, R., Hepp, R., Aubier, T. G., Dupin, A. A. M., ... & Hay, Y. A. (2018). GluD1, linked to schizophrenia, controls the burst firing of dopamine neurons. *Molecular psychiatry*, 23(3), 691.

Benato, F., Colletti, E., Skobo, T., Moro, E., Colombo, L., Argenton, F., & Dalla Valle, L. (2014). A living biosensor model to dynamically trace glucocorticoid transcriptional activity during development and adult life in zebrafish. *Molecular and cellular endocrinology, 392*(1-2), 60-72.

Benediktsson, R., Calder, A. A., Edwards, C. R., & Seckl, J. R. (1997). Placental 11β-hydroxysteroid dehydrogenase: a key regulator of fetal glucocorticoid exposure. *Clinical endocrinology*, *46*(2), 161-166.

Bennett, A. F., Hayes, N. V., & Baines, A. J. (1991). Site specificity in the interactions of synapsin 1 with tubulin. *Biochemical journal, 276*(3), 793-799.

Bennett, H. A., Einarson, A., Taddio, A., Koren, G., & Einarson, T. R. (2004). Prevalence of depression during pregnancy: systematic review. *Obstetrics & Gynecology*, 103(4), 698-709.

Bennetto, L., Keith, J. M., Allen, P. D., & Luebke, A. E. (2017). Children with autism spectrum disorder have reduced otoacoustic emissions at the 1 kHz mid-frequency region. *Autism Research*, 10(2), 337-345.

Bertram, I., Bernstein, H. G., Lendeckel, U. W. E., Bukowska, A., Dobrowolny, H., Keilhoff, G., ... & Bogerts, B. (2007). Immunohistochemical evidence for impaired neuregulin-1 signaling in the prefrontal cortex in schizophrenia and in unipolar depression. *Annals of the New York Academy of Sciences*, *1096*(1), 147-156.

Best, C., Kurrasch, D. M., & Vijayan, M. M. (2017). Maternal cortisol stimulates neurogenesis and affects larval behaviour in zebrafish. *Scientific reports*, *7*, 40905.

Blainey, P., Krzywinski, M., & Altman, N. (2014). Replication: quality is often more important than quantity. *Nature Methods, 11*(9), 879-881.

Bocchi, R., Egervari, K., Carol-Perdiguer, L., Viale, B., Quairiaux, C., De Roo, M., ... & Kiss, J. Z. (2017). Perturbed Wnt signaling leads to neuronal migration delay, altered interhemispheric connections and impaired social behavior. *Nature communications, 8*(1), 1158.

Bodaleo, F. J., Montenegro-Venegas, C., Henríquez, D. R., Court, F. A., & Gonzalez-Billault, C. (2016). Microtubule-associated protein 1B (MAP1B)-deficient neurons show structural presynaptic deficiencies in vitro and altered presynaptic physiology. *Scientific reports, 6*, 30069.

Bogdanova, N., Horst, J., Chlystun, M., Croucher, P. J., Nebel, A., Bohring, A., ... & Markoff, A. (2007). A common haplotype of the annexin A5 (ANXA5) gene promoter is associated with recurrent pregnancy loss. *Human molecular genetics*, 16(5), 573-578.

Bouillet, P., Sapin, V., Chazaud, C., Messaddeq, N., Décimo, D., Dollé, P., & Chambon, P. (1997). Developmental expression pattern of Stra6, a retinoic acid-responsive gene encoding a new type of membrane protein. *Mechanisms of development, 63*(2), 173-186.

Braithwaite, E. C., Kundakovic, M., Ramchandani, P. G., Murphy, S. E., & Champagne, F. A. (2015). Maternal prenatal depressive symptoms predict infant NR3C1 1F and BDNF IV DNA methylation. *Epigenetics*, *10*(5), 408-417.

Brennand, K. J., Simone, A., Jou, J., Gelboin-Burkhart, C., Tran, N., Sangar, S., ... & McCarthy, S. (2011). Modelling schizophrenia using human induced pluripotent stem cells. *Nature*, *473*(7346), 221.

Brennand, K., Savas, J. N., Kim, Y., Tran, N., Simone, A., Hashimoto-Torii, K., ... & Abdelrahim, M. (2015). Phenotypic differences in hiPSC NPCs derived from patients with schizophrenia. *Molecular psychiatry*, *20*(3), 361.

Briscoe, J., Pierani, A., Jessell, T. M., & Ericson, J. (2000). A homeodomain protein code specifies progenitor cell identity and neuronal fate in the ventral neural tube. *Cell, 101*(4), 435-445.

Brocco, M. A., Fernández, M. E., & Frasch, A. C. (2010). Filopodial protrusions induced by glycoprotein M6a exhibit high motility and aids synapse formation. *European Journal of Neuroscience, 31*(2), 195-202.

Brzózka, M. M., Radyushkin, K., Wichert, S. P., Ehrenreich, H., & Rossner, M. J. (2010). Cognitive and sensorimotor gating impairments in transgenic mice overexpressing the schizophrenia susceptibility gene Tcf4 in the brain. *Biological psychiatry*, 68(1), 33-40.

Bruchas, M. R., Schindler, A. G., Shankar, H., Messinger, D. I., Miyatake, M., Land, B. B., ... & Palmiter, R. D. (2011). Selective p38α MAPK deletion in serotonergic neurons produces stress resilience in models of depression and addiction. *Neuron, 71(*3), 498-511.

Bruschettini, M., Van Den Hove, D. L., Timmers, S., Welling, M., Steinbusch, H. P., Prickaerts, J., ... & Steinbusch, H. W. (2006). Cognition-and anxiety-related behavior, synaptophysin and MAP2 immunoreactivity in the adult rat treated with a single course of antenatal betamethasone. *Pediatric research, 60*(1), 50.

Burrows, R. C., Wancio, D., Levitt, P., & Lillien, L. (1997). Response diversity and the timing of progenitor cell maturation are regulated by developmental changes in EGFR expression in the cortex. *Neuron, 19*(2), 251-267.

Buss, C., Davis, E. P., Muftuler, L. T., Head, K., & Sandman, C. A. (2010). High pregnancy anxiety during mid-gestation is associated with decreased gray

matter density in 6–9-year-old children. *Psychoneuroendocrinology*, *35*(1), 141-153.

Buss, C., Davis, E. P., Shahbaba, B., Pruessner, J. C., Head, K., & Sandman, C. A. (2012). Maternal cortisol over the course of pregnancy and subsequent child amygdala and hippocampus volumes and affective problems. *Proceedings of the National Academy of Sciences*, 201201295.

Campion, C. G., Zaoui, K., Verissimo, T., Cossette, S., Matsuda, H., Solban, N., ... & Tremblay, J. (2018). COMMD5/HCaRG Hooks Endosomes on Cytoskeleton and Coordinates EGFR Trafficking. *Cell reports*, *24*(3), 670-684.

Capron, L. E., Glover, V., Pearson, R. M., Evans, J., O'Connor, T. G., Stein, A., ... & Ramchandani, P. G. (2015). Associations of maternal and paternal antenatal mood with offspring anxiety disorder at age 18 years. *Journal of affective disorders, 187*, 20-26.

Carmichael, S. L., Shaw, G. M., Yang, W., Abrams, B., & Lammer, E. J. (2007). Maternal stressful life events and risks of birth defects. *Epidemiology (Cambridge, Mass.)*, *18*(3), 356.

Carmona-Saez, P., Chagoyen, M., Tirado, F., Carazo, J. M., & Pascual-Montano, A. (2007). GENECODIS: a web-based tool for finding significant concurrent annotations in gene lists. *Genome biology, 8*(1), R3.

Chambers, S. M., Fasano, C. A., Papapetrou, E. P., Tomishima, M., Sadelain, M., & Studer, L. (2009). Highly efficient neural conversion of human ES and iPS cells by dual inhibition of SMAD signaling. *Nature biotechnology*, *27*(3), 275.

Chander, P., Kennedy, M. J., Winckler, B., & Weick, J. P. (2019). Neuron-Specific Gene 2 (NSG2) encodes an AMPA receptor interacting protein that modulates excitatory neurotransmission. *eNeuro, 6*(1).

Charbaut, E., Curmi, P. A., Ozon, S., Lachkar, S., Redeker, V., & Sobel, A. (2001). Stathmin family proteins display specific molecular and tubulin binding properties. *Journal of Biological Chemistry, 276*(19), 16146-16154.

Chen, J., Kanai, Y., Cowan, N. J., & Hirokawa, N. (1992). Projection domains of MAP2 and tau determine spacings between microtubules in dendrites and axons. *Nature, 360*(6405), 674.

Chen, E. Y., Tan, C. M., Kou, Y., Duan, Q., Wang, Z., Meirelles, G. V., ... & Ma'ayan, A. (2013). Enrichr: interactive and collaborative HTML5 gene list enrichment analysis tool. BMC bioinformatics, 14(1), 128.

Chen, R. R., Silva, E. A., Yuen, W. W., & Mooney, D. J. (2007). Spatio–temporal VEGF and PDGF delivery patterns blood vessel formation and maturation. *Pharmaceutical research, 24*(2), 258-264.

Chetty, S., Pagliuca, F. W., Honore, C., Kweudjeu, A., Rezania, A., & Melton, D. A. (2013). A simple tool to improve pluripotent stem cell differentiation. *Nature methods, 10*(6), 553.

Chong, S. C., Broekman, B. F., Qiu, A., Aris, I. M., Chan, Y. H., Rifkin-Graboi, A., ... & Saw, S. M. (2016). Anxiety and depression during pregnancy and temperament in early infancy: findings from a multi-ethnic, Asian, prospective birth cohort study. *Infant mental health journal*, *37*(5), 584-598.

Class, Q. A., Abel, K. M., Khashan, A. S., Rickert, M. E., Dalman, C., Larsson, H., ... & D'Onofrio, B. M. (2014). Offspring psychopathology following preconception, prenatal and postnatal maternal bereavement stress. *Psychological medicine, 44*(1), 71-84.

Conradt, E., Hawes, K., Guerin, D., Armstrong, D. A., Marsit, C. J., Tronick, E., & Lester, B. M. (2016). The contributions of maternal sensitivity and maternal depressive symptoms to epigenetic processes and neuroendocrine functioning. *Child development*, *87*(1), 73-85.

Conradt, E., Lester, B. M., Appleton, A. A., Armstrong, D. A., & Marsit, C. J. (2013). The roles of DNA methylation of NR3C1 and 11β-HSD2 and exposure to maternal mood disorder in utero on newborn neurobehavior. *Epigenetics*, *8*(12), 1321-1329.

Costa-Silva, J., Domingues, D., & Lopes, F. M. (2017). RNA-Seq differential expression analysis: An extended review and a software tool. *PloS one*, 12(12), e0190152.

Coyle, J. T. (2006). Glutamate and schizophrenia: beyond the dopamine hypothesis. *Cellular and molecular neurobiology*, 26(4-6), 363-382.

Curchoe, C. L., Russo, J., & Terskikh, A. V. (2012). hESC derived neuro-epithelial rosettes recapitulate early mammalian neurulation events; an in vitro model. *Stem cell research, 8*(2), 239-246.

Dalziel, S. R., Lim, V. K., Lambert, A., McCarthy, D., Parag, V., Rodgers, A., & Harding, J. E. (2005). Antenatal exposure to betamethasone: psychological functioning

and health related quality of life 31 years after inclusion in randomised controlled trial. *Bmj, 331*(7518), 665.

Davis, E. P., Head, K., Buss, C., & Sandman, C. A. (2017). Prenatal maternal cortisol concentrations predict neurodevelopment in middle childhood. *Psychoneuroendocrinology*, *75*, 56-63.

de la Torre-Ubieta, L., Stein, J. L., Won, H., Opland, C. K., Liang, D., Lu, D., & Geschwind, D. H. (2018). The dynamic landscape of open chromatin during human cortical neurogenesis. *Cell*, *172*(1-2), 289-304.

Denny, W. B., Valentine, D. L., Reynolds, P. D., Smith, D. F., & Scammell, J. G. (2000). Squirrel monkey immunophilin FKBP51 is a potent inhibitor of glucocorticoid receptor binding. *Endocrinology*, *141*(11), 4107-4113.

Devlin, A. M., Brain, U., Austin, J., & Oberlander, T. F. (2010). Prenatal exposure to maternal depressed mood and the MTHFR C677T variant affect SLC6A4 methylation in infants at birth. *PloS one*, *5*(8), e12201.

Dickinson, R. E., Fegan, K. S., Ren, X., Hillier, S. G., & Duncan, W. C. (2011). Glucocorticoid regulation of SLIT/ROBO tumour suppressor genes in the ovarian surface epithelium and ovarian cancer cells. *PLoS One*, *6*(11), e27792.

DiPietro, J. A., Novak, M. F., Costigan, K. A., Atella, L. D., & Reusing, S. P. (2006). Maternal psychological distress during pregnancy in relation to child development at age two. *Child development*, *77*(3), 573-587.

Dobreva, G., Chahrour, M., Dautzenberg, M., Chirivella, L., Kanzler, B., Fariñas, I., ... & Grosschedl, R. (2006). SATB2 is a multifunctional determinant of craniofacial patterning and osteoblast differentiation. *Cell*, *125*(5), 971-986.

Döcker, D., Schubach, M., Menzel, M., Munz, M., Spaich, C., Biskup, S., & Bartholdi, D. (2014). Further delineation of the SATB2 phenotype. *European Journal of Human Genetics*, *22*(8), 1034.

Duchek, P., Somogyi, K., Jékely, G., Beccari, S., & Rørth, P. (2001). Guidance of cell migration by the Drosophila PDGF/VEGF receptor. *Cell, 107*(1), 17-26.

Dulabon, L., Olson, E. C., Taglienti, M. G., Eisenhuth, S., McGrath, B., Walsh, C. A., ... & Anton, E. S. (2000). Reelin binds α3β1 integrin and inhibits neuronal migration. *Neuron, 27*(1), 33-44.

Edri, R., Yaffe, Y., Ziller, M. J., Mutukula, N., Volkman, R., David, E., ... & Gat-Viks, I. (2015). Analysing human neural stem cell ontogeny by consecutive isolation of Notch active neural progenitors. *Nature communications*, *6*, 6500.

Edvinsson, L. (2018). CGRP antibodies as prophylaxis in migraine. *Cell, 175*(7), 1719.

Ekonomou, A., Kazanis, I., Malas, S., Wood, H., Alifragis, P., Denaxa, M., ... & Episkopou, V. (2005). Neuronal migration and ventral subtype identity in the telencephalon depend on SOX1. *PLoS biology, 3*(6), e186.

Elkabetz, Y., Panagiotakos, G., Al Shamy, G., Socci, N. D., Tabar, V., & Studer, L. (2008). Human ES cell-derived neural rosettes reveal a functionally distinct early neural stem cell stage. *Genes & development*, *22*(2), 152-165.

Elkabetz, Y., & Studer, L. (2008). Human ESC-derived neural rosettes and neural stem cell progression. In *Cold Spring Harbor symposia on quantitative biology* (Vol. 73, pp. 377-387). Cold Spring Harbor Laboratory Press.

Emamian, E. (2012). AKT/GSK3 signaling pathway and schizophrenia. *Frontiers in molecular neuroscience*, *5*, 33.

Emamian, E. S., Hall, D., Birnbaum, M. J., Karayiorgou, M., & Gogos, J. A. (2004). Convergent evidence for impaired AKT1-GSK3β signaling in schizophrenia. *Nature genetics*, *36*(2), 131.

Enard, W., Przeworski, M., Fisher, S. E., Lai, C. S., Wiebe, V., Kitano, T., ... & Pääbo, S. (2002). Molecular evolution of FOXP2, a gene involved in speech and language. *Nature*, *418*(6900), 869.

Entringer, S., Kumsta, R., Hellhammer, D. H., Wadhwa, P. D., & Wüst, S. (2009). Prenatal exposure to maternal psychosocial stress and HPA axis regulation in young adults. *Hormones and behavior*, *55*(2), 292-298.

Evans, C., Hardin, J., & Stoebel, D. M. (2017). Selecting between-sample RNA-Seq normalization methods from the perspective of their assumptions. *Briefings in bioinformatics, 19*(5), 776-792.

Fadeev, A., Mendoza-Garcia, P., Irion, U., Guan, J., Pfeifer, K., Wiessner, S., ... & Palmer, R. H. (2018). ALKALs are in vivo ligands for ALK family receptor tyrosine kinases in the neural crest and derived cells. *Proceedings of the National Academy of Sciences, 115*(4), E630-E638.

Faedo, A., Borello, U., & Rubenstein, J. L. (2010). Repression of Fgf signaling by sprouty1-2 regulates cortical patterning in two distinct regions and times. *Journal of Neuroscience, 30*(11), 4015-4023.

Fasano, C. A., Phoenix, T. N., Kokovay, E., Lowry, N., Elkabetz, Y., Dimos, J. T., ... & Temple, S. (2009). Bmi-1 cooperates with Foxg1 to maintain neural stem cell self-renewal in the forebrain. *Genes & development, 23*(5), 561-574.

Fietz, S. A., Lachmann, R., Brandl, H., Kircher, M., Samusik, N., Schröder, R., ... & Distler, W. (2012). Transcriptomes of germinal zones of human and mouse fetal neocortex suggest a role of extracellular matrix in progenitor self-renewal. *Proceedings of the National Academy of Sciences*, *109*(29), 11836-11841.

Fineberg, A. M., Ellman, L. M., Schaefer, C. A., Maxwell, S. D., Shen, L., Chaudhury, N. H., ... & Brown, A. S. (2016). Fetal exposure to maternal stress and risk for schizophrenia spectrum disorders among offspring: differential influences of fetal sex. *Psychiatry research, 236*, 91-97.

FitzPatrick, D. R., Carr, I. M., McLaren, L., Leek, J. P., Wightman, P., Williamson, K., ... & Markham, A. F. (2003). Identification of SATB2 as the cleft palate gene on 2q32–q33. *Human molecular genetics*, *12*(19), 2491-2501.

Frahm, K. A., Peffer, M. E., Zhang, J. Y., Luthra, S., Chakka, A. B., Couger, M. B., ... & DeFranco, D. B. (2016). Research resource: the dexamethasone transcriptome in hypothalamic embryonic neural stem cells. *Molecular Endocrinology*, *30*(1), 144-154.

Francis, D., Diorio, J., Liu, D., & Meaney, M. J. (1999). Nongenomic transmission across generations of maternal behavior and stress responses in the rat. *Science*, *286*(5442), 1155-1158.

Franco, S. J., Martinez-Garay, I., Gil-Sanz, C., Harkins-Perry, S. R., & Müller, U. (2011). Reelin regulates cadherin function via Dab1/Rap1 to control neuronal migration and lamination in the neocortex. *Neuron*, *69*(3), 482-497.

Fukumoto, K., Morita, T., Mayanagi, T., Tanokashira, D., Yoshida, T., Sakai, A., & Sobue, K. (2009). Detrimental effects of glucocorticoids on neuronal migration during brain development. *Molecular psychiatry, 14*(12), 1119.

Garcia, A., Steiner, B., Kronenberg, G., Bick-Sander, A., & Kempermann, G. (2004). Age-dependent expression of glucocorticoid-and mineralocorticoid receptors on neural precursor cell populations in the adult murine hippocampus. *Aging cell*, 3(6), 363-371.

Garda, A. L., Puelles, L., Rubenstein, J. L. R., & Medina, L. (2002). Expression patterns of Wnt8b and Wnt7b in the chicken embryonic brain suggest a correlation with forebrain patterning centers and morphogenesis. *Neuroscience, 113*(3), 689-698.

Gedik, H. (2017). Investigation on Genetic Modifiers of Age at Onset of Major Depressive Disorder. Thesis.

Ghosh, B., Wood, C. R., Held, G. A., Abbott, B. D., & Lau, C. (2000). Glucocorticoid receptor regulation in the rat embryo: a potential site for developmental toxicity?. *Toxicology and Applied Pharmacology, 164*(2), 221-229.

Giamas, G., Filipović, A., Jacob, J., Messier, W., Zhang, H., Yang, D., ... & Castellano, L. (2011). Kinome screening for regulators of the estrogen receptor identifies LMTK3 as a new therapeutic target in breast cancer. *Nature medicine, 17*(6), 715.

Giancotti, F. G., & Ruoslahti, E. (1999). Integrin signaling. *Science, 285*(5430), 1028-1033.

Gifford, C. A., Ziller, M. J., Gu, H., Trapnell, C., Donaghey, J., Tsankov, A., ... & Zhang, X. (2013). Transcriptional and epigenetic dynamics during specification of human embryonic stem cells. Cell, 153(5), 1149-1163.

Gil-Sanz, C., Landeira, B., Ramos, C., Costa, M. R., & Müller, U. (2014). Proliferative defects and formation of a double cortex in mice lacking Mltt4 and Cdh2 in the dorsal telencephalon. *Journal of Neuroscience, 34*(32), 10475-10487.

Glessner, J. T., Wang, K., Sleiman, P. M., Zhang, H., Kim, C. E., Flory, J. H., ... & Mentch, F. (2010). Duplication of the SLIT3 locus on 5q35. 1 predisposes to major depressive disorder. *PloS one, 5*(12), e15463.

Goeden, N., Velasquez, J., Arnold, K. A., Chan, Y., Lund, B. T., Anderson, G. M., & Bonnin, A. (2016). Maternal inflammation disrupts fetal neurodevelopment via increased placental output of serotonin to the fetal brain. *Journal of Neuroscience, 36*(22), 6041-6049.

Goedert, M., Crowther, R. A., & Garner, C. C. (1991). Molecular characterization of microtubule-associated proteins tau and MAP2. *Trends in neurosciences, 14*(5), 193-199.

Goldman, A. S., Shapiro, B. H., & Katsumata, M. (1978). Human foetal palatal corticoid receptors and teratogens for cleft palate. *Nature*, *272*(5652), 464.

Gorospe, M., Wang, X., & Holbrook, N. J. (1999). Functional role of p21 during the cellular response to stress. *Gene expression, 7*(4-5), 377-388.

Götz, M., & Huttner, W. B. (2005). Developmental cell biology: The cell biology of neurogenesis. *Nature reviews Molecular cell biology*, *6*(10), 777.

Guidotti, A., Auta, J., Davis, J. M., Gerevini, V. D., Dwivedi, Y., Grayson, D. R., ... & Uzunov, D. (2000). Decrease in reelin and glutamic acid decarboxylase67 (GAD67) expression in schizophrenia and bipolar disorder: a postmortem brain study. *Archives of general psychiatry, 57*(11), 1061-1069.

Gustavsson, A., Svensson, M., Jacobi, F., Allgulander, C., Alonso, J., Beghi, E., ... & Gannon, B. (2011). Cost of disorders of the brain in Europe 2010. *European neuropsychopharmacology*, *21*(10), 718-779.

Hall, A. (1998). Rho GTPases and the actin cytoskeleton. *Science, 279*(5350), 509-514.

Hahn, C. G., Wang, H. Y., Cho, D. S., Talbot, K., Gur, R. E., Berrettini, W. H., ... & Gallop, R. J. (2006). Altered neuregulin 1–erbB4 signaling contributes to NMDA receptor hypofunction in schizophrenia. *Nature medicine*, *12*(7), 824.

Hayashi, Y., Sasaki, H., Suzuki, S., Nishiyama, T., Kitaori, T., Mizutani, E., ... & Sugiura-Ogasawara, M. (2013). Genotyping analyses for polymorphisms of ANXA5 gene in patients with recurrent pregnancy loss. *Fertility and sterility*, 100(4), 1018-1024.

Hill, M. N., McLaughlin, R. J., Morrish, A. C., Viau, V., Floresco, S. B., Hillard, C. J., & Gorzalka, B. B. (2009). Suppression of amygdalar endocannabinoid signaling by stress contributes to activation of the hypothalamic–pituitary–adrenal axis. *Neuropsychopharmacology*, *34*(13), 2733.

Hirabayashi, Y., & Gotoh, Y. (2010). Epigenetic control of neural precursor cell fate during development. *Nature Reviews Neuroscience*, *11*(6), 377.

Hirabayashi, K., Shiota, K., & Yagi, S. (2013). DNA methylation profile dynamics of tissue-dependent and differentially methylated regions during mouse brain development. *BMC genomics, 14*(1), 82.

Hirayasu, Y., Tanaka, S., Shenton, M. E., Salisbury, D. F., DeSantis, M. A., Levitt, J. J., ... & McCarley, R. W. (2001). Prefrontal gray matter volume reduction in first episode schizophrenia. *Cerebral Cortex, 11*(4), 374-381.

Hirvikoski, T., Nordenström, A., Lindholm, T., Lindblad, F., Ritzén, E. M., & Lajic, S. (2008). Long-term follow-up of prenatally treated children at risk for congenital adrenal hyperplasia: does dexamethasone cause behavioural problems?. *European Journal of Endocrinology*, *159*(3), 309-316.

Holland, K. D., Kearney, J. A., Glauser, T. A., Buck, G., Keddache, M., Blankston, J. R., ... & Meisler, M. H. (2008). Mutation of sodium channel SCN3A in a patient with cryptogenic pediatric partial epilepsy. *Neuroscience letters, 433*(1), 65-70.

Hompes, T., Izzi, B., Gellens, E., Morreels, M., Fieuws, S., Pexsters, A., ... & Verhaeghe, J. (2013). Investigating the influence of maternal cortisol and emotional state during pregnancy on the DNA methylation status of the glucocorticoid

receptor gene (NR3C1) promoter region in cord blood. *Journal of psychiatric research*, *47*(7), 880-891.

Hori, K., Nagai, T., Shan, W., Sakamoto, A., Taya, S., Hashimoto, R., ... & Nishioka, T. (2014). Cytoskeletal regulation by AUTS2 in neuronal migration and neuritogenesis. *Cell reports*, *9*(6), 2166-2179.

Horn, Z., Behesti, H., & Hatten, M. E. (2018). N-cadherin provides a cis and trans ligand for astrotactin that functions in glial-guided neuronal migration. *Proceedings of the National Academy of Sciences*, *115*(42), 10556-10563.

Hrdlickova, R., Toloue, M., & Tian, B. (2017). RNA-Seq methods for transcriptome analysis. *Wiley Interdisciplinary Reviews: RNA*, *8*(1), e1364.

Hur, E. M., & Zhou, F. Q. (2010). GSK3 signaling in neural development. *Nature Reviews Neuroscience*, 11(8), 539.

Hříbková, H., Grabiec, M., Klemová, D., Slaninová, I., & Sun, Y. M. (2018). Five steps to form neural rosettes: structure and function. *Journal of Cell Science*, jcs-206896.

Impagnatiello, F., Guidotti, A. R., Pesold, C., Dwivedi, Y., Caruncho, H., Pisu, M. G., ... & Pappas, G. D. (1998). A decrease of reelin expression as a putative vulnerability factor in schizophrenia. *Proceedings of the National Academy of Sciences, 95*(26), 15718-15723.

Ince-Dunn, G., Okano, H. J., Jensen, K. B., Park, W. Y., Zhong, R., Ule, J., ... & Yoo, J. (2012). Neuronal Elav-like (Hu) proteins regulate RNA splicing and

abundance to control glutamate levels and neuronal excitability. *Neuron, 75*(6), 1067-1080.

Inoue, T., Ota, M., Ogawa, M., Mikoshiba, K., & Aruga, J. (2007). Zic1 and Zic3 regulate medial forebrain development through expansion of neuronal progenitors. *Journal of Neuroscience, 27*(20), 5461-5473.

Irie, M., Hata, Y., Takeuchi, M., Ichtchenko, K., Toyoda, A., Hirao, K., ... & Südhof, T. C. (1997). Binding of neuroligins to PSD-95. *Science*, *277*(5331), 1511-1515.

Johnson, M. B., Kawasawa, Y. I., Mason, C. E., Krsnik, Ž., Coppola, G., Bogdanović, D., ... & Šestan, N. (2009). Functional and evolutionary insights into human brain development through global transcriptome analysis. *Neuron*, *62*(4), 494-509.

Johnson, W. E., Li, C., & Rabinovic, A. (2007). Adjusting batch effects in microarray expression data using empirical Bayes methods. *Biostatistics*, 8(1), 118-127.

Jones, J. R., Kong, L., Hanna IV, M. G., Hoffman, B., Krencik, R., Bradley, R., ... & Sherafat, M. A. (2018). Mutations in GFAP disrupt the distribution and function of organelles in human astrocytes. *Cell reports, 25*(4), 947-958.

Kamburov, A., Pentchev, K., Galicka, H., Wierling, C., Lehrach, H., & Herwig, R. (2010). ConsensusPathDB: toward a more complete picture of cell biology. *Nucleic acids research, 39*(suppl_1), D712-D717.

Kamiya, A., Kubo, K. I., Tomoda, T., Takaki, M., Youn, R., Ozeki, Y., ... & Ross, C. A. (2005). A schizophrenia-associated mutation of DISC1 perturbs cerebral cortex development. *Nature cell biology*, *7*(12), 1167.

Kessler, R. C., Berglund, P., Demler, O., Jin, R., Merikangas, K. R., & Walters, E. E. (2005). Lifetime prevalence and age-of-onset distributions of DSM-IV disorders in the National Comorbidity Survey Replication. *Archives of general psychiatry, 62*(6), 593-602.

Khalife, N., Glover, V., Taanila, A., Ebeling, H., Järvelin, M. R., & Rodriguez, A. (2013). Prenatal glucocorticoid treatment and later mental health in children and adolescents. *PloS one*, *8*(11), e81394.

Kim, K., Doi, A., Wen, B., Ng, K., Zhao, R., Cahan, P., ... & Yabuuchi, A. (2010). Epigenetic memory in induced pluripotent stem cells. *Nature, 467*(7313), 285.

Kim, S. E., Lee, W. J., & Choi, K. Y. (2007). The PI3 kinase-Akt pathway mediates Wnt3a-induced proliferation. *Cellular signalling, 19*(3), 511-518.

Kimura, J., Suda, Y., Kurokawa, D., Hossain, Z. M., Nakamura, M., Takahashi, M., ... & Aizawa, S. (2005). Emx2 and Pax6 function in cooperation with Otx2 and Otx1 to develop caudal forebrain primordium that includes future archipallium. *Journal of Neuroscience, 25*(21), 5097-5108.

Kingsbury, M., Weeks, M., MacKinnon, N., Evans, J., Mahedy, L., Dykxhoorn, J., & Colman, I. (2016). Stressful life events during pregnancy and offspring depression: evidence from a prospective cohort study. *Journal of the American Academy of Child & Adolescent Psychiatry, 55*(8), 709-716.

Kitamura, K., Yanazawa, M., Sugiyama, N., Miura, H., Iizuka-Kogo, A., Kusaka, M., ... & Matsuo, M. (2002). Mutation of ARX causes abnormal development of

forebrain and testes in mice and X-linked lissencephaly with abnormal genitalia in humans. *Nature genetics, 32*(3), 359.

Kirkeby, A., Grealish, S., Wolf, D. A., Nelander, J., Wood, J., Lundblad, M., ... & Parmar, M. (2012). Generation of regionally specified neural progenitors and functional neurons from human embryonic stem cells under defined conditions. *Cell reports*, 1(6), 703-714.

Kohli, M. A., Lucae, S., Saemann, P. G., Schmidt, M. V., Demirkan, A., Hek, K., ... & Hoehn, D. (2011). The neuronal transporter gene SLC6A15 confers risk to major depression. *Neuron*, 70(2), 252-265.

Konno, D., Iwashita, M., Satoh, Y., Momiyama, A., Abe, T., Kiyonari, H., & Matsuzaki, F. (2012). The mammalian DM domain transcription factor Dmrta2 is required for early embryonic development of the cerebral cortex. *PloS one, 7*(10), e46577.

Kreis, P., Gallrein, C., Rojas-Puente, E., Mack, T. G., Kroon, C., Dinkel, V., ... & Eickholt, B. J. (2019). ATM phosphorylation of the actin-binding protein drebrin controls oxidation stress-resistance in mammalian neurons and C. elegans. *Nature communications, 10*(1), 486.

Kriks, S., Shim, J. W., Piao, J., Ganat, Y. M., Wakeman, D. R., Xie, Z., ... & Yang, L. (2011). Dopamine neurons derived from human ES cells efficiently engraft in animal models of Parkinson's disease. *Nature*, 480(7378), 547.

Kuleshov, M. V., Jones, M. R., Rouillard, A. D., Fernandez, N. F., Duan, Q., Wang, Z., ... & McDermott, M. G. (2016). Enrichr: a comprehensive gene set enrichment analysis web server 2016 update. Nucleic acids research, 44(W1), W90-W97.

Kurokawa, D., Kiyonari, H., Nakayama, R., Kimura-Yoshida, C., Matsuo, I., & Aizawa, S. (2004). Regulation of Otx2 expression and its functions in mouse forebrain and midbrain. *Development, 131*(14), 3319-3331.

Lai, C. S., Fisher, S. E., Hurst, J. A., Vargha-Khadem, F., & Monaco, A. P. (2001). A forkhead-domain gene is mutated in a severe speech and language disorder. *Nature*, *413*(6855), 519.

Lai, T. J., Payne, M. E., Byrum, C. E., Steffens, D. C., & Krishnan, K. R. R. (2000). Reduction of orbital frontal cortex volume in geriatric depression. *Biological Psychiatry, 48*(10), 971-975.

La Manno, G., Gyllborg, D., Codeluppi, S., Nishimura, K., Salto, C., Zeisel, A., ... & Lönnerberg, P. (2016). Molecular diversity of midbrain development in mouse, human, and stem cells. *Cell, 167*(2), 566-580.

Lamminmäki, S., Massinen, S., Nopola-Hemmi, J., Kere, J., & Hari, R. (2012). Human ROBO1 regulates interaural interaction in auditory pathways. *Journal of Neuroscience*, *32*(3), 966-971.

Law, C. W., Chen, Y., Shi, W., & Smyth, G. K. (2014). voom: Precision weights unlock linear model analysis tools for RNA-seq read counts. *Genome biology, 15*(2), R29.

Law, A. J., Lipska, B. K., Weickert, C. S., Hyde, T. M., Straub, R. E., Hashimoto, R., ... & Weinberger, D. R. (2006). Neuregulin 1 transcripts are differentially expressed in schizophrenia and regulated by 5′ SNPs associated with the disease. *Proceedings of the National Academy of Sciences*, *103*(17), 6747-6752.

Leek, J. T., Johnson, W. E., Parker, H. S., Jaffe, A. E., & Storey, J. D. (2012). The sva package for removing batch effects and other unwanted variation in high-throughput experiments. *Bioinformatics, 28*(6), 882-883.

Leek, J. T., Scharpf, R. B., Bravo, H. C., Simcha, D., Langmead, B., Johnson, W. E., ... & Irizarry, R. A. (2010). Tackling the widespread and critical impact of batch effects in high-throughput data. *Nature Reviews Genetics*, 11(10), 733.

Leek, J. T., & Storey, J. D. (2007). Capturing heterogeneity in gene expression studies by surrogate variable analysis. *PLoS genetics*, 3(9), e161.

Lendahl, U., Zimmerman, L. B., & McKay, R. D. (1990). CNS stem cells express a new class of intermediate filament protein. *Cell, 60*(4), 585-595.

Leng, N., Dawson, J. A., Thomson, J. A., Ruotti, V., Rissman, A. I., Smits, B. M., ... & Kendziorski, C. (2013). EBSeq: an empirical Bayes hierarchical model for inference in RNA-seq experiments. *Bioinformatics*, *29*(8), 1035-1043.

Li, Z., Chen, J., Yu, H., He, L., Xu, Y., Zhang, D., ... & Song, Z. (2017). Genome-wide association analysis identifies 30 new susceptibility loci for schizophrenia. *Nature genetics*, *49*(11), 1576.

Li, H., Koo, Y., Mao, X., Sifuentes-Dominguez, L., Morris, L. L., Jia, D., ... & Billadeau, D. D. (2015). Endosomal sorting of Notch receptors through COMMD9-dependent pathways modulates Notch signaling. *Journal of Cell Biology, 211*(3), 605-617.

Li, J., Olsen, J., Vestergaard, M., & Obel, C. (2010). Attention-deficit/hyperactivity disorder in the offspring following prenatal maternal bereavement: a nationwide follow-up study in Denmark. *European child & adolescent psychiatry*, *19*(10), 747-753.

Li, M., & Yue, W. (2018). VRK2, a Candidate Gene for Psychiatric and Neurological Disorders. *Molecular neuropsychiatry, 4*(3), 119-133.

Lightman, S. L., & Conway-Campbell, B. L. (2010). The crucial role of pulsatile activity of the HPA axis for continuous dynamic equilibration. *Nature Reviews Neuroscience, 11*(10), 710.

Liu, Y., Zhou, J., & White, K. P. (2013). RNA-seq differential expression studies: more sequence or more replication?. *Bioinformatics, 30*(3), 301-304.

Lieberman, R., Kranzler, H. R., Levine, E. S., & Covault, J. (2017). Examining FKBP5 mRNA expression in human iPSC-derived neural cells. *Psychiatry research*, *247*, 172-181.

Liu, D., Diorio, J., Tannenbaum, B., Caldji, C., Francis, D., Freedman, A., ... & Meaney, M. J. (1997). Maternal care, hippocampal glucocorticoid receptors, and hypothalamic-pituitary-adrenal responses to stress. *Science*, *277*(5332), 1659-1662.

Liu, Y., Ferguson, J. F., Xue, C., Silverman, I. M., Gregory, B., Reilly, M. P., & Li, M. (2013). Evaluating the impact of sequencing depth on transcriptome profiling in human adipose. *PLoS One*, *8*(6), e66883.

Liu, Y., Zhou, J., & White, K. P. (2013). RNA-seq differential expression studies: more sequence or more replication?. *Bioinformatics, 30*(3), 301-304.

Long, H., Sabatier, C., Ma, L., Plump, A., Yuan, W., Ornitz, D. M., ... & Tessier-Lavigne, M. (2004). Conserved roles for Slit and Robo proteins in midline commissural axon guidance. *Neuron*, *42*(2), 213-223.

Loomes, R., Hull, L., & Mandy, W. P. L. (2017). What is the male-to-female ratio in autism spectrum disorder? A systematic review and meta-analysis. *Journal of the American Academy of Child & Adolescent Psychiatry*, *56*(6), 466-474.

López-Bendito, G., Cautinat, A., Sánchez, J. A., Bielle, F., Flames, N., Garratt, A. N., ... & Garel, S. (2006). Tangential neuronal migration controls axon guidance: a role for neuregulin-1 in thalamocortical axon navigation. *Cell*, *125*(1), 127-142.

Love, M. I., Huber, W., & Anders, S. (2014). Moderated estimation of fold change and dispersion for RNA-seq data with DESeq2. *Genome biology, 15*(12), 550.

Ma, F., Fuqua, B. K., Hasin, Y., Yukhtman, C., Vulpe, C. D., Lusis, A. J., & Pellegrini, M. (2019). A comparison between whole transcript and 3'RNA sequencing methods using Kapa and Lexogen library preparation methods. *BMC genomics, 20*(1), 9.

Ma, W., Tavakoli, T., Derby, E., Serebryakova, Y., Rao, M. S., & Mattson, M. P. (2008). Cell-extracellular matrix interactions regulate neural differentiation of human embryonic stem cells. *BMC developmental biology, 8*(1), 90.

MacArthur, B. A., Howie, R. N., Dezoete, J. A., & Elkins, J. (1982). School progress and cognitive development of 6-year-old children whose mothers were treated antenatally with betamethasone. *Pediatrics, 70*(1), 99-105.

Mackay, A. V. P. (1980). Positive and negative schizophrenic symptoms and the role of dopamine. *The British Journal of Psychiatry, 137*(4), 379-383.

Mairesse, J., Lesage, J., Breton, C., Bréant, B., Hahn, T., Darnaudéry, M., ... & Maccari, S. (2007). Maternal stress alters endocrine function of the feto-placental unit in rats. *American Journal of Physiology-Endocrinology and Metabolism*, *292*(6), E1526-E1533.

Maksimovic, J., Gordon, L., & Oshlack, A. (2012). SWAN: Subset-quantile within array normalization for illumina infinium HumanMethylation450 BeadChips. *Genome biology*, *13*(6), R44.

Maroof, A. M., Keros, S., Tyson, J. A., Ying, S. W., Ganat, Y. M., Merkle, F. T., ... & Widmer, H. R. (2013). Directed differentiation and functional maturation of cortical interneurons from human embryonic stem cells. *Cell stem cell, 12*(5), 559-572.

Martin, M. (2011). Cutadapt removes adapter sequences from high-throughput sequencing reads. *EMBnet. journal*, *17*(1), 10-12.

Matsumata, M., Sakayori, N., Maekawa, M., Owada, Y., Yoshikawa, T., & Osumi, N. (2012). The effects of Fabp7 and Fabp5 on postnatal hippocampal neurogenesis in the mouse. *Stem cells*, 30(7), 1532-1543.

McLean, C. Y., Bristor, D., Hiller, M., Clarke, S. L., Schaar, B. T., Lowe, C. B., ... & Bejerano, G. (2010). GREAT improves functional interpretation of cis-regulatory regions. *Nature biotechnology*, *28*(5), 495.

Meaney, M. J., Sapolsky, R. M., & McEwen, B. S. (1985). The development of the glucocorticoid receptor system in the rat limbic brain. I. Ontogeny and autoregulation. *Developmental Brain Research*, *18*(1-2), 159-164.

Mei, L., & Xiong, W. C. (2008). Neuregulin 1 in neural development, synaptic plasticity and schizophrenia. *Nature Reviews Neuroscience, 9*(6), 437.

Mertens, J., Paquola, A. C., Ku, M., Hatch, E., Böhnke, L., Ladjevardi, S., ... & Gonçalves, J. T. (2015). Directly reprogrammed human neurons retain aging-associated transcriptomic signatures and reveal age-related nucleocytoplasmic defects. *Cell stem cell, 17*(6), 705-718.

Meyer-Bahlburg, H. F., Dolezal, C., Baker, S. W., Carlson, A. D., Obeid, J. S., & New, M. I. (2004). Cognitive and motor development of children with and without congenital adrenal hyperplasia after early-prenatal dexamethasone. *The Journal of Clinical Endocrinology & Metabolism*, *89*(2), 610-614.

Meyer-Lindenberg, A., Miletich, R. S., Kohn, P. D., Esposito, G., Carson, R. E., Quarantelli, M., ... & Berman, K. F. (2002). Reduced prefrontal activity predicts

exaggerated striatal dopaminergic function in schizophrenia. *Nature neuroscience*, 5(3), 267.

Michibata, H., Okuno, T., Konishi, N., Kyono, K., Wakimoto, K., Aoki, K., ... & Taniguchi, T. (2009). Human GPM6A is associated with differentiation and neuronal migration of neurons derived from human embryonic stem cells. *Stem cells and development, 18*(4), 629-640.

Mikati, M. A., Grintsevich, E. E., & Reisler, E. (2013). Drebrin-induced stabilization of actin filaments. *Journal of Biological Chemistry, 288*(27), 19926-19938.

Millar, J. K., Wilson-Annan, J. C., Anderson, S., Christie, S., Taylor, M. S., Semple, C. A., ... & Porteous, D. J. (2000). Disruption of two novel genes by a translocation co-segregating with schizophrenia. *Human molecular genetics*, *9*(9), 1415-1423.

Miller, S. L., Chai, M., Loose, J., Castillo-Meléndez, M., Walker, D. W., Jenkin, G., & Wallace, E. M. (2007). The effects of maternal betamethasone administration on the intrauterine growth-restricted fetus. *Endocrinology, 148*(3), 1288-1295.

Miller, J. A., Ding, S. L., Sunkin, S. M., Smith, K. A., Ng, L., Szafer, A., ... & Arnold, J. M. (2014). Transcriptional landscape of the prenatal human brain. *Nature*, *508*(7495), 199.

Mills, E. L., Ryan, D. G., Prag, H. A., Dikovskaya, D., Menon, D., Zaslona, Z., ... & Szpyt, J. (2018). Itaconate is an anti-inflammatory metabolite that activates Nrf2 via alkylation of KEAP1. *Nature, 556*(7699), 113.

Mo, A., Mukamel, E. A., Davis, F. P., Luo, C., Henry, G. L., Picard, S., ... & Eddy, S. R. (2015). Epigenomic signatures of neuronal diversity in the mammalian brain. *Neuron, 86*(6), 1369-1384.

Moghaddam, B., & Javitt, D. (2012). From revolution to evolution: the glutamate hypothesis of schizophrenia and its implication for treatment. *Neuropsychopharmacology, 37*(1), 4.

Mohn, F., Weber, M., Rebhan, M., Roloff, T. C., Richter, J., Stadler, M. B., ... & Schübeler, D. (2008). Lineage-specific polycomb targets and de novo DNA methylation define restriction and potential of neuronal progenitors. *Molecular cell*, *30*(6), 755-766.

Monk, C., Feng, T., Lee, S., Krupska, I., Champagne, F. A., & Tycko, B. (2016). Distress during pregnancy: epigenetic regulation of placenta glucocorticoid-related genes and fetal neurobehavior. *American Journal of Psychiatry*, *173*(7), 705-713.

Moreno, M. A., Furtner, F., & Rivara, F. P. (2012). Preventing birth defects with a healthy pregnancy diet. *Archives of pediatrics & adolescent medicine, 166*(2), 200-200.

Mostaid, M. S., Lloyd, D., Liberg, B., Sundram, S., Pereira, A., Pantelis, C., ... & Bousman, C. A. (2016). Neuregulin-1 and schizophrenia in the genome-wide association study era. *Neuroscience & Biobehavioral Reviews*, *68*, 387-409.

Mulligan, C., D'Errico, N., Stees, J., & Hughes, D. (2012). Methylation changes at NR3C1 in newborns associate with maternal prenatal stress exposure and newborn birth weight. *Epigenetics*, *7*(8), 853-857.

Muraki, K., & Tanigaki, K. (2015). Neuronal migration abnormalities and its possible implications for schizophrenia. *Frontiers in neuroscience*, 9, 74.

Muralidharan, B., Khatri, Z., Maheshwari, U., Gupta, R., Roy, B., Pradhan, S. J., ... & Kolthur-Seetharam, U. (2017). LHX2 interacts with the NuRD complex and regulates cortical neuron subtype determinants Fezf2 and Sox11. *Journal of Neuroscience, 37*(1), 194-203.

Murphy, B. P., Inder, T. E., Huppi, P. S., Warfield, S., Zientara, G. P., Kikinis, R., ... & Volpe, J. J. (2001). Impaired cerebral cortical gray matter growth after treatment with dexamethasone for neonatal chronic lung disease. *Pediatrics*, *107*(2), 217-221.

Mychasiuk, R., Gibb, R., & Kolb, B. (2011). Prenatal stress produces sexually dimorphic and regionally specific changes in gene expression in hippocampus and frontal cortex of developing rat offspring. *Developmental Neuroscience*, *33*(6), 531-538.

Mzoughi, S., Zhang, J., Hequet, D., Teo, S. X., Fang, H., Xing, Q. R., ... & Wollmann, H. (2017). PRDM15 safeguards naive pluripotency by transcriptionally regulating WNT and MAPK–ERK signaling. *Nature genetics*, *49*(9), 1354.

Narayan, G., Goparaju, C., Arias-Pulido, H., Kaufmann, A. M., Schneider, A., Dürst, M., ... & Murty, V. V. (2006). Promoter hypermethylation-mediated inactivation

of multiple Slit-Robo pathway genes in cervical cancer progression. *Molecular cancer*, *5*(1), 16.

Nesan, D., Kamkar, M., Burrows, J., Scott, I. C., Marsden, M., & Vijayan, M. M. (2012). Glucocorticoid receptor signaling is essential for mesoderm formation and muscle development in zebrafish. *Endocrinology*, *153*(3), 1288-1300.

Nesan, D., & Vijayan, M. M. (2013). The transcriptomics of glucocorticoid receptor signaling in developing zebrafish. *PLoS One, 8(*11), e80726.

Ni, L., Pan, Y., Tang, C., Xiong, W., Wu, X., & Zou, C. (2018). Antenatal exposure to betamethasone induces placental 11β-hydroxysteroid dehydrogenase type 2 expression and the adult metabolic disorders in mice. *PloS one, 13*(9), e0203802.

Nimkarn, S., & New, M. I. (2007). Prenatal diagnosis and treatment of congenital adrenal hyperplasia owing to 21-hydroxylase deficiency. *Nature Reviews Endocrinology*, *3*(5), 405.

Ninomiya, E., Hattori, T., Toyoda, M., Umezawa, A., Hamazaki, T., & Shintaku, H. (2014). Glucocorticoids promote neural progenitor cell proliferation derived from human induced pluripotent stem cells*. Springerplus*, 3(1), 527.

Niwa, M., Kamiya, A., Murai, R., Kubo, K. I., Gruber, A. J., Tomita, K., ... & Hiyama, H. (2010). Knockdown of DISC1 by in utero gene transfer disturbs postnatal dopaminergic maturation in the frontal cortex and leads to adult behavioral deficits. *Neuron*, 65(4), 480-489.

Nogales-Cadenas, R., Carmona-Saez, P., Vazquez, M., Vicente, C., Yang, X., Tirado, F., ... & Pascual-Montano, A. (2009). GeneCodis: interpreting gene lists through enrichment analysis and integration of diverse biological information. *Nucleic acids research, 37(suppl_2)*, W317-W322.

Nojima, H., Adachi, M., Matsui, T., Okawa, K., Tsukita, S., & Tsukita, S. (2008). IQGAP3 regulates cell proliferation through the Ras/ERK signaling cascade. *Nature cell biology*, 10(8), 971.

Nopoulos, P., Boes, A. D., Jabines, A., Conrad, A. L., Canady, J., Richman, L., & Dawson, J. D. (2010). Hyperactivity, impulsivity, and inattention in boys with cleft lip and palate: relationship to ventromedial prefrontal cortex morphology. *Journal of neurodevelopmental disorders*, *2*(4), 235.

Nulman, I., Koren, G., Rovet, J., Barrera, M., Pulver, A., Streiner, D., & Feldman, B. (2012). Neurodevelopment of children following prenatal exposure to venlafaxine, selective serotonin reuptake inhibitors, or untreated maternal depression. *American Journal of Psychiatry*, *169*(11), 1165-1174.

Oberlander, T. F., Weinberg, J., Papsdorf, M., Grunau, R., Misri, S., & Devlin, A. M. (2008). Prenatal exposure to maternal depression, neonatal methylation of human glucocorticoid receptor gene (NR3C1) and infant cortisol stress responses. *Epigenetics*, *3*(2), 97-106.

O'Donnell, K. J., Glover, V., Barker, E. D., & O'Connor, T. G. (2014). The persisting effect of maternal mood in pregnancy on childhood psychopathology. *Development and psychopathology*, *26*(2), 393-403.

Ogino, H., Hisanaga, A., Kohno, T., Kondo, Y., Okumura, K., Kamei, T., ... & Hattori, M. (2017). Secreted metalloproteinase ADAMTS-3 inactivates reelin. *Journal of Neuroscience, 37*(12), 3181-3191.

Oikari, L. E., Okolicsanyi, R. K., Qin, A., Yu, C., Griffiths, L. R., & Haupt, L. M. (2016). Cell surface heparan sulfate proteoglycans as novel markers of human neural stem cell fate determination. *Stem cell research, 16*(1), 92-104.

O'Neill, A. C., Kyrousi, C., Einsiedler, M., Burtscher, I., Drukker, M., Markie, D. M., ... & Cappello, S. (2018). Mob2 Insufficiency Disrupts Neuronal Migration in the Developing Cortex. *Frontiers in cellular neuroscience*, *12*, 57.

Ostlund, B. D., Conradt, E., Crowell, S. E., Tyrka, A. R., Marsit, C. J., & Lester, B. M. (2016). Prenatal stress, fearfulness, and the epigenome: exploratory analysis of sex differences in DNA methylation of the glucocorticoid receptor gene. *Frontiers in behavioral neuroscience*, *10*, 147.

Paakinaho, V., Presman, D. M., Ball, D. A., Johnson, T. A., Schiltz, R. L., Levitt, P., ... & Hager, G. L. (2017). Single-molecule analysis of steroid receptor and cofactor action in living cells. *Nature communications, 8*, 15896.

Pantha, S., Hayes, B., Yadav, B. K., Sharma, P., Shrestha, A., & Gartoulla, P. (2014). Prevalence of Stress among Pregnant Women Attending Antenatal Care in a Tertiary Maternity Hospital in Kathmandu. *Journal of Women's Health Care*, *3*(5), 183.

Patro, R., Duggal, G., Love, M. I., Irizarry, R. A., & Kingsford, C. (2017). Salmon provides fast and bias-aware quantification of transcript expression. *Nature methods*, *14*(4), 417.

Pardiñas, A. F., Holmans, P., Pocklington, A. J., Escott-Price, V., Ripke, S., Carrera, N., ... & Han, J. (2018). Common schizophrenia alleles are enriched in mutation-intolerant genes and in regions under strong background selection. *Nature genetics*, *50*(3), 381.

Pearson, R. M., Evans, J., Kounali, D., Lewis, G., Heron, J., Ramchandani, P. G., ... & Stein, A. (2013). Maternal depression during pregnancy and the postnatal period: risks and possible mechanisms for offspring depression at age 18 years. *JAMA psychiatry, 70*(12), 1312-1319.

Peffer, M. E., Zhang, J. Y., Umfrey, L., Rudine, A. C., Monaghan, A. P., & DeFranco, D. B. (2015). Minireview: the impact of antenatal therapeutic synthetic glucocorticoids on the developing fetal brain. *Molecular Endocrinology*, *29*(5), 658-666.

Petridis, A. K., El Maarouf, A., & Rutishauser, U. (2004). Polysialic acid regulates cell contact-dependent neuronal differentiation of progenitor cells from the subventricular zone. *Developmental dynamics: an official publication of the American Association of Anatomists, 230*(4), 675-684.

Perroud, N., Rutembesa, E., Paoloni-Giacobino, A., Mutabaruka, J., Mutesa, L., Stenz, L., ... & Karege, F. (2014). The Tutsi genocide and transgenerational transmission of maternal stress: epigenetics and biology of the HPA axis. *The World Journal of Biological Psychiatry*, *15*(4), 334-345.

Pfefferbaum, A., Mathalon, D. H., Sullivan, E. V., Rawles, J. M., Zipursky, R. B., & Lim, K. O. (1994). A quantitative magnetic resonance imaging study of changes in brain morphology from infancy to late adulthood. *Archives of neurology*, 51(9), 874-887.

Pickles, A., Sharp, H., Hellier, J., & Hill, J. (2017). Prenatal anxiety, maternal stroking in infancy, and symptoms of emotional and behavioral disorders at 3.5 years. *European child & adolescent psychiatry*, *26*(3), 325-334.

Pikulkaew, S., Benato, F., Celeghin, A., Zucal, C., Skobo, T., Colombo, L., & Valle, L. D. (2011). The knockdown of maternal glucocorticoid receptor mRNA alters embryo development in zebrafish. *Developmental dynamics, 240*(4), 874-889.

Plant, D. T., Pariante, C. M., Sharp, D., & Pawlby, S. (2015). Maternal depression during pregnancy and offspring depression in adulthood: role of child maltreatment. *The British Journal of Psychiatry, 207*(3), 213-220.

Plant, D. T., Pawlby, S., Sharp, D., Zunszain, P. A., & Pariante, C. M. (2016). Prenatal maternal depression is associated with offspring inflammation at 25 years: a prospective longitudinal cohort study. *Translational psychiatry*, *6*(11), e936.

Plump, A. S., Erskine, L., Sabatier, C., Brose, K., Epstein, C. J., Goodman, C. S., ... & Tessier-Lavigne, M. (2002). Slit1 and Slit2 cooperate to prevent premature midline crossing of retinal axons in the mouse visual system. *Neuron, 33*(2), 219-232.

Popoli, M., Yan, Z., McEwen, B. S., & Sanacora, G. (2012). The stressed synapse: the impact of stress and glucocorticoids on glutamate transmission. *Nature Reviews Neuroscience*, *13*(1), 22.

Porter, F. D., Drago, J., Xu, Y., Cheema, S. S., Wassif, C., Huang, S. P., ... & Alt, F. (1997). Lhx2, a LIM homeobox gene, is required for eye, forebrain, and definitive erythrocyte development. *Development, 124*(15), 2935-2944.

Pratt, W. B., Morishima, Y., Murphy, M., & Harrell, M. (2006). Chaperoning of glucocorticoid receptors. In *Molecular Chaperones in Health and Disease* (pp. 111-138). Springer, Berlin, Heidelberg.

Qi, Y., Zhang, X. J., Renier, N., Wu, Z., Atkin, T., Sun, Z., ... & Ganat, Y. (2017). Combined small-molecule inhibition accelerates the derivation of functional cortical neurons from human pluripotent stem cells. *Nature biotechnology, 35*(2), 154.

Qiu, A., Shen, M., Buss, C., Chong, Y. S., Kwek, K., Saw, S. M., ... & Karnani, N. (2017). Effects of antenatal maternal depressive symptoms and socio-economic status on neonatal brain development are modulated by genetic risk. *Cerebral Cortex*, *27*(5), 3080-3092.

Qu, X., Zou, Z., Sun, Q., Luby-Phelps, K., Cheng, P., Hogan, R. N., ... & Levine, B. (2007). Autophagy gene-dependent clearance of apoptotic cells during embryonic development. *Cell, 128*(5), 931-946.

Rai, D., Golding, J., Magnusson, C., Steer, C., Lewis, G., & Dalman, C. (2012). Prenatal and early life exposure to stressful life events and risk of autism spectrum

disorders: population-based studies in Sweden and England. *PloS one*, 7(6), e38893.

Rajagopalan, S., Deitinghoff, L., Davis, D., Conrad, S., Skutella, T., Chedotal, A., ... & Strittmatter, S. M. (2004). Neogenin mediates the action of repulsive guidance molecule. *Nature cell biology, 6*(8), 756.

Reul, J. M., Gesing, A., Droste, S., Stec, I. S., Weber, A., Bachmann, C., ... & Linthorst, A. C. (2000). The brain mineralocorticoid receptor: greedy for ligand, mysterious in function. *European journal of pharmacology*, *405*(1-3), 235-249.

Rijlaarsdam, J., Pappa, I., Walton, E., Bakermans-Kranenburg, M. J., Mileva-Seitz, V. R., Rippe, R. C., ... & Cecil, C. A. (2016). An epigenome-wide association meta-analysis of prenatal maternal stress in neonates: A model approach for replication. *Epigenetics*, *11*(2), 140-149.

Rijlaarsdam, J., van IJzendoorn, M. H., Verhulst, F. C., Jaddoe, V. W., Felix, J. F., Tiemeier, H., & Bakermans-Kranenburg, M. J. (2017). Prenatal stress exposure, oxytocin receptor gene (OXTR) methylation, and child autistic traits: the moderating role of OXTR rs53576 genotype. *Autism Research, 10*(3), 430-438.

Ring, R. H., Valo, Z., Gao, C., Barish, M. E., & Singer-Sam, J. (2003). The Cdkn1a gene (p21Waf1/Cip1) is an inflammatory response gene in the mouse central nervous system. *Neuroscience letters, 350*(2), 73-76.

Ripke, S., Neale, B. M., Corvin, A., Walters, J. T., Farh, K. H., Holmans, P. A., ... & Pers, T. H. (2014). Biological insights from 108 schizophrenia-associated genetic loci. *Nature*, *511*(7510), 421.

Ripke, S., Sanders, A. R., Kendler, K. S., Levinson, D. F., Sklar, P., Holmans, P. A., ... & Scolnick, E. (2011). Genome-wide association study identifies five new schizophrenia loci. *Nature genetics, 43*(10), 969.

Ritchie, ME, Phipson, B, Wu, D, Hu, Y, Law, CW, Shi, W, and Smyth, GK (2015). limma powers differential expression analyses for RNA-sequencing and microarray studies. *Nucleic Acids Research, 43*(7), e47.

Rivals, I., Personnaz, L., Taing, L., & Potier, M. C. (2006). Enrichment or depletion of a GO category within a class of genes: which test? *Bioinformatics*, *23*(4), 401-407.

Robertson, S., Rohwer, J. M., Hapgood, J. P., & Louw, A. (2013). Impact of glucocorticoid receptor density on ligand-independent dimerization, cooperative ligand-binding and basal priming of transactivation: a cell culture model. *PloS one*, *8*(5), e64831.

Robinson, E. (1963). Effect of amygdalectomy on fear-motivated behavior in rats. *Journal of Comparative and Physiological Psychology, 56*(5), 814-820.

Robinson, M. D., McCarthy, D. J., & Smyth, G. K. (2010). edgeR: a Bioconductor package for differential expression analysis of digital gene expression data. *Bioinformatics, 26*(1), 139-140.

Roca, C. P., Gomes, S. I., Amorim, M. J., & Scott-Fordsmand, J. J. (2017). Variation-preserving normalization unveils blind spots in gene expression profiling. *Scientific reports, 7*, 42460.

Rohr, K. B., Schulte-Merker, S., & Tautz, D. (1999). Zebrafish zic1 expression in brain and somites is affected by BMP and hedgehog signalling. *Mechanisms of development, 85*(1-2), 147-159.

Ronald, A., Pennell, C. E., & Whitehouse, A. J. (2011). Prenatal maternal stress associated with ADHD and autistic traits in early childhood. *Frontiers in psychology*, *1*, 223.

Rouse, M. H., & Goodman, S. H. (2014). Perinatal depression influences on infant negative affectivity: timing, severity, and co-morbid anxiety. *Infant Behavior and Development*, *37*(4), 739-751.

Roussa, E., Wiehle, M., Dünker, N., Becker-Katins, S., Oehlke, O., & Krieglstein, K. (2006). Transforming growth factor β is required for differentiation of mouse mesencephalic progenitors into dopaminergic neurons in vitro and in vivo: ectopic induction in dorsal mesencephalon. *Stem Cells, 24*(9), 2120-2129.

Russell, G. M., Henley, D. E., Leendertz, J., Douthwaite, J. A., Wood, S. A., Stevens, A., ... & Veldhuis, J. D. (2010). Rapid glucocorticoid receptor-mediated inhibition of hypothalamic–pituitary–adrenal ultradian activity in healthy males. *Journal of Neuroscience, 30*(17), 6106-6115.

Sakakibara, S. I., Nakamura, Y., Satoh, H., & Okano, H. (2001). Rna-binding protein Musashi2: developmentally regulated expression in neural precursor cells

and subpopulations of neurons in mammalian CNS. *Journal of Neuroscience, 21*(20), 8091-8107.

Sandman, C. A., Buss, C., Head, K., & Davis, E. P. (2015). Fetal exposure to maternal depressive symptoms is associated with cortical thickness in late childhood. *Biological psychiatry*, *77*(4), 324-334.

Sanjuán, J., Tolosa, A., González, J. C., Aguilar, E. J., Pérez-Tur, J., Nájera, C., ... & de Frutos, R. (2006). Association between FOXP2 polymorphisms and schizophrenia with auditory hallucinations. *Psychiatric genetics*, 16(2), 67-72.

Santarelli, S., Wagner, K. V., Labermaier, C., Uribe, A., Dournes, C., Balsevich, G., ... & Müller, M. B. (2016). SLC6A15, a novel stress vulnerability candidate, modulates anxiety and depressive-like behavior: involvement of the glutamatergic system. *Stress*, 19(1), 83-90.

Sarkar, S., Craig, M. C., Dell'Acqua, F., O'Connor, T. G., Catani, M., Deeley, Q., ... & Murphy, D. G. (2014). Prenatal stress and limbic-prefrontal white matter microstructure in children aged 6–9 years: a preliminary diffusion tensor imaging study. *The World Journal of Biological Psychiatry*, *15*(4), 346-352.

Sausenthaler, S., Rzehak, P., Chen, C. M., Arck, P., Bockelbrink, A., Schäfer, T., ... & Von Berg, A. (2009). 9 Stress-Related Maternal Factors During Pregnancy in Relation to Childhood Eczema: Results From the LISA Study. *Journal of investigational allergology & clinical immunology*, *19*(6), 481.

Schechter, J. C., Brennan, P. A., Smith, A. K., Stowe, Z. N., Newport, D. J., & Johnson, K. C. (2017). Maternal prenatal psychological distress and preschool cognitive functioning: The protective role of positive parental engagement. _Journal of abnormal child psychology_, _45_(2), 249-260.

Scheepens, A., van de Waarenburg, M., van den Hove, D., & Blanco, C. E. (2003). A single course of prenatal betamethasone in the rat alters postnatal brain cell proliferation but not apoptosis. _The Journal of physiology, 552_(1), 163-175.

Schmidt, M. V., Schülke, J. P., Liebl, C., Stiess, M., Avrabos, C., Bock, J., ... & Trümbach, D. (2011). Tumor suppressor down-regulated in renal cell carcinoma 1 (DRR1) is a stress-induced actin bundling factor that modulates synaptic efficacy and cognition. _Proceedings of the National Academy of Sciences, 108_(41), 17213-17218.

Schroeder, M., Jakovcevski, M., Polacheck, T., Lebow, M., Drori, Y., Engel, M., ... & Chen, A. (2017). A methyl-balanced diet prevents CRF-induced prenatal stress-triggered predisposition to binge eating-like phenotype. _Cell metabolism, 25_(6), 1269-1281.

Schurch, N. J., Schofield, P., Gierliński, M., Cole, C., Sherstnev, A., Singh, V., ... & Blaxter, M. (2016). How many biological replicates are needed in an RNA-seq experiment and which differential expression tool should you use?. _Rna, 22_(6), 839-851.

Schwartz, M. P., Hou, Z., Propson, N. E., Zhang, J., Engstrom, C. J., Costa, V. S., ... & Wang, Y. (2015). Human pluripotent stem cell-derived neural constructs for

predicting neural toxicity. *Proceedings of the National Academy of Sciences, 112*(40), 12516-12521.

Seckl, J. R. (1997). Glucocorticoids, feto-placental 11β-hydroxysteroid dehydrogenase type 2, and the early life origins of adult disease. *Steroids, 62*(1), 89-94.

Seckl, J. R., & Holmes, M. C. (2007). Mechanisms of disease: glucocorticoids, their placental metabolism and fetal 'programming' of adult pathophysiology. *Nature Reviews Endocrinology*, *3*(6), 479.

Seth, S., Lewis, A. J., Saffery, R., Lappas, M., & Galbally, M. (2015). Maternal prenatal mental health and placental 11β-HSD2 gene expression: initial findings from the mercy pregnancy and emotional wellbeing study. *International journal of molecular sciences*, *16*(11), 27482-27496.

Sharp, H., Hill, J., Hellier, J., & Pickles, A. (2015). Maternal antenatal anxiety, postnatal stroking and emotional problems in children: outcomes predicted from pre- and postnatal programming hypotheses. *Psychological medicine*, *45*(2), 269-283.

Sharp, H., Pickles, A., Meaney, M., Marshall, K., Tibu, F., & Hill, J. (2012). Frequency of infant stroking reported by mothers moderates the effect of prenatal depression on infant behavioural and physiological outcomes. *PloS one*, *7*(10), e45446.

Sherman, B. T., & Lempicki, R. A. (2009). Systematic and integrative analysis of large gene lists using DAVID bioinformatics resources. *Nature protocols, 4*(1), 44-57.

Shin, J., Syme, C., Wang, D., Richer, L., Pike, G. B., Gaudet, D., ... & Pausova, Z. (2019). Novel genetic locus of visceral fat and systemic inflammation. *The Journal of Clinical Endocrinology & Metabolism.*

Slopen, N., Loucks, E. B., Appleton, A. A., Kawachi, I., Kubzansky, L. D., Non, A. L., ... & Gilman, S. E. (2015). Early origins of inflammation: An examination of prenatal and childhood social adversity in a prospective cohort study. *Psychoneuroendocrinology*, *51*, 403-413.

Smyth G. K. (2014). Linear models and empirical Bayes methods for assessing differential expression in microarray experiments. *Statistical Applications in Genetics and Molecular Biology. 3*(1):3.

Soneson C, Love MI, Robinson MD (2015). "Differential analyses for RNA-seq: transcript-level estimates improve gene-level inferences." *F1000Research*, 4. doi: 10.12688/f1000research.7563.1.

Steel, Z., Marnane, C., Iranpour, C., Chey, T., Jackson, J. W., Patel, V., & Silove, D. (2014). The global prevalence of common mental disorders: a systematic review and meta-analysis 1980–2013. *International Journal of Epidemiology*, *43*(2), 476–493.

Stein, J. L., de la Torre-Ubieta, L., Tian, Y., Parikshak, N. N., Hernández, I. A., Marchetto, M. C., ... & Wexler, E. M. (2014). A quantitative framework to evaluate modeling of cortical development by neural stem cells. *Neuron*, *83*(1), 69-86.

Steinberg, S., de Jong, S., Andreassen, O. A., Werge, T., Børglum, A. D., Mors, O., ... & Demontis, D. (2011). Common variants at VRK2 and TCF4 conferring risk of schizophrenia. *Human molecular genetics, 20*(20), 4076-4081.

Stiles, J., & Jernigan, T. L. (2010). The basics of brain development. *Neuropsychology review*, *20*(4), 327-348.

Stone, J. M., Morrison, P. D., & Pilowsky, L. S. (2007). Glutamate and dopamine dysregulation in schizophrenia—a synthesis and selective review. *Journal of psychopharmacology*, 21(4), 440-452.

Studer, L. (2017). Strategies for bringing stem cell-derived dopamine neurons to the clinic—the NYSTEM trial. In *Progress in brain research* (Vol. 230, pp. 191-212). Elsevier.

Suarez, L., Cardarelli, K., & Hendricks, K. (2003). Maternal stress, social support, and risk of neural tube defects among Mexican Americans. *Epidemiology*, *14*(5), 612-616.

Sudmant, P. H., Lee, H., Dominguez, D., Heiman, M., & Burge, C. B. (2018). Widespread Accumulation of Ribosome-Associated Isolated 3′ UTRs in Neuronal Cell Populations of the Aging Brain. *Cell reports*, *25*(9), 2447-2456.

Sun, Q., Yang, Y., Li, X., He, B., Jia, Y., Zhang, N., & Zhao, R. (2016). Folate deprivation modulates the expression of autophagy-and circadian-related genes in HT-

22 hippocampal neuron cells through GR-mediated pathway. *Steroids, 112,* 12-19.

Soneson, C., & Delorenzi, M. (2013). A comparison of methods for differential expression analysis of RNA-seq data. *BMC bioinformatics*, *14*(1), 91.

Stoykova, A., Gotz, M., Gruss, P., & Price, J. (1997). Pax6-dependent regulation of adhesive patterning, R-cadherin expression and boundary formation in developing forebrain. *Development, 124*(19), 3765-3777.

Sumner, C. J., d'Ydewalle, C., Wooley, J., Fawcett, K. A., Hernandez, D., Gardiner, A. R., ... & Stanescu, H. C. (2013). A dominant mutation in FBXO38 causes distal spinal muscular atrophy with calf predominance. *The American Journal of Human Genetics, 93*(5), 976-983.

St-Hilaire, A., Steiger, H., Liu, A., Laplante, D. P., Thaler, L., Magill, T., & King, S. (2015). A prospective study of effects of prenatal maternal stress on later eating-disorder manifestations in affected offspring: Preliminary indications based on the project ice storm cohort. *International Journal of Eating Disorders, 48*(5), 512-516.

Tabas-Madrid, D., Nogales-Cadenas, R., & Pascual-Montano, A. (2012). GeneCodis3: a non-redundant and modular enrichment analysis tool for functional genomics. *Nucleic acids research, 40*(W1), W478-W483.

Talkowski, M. E., Mullegama, S. V., Rosenfeld, J. A., Van Bon, B. W., Shen, Y., Repnikova, E. A., ... & Chiang, C. (2011). Assessment of 2q23. 1 microdeletion syndrome implicates MBD5 as a single causal locus of intellectual disability,

epilepsy, and autism spectrum disorder. *The American Journal of human genetics*, *89*(4), 551-563.

Talkowski, M. E., Rosenfeld, J. A., Blumenthal, I., Pillalamarri, V., Chiang, C., Heilbut, A., ... & Pereira, S. (2012). Sequencing chromosomal abnormalities reveals neurodevelopmental loci that confer risk across diagnostic boundaries. *Cell*, *149*(3), 525-537.

Tan W.-H., Gilmore E. C., Baris H. N., Chapter 15 - Human Developmental Genetics. In D. Rimoin, R. Pyeritz, B. Korf (Eds.). *Emery and Rimoin's Principles and Practice of Medical Genetics*. Academic Press, 2013, Pages 1-63.

Tanabe, K., Ang, C. E., Chanda, S., Olmos, V. H., Haag, D., Levinson, D. F., ... & Wernig, M. (2018). Transdifferentiation of human adult peripheral blood T cells into neurons. *Proceedings of the National Academy of Sciences, 115*(25), 6470-6475.

Tanahashi, T., Mune, T., Morita, H., Tanahashi, H., Isomura, Y., Suwa, T., ... & Yasuda, K. (2002). Glycyrrhizic acid suppresses type 2 11β-hydroxysteroid dehydrogenase expression in vivo. *The Journal of steroid biochemistry and molecular biology*, *80*(4-5), 441-447.

Tandonnet, S., & Torres, T. T. (2017). Traditional versus 3′ RNA-seq in a non-model species. *Genomics data*, 11, 9-16.

Tang, Y., Liu, M. L., Zang, T., & Zhang, C. L. (2017). Direct reprogramming rather than iPSC-based reprogramming maintains aging hallmarks in human motor neurons. *Frontiers in molecular neuroscience, 10*, 359.

Theil, T., Aydin, S., Koch, S., Grotewold, L., & Rüther, U. (2002). Wnt and Bmp signalling cooperatively regulate graded Emx2 expression in the dorsal telencephalon. *Development*, *129*(13), 3045-3054.

Thier, M., Wörsdörfer, P., Lakes, Y. B., Gorris, R., Herms, S., Opitz, T., ... & Brüstle, O. (2012). Direct conversion of fibroblasts into stably expandable neural stem cells. *Cell stem cell, 10*(4), 473-479.

Tiscia, G., Colaizzo, D., Chinni, E., Pisanelli, D., Sciannamè, N., Favuzzi, G., ... & Grandone, E. (2009). Haplotype M2 in the annexin A5 (ANXA5) gene and the occurrence of obstetric complications. *Thrombosis and haemostasis*, 102(08), 309-313.

Tomov, M. L., Olmsted, Z. T., Dogan, H., Gongorurler, E., Tsompana, M., Otu, H. H., ... & Paluh, J. L. (2016). Distinct and Shared Determinants of Cardiomyocyte Contractility in Multi-Lineage Competent Ethnically Diverse Human iPSCs. *Scientific reports, 6*, 37637.

Topol, A., Tran, N. N., & Brennand, K. J. (2015). A guide to generating and using hiPSC derived NPCs for the study of neurological diseases. *JoVE (Journal of Visualized Experiments)*, (96), e52495.

Topol, A., Zhu, S., Tran, N., Simone, A., Fang, G., & Brennand, K. J. (2015). Altered WNT signaling in human induced pluripotent stem cell neural progenitor cells derived from four schizophrenia patients. *Biological psychiatry*, *78*(6), e29-e34.

Torr, E. E., Gardner, D. H., Thomas, L., Goodall, D. M., Bielemeier, A., Willetts, R., ... & Devitt, A. (2012). Apoptotic cell-derived ICAM-3 promotes both macrophage chemoattraction to and tethering of apoptotic cells. *Cell death and differentiation, 19*(4), 671.

Tran, K. A., Jackson, S. A., Olufs, Z. P., Zaidan, N. Z., Leng, N., Kendziorski, C., ... & Sridharan, R. (2015). Collaborative rewiring of the pluripotency network by chromatin and signalling modulating pathways. *Nature communications, 6*, 6188.

Trautman, P. D., Meyer-Bahlburg, H. F., Postelnek, J., & New, M. I. (1995). Effects of early prenatal dexamethasone on the cognitive and behavioral development of young children: results of a pilot study. *Psychoneuroendocrinology*, *20*(4), 439-449.

Tsankov, A. M., Gu, H., Akopian, V., Ziller, M. J., Donaghey, J., Amit, I., ... & Meissner, A. (2015). Transcription factor binding dynamics during human ES cell differentiation. *Nature*, *518*(7539), 344.

Tsiarli, M. A., Rudine, A., Kendall, N., Pratt, M. O., Krall, R., Thiels, E., ... & Monaghan, A. P. (2017). Antenatal dexamethasone exposure differentially affects distinct cortical neural progenitor cells and triggers long-term changes in murine cerebral architecture and behavior. *Translational psychiatry*, *7*(6), e1153.

Tyzio, R., Nardou, R., Ferrari, D. C., Tsintsadze, T., Shahrokhi, A., Eftekhari, S., ... & Lemonnier, E. (2014). Oxytocin-mediated GABA inhibition during delivery attenuates autism pathogenesis in rodent offspring. *Science, 343*(6171), 675-679.

Uenishi, G. I., Jung, H. S., Kumar, A., Park, M. A., Hadland, B. K., McLeod, E., ... & Swanson, S. (2018). NOTCH signaling specifies arterial-type definitive hemogenic endothelium from human pluripotent stem cells. *Nature communications, 9*(1), 1828.

Ursini, G., Punzi, G., Chen, Q., Marenco, S., Robinson, J. F., Porcelli, A., ... & Seidel, J. (2018). Convergence of placenta biology and genetic risk for schizophrenia. *Nature medicine*, *24*(6), 792.

Vadodaria, K. C., Mertens, J., Paquola, A., Bardy, C., Li, X., Jappelli, R., ... & Koch, P. (2016). Generation of functional human serotonergic neurons from fibroblasts. *Molecular psychiatry, 21*(1), 49.

van de Leemput, J., Boles, N. C., Kiehl, T. R., Corneo, B., Lederman, P., Menon, V., ... & Yao, S. (2014). CORTECON: a temporal transcriptome analysis of in vitro human cerebral cortex development from human embryonic stem cells. *Neuron, 83*(1), 51-68.

Van Den Ameele, J., Tiberi, L., Vanderhaeghen, P., & Espuny-Camacho, I. (2014). Thinking out of the dish: what to learn about cortical development using pluripotent stem cells. *Trends in neurosciences*, *37*(6), 334-342.

Van den Bergh, B. R., Van Calster, B., Smits, T., Van Huffel, S., & Lagae, L. (2008). Antenatal maternal anxiety is related to HPA-axis dysregulation and self-reported depressive symptoms in adolescence: a prospective study on the fetal origins of depressed mood. *Neuropsychopharmacology*, *33*(3), 536.

Van den Bergh, B. R., van den Heuvel, M. I., Lahti, M., Braeken, M., de Rooij, S. R., Entringer, S., ... & Schwab, M. (2017). Prenatal developmental origins of behavior and mental health: The influence of maternal stress in pregnancy. *Neuroscience & Biobehavioral Reviews*.

Van Der Kooij, M. A., Fantin, M., Rejmak, E., Grosse, J., Zanoletti, O., Fournier, C., ... & Sandi, C. (2014). Role for MMP-9 in stress-induced downregulation of nectin-3 in hippocampal CA1 and associated behavioural alterations. *Nature communications, 5*, 4995.

Van Os, J., & Selten, J. P. (1998). Prenatal exposure to maternal stress and subsequent schizophrenia: the May 1940 invasion of the Netherlands. *The british journal of psychiatry*, 172(4), 324-326.

Van Wegberg, A. M. J., MacDonald, A., Ahring, K., Bélanger-Quintana, A., Blau, N., Bosch, A. M., ... & Huijbregts, S. C. (2017). The complete European guidelines on phenylketonuria: diagnosis and treatment. *Orphanet journal of rare diseases, 12*(1), 162.

Varon, R., Vissinga, C., Platzer, M., Cerosaletti, K. M., Chrzanowska, K. H., Saar, K., ... & Stumm, M. (1998). Nibrin, a novel DNA double-strand break repair protein, is mutated in Nijmegen breakage syndrome. *Cell*, 93(3), 467-476.

Velders, F. P., Dieleman, G., Cents, R. A., Bakermans-Kranenburg, M. J., Jaddoe, V. W., Hofman, A., ... & Tiemeier, H. (2012). Variation in the glucocorticoid receptor gene at rs41423247 moderates the effect of prenatal maternal psychological symptoms on child cortisol reactivity and behavior. *Neuropsychopharmacology*, 37(11), 2541.

Veraksa, A., Del Campo, M., & McGinnis, W. (2000). Developmental patterning genes and their conserved functions: from model organisms to humans. *Molecular genetics and metabolism, 69*(2), 85-100.

Vieceli, F. M., & Bronner, M. E. (2018). Leukocyte Receptor Tyrosine Kinase interacts with secreted midkine to promote survival of migrating neural crest cells. *Development, 145*(20), dev164046.

Walder, D. J., Laplante, D. P., Sousa-Pires, A., Veru, F., Brunet, A., & King, S. (2014). Prenatal maternal stress predicts autism traits in 6½ year-old children: Project Ice Storm. *Psychiatry research,* 219(2), 353-360.

Wang, Z., Gerstein, M., & Snyder, M. (2009). RNA-Seq: a revolutionary tool for transcriptomics. *Nature reviews genetics*, 10(1), 57.

Wang, X., Jiang, X., Yu, X., Liu, H., Tao, Y., Jiang, G., & Hong, M. (2017). Cimifugin suppresses allergic inflammation by reducing epithelial derived initiative key factors via regulating tight junctions. Journal of cellular and molecular medicine, 21(11), 2926-2936.

Wang, S., Watanabe, T., Noritake, J., Fukata, M., Yoshimura, T., Itoh, N., ... & Kaibuchi, K. (2007). IQGAP3, a novel effector of Rac1 and Cdc42, regulates neurite outgrowth. *Journal of Cell Science*, 120(4), 567-577.

Weinstein, J. J., Chohan, M. O., Slifstein, M., Kegeles, L. S., Moore, H., & Abi-Dargham, A. (2017). Pathway-specific dopamine abnormalities in schizophrenia. *Biological psychiatry, 81*(1), 31-42.

Wen, D. J., Poh, J. S., Ni, S. N., Chong, Y. S., Chen, H., Kwek, K., ... & Qiu, A. (2017). Influences of prenatal and postnatal maternal depression on amygdala volume and microstructure in young children. *Translational psychiatry*, 7(4), e1103.

Whitton, L., Apostolova, G., Rieder, D., Dechant, G., Rea, S., Donohoe, G., & Morris, D. W. (2018). Genes regulated by SATB2 during neurodevelopment contribute to schizophrenia and educational attainment. *PLoS genetics*, 14(7), e1007515.

Winsper, C., Wolke, D., & Lereya, T. (2015). Prospective associations between prenatal adversities and borderline personality disorder at 11–12 years. *Psychological medicine, 45*(5), 1025-1037.

Wochnik, G. M., Rüegg, J., Abel, G. A., Schmidt, U., Holsboer, F., & Rein, T. (2005). FK506-binding proteins 51 and 52 differentially regulate dynein interaction and nuclear translocation of the glucocorticoid receptor in mammalian cells. *Journal of Biological Chemistry, 280*(6), 4609-4616.

World Health Organization (2015). Health in 2015: from MDGs, millennium development goals to SDGs, sustainable development goals.

Wray, N. R., Ripke, S., Mattheisen, M., Trzaskowski, M., Byrne, E. M., Abdellaoui, A., ... & Bacanu, S. A. (2018). Genome-wide association analyses identify 44 risk variants and refine the genetic architecture of major depression. *Nature genetics*, 50(5), 668.

Xiong, Y., Soumillon, M., Wu, J., Hansen, J., Hu, B., Van Hasselt, J. G., ... & Bochicchio, J. (2017). A comparison of mRNA sequencing with random primed and 3′-directed libraries. *Scientific reports, 7*(1), 14626.

Ye, Y., Lukinova, N., & Fortini, M. E. (1999). Neurogenic phenotypes and altered Notch processing in Drosophila Presenilin mutants. *Nature, 398*(6727), 525.

Yehuda, R., Engel, S. M., Brand, S. R., Seckl, J., Marcus, S. M., & Berkowitz, G. S. (2005). Transgenerational effects of posttraumatic stress disorder in babies of mothers exposed to the World Trade Center attacks during pregnancy. *The Journal of Clinical Endocrinology & Metabolism*, *90*(7), 4115-4118.

Yoon, K. J., Ringeling, F. R., Vissers, C., Jacob, F., Pokrass, M., Jimenez-Cyrus, D., ... & Kim, S. (2017). Temporal control of mammalian cortical neurogenesis by m6A methylation. *Cell*, *171*(4), 877-889.

Yoshida, M., Suda, Y., Matsuo, I., Miyamoto, N., Takeda, N., Kuratani, S., & Aizawa, S. (1997). Emx1 and Emx2 functions in development of dorsal telencephalon. *Development, 124*(1), 101-111.

Young, E. A., Abelson, J., & Lightman, S. L. (2004). Cortisol pulsatility and its role in stress regulation and health. *Frontiers in neuroendocrinology, 25*(2), 69-76.

Young, F. I., Keruzore, M., Nan, X., Gennet, N., Bellefroid, E. J., & Li, M. (2017). The doublesex-related Dmrta2 safeguards neural progenitor maintenance involving transcriptional regulation of Hes1. *Proceedings of the National Academy of Sciences, 114*(28), E5599-E5607.

Yu, G., Wang, L. G., & He, Q. Y. (2015). ChIPseeker: an R/Bioconductor package for ChIP peak annotation, comparison and visualization. *Bioinformatics*, *31*(14), 2382-2383.

Zanotelli, M. R., Ardalani, H., Zhang, J., Hou, Z., Nguyen, E. H., Swanson, S., ... & Xie, A. W. (2016). Stable engineered vascular networks from human induced pluripotent stem cell-derived endothelial cells cultured in synthetic hydrogels. *Acta biomaterialia*, 35, 32-41.

Zhang, X., Cai, J., Zheng, Z., Polin, L., Lin, Z., Dandekar, A., ... & Yang, Z. Q. (2015). A novel ER–microtubule-binding protein, ERLIN2, stabilizes Cyclin B1 and regulates cell cycle progression. *Cell discovery, 1*, 15024.

Zhang, S., Li, J., Lea, R., Vleminckx, K., & Amaya, E. (2014). Fezf2 promotes neuronal differentiation through localised activation of Wnt/β-catenin signalling during forebrain development. *Development, 141*(24), 4794-4805.

Zhang, J., Schwartz, M. P., Hou, Z., Bai, Y., Ardalani, H., Swanson, S., ... & Bolin, J. (2017). A genome-wide analysis of human pluripotent stem cell-derived endothelial cells in 2D or 3D culture. *Stem cell reports*, *8*(4), 907-918.

Zhao, B., Wang, J., Liu, L., Li, X., Liu, S., Xia, Q., & Shi, J. (2016). Annexin A1 translocates to nucleus and promotes the expression of pro-inflammatory cytokines in a PKC-dependent manner after OGD/R. *Scientific reports, 6,* 27028.

Zhu, X., Gu, H., Liu, Z., Xu, Z., Chen, X., Sun, X., ... & Deng, X. (2013). Associations between TCF4 gene polymorphism and cognitive functions in schizophrenia patients and healthy controls. *Neuropsychopharmacology, 38*(4), 683.

Zhu, P., Hao, J. H., Tao, R. X., Huang, K., Jiang, X. M., Zhu, Y. D., & Tao, F. B. (2015). Sex-specific and time-dependent effects of prenatal stress on the early behavioral symptoms of ADHD: a longitudinal study in China. *European child & adolescent psychiatry, 24*(9), 1139-1147.

Zill, P., Baghai, T. C., Zwanzger, P., Schüle, C., Eser, D., Rupprecht, R., ... & Ackenheil, M. S. N. P. (2004). SNP and haplotype analysis of a novel tryptophan hydroxylase isoform (TPH2) gene provide evidence for association with major depression. *Molecular psychiatry, 9*(11), 1030.

Ziller, M. J., Edri, R., Yaffe, Y., Donaghey, J., Pop, R., Mallard, W., ... & Gu, H. (2015). Dissecting neural differentiation regulatory networks through epigenetic footprinting. *Nature*, *518*(7539), 355.

Ziller, M. J., Hansen, K. D., Meissner, A., & Aryee, M. J. (2015). Coverage recommendations for methylation analysis by whole-genome bisulfite sequencing. *Nature methods, 12*(3), 230.

Zohsel, K., Holz, N. E., Hohm, E., Schmidt, M. H., Esser, G., Brandeis, D., ... & Laucht, M. (2017). Fewer self-reported depressive symptoms in young adults exposed to maternal depressed mood during pregnancy. *Journal of affective disorders*, *209*, 155-162.

Zweifel, S., Marcy, G., Guidice, Q. L., Li, D., Heinrich, C., Azim, K., & Raineteau, O. (2018). HOPX Defines Heterogeneity of Postnatal Subventricular Zone Neural Stem Cells. *Stem cell reports, 11*(3), 770-783.

7.　Supplementary Information

7.1　Supplementary Analyses

First, a regression model without the inclusion of covariates was computed on SWAN normalised data that had not been corrected for batches. Results obtained with this analysis therefore best represent differences between methylation beta values as measured. It will be referred to as basic model. The data structure does therefore not undergo any further alterations other than those described following the normalization procedure.

Second, an alternative regression model was run with biological replicate as random or "within-subject" factor. In this model, from here on referenced as model 2, normalised beta values were batch corrected for array sentrix position without prior specification of the regression model.

Consequences of the alternative preprocessing pipeline on the data structure were once again assessed by multidimensional scaling plots, correlation analyses with principal components, and variance partitioning.

Multidimensional scaling plots following the preprocessing procedure for model 2 showed increased variance compared to normalised data without batch correction reflecting that some of the variance explained by these factors was removed alongside batch correction for array position (**Supplementary Fig. 1**). Within individual stages of differentiation, stem cells were best distinguished by cell line and neuronal progenitors by biological replicate or differentiation batch, whereas differentiated neurons revealed no clustering (**Supplementary Fig. 2**).
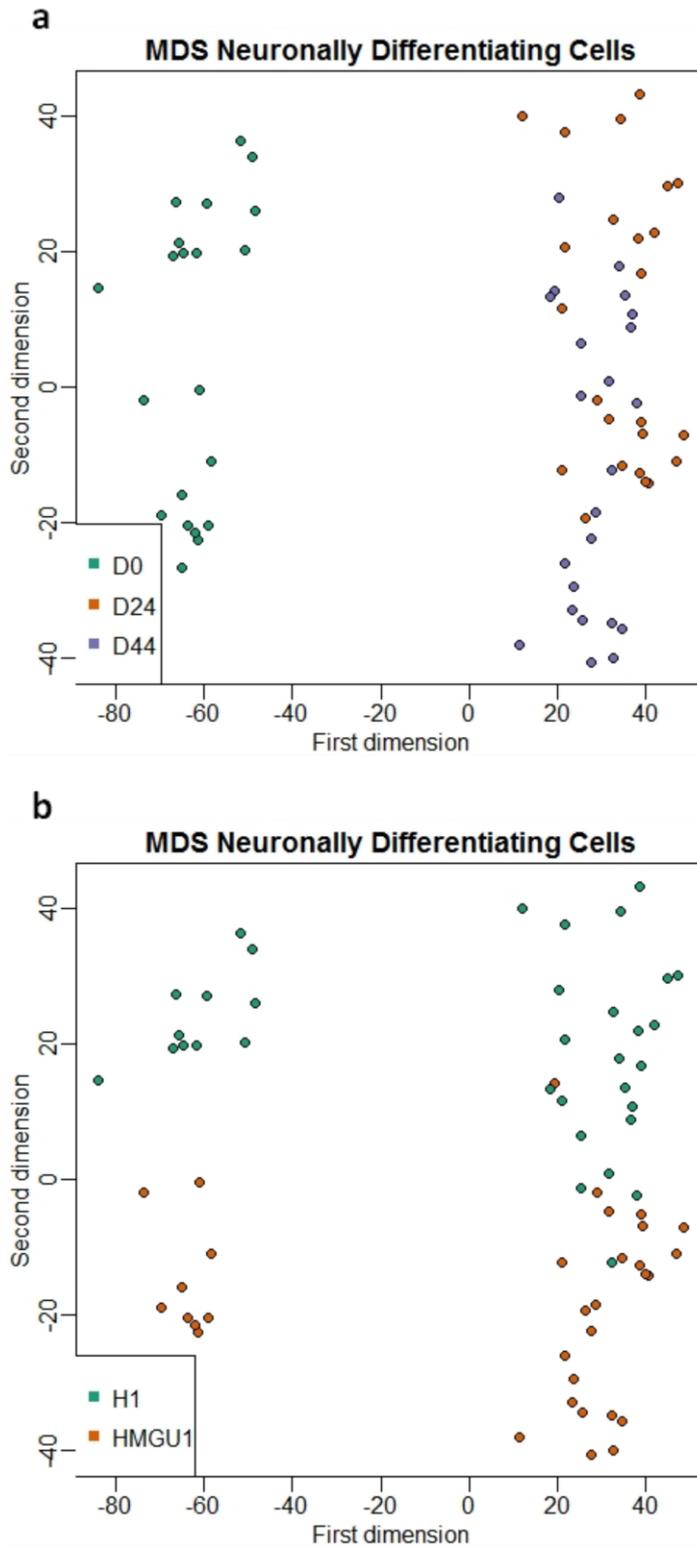
Supplementary Figure 1. Multidimensional scaling plots following batch correction (model 2). SWAN normalised batch-corrected data by **a)** differentiation stage and **b)** cell line (N=70 samples; n=792 780 probes).

combat corrected betas model 2
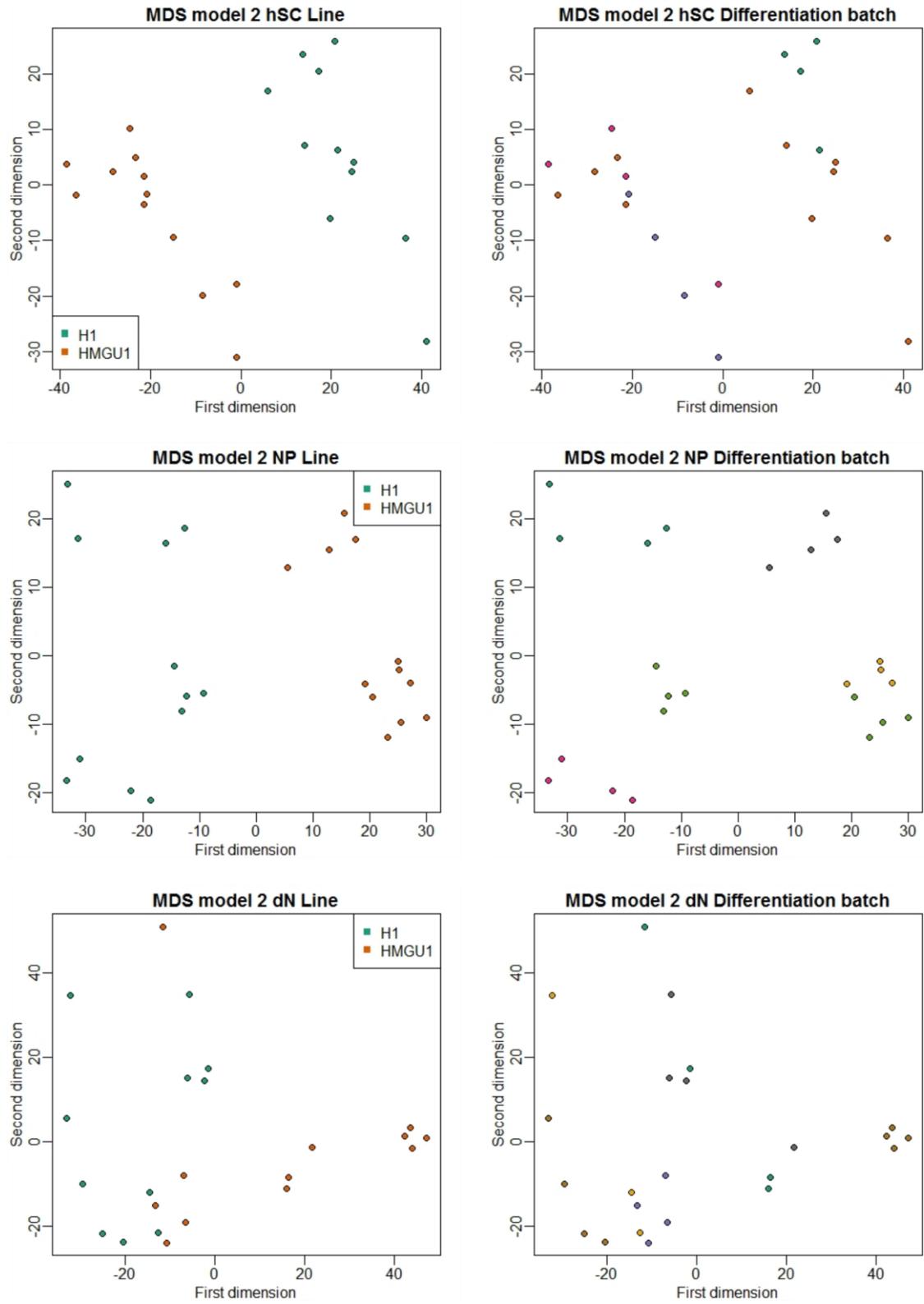
Supplementary Figure 2. Multidimensional scaling plot (model 2). Beta values after batch correction for model 2 (N=70, n=792 780 probes).

The correlation structure of known variables with principal components following model 2 batch correction (**Supplementary Fig. 3**) showed that stage of differentiation remained highly correlated to the first principal component, and cell line to the second principal component. Meanwhile, EPIC methylation chip as confounding variable remained correlated to PC8, PC11, and PC17. Following this preprocessing procedure, treatment and duration did not cluster with individual principal components.

Variance partition after batch correction for array position showed a reduction of variance explained by this factor in the complete data set from 30% before batch correction down to around 10% (**Supplementary Fig. 4**). Again, reductions were less pronounced within individual stages of neuronal development. Variance explained by predictor variables stage of differentiation, treatment, and duration slightly decreased in the corrected data set.
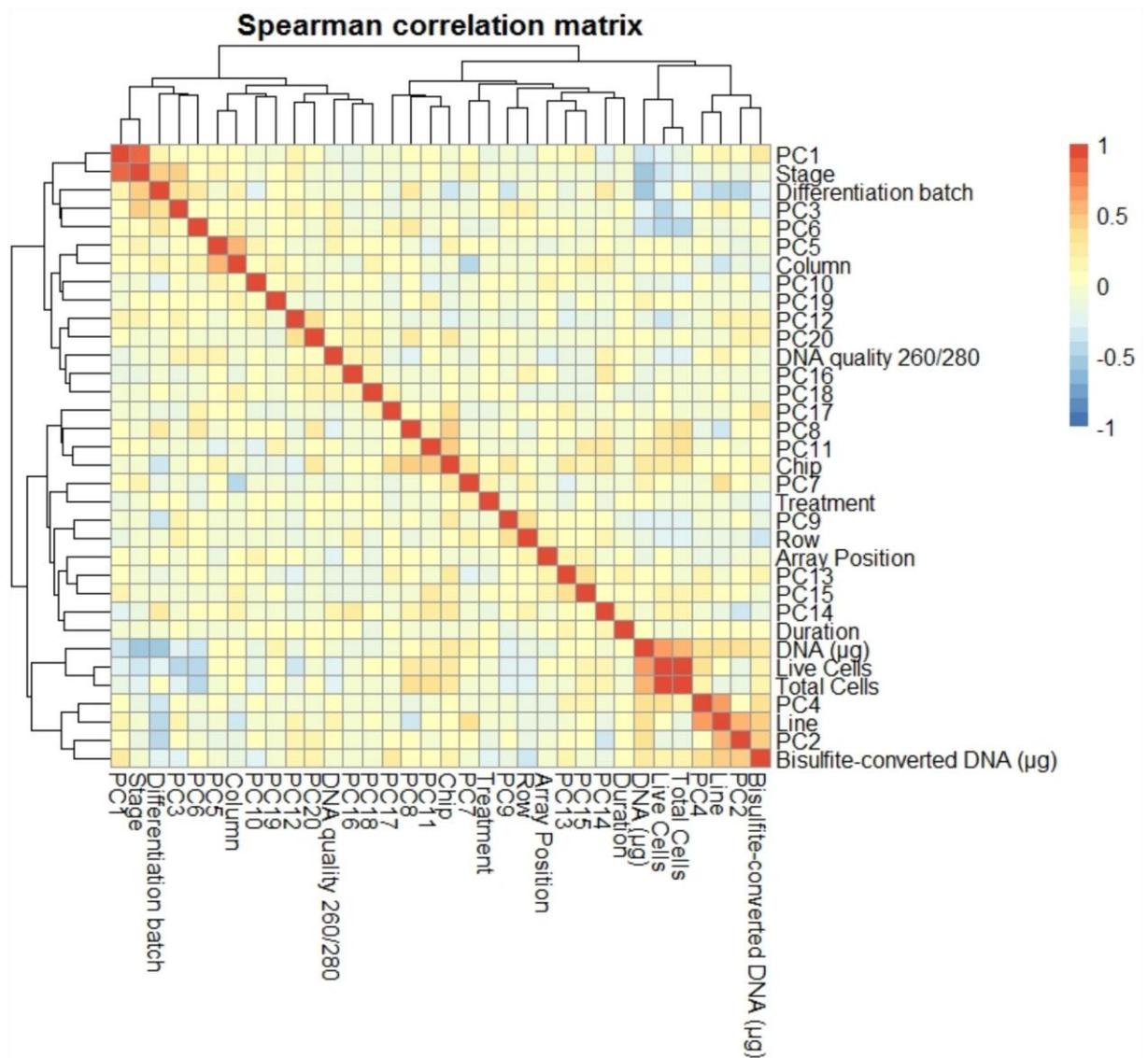
Supplementary Figure 3. Correlation matrix between PCA 1-20 and potential predictor variables (model 2). Methylation beta values were SWAN normalised and batch-corrected for array sentrix position (N=70 samples; n=792 780 probes).
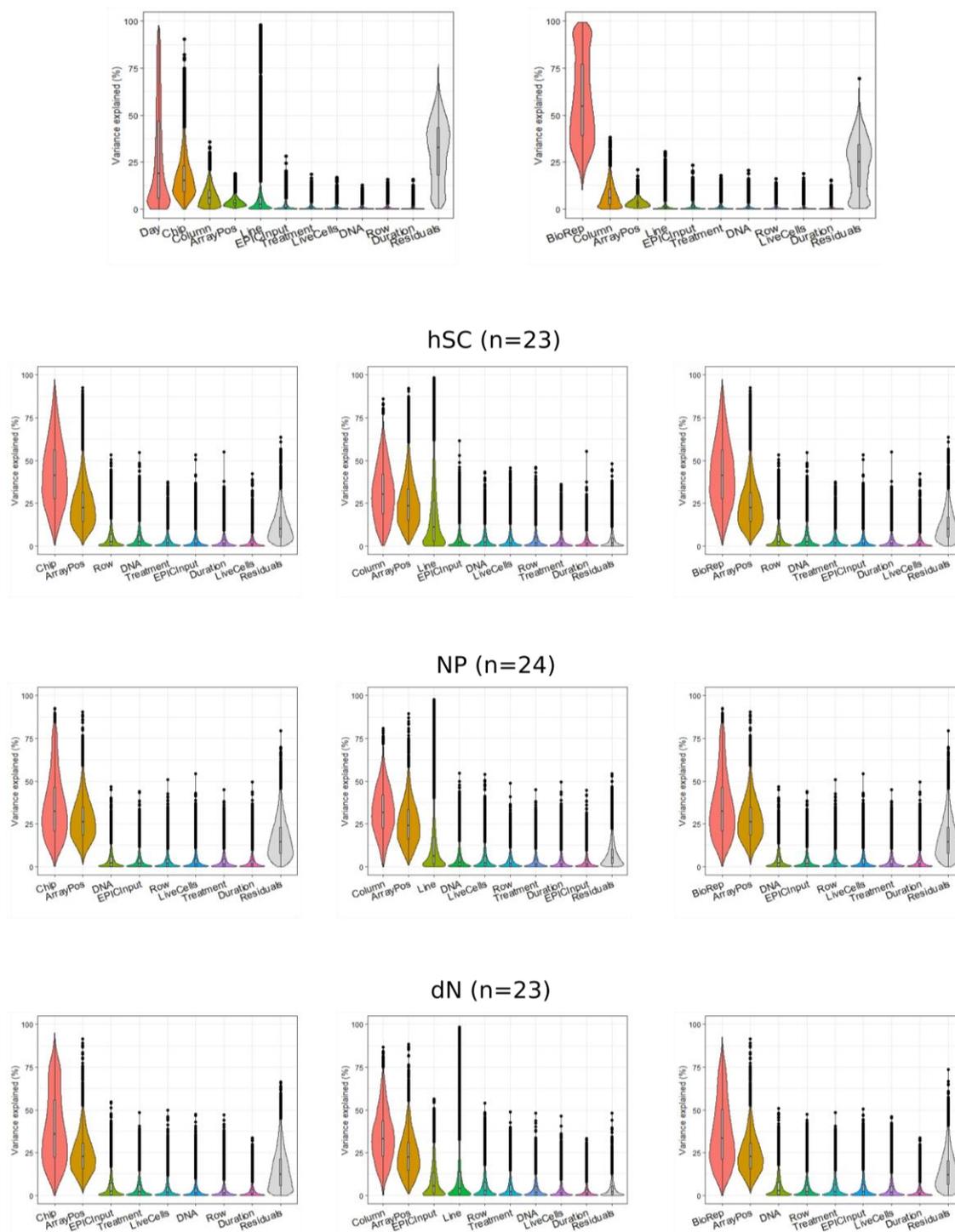
Supplementary Figure 4. Variance partition in combat corrected methylation beta values (N=70 samples; n=10 000 probes). Chip = EPIC methylation chip, ArrayPos = sentrix position, LiveCells = number of living cells, DNA = DNA input amount for bisulfite conversion, EPICInput = amount of bisulfite-converted DNA.

An exemplary visualisation of the influence of preprocessing choice and inclusion of covariates on identification of differentially methylated positions (DMPs) is given for differentiated neurons (D44) following dexamethasone stimulation (beta change ≥ 5%, no significance cutoff) (**Supplementary Fig. 5**). The regression model specified in the main analyses of the thesis is referred to as model 1. Model 1 identified 78% of DMPs in the basic comparison, reduced differences below the 5% cutoff between 1 664 probes, and increased differences between 2 123 probes (**Supplementary Fig. 5a**). Combat correction in model 1 reduced differences below cutoff in n=2 889 probes, and increased differences in 1 209 probes (**Supplementary Fig. 5b**). Thus, batch correction making use of the model specification in ComBat and the inclusion of covariates resulted in a balanced correction without bias towards either unilaterally increasing or decreasing differences between probes.

Model 2 identified 48% of DMPs in the basic comparison, reduced differences between 4 019 probes below cutoff, and increased differences between 32 probes (**Supplementary Fig. 5c**). ComBat correction in model 2 reduced differences below cutoff in n=3 013 probes, and increased differences in 29 probes (**Supplementary Fig. 5d**). 95% of DMPs called in model 2 are also identified in model 1 with 43% of probes in model 1 not identified by model 2 (**Supplementary Fig. 5d**). Given that 95% of DMPs identified in model 2 were identified by model 1, overall interpretation of results should be unaffected by choice of preprocessing and covariates.

Spearman correlations between beta changes estimated by the different regression models are shown in **Table 13**.

Overall convergence on estimates of absolute differences obtained with either regression model was high throughout contrasts.

Table 13. Correlations between beta changes estimated with model 1, the basic model and model 2.

	Model 1 – Basic model		Model 1 – Model 2	
	r	*p*-value	r	*p*-value
hSC – NP	0.99	0	0.99	0
NP – dN	0.98	0	0.98	0
hSC DEX	0.95	0	0.94	0
NP DEX	0.96	0	0.96	0
dN DEX	0.96	0	0.96	0

Annotations. hSC = human stem cells, NP = neuronal progenitors, dN = differentiated neurons, DEX = dexamethasone.

Results for differentially methylated positions are reported for all regression models in **Supplementary Tables 2-3 & 5-7**.
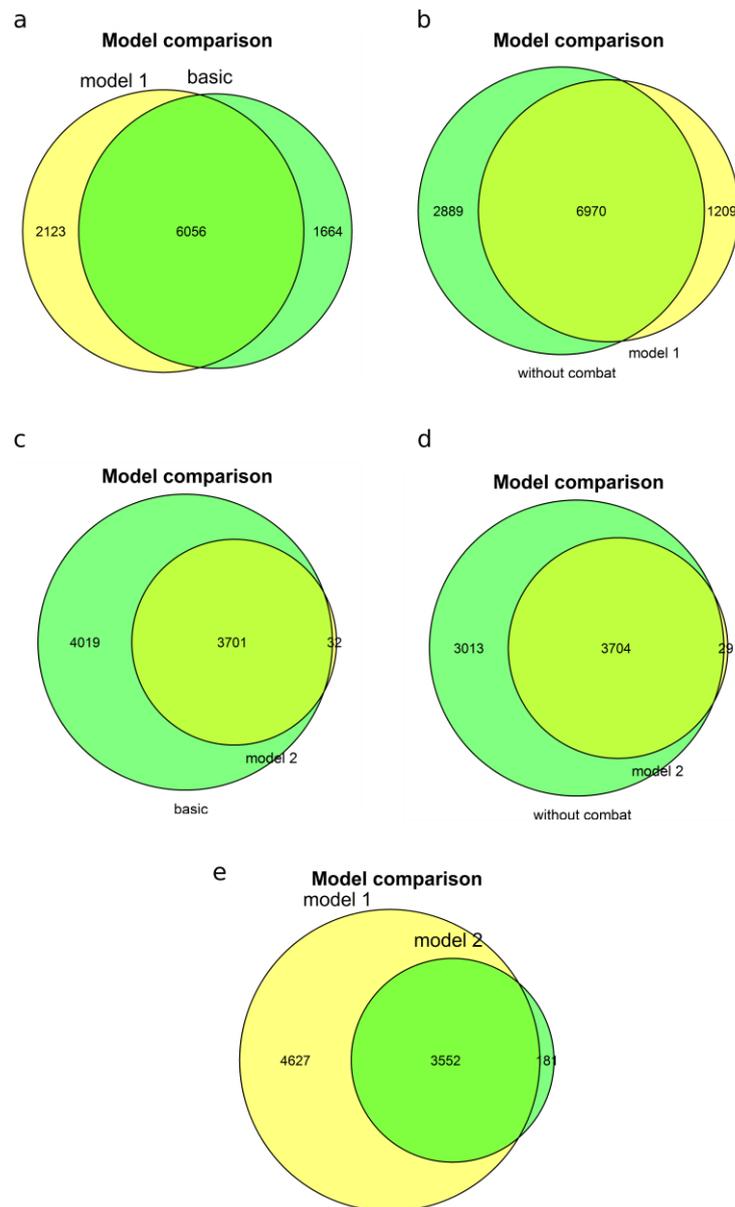
Supplementary Figure 5. Venn diagrams of DMPs (beta change ≥ 5%, no significance cutoff) identified in dNs (D44) following dexamethasone stimulation in regression models 1 and 2 (N = 70 samples; n = 792 780 probes). basic = unadjusted comparison, no combat correction or inclusion of covariates, simple contrast between stimulated and unstimulated samples in normalised data; Model 1 = combat correction for array and sentrix position, protected for differentiation stage, treatment, and duration as well as covariates cell line and DNA (µg); Model 2 = combat correction for array, no protection for variables of interest or covariates, run with line as covariate and biological replicate as random factor; without combat = model 1 or 2 run without respective approach to batch correction.

[241]

7.2 REAGENTS AND RESOURCES

REAGENT or RESOURCE	SOURCE	IDENTIFIER (if applicable)
Antibodies		
OCT4	Millipore	Cat# ABD116
NANOG	Millipore	Cat# MABD24
TRA1-60	Millipore	Cat# MAB4360
SOX2	Cell Signaling	Cat# 2748
FOXG1	Abcam	Cat# ab18259
PAX6	Biozol	Cat# BLD-901301
OTX2	R&D	Cat# AF1979
NESTIN	Santa Cruz	Cat# sc-23927
ZO1	BD Bioscience	Cat# 610966
MAP2	Abcam	Cat# AB5392
VGLUT1	Synaptic Systems	Cat# 135303
VGAT2	Synaptic Systems	Cat# 131011
SYN1	Synaptic Systems	Cat# 106001
PSD95	Invitrogen	Cat# 51-6900
GFAP	Dako	Cat# Z0334
GR	Santa Cruz	Cat# sc-8992X
GR	Cell Signaling	Cat# 12041
HSP70	Cell Signaling	Cat# 4872

HSP90	Thermo Scientific	Cat# PA3-013
FKBP51	Santa Cruz	Cat# 11518 (F14)
β-ACTIN	Cell Signaling	Cat# 4967
Alexa 488 Donkey Anti-rabbit	Dianova	Cat# 711-545-152
Alexa 488 Donkey Anti-mouse	Dianova	Cat# 715-545-150
Alexa 488 Donkey Anti-chicken	Dianova	Cat# 703-545-155
Alexa 594 Donkey Anti-rabbit	Life Technologies	Cat# A21207
Alexa 594 Donkey Anti-mouse	Dianova	Cat# 715-585-150
Alexa 594 Donkey Anti-goat	Dianova	Cat# 705-585-147
DyLight 647 Donkey Anti-rabbit	Dianova	Cat# 711-605-152
Alexa 647 Donkey Anti-mouse	Life Technologies	Cat# A31571
Anti-rabbit IgG, HRP-linked Antibody	Cell Signaling	Cat# 7074S
HRP-conjugated secondary antibody anti-goat	Santa Cruz	Cat# sc-2028
HRP-conjugated secondary antibody anti-rabbit	Cell Signaling	Cat# 7074S

| **Chemicals, Peptides, and Recombinant Proteins**		
L-Ascorbic Acid	Sigma Aldrich	Cat# A8960
BDNF	PeproTech	Cat# 450-02-10
GDNF	PeproTech	Cat# 450-10-10
cAMP	Enzo Life Sciences	Cat# BML-CN125-0100
N2	Thermo Fisher Scientific	Cat# 17502048
B27-RA	Thermo Fisher Scientific	Cat# 12587010
Laminin	Sigma	Cat# L2020
Matrigel	CORNING	Cat# 354277
ROCK inhibitor (Y-27632)	STEMCell	Cat# 72304
cOmplete protease inhibitor cocktail	Roche	Cat# 11697498001
Roti-Load	Roth	Cat# K929.1
Immobilon Western HRP Substrate	Merck	Cat# WBKLS0500
Arabinofuranosyl-cytosine (*ara*-C)	Jena BioScience	N-20307-5
Critical Commercial Assays		
QuantSeq 3′ mRNA-Seq Library Prep Kit FWD for Illumina	Lexogen	SKU: 015.2X96
Infinium Methylation EPIC Bead Chip Kit	Illumina	WG-317-1003

| chemagic RNA Blood Kit special	PerkinElmer	CMG-1084
chemagic DNA Blood Kit special	PerkinElmer	CMG-1091
AggreWell 800	STEMCELL Technologies	Cat# 34811
STEMdiff Neural Induction Medium	STEMCELL Technologies	Cat# 05839
STEMdiff Neural Progenitor Medium	STEMCELL Technologies	Cat# 05833
BrainPhys Neuronal Medium	STEMCELL Technologies	Cat# 05790
Experimental Models: Cell Lines		
WA01	Robert Koch Institute, Berlin	
HMGU1	German Research Center for Environmental Health, Munich	

7.3 SUPPLEMENTARY TABLES

All supplementary tables are available as Excel-files:

1. Suppl.Table_1_DEG_Development_EBSeq_DESeq2.xlsx

2. Suppl.Table_2_Methylation_Development_NP_Over_hSC.xlsx

3. Suppl.Table_3_Methylation_Development_dN_Over_NP.xlsx

4. Suppl.Table_4_DEG_DEX_EBSeq.xlsx

5. Suppl.Table_5_Methylation_DEX_hSC.xlsx

6. Suppl.Table_6_Methylation_DEX_NP.xlsx

7. Suppl.Table_7_Methylation_DEX_dN.xlsx

8. Suppl.Table_8_Functional_Enrichment_NP_Over_hSC_DMR_q0.01_betafc10%.xlsx

9. Suppl.Table_9_Functional_Enrichment_dN_Over_NP_DMR_q0.01_betafc10%.xlsx

10. Suppl.Table_10_Functional_Enrichment_dN_DEX_DMR_q0.1.xlsx

7.4   SUPPLEMENTARY FIGURES
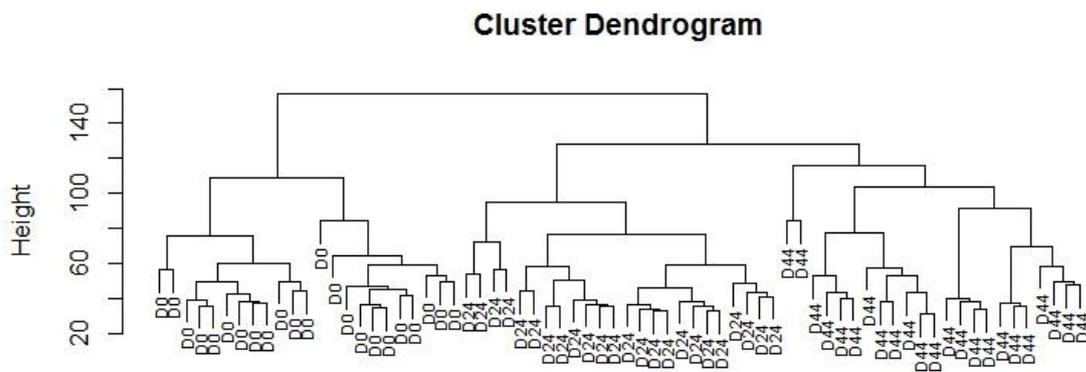
Supplementary Figure 6. Cluster dendrogram of differentiated cells. Normalized methylation beta values (N=70, n=866 091 probes).
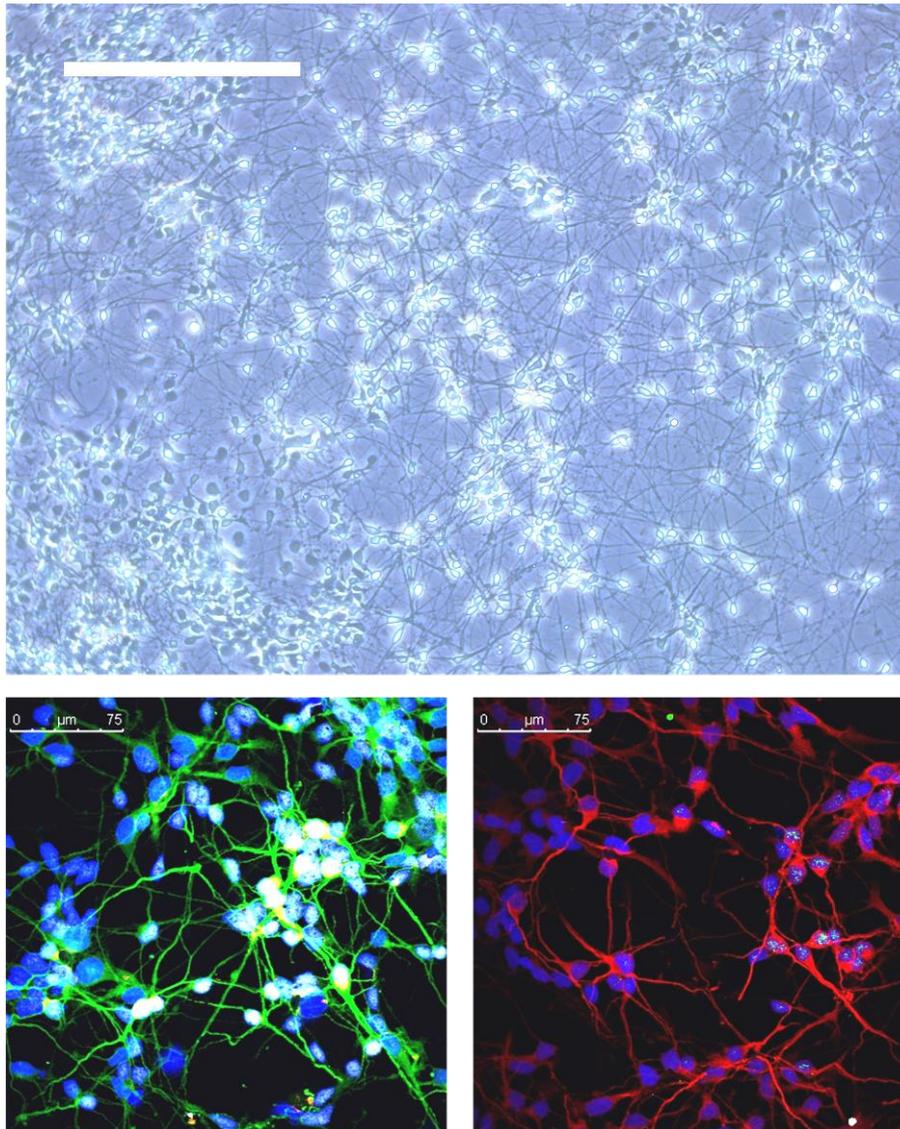
Supplementary Figure 7. Neuronal biological replicate excluded from RNA-Seq analyses. Upper panel: morphology in culture on day of experiment (scale bar: 50 μm). Lower panel (left): ICC marker expression for MAP2 (green) and FOXG1 (white). Lower panel (right): ICC marker expression for MAP2 (red) and vGlut1 (green).

DISCLOSURE OF AUTHOR CONTRIBUTIONS

Figures 1-5 were created by the author modifying individual components from Servier Medical Art, licensed under a Creative Commons Attribution 3.0 Unported (CC BY 3.0) License. http://smart.servier.com/.

The author conducted literature research, all cell culture experiments including the establishment of the glucocorticoid receptor translocation assay and differentiation protocol, all directed differentiation experiments, dexamethasone stimulation experiments, immunocytochemistry, and microscopy. The author also wrote the R scripts used for biostatistical analyses of differential methylation and differential gene expression, conducted the statistical analyses, and generated all plots and figures. Individual sections of R code were obtained from members of the department, as indicated below, and modified as required.

Preparation of EPIC methylation arrays and Lexogen QuantSeq 3' mRNA libraries was carried out by Susann Sauer and Maik Ködel. The qPCR was also conducted by Maik Ködel. Western Blot experiments were run by Denis Ciato who also helped with the establishment of an ImageJ processing pipeline fur computing nuclear translocation. Darina Czamara supervised EPIC methylation analyses and provided a script for preprocessing. Preprocessing of RNA-Seq data was carried out by Simone Röh, who also provided a script for permutation of *p*-values in Fisher's exact test. The large expression dataset for visualisation of developmental gene expression was provided by Michael Breen, analyses were run by the author. A list of Glucocorticoid Response Elements was obtained from Janine Arloth. The HMGU1 iPSC line was reprogrammed by Ejona Rusha. Dietmar Spengler gave literature recommendations and provided feedback on differentiation protocols and translocation experiments.

ACKNOWLEDGEMENTS

I would first like to thank Elisabeth Binder for setting the grounds for truly translational research in bringing a broad array of disciplines together and of course for enabling this study.

I would also like to thank the members of my Thesis Advisory Committee, Michael Ziller and Moritz Rossner, as well as Darina Czamara and Simone Röh for excellent advice and constructive criticism. In addition, I would like to thank everyone in the cell culture lab, and especially Christine, Tamara, Susanne and Ruhel for taking turns with weekend duties caring for those needy cells of mine.

My deep gratitude goes to the Graduate School of Systemic Neurosciences staff, and especially Lena Bittl, for their great administrative support.

Спасибо также моим родителям за их постоянную поддержку и заботу.

My very special thanks goes to Lisa, Lena, and Johannes for listening to my incomprehensible lab gibberish and finding all the right words nonetheless.

Lastly, thanks to Denis for sharing the GR antibody with me and for becoming such an important part of my life.

LIST OF PUBLICATIONS

Ciato, D., Li, R., Garcia, J. L. M., **Papst, L.**, D'Annunzio, S., Hristov, M., ... & Theodoropoulou, M. (2019). Inhibition of HSF1 enhances repressive molecular mechanisms on POMC promoter. *Neuroendocrinology*.

Submitted

Papst, L. & Binder, E.B. How Genes and Environment Interact to Shape Risk and Resilience to Stress-Related Psychiatric Disorders. In A. Chen (Ed.). *Stress Resilience*. Amsterdam, Elsevier.

In preparation

Papst, L., et al., Investigating prenatal stress in a stem cell model of human neuronal development.

AFFIDAVIT

Hiermit versichere ich an Eides statt, dass ich die vorliegende Dissertation

Investigating prenatal stress in a stem cell model of human neuronal development

selbstständig angefertigt habe, mich außer der angegebenen keiner weiteren Hilfsmittel bedient und alle Erkenntnisse, die aus dem Schrifttum ganz oder annähernd übernommen sind, als solche kenntlich gemacht und nach ihrer Herkunft unter Bezeichnung der Fundstelle einzeln nachgewiesen habe.

München, den 27.05.2019   Unterschrift Lilia Papst